The Dynamics of First Order Phase Transitions

J. D. Gunton, M. San Miguel and P.S. Sahni,

Phase Transitions and Critical Phenomena,
vol. 8 pp. 269-466.

Academic Press, London (1983)
Eds. C. Domb and J. Lebowitz.

Wegner, F. J. (1972). *Phys. Rev. B* **5**, 4529.
Widom, A. (1970). *Phys. Rev. A* **3**, 2042.
Widom, B. (1972). *In* "Phase Transitions and Critical Phenomena", Vol. 2 (C. Domb and M. S. Green, eds), Academic Press, London, p. 79.
Wiechert, H. and Wupperfeld, G. (1978). *J. Phys. (Paris)* **39** (Suppl.), C6–324.
Wilson, K. G. and Kogut, J. (1974). *Phys. Reports* **12C**, 77.
Wimp, J. (1981). "Sequence Transformations and Their Applications", Academic Press, New York.
Wolfram, T., de Wames, R. E., Hall, W. F. and Palmberg, P. W. (1971). *Surf. Sci.* **28**, 45.
Wu, F. Y. (1971). *Phys. Rev. B* **4**, 2312.
Wu, F. Y. (1982). *Rev. Mod. Phys.* **54**, 235.
Wynn, P. (1966). *Numer. Math.* **8**, 264.
Yahata, H. and Suzuki, M. (1969). *J. Phys. Soc. Japan* **27**, 1421.
Yalabik, M. C. and Gunton, J. D. (1979). *Prog. Theoret. Phys.* **62**, 1573.
Yang, C. N. and Lee, T. D. (1952). *Phys. Rev.* **87**, 404, 410.
Young, A. P. (1979). *Phys. Rev. B* **19**, 1855.
Ziman, J. M. (1953). *Phil. Mag.* **44**, 548.

3. The Dynamics of First-order Phase Transitions

J. D. Gunton

Physics Department, Temple University, Philadelphia, Pennsylvania 19122, USA
and
Département de Physique Théorique, Université de Genève, 1211 Genève 4, Switzerland

M. San Miguel

Departamento di Fisica Teorica, Universidad de Barcelona, Barcelona 28, Spain

and

Paramdeep S. Sahni

Corporate Research Science Laboratories, Exxon Research and Engineering Co., PO Box 45, Linden, New Jersey 07046, USA

PHASE TRANSITIONS
VOLUME 8 ISBN 0-12-220308-9

I. Introduction

In this article we review existing experimental and theoretical studies of the dynamical properties of a large class of first-order transitions. These involve such phenomena as nucleation, spinodal decomposition and late stage growth and coarsening. In the typical situation which we will consider, a system is rapidly quenched from a one-phase, thermal equilibrium state to a one-phase, nonequilibrium state inside its coexistence curve (Fig. 1). Such a quenched system then gradually evolves from this nonequilibrium state to an equilibrium thermodynamic state which consists of two coexisting phases. It does so by the temporal development of spatial fluctuations

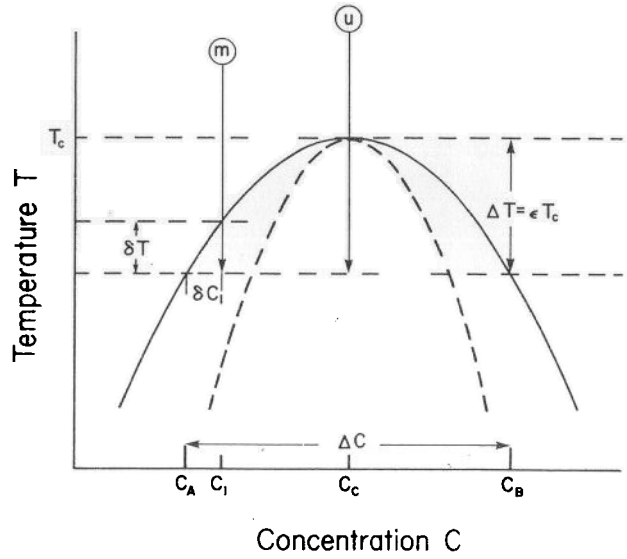

FIG. 1. The coexistence curve (solid line) and classical spinodal curve (dashed line) are shown schematically for a system such as a binary fluid or binary alloy. Typical quenches into the metastable (m) and the unstable (u) regions are also shown. In the former case the system is under-cooled by an amount δT, corresponding to an initial supersaturation $\delta c_1 = c_1 - c_A$, at a temperature $T = T_c - \Delta T$ below the critical point.

which take the initially homogeneous system through a sequence of highly inhomogeneous states which are far from equilibrium. This dynamical evolution is highly nonlinear. Thus the problem of pattern formation in systems which are spontaneously attempting to reach equilibrium provides a fascinating example of nonlinear, nonequilibrium phenomena. In spite of extensive experimental and theoretical studies of these first-order transitions, a first principles understanding does not yet exist. It should be noted that the prototype first-order phase transition which we consider here is associated with a second-order phase transition which occurs at a critical point (Fig. 1). (This dynamical prototype obviously involves a first-order phase transition, since discontinuities in the order parameter, entropy and other extensive variables characterize the two-phase equilibrium states.) We will in general not consider here the dynamical behavior of first-order phase transitions which do not involve a critical point, such as the liquid–solid transition (e.g. undercooling water). Much of the theoretical formalism which we describe, however, can rather straightforwardly be applied to this latter class of phenomena.

It should also be observed that the dynamical evolution toward thermodynamic equilibrium with which we concern ourselves here differs somewhat from other interesting nonlinear phenomena in which pattern formation is involved. For example, in problems such as the Rayleigh–Benard instability or Couette flow, ordered structures also develop, but the final state in such cases is a nonequilibrium state. The pattern formation is a consequence of nonequilibrium boundary conditions. (Recent reviews of hydrodynamic instabilities include Swinney and Gollub, 1981, and Eckmann, 1981.)

In our case, since the final state is in thermodynamic equilibrium, its properties are in principle well known from first principles. In addition, for the phenomena with which we are concerned, a well defined free energy functional exists, which provides the driving force for the dynamical evolution. In nonlinear problems in which the final state is in nonequilibrium, such a free energy functional often does not exist. (For a discussion of free energy functionals in this case see Graham, 1975, 1981, 1982.)

In the classical theory of first-order phase transitions one distinguishes between two different types of instability which characterize the early stages of phase separation in such systems. The first is an instability against finite amplitude, localized (droplet-like) fluctuations which leads to the initial decay of a metastable state. The rate of birth of such droplets is described by homogeneous nucleation theory. The second is an instability against infinitesimal amplitude, nonlocalized (long wavelength) fluctuations which leads to the initial decay of an unstable state. This latter instability is termed spinodal decomposition. In the classical picture there is a sharp distinction between metastable and unstable states. This is provided by the

spinodal curve which in the classical (mean field) theory is the locus of points inside the coexistence curve for which an appropriate susceptibility (such as the concentration susceptibility $(\partial c/\partial \mu)_T$ for binary fluids or the isothermal susceptibility for simple fluids) diverges. As is shown in Fig. 2, the classical theory predicts a van der Waals loop in the two-phase, nonequilibrium region. In this picture metastable states are those for which the appropriate susceptibility is positive, while unstable states are those for which this susceptibility is negative. The spinodal curve separates these two states. This distinction was originally proposed by Gibbs (1906).

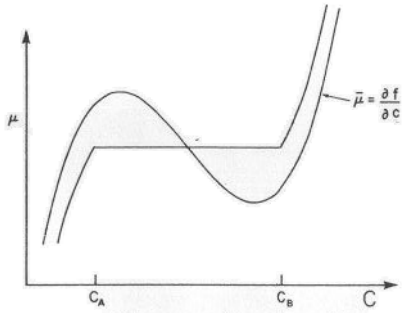

FIG. 2. The chemical potential μ as a function of concentration c for $T < T_c$, as predicted by mean field theory. The horizontal line indicates the equilibrium chemical potential, while the van der Waals loop indicates the regions of metastability and instability. The classical spinodal points are the two points on the loop for which $(\partial \mu/\partial c)_T = 0$.

Although the classical spinodal curve still provides a convenient way to distinguish loosely between metastable and unstable states, recent research suggests that there is in fact no sharp distinction between such states. Rather, there is a gradual transition in the dynamical behavior of a quenched system as one varies the quench concentration in the vicinity of the classical spinodal curve in Fig. 1. This point is discussed in detail in several sections of this article (Sections III, V, VII, IX–XI).

To get an understanding of the qualitative features of the dynamical properties of metastable and unstable states, it is helpful to note two experimental methods used in the study of first-order phase transitions. These are direct microscopic observations and small angle scattering measurements. We discuss the former method first. In Fig. 3 we show the results of a transmission electron microscope study of the alloy Fe–Al (Oki *et al.*, 1977). The extreme left and right sets show the growth of droplets for various times following quenches of the alloy into two metastable regions of its phase diagram. The center set of figures shows the result of

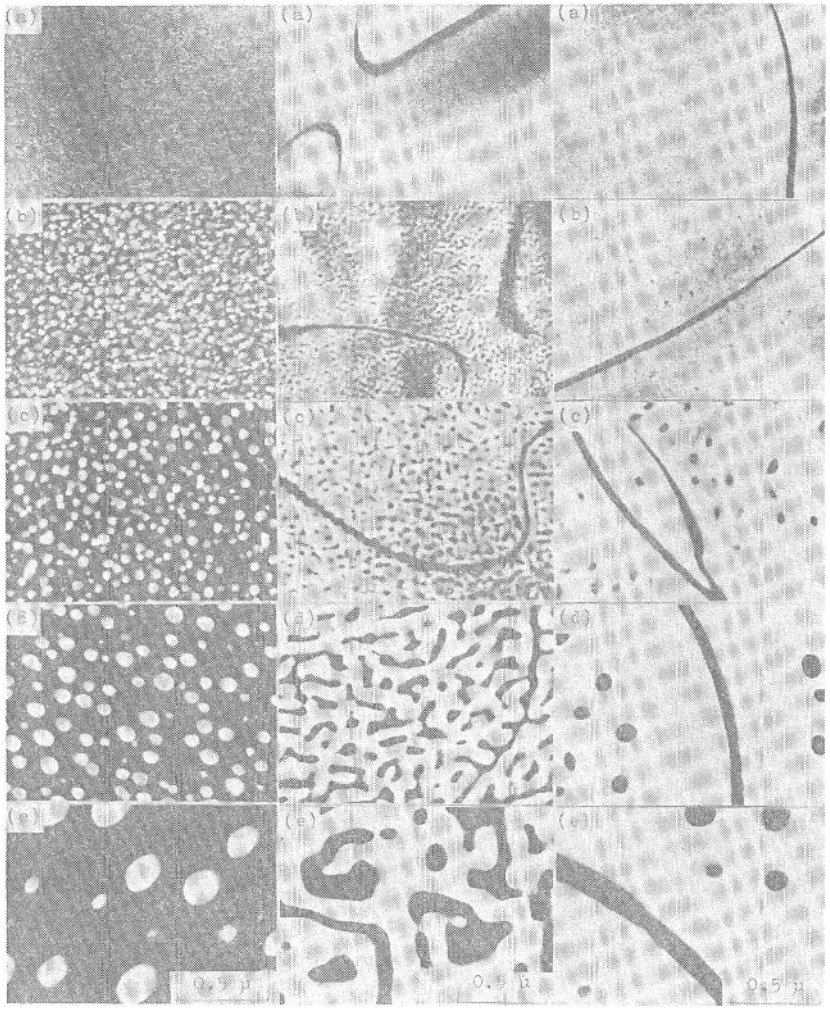

FIG. 3. Domain structures imaged with B_2 superlattice reflection in 23.0, 24.7 and 24.9 at% Al alloys, from left to right. The samples are quenched from 630°C and annealed at 570°C in the case of 23.0 and 24.7 at% Al alloys and at 568°C in the case of 24.9 at% Al alloy. (a) As quenched; (b) annealed for 15 min in 23.0 and 24.9 at% Al and for 10 min in 24.7 at% Al alloy; (c) 100 min; (d) 1000 min; (e) 10000 min. (From Oki *et al.*, 1977.)

a quench into an unstable region of the Fe–Al phase diagram. This shows the characteristic interconnectivity of phases which is often used as a mark of spinodal decomposition. The reaction following a quench into the region of instability starts with the appearance of a fine, uniformly dispersed precipitate. This shows the long wavelength instability mentioned above.

The interface between the phases is initially very diffuse, but sharpens with time. In the later stages of the reaction the pattern coarsens and surface energy effects become important, as in the late stage growth following nucleation events. Features qualitatively similar to those in Fig. 3 have also been observed in optical microscope studies of binary fluids. It is clear that these microscopic measurements yield interesting, detailed, dynamical information about the phase separation process. One can determine, for example, the distribution of droplet sizes as a function of time by this method. This droplet distribution function is obviously a quantity of fundamental interest and is discussed in sections VI, VII and IX of this article. It should be noted that the advent of high resolution electron microscopy has enormously advanced our understanding of nucleation phenomena in solids (Russell, 1980). However, light microscope studies of nucleation and growth in binary fluids have just recently begun, as we mention in Section X.

Before discussing small angle scattering methods we add a word of warning concerning the interpretation of the interesting morphological distinction between the droplet-like and interconnected structures shown in Fig. 3. Such a distinction was originally used in the literature to try to distinguish between metastable and unstable dynamical processes. Namely, it was originally assumed that the appearance of the interconnected structure meant that the decay of an unstable state was being observed. It was then noted, however, that a similar interconnected structure could be obtained from a superposition of many droplets, i.e. as a result of the nucleation and growth from a metastable state. Thus it has been pointed out by Hilliard (1970) and Herman and MacCrone (1971) that morphology alone cannot be used to determine unambiguously whether a process of phase decomposition begins by spinodal decomposition. An extensive discussion of this point is given by Jantzen and Herman (1978). For the purpose of this review article, however, the origin of the interconnected structure is not crucial. Whenever such a structure develops, it can be important, as for example in the case of binary fluids. In this situation unusual hydrodynamic effects can result (Sections V and XI). Whether this interconnectivity results from an "unstable" or a "metastable" quench is, from our point of view, less important, although in principle interesting.

The second experimental technique of relevance to us involves small angle scattering. A very good summary of the use of small angle scattering of X-rays and neutrons in first-order phase transitions has been given by Gerold and Kostorz (1978). When multiple scattering effects can be either neglected or corrected for, one obtains the structure function of the system from the measured intensity of scattered radiation. (When multiple scattering effects can be neglected, this intensity is proportional to the structure function.) This structure factor is a time-dependent, nonequilibrium cor-

relation function. For example, for binary alloys or binary fluids it is the Fourier transform of the nonequilibrium average (at a given time) of the product of the local concentrations at two different spatial positions in the system (Sections V and XI). This function is obviously of considerable experimental and theoretical interest and is discussed extensively throughout this article (Sections V, VII–IX and XI).

It is worth noting what one sees in typical scattering experiments following a quench of a system into an unstable region. For a binary fluid, for example, one observes the (almost) instantaneous appearance of a halo of scattered light. This ring subsequently brightens and collapses as phase separation proceeds (Sections V, IX and XI). The peak in the scattering intensity is used as a measure of a characteristic inverse length, such as a domain size, of the phase-separating system. A similar behavior in the intensity can also result from scattering due to a distribution of growing droplets, following their formation via nucleation, as we discuss in Sections VII and VIII.

Before turning to an outline of this review we first describe a typical nucleation experiment in a binary fluid, in order to introduce some useful concepts and notation. In such an experiment the system is undercooled by an amount δT, corresponding to an initial supersaturation δc_1 (as defined in Fig. 1). The metastable system is then observed for some finite period of time. If no significant nucleation occurs during this time, as measured say by a detectable attenuation of an incident laser beam, the system is undercooled further. Eventually, by repeating this procedure, the experimentalist can determine the location of the so-called cloud point, which is the maximum value of undercooling possible before significant nucleation occurs (on the time scale of the experiment), such that a dramatic attenuation in the intensity of the laser beam occurs. The system becomes cloudy in appearance due to the formation of a large number of detectable droplets. Nucleation theories (Sections II, IV and VII) predict the rate of formation of the droplets of the nucleating phase as a function of the undercooling or supersaturation. These theories predict a large increase in droplet formation in a very narrow region of undercooling (the cloud point), so that a comparison of theory and experiment is possible (Section X). It should be noted, however, that the cloud point is clearly a dynamical property of the system, rather than an intrinsic limit of metastability, since its determination involves the time scale of observation of the experiment. As we note in Section X, a more meaningful characterization of metastability is a so-called completion time, which is the time, say, that it takes the reaction (produced by nucleation) to go half-way toward completion. It should also be remarked that as long as the system remains truly metastable (i.e. does not decay), it is possible to perform experimental measurements of thermodynamic quantities such as the specific heat for

the metastable state. An interesting and fundamental question is how to describe from a statistical point of view these "equilibrium" properties of a metastable state. We give some discussion of this point in Sections II and IV when considering the problem of defining the analytic continuation of a stable state into the metastable phase. An interesting discussion of the equilibrium properties of a metastable state in terms of a constrained ensemble of states is given by Penrose and Lebowitz (1979). A complete description of metastability requires a discussion of dynamics and involves concepts such as nucleation rate (Sections II, IV, VII and X), completion time (Section X) and the nonlinear relaxation time (Section XIII).

The outline of this review is as follows. In Section II we summarize the classical Becker–Döring (1935) theory of nucleation. In addition to being a useful approximation in many applications of nucleation theory, this classical theory also introduces many of the basic concepts used in the more sophisticated theories which we discuss in Sections IV and VII. In Section III we discuss the semi-phenomenological equations of motion involved in the continuum theories of nucleation and spinodal decomposition. These models involve Fokker–Planck equations for the time-dependent probability distribution functional for a given system. An equivalent formulation can be given in terms of nonlinear Langevin equations for the semi-macroscopic dynamical variables of interest. In both the Fokker–Planck and Langevin equations a basic ingredient is a "coarse-grained" Helmholtz free energy functional. This is usually taken to be given by a Ginzburg–Landau form. We also summarize in Section III recent renormalization group calculations of this free energy functional for first-order phase transitions. In this case one must renormalize a double well potential. Such calculations show that there is no unique spinodal curve. Rather, its location depends on the coarse-graining size considered. In Section IV we discuss a field theoretic generalization of the classical nucleation theory due to Langer (1969). This seems to provide a first principles theory of nucleation for systems describable by continuum models. We illustrate this approach by summarizing a calculation of the nucleation rate for a binary fluid near its critical point. We also state the results for the essentially equivalent problem of a liquid–gas transition. Finally, we discuss a problem closely related to nucleation theory. This involves the determination of the analytic continuation of the free energy of a stable state to a metastable state. The free energy is predicted to have an essential singularity at any point on the coexistence curve, which, however, is so weak as to be experimentally unobservable.

In Section V we summarize various theories of spinodal decomposition for binary alloys. These include the linear theory of Cahn (1961) and a nonlinear theory of Langer, Bar-on and Miller (1975). We also note there the need for further theoretical work in this area, since no fully satisfactory

theory yet exists. In addition, we discuss interesting hydrodynamic effects on the spinodal decomposition and late stage coarsening in binary fluids. A particularly interesting effect arises from surface tension-driven flow in interconnected droplets, for quenches inside the percolation limit (Siggia, 1979). Our current theoretical understanding of such hydrodynamic effects is at best semi-quantitative. We also discuss power law approximations that have been used to analyze various dynamical quantities of experimental interest. We note that such approximations should be viewed with a certain degree of caution. In Section VI we discuss the late stage growth theory of Lifshitz and Slyozov (1961) and Wagner (1961), applicable to systems such as binary alloys and binary fluids in the limit of small "supersaturation". We also outline the late stage growth theory of Allen and Cahn (1979a, b) for systems in which the order parameter is not conserved. In addition, we mention other interesting work in this area of interface dynamics.

In Section VII we present a cluster dynamics theory of nucleation and growth due primarily to Binder, in collaboration with Stauffer, Müller-Krumbhaar and others. This theory is more microscopic than the continuum formulation and has led to several useful qualitative insights concerning the dynamics of first-order phase transitions which we summarize. These include a scaling theory of nucleation, theories of cluster growth and a qualitative theory of spinodal decomposition as a generalized nucleation phenomenon. We also contrast the current cluster picture of a gradual transition from the metastable to the unstable domain with the classical picture of Cahn and Hilliard (1958). In the latter theory the classical spinodal curve provides a sharp distinction between metastable and unstable states. We also describe in Section VII some of the difficulties involved in obtaining a quantitatively successful theory of cluster dynamics. In Section VIII we summarize various phenomenological theories for a dynamic scaling of the nonequilibrium structure factor, for systems such as binary alloys and binary fluids. We also discuss scaling theories for the somewhat simpler problem in which the order parameter is not conserved. This scaling behavior has been confirmed in experimental and computer simulation studies of several systems (Sections VIII, IX, XI and XII). These include cases in which the order parameter is conserved as well as cases in which it is nonconserved. It also appears likely that small deviations from the simple scaling behavior have been observed (Sections VIII, IX, XI and XII). Further theoretical investigation of this scaling is clearly necessary.

In Section IX we present the results of extensive computer simulation studies of an Ising model of a binary alloy by Lebowitz, Kalos and collaborators. These studies have led to many interesting results for the structure factor for this model. These include the observation of a gradual transition from the metastable to unstable domain, the invalidity of the linear theory for the observable time domain and a scaling behavior for the structure

function. We also discuss the results of the Monte Carlo studies of cluster growth in the Ising model, as well as various theoretical analyses of these results due to Penrose, Lebowitz and collaborators.

In Section X we discuss the results of several experimental studies of homogeneous nucleation in near-critical fluids. These careful investigations revealed an apparent breakdown of nucleation theory in the vicinity of a critical point. However, as we note in Section X, it now appears that this is not the case. Rather, the anomalously large undercoolings observed in these cloud point studies seem to be due to the effects of critical slowing down (Binder and Stauffer, 1976), although this is not a completely settled issue. Such a slowing down decreases the growth rate of the nucleating droplets and prevents their observation in conventional cloud point experiments. These experiments have served to remind us that metastability is intrinsically a dynamical problem. They have raised the interesting and difficult theoretical problem of describing simultaneously the nucleation and growth of droplets. We summarize in Section X the first detailed theoretical study of this problem (Langer and Schwartz, 1980) and compare this theory with the experimental studies of near-critical fluids. We also mention in this section a very interesting experiment by Krishnamurty and Goldburg (1980), who have attempted to study with a microscope the birth and growth of droplets near a binary fluid critical point. This work seems to provide the direction for future research in this field. We also note in Section X that the coupling between nucleation and growth means that no definitive test of homogeneous nucleation theory yet exists.

In Section XI we discuss a variety of experimental studies of spinodal decomposition. In particular we review recent neutron scattering studies of the alloy Al–Zn (Hennion *et al.* 1982; Guyot and Simon, 1982). These careful studies on single crystals have revealed features for the structure function which are very similar to those found in Monte Carlo studies of the Ising model (discussed in Section IX). Indeed, with a suitable rescaling of coordinates the experimental and Monte Carlo results are in close agreement. This agreement is to some extent surprising given differences between the Al–Zn and Ising model dynamics which we mention in Section XI. We also discuss very nice light scattering studies on near-critical binary fluids (e.g. Chou and Goldburg, 1981; Knobler and Wong, 1981). These studies show that the structure function for binary fluids satisfies a scaling behavior, although small deviations seem to occur (Knobler and Wong, 1981). These experiments also reveal the important effects of hydrodynamics mentioned earlier. In particular, Wong and Knobler (1981) have confirmed that the predictions of Siggia (1979) for the late stage growth rate are qualitatively correct. This experimental study also shows that a more quantitative theory of the effects of hydrodynamics on growth rates and the structure factor is necessary.

In Section XII we present theoretical, Monte Carlo and experimental results for the dynamics of systems quenched below a tricritical point. These include theoretical and experimental studies of ^{3}He–^{4}He mixtures. The latter experiments have revealed both a scaling behavior as well as interesting effects due to gravity. We also discuss results of theoretical and Monte Carlo studies of a simple relaxation model involving two order parameters. This model provides a simplified description of metamagnets, binary alloys and chemisorption, as we mention in Section XII. We also note various similarities and differences between the dynamical properties of critical and tricritical systems in this section.

Finally, in Section XIII, we discuss a variety of topics not treated in the main text. These include studies of a nonlinear relaxation function, a quantity which seems to provide an important theoretical tool for the study of first-order phase transitions. We also discuss very recent theoretical work on the dynamical behavior of systems under various quench conditions. These include a periodic variation in the temperature which can lead to periodic spinodal decomposition. Other novel effects are predicted under certain quench conditions. We also summarize theoretical and experimental studies of the dynamics of first-order phase transitions in several systems other than the prototype binary alloy and binary fluid systems discussed in the text. These include superfluids and superconductors, electron–hole condensation in semiconductors, physisorption and chemisorption systems, intercalation compounds, polymer blends, percolation, geological systems, pattern formation in chemical reactions, gels, optical instabilities and molecular dynamics. (The molecular dynamics section contains a summary of recent work on spinodal decomposition in a two-dimensional fluid, as well as crystal nucleation in supercooled liquids.) In our opinion one rich area for future research in first-order phase transitions lies in the direction of studying a wider range of physical systems. It would seem likely that one will encounter interesting new effects in nucleation and spinodal decomposition by such efforts, similar to the interesting differences found between binary alloys and binary fluids in recent studies.

We should also note some topics which we do not discuss in this article. First, it is impossible to review all of the (enormous) literature on homogeneous nucleation. We have restricted our attention primarily to nucleation in near-critical fluids, although the formal theories which we describe are not limited to this domain. Our reasons for this choice are the following. First, fluids are excellent systems in which to study homogeneous (rather than heterogeneous) nucleation. Second, far below the critical point fluids are reasonably well described by Becker–Döring-type theories. This is in part due to the limited accuracy of experimental data, so that more refined theories are not warranted. As well, for such fluids the attempt frequency (Sections II, IV and VII) is so large that nucleation is significant whenever

the activation energy barrier for the formation of droplets of a critical size is less than about $50k_BT$. For these high energy barriers the classical theory is a reasonable first approximation (Binder, 1980a). On the other hand, for fluids very near the critical point a much stricter test of nucleation theory is possible. The attempt frequency and activation energy are much smaller here. By changing the temperature one can vary the relevant time scale by several orders of magnitude (because of critical slowing down) so that an accurate test of theory is possible. Studies near the critical point have the additional advantages that the nucleating droplets are of macroscopic size and that nucleation takes place over times which are conveniently measurable. Considerable experimental data is now available in this domain (Section X). We should also note that solids do not provide as good a test of homogeneous nucleation theory as fluids. This is due to the fact that in most cases heterogeneous nucleation is more important. (Such nucleation occurs at dislocations, grain boundaries, etc.) As well, the theoretical analysis of nucleation in solids is more complicated, due to the need to take into account elastic and anisotropic effects when discussing the energy of formation of a droplet. Thus we do not discuss nucleation in solids here. An excellent recent review of this important subject has been given by Russell (1980), who discusses metals, semiconductors, glass and crystalline ceramics and minerals. Another significant topic which we do not treat concerns rigorous results about metastability. In view of the extreme difficulty involved in obtaining a first principles understanding of metastability, rigorous results are very helpful. However, this field has not developed as much as one would like. A very good review of existing work on this topic is that of Penrose and Lebowitz (1979). Discussions of other topics in homogeneous nucleation omitted here can be found in the texts of Abraham (1974a) and Skripov (1974). The text by Abraham also contains a summary of other important experimental tools for the study of homogeneous nucleation not mentioned in our article. These include the expansion and diffusion cloud chambers as well as the supersonic nozzle technique. Finally we note that some aspects of spinodal decomposition not covered here are treated in review articles by Metiu *et al.* (1979) and Skripov and Skripov (1979), as well as in several references given in Section XI.

II. Classical Theory of Nucleation

A. Classical droplet model

Modern nucleation theory is based on the "classical" theory for the rate of formation of nucleating droplets. This nucleation rate is derived in the

text by Frenkel (1946) who attributes its origin to Becker and Döring (1935) and Zeldovich (1943). Prior to this, important contributions were made by Gibbs (1906), Volmer and Weber (1926) and Farkas (1927). The work of Gibbs in particular involved a thermodynamic theory of curved surfaces which still provides a basic starting point for understanding droplet formation. Since the classical theory captures much of the essential physics of metastability, we review it briefly here. It should be pointed out, however, that although the subject of homogeneous nucleation is an old and rich field, fundamental questions still remain. As a practical illustration of this we note that the anomalous undercooling observed in near critical binary fluids (Section X) originally was interpreted as implying an error in nucleation theory of about 10^{20}. As we will see in Section X, a complete understanding of such binary fluids is still lacking.

We begin by first discussing the equilibrium properties of the classical droplet model which underlies the dynamical theory. This model provides a useful insight into the mechanism of decay of a metastable state. In addition, its free energy has a very weak, essential singularity at the condensation point which is present (in a somewhat altered form) in more sophisticated theories which we review later. Finally, this model serves as a convenient introduction to the field theory model discussed in Section IV.

This classical picture of condensation was put forth independently by Bijl (1938), Band (1939) and Frenkel (1939). It is particularly easy to describe for the Ising model of a ferromagnet (discussed in more detail in Section IX.A). Imagine an Ising lattice of N spins (each of which can either be up or down) in a small positive magnetic field H, at a temperature T sufficiently below the critical temperature T_c that almost all the spins are up. If one slowly changes H to negative values, it is possible to prepare this system in a metastable state, in which the average value of the magnetization remains positive. The problem is to explain how such a state eventually decays into a more stable state. The classical picture is that for positive H, the typical configurations of this ferromagnet consists of small droplets (clusters) of down spins dispersed in a background of up spins. Further, typical distances between these droplets are sufficiently large such that one can treat the system as a "gas" of noninteracting droplets. The number of clusters of size l (i.e. of l spins) is then given by the Boltzmann factor

$$n_l = N\,\mathrm{e}^{-\beta\varepsilon_l}, \tag{2.1}$$

where ε_l is a "free energy" of formation of a cluster and $\beta = 1/k_B T$. The crucial problem is then to determine ε_l. The classical assumption is that

$$\varepsilon_l = 2Hl + \sigma l^{(d-1)/d} \tag{2.2}$$

for a d-dimensional system. The bulk term is the energy required to flip l spins, while the surface term involves a "surface tension" σ. These droplets are assumed to be sufficiently compact that one has a "normal" surface to volume ratio, in contrast to "sea-weed-like" clusters, say. The condensation mechanism implicit in this model can then be seen from considering the behavior of n_l as a function of the droplet size l, as shown in Fig. 4. For positive H, n_l decreases rapidly as l increases, so that the clusters which determine the physical properties of the system are all microscopically small. On the other hand, if one considers the case with negative H, the situation is quite different. Then there is a competition between the bulk and surface terms, with the surface term dominating for small l and the bulk term dominating for large l. As a consequence, there is a critical size droplet l_c (with a critical radius R_c) such that droplets for which $l > l_c$ are energetically favored and grow. These droplets thus provide the nucleating mechanism by which the metastable state decays. This theory certainly captures the qualitative properties of nucleation correctly, but, as discussed in Section VII, it is in general not quantitatively accurate.

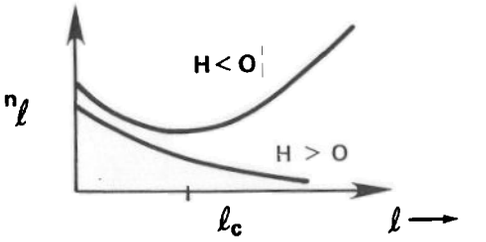

FIG. 4. The classical droplet distribution function n_l as a function of the droplet size l, for stable and metastable values of the magnetic field H.

Also implicit in this picture is a prediction that at a condensation point $H = 0$, $T < T_c$, the free energy has an essential singularity. This point has been discussed by several authors, notably Andreev (1964), Fisher (1967a) and Langer (1967). This singularity results from the droplet contribution to the free energy, $F(H)$, which is given (Langer, 1967) by

$$F(H) = N^{-1}\sum_{l=1}^{\infty} n_l(H), \tag{2.3}$$

and which, from (2.1), (2.2) and (2.3), can be written as a Mayer-like cluster expansion (Mayer and Mayer, 1940),

$$F(H) = \sum_{l=1}^{\infty} b_l z^l, \tag{2.4}$$

with

$$z = e^{-2\beta H}, \tag{2.5}$$

$$b_l = e^{-\beta\sigma l^{(d-1)/d}}. \tag{2.6}$$

The form (2.6) is a rather crude droplet model approximation for the Mayer cluster coefficients b_l. It is clear that one should identify the free energy of the metastable phase in this model as

$$\tilde{F}(H) \cong \frac{1}{N}\sum_{l=1}^{l_c} b_l z^l, \tag{2.7}$$

where the cut-off is the critical droplet size $l_c \propto R_c^d$, and where the critical size is given by

$$l_c = \left(\frac{(d-1)\sigma}{2d|H|}\right)^d. \tag{2.8}$$

This critical size follows from determining the minimum in $n_l(H)$ from (2.1) and (2.2). The remaining contribution of the droplets in (2.4) gives rise to an essential singularity in $F(H)$, as has been discussed thoroughly by Fisher (1967a) and Langer (1967). A simple version of this treatment which illuminates the role played by the critical droplet in the determination of the essential singularity has been given by Wallace (1980). If one converts the sum in (2.4) into an integral and replaces l by the droplet radius R, one obtains for the droplet free energy per unit volume

$$F(h) \propto \int_0^\infty dR\, e^{-(hR^d + R^{d-1})} \tag{2.9}$$

in appropriate dimensionless variables, where $h \propto H$. (In obtaining (2.9) Wallace neglects for simplicity the volume term R^{d-1}.) If one then expands (2.9) as a power series in h, it is easy to see that the radius of convergence of the resulting power series is zero. The free energy $F(h)$ is singular at $h = 0$, but the singularity is extremely weak, since one can show that all derivatives of F exist at $h = 0$. The nature of this singularity can be investigated by determining the analytic continuation of $F(h)$ from $h > 0$ through complex values of h to $h < 0$. This can be done by the standard method of steepest descent, choosing an appropriate contour in the complex R plane as shown in Fig. 5. This analytic continuation of $F(h)$ yields a complex free energy, which has a branch-point singularity at $h = 0$. The fact that $F(h)$ is complex is easily understood, since the analytic continuation of (2.9) in the complex h-plane from $h > 0$ to $h < 0$ requires that $\mathrm{Re}\, hR^d > 0$, in order that the integral in (2.9) converges at the upper limit. Thus to reach $\arg h = \pm\pi$, one must rotate the contour of integration in the R-plane in the opposite direction, through an angle $\arg R = \mp\pi/d$, as

in Fig. 5. Since this contour of integration lies in the complex R-plane for $h < 0$, it is not surprising that $F(h)$ is complex.

The imaginary part of $F(h)$ can be determined for small h from a saddle point located at R_c. The result is

$$\mathrm{Im}\, F(\arg h = \pm\pi) = \mp B|h|^b \exp\{-A|h|^{d-1}\}, \tag{2.10}$$

where $b = (d-3)/2$ and A and B are constants. It is noteworthy that the critical droplet is responsible for this imaginary part, in the sense that the saddle point is at R_c.

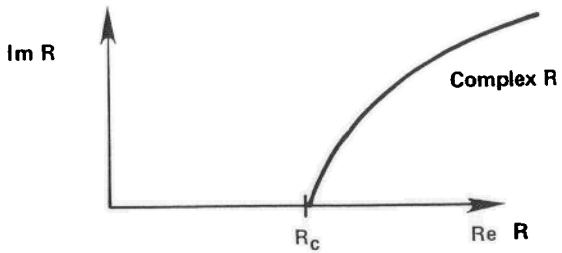

FIG. 5. Contour of integration for the steepest descent evaluation of the free energy for the simplified classical droplet model discussed in the text.

We conclude this section with two observations. The first is that more sophisticated theories also predict that the free energy is singular at such a condensation point (Sections IV and VII). However, the nature of this singularity is still a controversial subject, as we discuss in more detail later on. It is, however, of more mathematical than physical interest, since it would seem to be such a weak singularity as to be unobservable experimentally. The second remark is that subsequent generalizations of the classical droplet model have taken two quite different directions. The first approach attempts to improve this droplet model in a very detailed way, by giving a more precise definition of droplets and attempting to develop a more accurate statistical theory of their contribution to $F(H)$. We briefly summarize this approach in Section VII. The second approach attempts to avoid all the difficulties associated with developing a precise cluster theory. The resulting field theoretic model replaces the sum over droplets of all different sizes by a single length problem, which involves perturbation about the critical droplet size R_c. This approach is reviewed in Section IV. This theory gives a singularity similar to (2.10) but with a different value of the exponent b. In addition, there is a physical significance associated with the imaginary free energy in this model, as it is proportional to the nucleation rate. Finally, we note that it is easy to extend the above discussion to other systems. For example, for simple fluids the magnetic

field H is replaced by the chemical potential difference $\mu - \mu_c$, where μ_c is the condensation value of μ. The classical model thus can be used to describe such systems as simple fluids, binary fluids and binary alloys.

B. Becker–Döring theory

Since metastability is a dynamical problem, we now consider the kinetics of cluster formation, as formulated in particular by Becker and Döring (1935). This classical theory is presented in many texts, such as Frenkel (1946) and Abraham (1974a). We therefore only briefly discuss the basic ideas involved in this calculation of the nucleation rate. There is an extensive literature on cluster dynamics dealing with subsequent attempts to improve the Becker–Döring theory, which we will summarize in Sections VII and IX. Recent discussions of these attempts include Binder and Stauffer (1976), Mirold and Binder (1977), Penrose *et al.* (1978), Katz and Donohue (1979) and Penrose and Lebowitz (1979).

The starting point of the Becker–Döring theory is a kinetic equation for a time-dependent $n_l(t)$, where $n_l(t)$ is the average number of droplets of size l present at time t. The basic assumption of their theory is that the time evolution of $n_l(t)$ is only due to an evaporation–condensation mechanism, in which a droplet of size l gains or loses a single molecule. Therefore, effects such as the coagulation of two droplets are not considered, so that the equation of motion for $n_l(t)$ can be written as

$$\frac{\partial n_l(t)}{\partial t} = J_{l-1} - J_l, \qquad l \geq 2, \tag{2.11}$$

where

$$J_l = R_l n_l(t) - R'_{l+1} n_{l+1}(t) \tag{2.12}$$

is the rate per unit volume at which droplets of size l grow to droplets of size $l+1$. Equation (2.11) does not hold for single particle clusters, since such clusters are not constrained to events involving other one-particle clusters. Becker and Döring essentially assumed that n_1 remains constant, as we will do. An alternative treatment has been proposed by Penrose and Lebowitz (1979), who determine n_1 from the conservation of the total number of particles in the system.

Equation (2.12) expresses the assumption that the evaporation and condensation rates which determine J_l are proportional to the number of droplets present of sizes $l+1$ and l respectively, with corresponding proportionality coefficients R'_{l+1} and R_l. These kinetic coefficients are related via a detailed balance argument, which follows from requiring that the

equilibrium droplet distribution function n_l given by eqn (2.1) is a time-independent solution of (2.11). This yields

$$R_{l-1} e^{-\varepsilon_{l-1}/k_B T} = R'_l e^{-\varepsilon_l/k_B T}. \tag{2.13}$$

With this relation one can write (2.11) as

$$\frac{\partial n_l(t)}{\partial t} = -\frac{\partial J_l}{\partial l} = \frac{\partial}{\partial l}\left[\frac{R_l}{k_B T}\frac{\partial \varepsilon_l}{\partial l} n_l(t) + R_l \frac{\partial}{\partial l} n_l(t)\right], \tag{2.14}$$

treating l as a continuous variable. This is a Fokker–Planck equation with an l-dependent diffusion coefficient R_l. One can thus interpret the Becker–Döring theory as a stochastic process in l-space. The details of the kinetics are included in R_l, which we have yet to specify. The Becker–Döring assumption is that the rate at which molecules condense on a droplet of size l is proportional to its surface area, so that in three dimensions

$$R_l \propto l^{2/3}. \tag{2.15}$$

Other choices for R_l are possible, however, as will be discussed in connection with the Lifshitz–Slyozov theory in Section VII. It should be noted that the solution of (2.14) does not take into account the conservation of particles, since it is not important in nucleation events. (See Sections VII and X.)

The quantity J_l which occurs in (2.11) and (2.12) is just the current of the continuity equation (2.14). The value $J_l = 0$ corresponds to the equilibrium solution. Nucleation theory, on the other hand, is based on a nonequilibrium, steady state solution of (2.14), with $J_l = I =$ constant. The quantity I is called the nucleation rate and measures the rate of production of droplets (larger than the critical size) in the nonequilibrium steady state determined by a time-independent solution n_l^s of (2.14). The method which Becker and Döring used to obtain this solution involves the following choice of boundary conditions:

$$n_l^s \xrightarrow[l\to 0]{} n_1, \qquad n_l^s \xrightarrow[l\to\infty]{} 0. \tag{2.16}$$

This describes a steady state in which we have a source of droplets at $l = 0$. Furthermore, it assumes that once a cluster grows to a specified large size (greater than l_c), it is removed from the system. This choice of "source and sink" boundary conditions is also employed by Langer (1967) in this field theory formulation. The steady state solution of (2.14) which one obtains using (2.16) is

$$I = \left[\int_0^\infty (n_l R_l)^{-1}\, dl\right]^{-1}, \tag{2.17}$$

$$n_l^s = I \int_l^\infty \frac{1}{R_{l'}} \frac{n_l}{n_{l'}}\, dl'. \tag{2.18}$$

It is possibly useful to note that this steady state situation is completely analogous to the one considered when calculating the tunnelling of a Brownian particle across a potential barrier. The potential barrier in the nucleation problem is ε_l and has a maximum at the critical size l_c. We should also note that the steady state solution given here can be at best an approximate description of the real process of nucleation. For example, for a gas–liquid system the formation of liquid droplets produces a decrease of the initial supersaturation, δc, which implies that the chemical potential difference, $\delta\mu = \mu - \mu_c$ is a time-dependent quantity. This phenomenon is called the depletion effect and is not taken into account in this steady state solution, since $\delta\mu$ is kept fixed at its initial value. This shortcoming is also present in the field theoretical approach which we discuss in Section IV. The completion time theory discussed in Section X takes this depletion effect into account in an approximate way.

For the small fields (or small initial "supersaturations") which we consider here, ε_l has a sharp maximum at l_c, so that the integral in (2.17) can be evaluated by expanding the integrand around l_c. We then have

$$I = I_0 \, e^{-\varepsilon_{l_c}/k_B T}, \tag{2.19}$$

$$I_0 = CR_c \left(\frac{\varepsilon_{l_c}''}{2k_B T} \right)^{1/2} \tag{2.20}$$

where C is a constant and $\varepsilon_l'' = \partial^2 \varepsilon_l / \partial l^2$. This is the Becker–Döring result for the nucleation rate and describes a thermally activated process. The quantity ε_{l_c} is an activation energy (the energy of formation of the critical droplet) and I_0 is the so-called nucleation rate "prefactor". It should be noted that this nucleation rate depends very strongly on the exponential term. The implication of this for experimental measurements of cloud points is discussed in Section X.

We conclude this section by noting that it is beyond the scope of this article to discuss the extensive applications of this classical theory to the many areas involving homogeneous nucleation. There are many excellent reviews of such applications in the literature, including Pound (1972), Abraham (1974a) and Russell (1980). As mentioned in Section I, we will confine ourselves here to a discussion of nucleation in simple and binary fluids near the critical point, which we present in Section X. A scaling version of (2.19) will be given in Sections IV, VII and X, in a form appropriate for the critical region. We should also note that a controversial modification of the Becker–Döring theory proposed by Lothe and Pound (1962) has received considerable attention in the literature. A discussion of this work and additional references to it may be found in Abraham's book (1974a).

III. Field Theory Models

A. Semi-phenomenological equations of motion

We now turn to a field theoretic approach to the nonequilibrium dynamics of metastable states, which provides an alternative to the cluster dynamics theory of the preceding section. This continuum description will also be of use in developing a theory for spinodal decomposition, as we will discuss later. In this section we present the semi-phenomenological dynamical equations of motion which provide a starting point for a dynamical theory of metastable and unstable states. The rationale for these equations is similar to the situation in critical dynamics. Namely, one recognizes that it is hopeless to obtain a detailed microscopic theory at the level of solving the Liouville equations. Therefore one focuses attention on a small set of semi-macroscopic variables $\{\psi_i\}$, $i = 1, 2, \ldots, N$, whose dynamical evolution is "slow" compared to the remaining microscopic degrees of freedom. Dynamical equations of motion for the variables ψ_i are then obtained, either by phenomenological arguments or formal projection operator techniques (Zwanzig, 1961; Mori, 1965; Kawasaki, 1973; Ma and Mazenko, 1975). In these equations the remaining microscopic ("fast") variables enter only in the form of random forces. This phenomenological approach is particularly useful for the study of metastable and unstable states if the system of interest is in the immediate vicinity of its critical point, where it has a large correlation length and long time scales.

The choice of this set of variables is an important issue. Just as in critical dynamics one must choose the set $\{\psi_i\}$ with care, in order not to omit any essential physics nor introduce any unnecessary complexity into the theoretical description. The ultimate test of such a theory and its underlying assumptions is, of course, its ability to explain the experimentally observed dynamical phenomena. In general this set of slow variables includes the order parameter ψ and hydrodynamic variables, as we discuss below for several models.

In much of our illustrative discussion of the formal theory of metastability and spinodal decomposition we will use as a prototype a simple diffusion model of a binary alloy, with the order parameter ψ being the local concentration $c(\vec{r})$, of one of the two component species. The same model can be used in a simplified treatment of nucleation of a binary fluid, with an appropriate relabeling of variables.

The general dynamical model used in the continuum theory involves a Fokker–Planck equation for the probability distribution functional $\rho(\{\psi_i\}, t)$. This takes the form of a continuity equation in the space of

variables $\{\psi_i\}$, namely

$$\frac{\partial \rho}{\partial t} = -\sum_{i=1}^{N} \frac{\partial J_i}{\partial \psi_i}, \tag{3.1}$$

where the probability current J_i is given by

$$J_i = -\sum_{j=1}^{N} M_{ij}\left(\frac{\partial F}{\partial \psi_j}\rho + k_B T \frac{\partial \rho}{\partial \psi_j}\right).$$

We have used a condensed notation in the above in which a sum over i represents an integration over $\vec{r}$ and a sum over the semi-macroscopic variables. The quantity $F\{\psi_i\}$ is a so-called "coarse-grained" free energy functional (which we will discuss in more detail later). It contains a spatial integral over a free energy density. An essential feature of this free energy density is that below a critical point it has a double well structure. This double well describes the equilibrium situation in which two phases coexist. In the cases with which we will primarily concern outselves here, F is usually assumed to be given by a Ginzburg–Landau Hamiltonian for an appropriately chosen wavenumber cut-off Λ. The matrix M_{ij} in general consists of a symmetric and an antisymmetric part. The symmetric part corresponds to a set of generalized Onsager coefficients while the antisymmetric part corresponds to any nondissipative terms. As a specific example of this Fokker–Planck equation we consider a simple binary alloy in which the order parameter can be chosen to be the local concentration $c(\vec{r})$ of one of the two species of A and B atoms. Then (3.1) and (3.2) are given by

$$\frac{\partial \rho(\{c\}, t)}{\partial t} = -\int d\vec{r}\, \frac{\delta J}{\delta c(\vec{r})},$$

where

$$J(\vec{r}) = -M\nabla^2\left(\frac{\delta F}{\delta c(\vec{r})}\rho + k_B T \frac{\delta \rho}{\delta c(\vec{r})}\right), \tag{3.4}$$

where M is a mobility. (We have neglected here the possibility of M depending on c, in which case $M\nabla^2$ should be replaced by $\nabla \cdot M\nabla$.) The Fokker–Planck equations have been derived and discussed by a variety of authors. In particular Langer and coworkers have discussed them in the context of first-order phase transitions (Langer, 1967; Langer and Turski, 1973).

An equivalent formulation of the dynamical models can be given in terms of nonlinear Langevin equations for the variables ψ_i:

$$\frac{\partial \psi_i}{\partial t} = -\sum M_{ij}\frac{\partial F}{\partial \psi_j} + \zeta_i, \tag{3.5}$$

where ζ_i is a Langevin noise term (random force) which is taken to be Gaussian distributed. Its mean value and correlation are

$$\langle \zeta_i(\vec{r}, t)\rangle = 0 \tag{3.6}$$

and

$$\langle \zeta_i(\vec{r}, t)\, \zeta_j(\vec{r}\,', t')\rangle = 2k_B T \Gamma_{ij}\delta(\vec{r} - \vec{r}\,')\, \delta(t - t'), \tag{3.7}$$

where Γ_{ij} is the symmetric part of the matrix M_{ij} (generalized Onsager coefficients). We will now discuss several models of relevance to this article, which are particular examples of (3.5)–(3.7). Reviews of these models within the context of critical dynamics have been given by Kawasaki (1970, 1973), Hohenberg and Halperin (1977) and Gunton (1979). We will in general follow the model designation given in Hohenberg and Halperin (1977). Their article contains a comprehensive discussion of these phenomenological models and has an excellent summary of the applicability of these models to a variety of physical systems.

One of the systems which we will primarily consider in this article is a simple binary alloy consisting of two atomic species A and B. (Its magnetic analog is an Ising ferromagnet.) Below its critical point such an alloy phase separates into an A-rich and an A-poor phase. The dynamical model for this system is taken to be

$$\frac{\partial c(\vec{r}, t)}{\partial t} = -\nabla \cdot \vec{j}(\vec{r}, t) + \zeta(\vec{r}, t), \tag{3.8}$$

where as noted above the order parameter $\psi = c(\vec{r}, t)$ denotes the local concentration of one of the species. The interdiffusion current $\vec{j}(\vec{r})$ is

$$\vec{j}(\vec{r}) = -M\nabla \frac{\delta F}{\delta c(\vec{r})}, \tag{3.9}$$

where M is a mobility. The local chemical potential is

$$\mu(\vec{r}) = \frac{\delta F}{\delta c(\vec{r})} \tag{3.10}$$

so that (3.8)–(3.9) describe a diffusion process. The Ginzburg–Landau free energy functional $F\{c\}$ is

$$F\{c\} = \int d\vec{r}\,\{\tfrac{1}{2}K|\nabla c|^2 + f(c)\}, \tag{3.11}$$

where it is assumed that $c(\vec{r})$ contains only spatial variation with wavevector smaller than some cut-off Λ. The usual "c^4" approximation for $f(c)$ is

$$f(c) = -\frac{1}{2}rc^2 + \frac{u}{4}c^4, \tag{3.12}$$

where $r > 0$ for $T < T_c$. Thus, below the critical point, $f(c)$ has the double well structure mentioned earlier. The same free energy functional F was introduced independently by Cahn and Hilliard (1958, 1959) in a study of metastable states. (They discussed the droplet profile, activation energy and surface tension, as we briefly summarize in Section VII.G.) The noise term ζ satisfies (3.6) and (3.7), the latter taking the form

$$\langle \zeta(\vec{r}, t)\, \zeta(\vec{r}\,', t')\rangle = -2k_B T M \nabla^2 \delta(\vec{r} - \vec{r}\,')\, \delta(t - t'). \tag{3.13}$$

The physical source of this noise term ζ is assumed to be the phonon modes of the alloy, whose time scale is much smaller than the slow diffusive process of interest here. The equations (3.8), (3.9) and (3.11) yield the explicit nonlinear diffusion equation

$$\frac{\partial c}{\partial t} = M\nabla^2\left\{-K\nabla^2 c + \frac{\partial f}{\partial c}\right\} + \zeta. \tag{3.14}$$

With (3.12) this becomes

$$\frac{\partial c}{\partial t} = M\nabla^2\{(-K\nabla^2 - r)c + uc^3\} + \zeta. \tag{3.15}$$

This model is known as model B in critical dynamics (Hohenberg and Halperin, 1977). It is the continuum analog of a kinetic Ising model in which neighboring A and B atoms are allowed to exchange lattice site positions with some specified transition probability (Kawasaki, 1972). The dynamical properties of this lattice model have been studied in cluster dynamics theories of nucleation and spinodal decomposition (Section VII) and in computer simulation studies (Section IX).

A closely related model is model A, in which the order parameter ψ is not conserved (in contrast to model B). Its equation of motion is thus given by the analog of (3.14) or (3.15), i.e.

$$\frac{\partial \psi(\vec{r})}{\partial t} = -M\left\{-K\nabla^2 + \frac{\partial f(\psi)}{\partial \psi}\right\} + \zeta(\vec{r}) \tag{3.16}$$

or

$$\frac{\partial \psi(\vec{r})}{\partial t} = -M\{(-K\nabla^2 - r)\psi + u\psi^3\} + \zeta(\vec{r}) \tag{3.17}$$

with the Gaussian noise $\zeta(\vec{r})$ satisfying (3.6) and (3.13), with $-M\nabla^2 \to M$. Model B is the continuum analog of a kinetic Ising model in which a single "spin" at a lattice site is allowed to flip with some specified transition probability (Glauber, 1963). We will discuss various nucleation and domain growth properties of model A in Sections VI, VII and XIII. This model is thought to describe the critical dynamics of various alloys, such as Fe_3Al, Ni_3Mn and CuZn (β-brass), which undergo an order–disorder transition. The equilibrium properties of such alloys can be described in terms of an antiferromagnetic Ising model (It should be noted that models A and B are often called time-dependent Ginzburg–Landau (TDGL) models.)

Another model of interest involves the coupling of two dynamical variables, a nonconserved order parameter ψ and a locally conserved variable c. This is model C, whose equations of motion are

$$\frac{\partial \psi}{\partial t} = -\Gamma_\psi \frac{\delta F}{\delta \psi} + \zeta_\psi, \tag{3.18}$$

$$\frac{\partial c}{\partial t} = \Gamma_c \nabla^2 \frac{\delta F}{\delta c} + \zeta_c, \tag{3.19}$$

with

$$F = \int d\vec{r}\left\{\frac{1}{2}K|\nabla\psi|^2 - \frac{1}{2}r|\psi|^2 + \frac{u}{4}|\psi|^4 + \frac{v}{6}|\psi|^6 + \frac{\beta}{2}|\nabla c|^2 + \frac{\chi_n^{-1}}{2}c^2 - \Delta c + \gamma c|\psi|^2\right\}. \tag{3.20}$$

(We have included a gradient term in c and a ψ^6 term which are neglected in the Hohenberg–Halperin (1977) definition. It should also be noted that ψ is real for model C. However, the same free energy appears later on, in (3.30), but in the latter case ψ is complex.) The noise terms ζ_ψ and ζ_c satisfy (3.6) and the relations

$$\langle \zeta_\psi(\vec{r}, t)\zeta_\psi(\vec{r}\,', t')\rangle = 2k_B T \Gamma_\psi \delta(\vec{r} - \vec{r}\,')\delta(t - t'), \tag{3.21}$$

$$\langle \zeta_c(\vec{r}, t)\zeta_c(\vec{r}\,', t')\rangle = -2k_B T \Gamma_c \nabla^2 \delta(\vec{r} - \vec{r}\,')\delta(t - t'). \tag{3.22}$$

The cross-correlation functions are zero. The free energy functional in (3.20) was proposed by Halperin, Hohenberg and Ma (1974) for their models C and D. It has also been derived for metamagnets by Nelson and Fisher (1975). (The physical significance of various coefficients in (3.20) is discussed in both these papers.) In the latter case ψ represents the local staggered (or sublattice) magnetization and c the local magnetization. A discussion of nucleation and spinodal decomposition below this metamagnet *tricritical* point, which is based on (3.18)–(3.22), is reviewed in Section XII. The results of a computer simulation study of a two-dimensional meta-

magnet with Kawasaki spin exchange (which is a lattice analog of model C) is also given in Section XII. Various other applications of model C, as well as an analysis of its critical and tricritical behavior, are discussed by Siggia and Nelson (1977) and Hohenberg and Halperin (1977).

Models A, B and C are purely relaxational models. (The antisymmetric part of M_{ij} in (3.2) is zero for these models.) For many interesting phase transitions, however, such as the gas–liquid and binary fluid critical point transitions and the ^{3}He–^{4}He tricritical and λ-line transitions, hydrodynamic modes occur in the equations of motion. For a pure fluid it is well known that there are four hydrodynamic modes (Landau and Lifshitz, 1959). These include two viscous modes and a thermal diffusion mode, as well as a sound wave. However, sufficiently near the critical point and for frequencies small compared to ck and $c\xi^{-1}$ (where c is the sound velocity and ξ is the correlation length) one can ignore the sound waves (whose frequencies are much higher than the diffusive modes for $k \sim \xi^{-1}$). Thus a model H has been proposed to describe the critical dynamics of fluids, whose equations are

$$\frac{\partial \psi}{\partial t} = \lambda_0 \nabla^2 \frac{\delta F}{\delta \psi} - g_0 \nabla \psi \cdot \frac{\delta F}{\delta \vec{j}} + \zeta_\psi, \tag{3.23}$$

$$\frac{\partial \vec{j}}{\partial t} = \boldsymbol{T} \cdot \left[\eta_0 \nabla^2 \frac{\delta F}{\delta \vec{j}} + g_0 (\nabla \psi) \frac{\delta F}{\delta \psi} + \vec{\zeta} \right], \tag{3.24}$$

$$F = F_0 - \int \mathrm{d}\vec{r} \{ h(\vec{r}, t)\, \psi + \vec{A}(r, t) \cdot \vec{j} \}, \tag{3.25}$$

$$F_0 = \int \mathrm{d}\vec{r} \{ \tfrac{1}{2} K |\nabla \psi|^2 - \tfrac{1}{2} r \psi^2 + \frac{u}{4} \psi^4 + \tfrac{1}{2} \vec{j}^{\,2} \}. \tag{3.26}$$

These are the Hohenberg–Halperin (1977) equations for model H, as developed by Kawasaki (1970), Halperin *et al.* (1974) and Siggia *et al.* (1976). The various quantities involved are the transverse part, $\vec{j}$, of the momentum density, a thermal conductivity λ_0 and shear viscosity η_0, a coupling constant g_0 and infinitesimal applied fields h and $\vec{A}$. The operator $\boldsymbol{T}$ projects out the transverse part of the vector on which it operates ($T_{\alpha\beta} = \delta_{\alpha\beta} - k_\alpha k_\beta / k^2$). The noise terms ζ_ψ and $\vec{\zeta}$ satisfy the appropriate fluctuation–dissipation analogs of (3.6) and (3.7). Finally, the order parameter ψ in (3.23) is a certain linear combination of the local energy and mass densities (Hohenberg and Halperin, 1977). Nucleation theories for pure fluids have been developed which are based on versions of model H, as we discuss in Section IV.

It is well known that model H also describes the critical dynamics of binary fluids. This is not immediately obvious, since a binary fluid has six conserved dynamical variables, its energy density, two mass densities (for

the A and B constituents respectively) and the three components of the momentum density $\vec{j}$. There are five hydrodynamic modes (Landau and Lifshitz, 1959), four of which are diffusive. These consist of a thermal diffusion mode, a concentration diffusion mode and viscous relaxation modes for the two transverse components of $\vec{j}$. The fifth mode is a propagating sound mode. As has been shown by a variety of authors (see Hohenberg and Halperin, 1977) the binary fluid belongs to the same dynamic universality class as pure fluids. Thus with an appropriate identification of variables, model H can be used to describe binary fluids. Theories of nucleation and spinodal decomposition in binary fluids have been given, based on simplified versions of model H, as we review in Sections IV, V and X. However, it should be noted that no first principles, nonlinear theory of spinodal decomposition has been developed for model H itself, due to the complexity of the equations of motion.

A final model which we will discuss in this review describes ^{3}He–^{4}He mixtures (Siggia and Nelson, 1977). The equations of motion are given by

$$\frac{\partial \psi}{\partial t} = -2\Gamma_0 \frac{\delta W}{\partial \psi^*} - i g_1 \psi \frac{\delta W}{\delta q} - i g_2 \psi \frac{\delta W}{\delta c} + \zeta_\psi, \tag{3.27}$$

$$\frac{\partial c}{\partial t} = \lambda_0 \nabla^2 \frac{\delta W}{\delta c} + L_0 \nabla^2 \frac{\delta W}{\delta q} + 2 g_2 \operatorname{Im}\left(\psi^* \frac{\delta W}{\delta \psi^*} \right) + \zeta_c, \tag{3.28}$$

$$\frac{\partial q}{\partial t} = K_0 \nabla^2 \frac{\delta W}{\delta q} + L_0 \nabla^2 \frac{\delta W}{\delta c} + 2 g_1 \operatorname{Im}\left(\psi^* \frac{\delta W}{\delta \psi^*} \right) + \zeta_q, \tag{3.29}$$

where

$$W = F + \tfrac{1}{2} \int \mathrm{d}\vec{r}\, C^{-1} q^2 \tag{3.30}$$

with F defined by (3.20). (This choice of W includes as term Δc not included in the original Siggia and Nelson (1977) model, but introduced by Hohenberg and Nelson (1979).) The noise terms have correlations given by

$$\langle \zeta_\psi(\vec{r}, t)\, \zeta_{\psi^*}(\vec{r}\,', t') \rangle = 4\, \mathrm{Re}\, \Gamma_0 \delta(\vec{r} - \vec{r}\,') \delta(t - t'), \tag{3.31}$$

$$\langle \zeta_c(\vec{r}, t)\, \zeta_c(\vec{r}\,', t') \rangle = -2\lambda_0 \nabla^2 \delta(\vec{r} - \vec{r}\,') \delta(t - t'), \tag{3.32}$$

$$\langle \zeta_q(\vec{r}, t)\, \zeta_q(\vec{r}\,', t') \rangle = -2K_0 \nabla^2 \delta(\vec{r} - \vec{r}\,') \delta(t - t'), \tag{3.33}$$

$$\langle \zeta_c(\vec{r}, t)\, \zeta_q(\vec{r}\,', t') \rangle = -2L_0 \nabla^2 \delta(\vec{r} - \vec{r}\,') \delta(t - t'), \tag{3.34}$$

with all other cross-correlations equal to zero. The superfluid order parameter ψ is complex, with an amplitude $|\psi|$ and phase θ. The variables c and q are the local concentration of ^{3}He and the "entropy" respectively. An interesting feature of superfluid ^{3}He–^{4}He mixtures is the existence of a second sound mode not present in normal binary fluid mixtures. The physical significance of the various kinetic coefficients Γ_0, K_0, L_0, λ_0 as

well as coupling constants g_1 and g_2 are discussed by Siggia and Nelson (1977) and Hohenberg and Nelson (1979). We will summarize a linearized theory of spinodal decomposition ^{3}He–^{4}He (quenched below its tricritical point) in Section XII. As well, we discuss some aspects of a nucleation theory for this system in the same section.

Finally, we should note that all the dynamical coefficients which have been introduced in the models discussed here (i.e. the matrix M_{ij} in (3.2) or the various coefficients corresponding to its symmetric part Γ_{ij} in (3.7)) are so-called "bare" coefficients. Their values depend on the particular cut-off Λ implicit in the equations of motion. Namely, spatial variations in the order parameter only include Fourier components for which the magnitude of the wavevector $\vec{k}$ is less than Λ. These bare coefficients are finite at a critical point. However, when one renormalizes these equations of motion by including fluctuations on a length scale of the order of the correlation length ξ, the renormalized coefficients usually become singular at the critical point (some vanish at T_c for the relaxational models while others diverge at T_c for models with hydrodynamic modes (Hohenberg and Halperin, 1977). It should be noted that in the theories of nucleation and spinodal decomposition which we review in this article it is the physically meaningful, renormalized coefficients which occur in the final results.

Since some of our discussion of first-order phase transitions involves studies near a critical point, we summarize in Table I some of the standard critical exponent notation used in this article. (It should be noted in Table I that for $T > T_c$ similar exponents can be defined, but without primes. Scaling theories assume that the corresponding exponents for $T \gtrless T_c$ are

TABLE I. Notation for critical exponents. $\langle\psi\rangle$ denotes the order parameter, H its conjugate field and $\varepsilon = (T_c/T - 1) \geq 0$. For simplicity, we consider only "Ising-like" systems, for $T \leq T_c$.

		Conditions		
Exponent	Definition	H	$\langle\psi\rangle$	Quantity
α'	$C_H \sim \varepsilon^{-\alpha'}$	0	0	Specific heat at constant field
β	$\langle\psi\rangle \sim \varepsilon^{\beta}$	0	$\neq 0$	Coexistence curve value of $\langle\psi\rangle$
γ'	$\chi_T \sim \varepsilon^{-\gamma'}$	0	$\neq 0$	Zero field isothermal susceptibility
δ	$H \sim \lvert\langle\psi\rangle\rvert^{\delta}\,\mathrm{sign}(\langle\psi\rangle)$	$\neq 0$	$\neq 0$	Critical isotherm
ν'	$\xi \sim \varepsilon^{-\nu'}$	0	$\neq 0$	Correlation length
z	$\tau \sim (\varepsilon^{-\nu'})^{z}$	0	$\neq 0$	Characteristic time constant

equal.) Detailed reviews of critical phenomena are given in the texts by Stanley (1971), Pfeuty and Toulouse (1975) and Ma (1976).

B. Coarse-grained free energy functional

At this point we discuss in more detail the coarse-graining procedure involved in obtaining the free energy functional F for the continuum models defined by (3.1) and (3.2) or (3.5)–(3.7). For simplicity we will restrict our attention to a simple binary alloy, such as model B, whose free energy functional given by (3.11) and (3.12) contains the essential features common to most systems of interest. We consider a microscopic model of a binary alloy in which a given site i of the lattice can be occupied by either an A or a B atom. Such a model can be described in Ising-like language, where one introduces a variable $c_i = \pm 1$ to specify that the site is occupied by an A or B atom respectively. (A more complete discussion of such a model is given in Section IX.A, using a slightly different notation in which $c_i \to \sigma_i$.) A microscopic state of this model is then given by some specific configuration $\{c_i\}$, with a corresponding Hamiltonian $H\{c_i\}$. The appropriate Boltzmann factor for finding such a state is, of course,

$$P\{c_i\} = e^{-\beta H\{c_i\}}/Z, \tag{3.35}$$

where Z is the partition function

$$Z = \sum_{\{c_i\}} e^{-\beta H\{c_i\}}. \tag{3.36}$$

A coarse graining of this system can be carried out by dividing the original lattice into hypercubical cells, of edge size L. One then introduces an average concentration variable c_α for the αth cell,

$$c_\alpha = L^{-1} \sum_{i \in \alpha\text{th cell}} c_i \tag{3.37}$$

and defines a coarse-grained Helmholtz free energy functional $F\{c_\alpha\}$

$$e^{-\beta F\{c_\alpha\}} \equiv \sum_{\{c_i\}}{}' e^{-\beta H\{c_i\}}. \tag{3.38}$$

The prime in (3.38) denotes that the sum is over all microscopic configurations $\{c_i\}$ consistent with the constraint that the cell configuration is specified by $\{c_\alpha\}$, with a specified average concentration c_0. One seldom explicitly calculates the partial trace in (3.38). Rather, one assumes that the result is given by a lattice version of the Ginzburg–Landau free energy functional, i.e.

$$F\{c_\alpha\} = \sum_\alpha f(c_\alpha) + \sum_{\langle\alpha\beta\rangle} \tfrac{1}{2} K_L (c_\alpha - c_\beta)^2 + \ldots \tag{3.39}$$

with the free energy density $f(c_\alpha)$ approximated by

$$f(c_\alpha) = -\tfrac{1}{2}r_L c_\alpha^2 + \tfrac{1}{4}u_L c_\alpha^4 + \ldots . \tag{3.40}$$

The sum $\langle\alpha\beta\rangle$ in (3.39) is over nearest neighbor cells. The coupling constants $(r_L, u_L, K_L, \ldots)$ depend on the initial choice of cell size L. For such an expansion to be valid, with the coupling constants depending on temperature in a nonsingular way, it is necessary that $L \ll \xi$, where ξ is the correlation length. Sufficiently near T_c, where ξ becomes arbitrarily large, one can choose $L \gg a_0$ (where a_0 is the lattice spacing). One can then replace (3.39) by a continuum approximation in which $F\{c_\alpha\} \to F\{c\}$, given by (3.11) and (3.12). In eqns (3.11) and (3.12) only Fourier components $\{c_{\vec{k}}\}$ of $c(r)$ with $|\vec{k}| < \Lambda$ are included, where Λ is a cut-off analogous to L^{-1}.

The above coarse-graining procedure is well known and is the starting point for various renormalization group calculations (Wilson and Kogut, 1974; Binder, 1981b). The interesting point for first-order phase transitions is that below T_c the free energy density f, given by (3.12) or (3.40), is a double well potential, as shown in Fig. 6. Furthermore, the *shape* of this

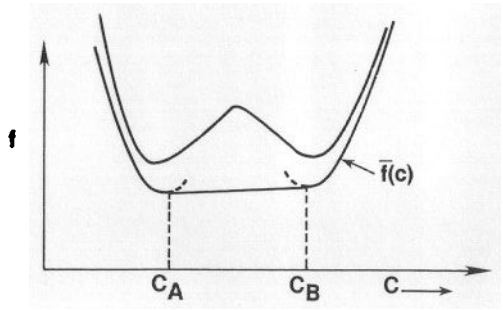

FIG. 6. The coarse-grained free energy $f(c)$. The function $\bar{f}$ is the corresponding equilibrium function in the limit of an infinite coarse-graining size.

double well potential and in particular the location of its spinodal points (where $\partial^2 f/\partial c^2 = 0$) depends on the (arbitrary) choice of cut-off (L^{-1} or Λ) which one chooses. We will discuss the implications of this latter point in Section III.C.

Before doing so, we note two important points with respect to this coarse-graining procedure. The first is that if one performs the remaining partial trace over the $\{c_\alpha\}$ in (3.38) (or the analogous functional integral over the functions $c(\vec{r})$ using (3.11)), one will obtain the equilibrium free energy density $\bar{f}(c_0)$, where c_0 is the average concentration of one of the components of the binary mixture. Namely,

$$\bar{f}(c_0) = -k_B T \lim_{V\to\infty} V^{-1} \ln \int \delta c \, e^{-F\{c\}/k_B T}, \tag{3.41}$$

where the integral denotes the functional integral over the space of functions $\{c(\vec{r})\}$, subject to the constraint

$$c_0 = V^{-1} \int c(\vec{r}) \, d\vec{r}, \tag{3.42}$$

with $F\{c\}$ given by (3.11). The resulting free energy density $\bar{f}(c_0)$ is a convex function of the concentration, in contrast to $f(c)$, as shown schematically in Fig. 6. The corresponding chemical potentials for $f(c)$ and $\bar{f}(c)$ are shown in Fig. 7. Since $\bar{f}(c)$ is simply a straight line between the equilibrium concentration values c_A and c_B, it clearly contains no useful information about metastable and unstable states. On the other hand, one can define the analytic continuation of the equilibrium free energy density $\bar{f}(c_0)$ of

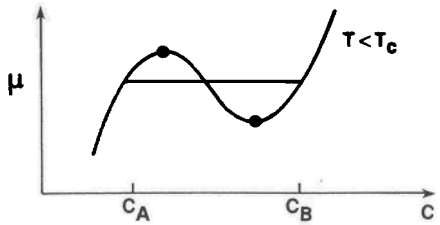

FIG. 7. The chemical potentials $\mu(c)$ and $\bar{\mu}(c)$ corresponding to the coarse-grained free energy $f(c)$ and equilibrium free energy $\bar{f}(c)$ respectively.

the stable state into the metastable state. This has been discussed in Section II within the context of a classical droplet model. We discuss a much better field theoretical derivation of this analytic continuation in Sections IV.B and IV.E. The interpretation of this is that the real part of the analytic continuation of $\bar{f}(c_0)$ (shown as the dotted lines in Fig. 6) describes the *equilibrium* properties of the metastable state (Section IV). On the other hand, the coarse-grained free energy function, $f(c)$, defined by (3.12), say, is crucial for understanding the *nonequilibrium* properties of metastable and unstable states as described by equations of motion such as (3.14) or (3.15). Thus there are two quite different free energies, the coarse-grained $f(c)$ and the analytic continuation of the equilibrium free energy $\bar{f}(c)$, which arise in describing metastable states. This important point has been made most explicitly by Langer (1974).

Finally, we discuss a major issue concerning the coarse-grained free energy functional. Namely, what is an appropriate choice for the cut-off Λ implicit in the equations (3.11) and (3.12) (or more generally in the appropriate free energy functional for any one of the phenomenological

models of interest). This choice is determined by the fact that one is interested in describing the dynamics of these phase separation processes on a length scale of the bulk correlation length ξ, at the temperature $T < T_c$ to which a given system is quenched. Therefore, one chooses this cut-off to be $\Lambda^{-1} = \alpha\xi$, where ξ is the equilibrium correlation length at the temperature $T < T_c$ and α is a number of order unity. The rationale for this choice is the following: first, the cut-off Λ^{-1} must be large enough that the continuum approximation makes sense, i.e. $\Lambda^{-1} \gg a_0$, where a_0 is the lattice constant. Second, it cannot be much larger than the correlation length ξ because then the cell could contain two phases and one would have lost the details of the phase separation which one is interested in describing. Another practical reason for choosing $\Lambda^{-1} = \alpha\xi$ is that one has included all the critical fluctuations in the partial sum involved in (3.38). Thus one would expect that in the dynamical theory to be described later various quantities can be reasonably well approximated by their thermodynamic values.

C. Renormalization group theory

Since the determination of the free energy functional for a coarse-graining size of the order of ξ is important for a dynamical description of a given system, we summarize here existing work on this subject. The first attempts were quite phenomenological. They involved determining relevant parameters in (3.11) from extrapolations of measured thermodynamic quantities (Rundman and Hilliard, 1967; de Fontaine, 1967). Later, in a theory of spinodal decomposition discussed in Section V, Langer *et al.* (1975) assumed that near the critical point $f(c)$ was given by a scaled version of (3.12), for a coarse-graining size $\Lambda^{-1} = \alpha\xi$ (with a specified value of α). Only one system-dependent parameter, f_0, entered their approximation for f. Its value was determined from known critical exponents and critical amplitudes of the three-dimensional Ising model.

Subsequent to these phenomenological approaches it was noted that the evaluation of a free energy functional such as $F\{c\}$ in (3.11) (or its lattice analog (3.38)) for different coarse-graining sizes is an example of a renormalization group calculation. In contrast to the usual applications of the renormalization group (Wilson and Kogut, 1974), however, one must consider double well potentials, such as is shown in Fig. 7. The first renormalization group calculation of the coarse-grained Helmholtz free energy functional (3.11) was carried out by Kawasaki *et al.* (1981). Their starting point was the usual Ginzburg–Landau free energy functional ((3.11) and (3.12)) with "bare" coupling constants r and u and an initial cut-off Λ_0. (That is, the original functional only includes Fourier components of

the order parameter $\{c_{\vec{k}}; |\vec{k}| < \Lambda_0\}$.) A renormalized free energy functional with a new $\Lambda_l = \Lambda_0 e^{-l}$, where e^{-l} is the length rescaling parameter, was then computed to first order in $\varepsilon = 4 - d$, using differential renormalization group equations formulated by Nicoll *et al.* (1976). As one would expect, the shape of the double well potential $f(c)$ changes as l varies. (This is due to coupling constants such as r and u becoming l-dependent.) In particular, the spinodal curve (the locus of points for which $\partial^2 f/\partial c^2 = 0$) is l-dependent. That is, there is not a unique spinodal curve, but rather a family of such curves, specified by the coarse-graining size $\Lambda_0^{-1}e^l$. The free energy functional at the coarse-graining size proportional to ξ was compared with the phenomenological form used by Langer *et al.* (1975). It differed from their approximate form by additional higher order terms in the fourth-order polynomial (3.12). (This is to be expected.) In addition, the value of the parameter f_0 obtained in the first-order calculation was significantly less than that of Langer *et al.*, but this could be at least in part due to the limitations of a first-order calculation for $\varepsilon \geq 1$.

It should be noted that the renormalization group result that the spinodal curve is dependent on the coarse-graining size had been implicit in an earlier cluster theory result of Kikuchi (1967). It is also consistent with predictions by Langer (1974) and Binder *et al.* (1978) that the dynamical transition between nucleation and spinodal decomposition mechanisms is intrinsically smooth; that is, no sharp spinodal line exists in the dynamical theory.

An alternative Monte Carlo "renormalization group" method has recently been developed by Binder (1981b) which promises to be very useful in determining a coarse-grained free energy functional from microscopic models of binary alloys, binary fluids and other systems of interest. In this approach, a real space "renormalization group" method is implemented by Monte Carlo simulation techniques. One can directly compute various reduced distribution functionals in the two-phase region, as a function of cell size. For example, one can compute the joint distribution functional $\rho_L(c_\alpha, c_\beta)$ for finding cells α and β with concentrations c_α and c_β respectively, for a given cell size L (using the notation of (3.37)). One can then parametrize this distribution functional by a Ginzburg–Landau-type approximation and obtain the coupling constants analogous to K_L, r_L and u_L in (3.39) and (3.40) as a function of cell size. Preliminary results (Kaski *et al.*, 1983) of such a study of the three-dimensional Ising model of a binary alloy (Section IX) are shown in Fig. 8, where the coarse-grained "spinodal curve" for different choices of cell size are shown.

Finally, we note that in principle one should renormalize the dynamical equations of motion, such as (3.3) or (3.14), rather than just the free energy functional. An approximate renormalization has been carried out by Horner and Jüngling (1979) to first order in $\varepsilon = 4 - d$, for models A

and B. Renormalized Fokker–Planck equations (such as (3.3) and (3.4)) are obtained for a new field variable (which is a type of coarse-grained order parameter), by a formulation in terms of path integrals. Although this approach appears to be quite interesting, the authors used a simple factorization scheme to solve the resulting approximate renormalized equations. This factorization yields some qualitatively correct features of the dynamics of phase separation, but is quantitatively inaccurate.

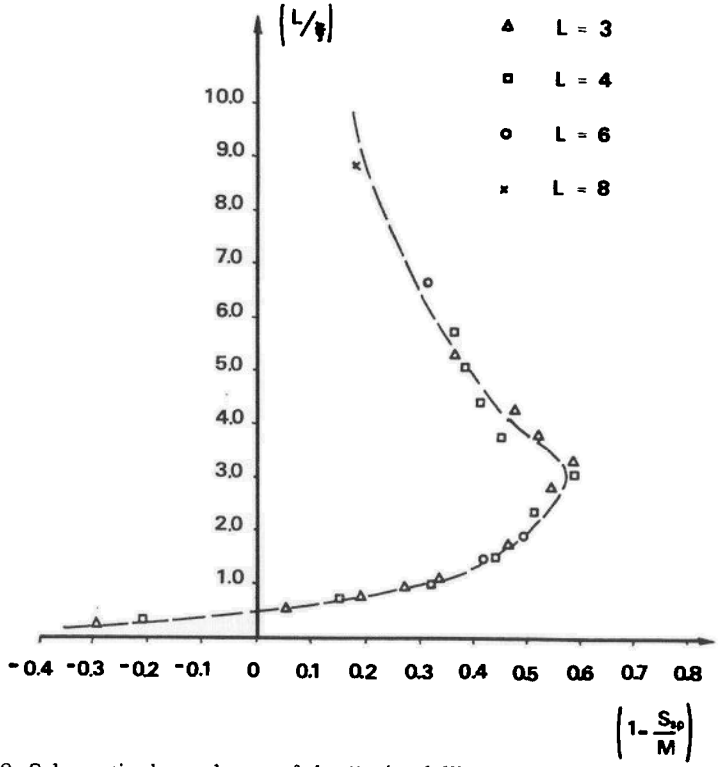

FIG. 8. Schematic dependence of the "spinodal" curve on the coarse-graining cell size L. A scaled form is shown in which the ratio L/ξ is plotted versus the ratio of the spinodal value S_{sp} to the equilibrium value M of the order parameter.

IV. A Field Theoretic Nucleation Theory

A. Basic ideas

We now discuss a formal theory of nucleation due to Langer (1969), which is based on the semi-phenomenological Fokker–Planck or nonlinear Lan-

gevin equations discussed in Section III. This formalism has been applied by Langer and others to a variety of problems including the liquid–vapor transition (Langer and Turski, 1973; Turski and Langer, 1980), binary fluids (Langer, 1980), superconductivity (Langer and Ambegaokar, 1967; McCumber and Halperin, 1970) and superfluidity (Langer and Fisher, 1967; Langer and Reppy, 1970). A variation of this field theory approach has also been applied by Kawasaki to the liquid–vapor and binary fluid systems (Kawasaki, 1975a, b; Kawasaki and Gunton, 1976). Although this theory has only been derived under conditions which require one to be somewhat below the critical point, it has often been used in the critical region (Langer and Turski, 1973; Langer, 1980; Kawasaki, 1975b). It seems quite likely that its applicability near the critical point is justified. However, the only theoretical work which substantiates this is a "one-loop" renormalization group calculation by Houghton and Lubensky (1981) valid to lowest order in ε, where $\varepsilon = 4 - d$. Further theoretical work in this area would be quite useful.

In this chapter we outline the formal structure of the theory and briefly summarize its application to the liquid–gas and binary fluid systems. We then discuss within the same formalism the closely related problem of the mathematical description of the condensation point which we discussed in Section II in the context of the classical droplet model. An elegant result emerges from this analysis (also due to Langer, 1969). Namely, the nucleation rate is proportional to the imaginary part of the analytic continuation of the free energy from the stable to the metastable phase. This gives a physical significance to the analytic continuation which is absent in a purely static treatment. We summarize applications of the field theoretic nucleation theory to superfluidity and superconductivity in Section XII.

Before discussing the formalism we should note some important qualitative similarities and differences between the continuum and the cluster dynamics theory. To begin with, the two theories have in common the concept that a metastable state decays via the thermal activation of a localized, unstable fluctuation. For the case of a gas–liquid or binary fluid mixture, for example, this corresponds to a droplet of critical size ("critical droplet"). In contrast to the classical theory of Becker and Döring, however, this critical droplet need not be a physical droplet of the condensing phase, as first pointed out by Cahn and Hilliard (1959), but rather characterizes a certain saddle point configuration. Secondly, no detailed theory of droplet formation is required in the field theory approach. Indeed only the critical droplet and its surface deformation, as well as its initial growth rate, are required. This is on the one hand a great advantage in that one need not worry about the difficulties involved in giving a precise definition of clusters or in obtaining a mathematical solution of their kinetic equations (Section VII). On the other hand, it is a disadvantage if, in addition to discussing

the birth of droplets (nucleation theory), one needs also to discuss their growth. Unfortunately a satisfactory theory of recent experiments on binary fluids near the critical point requires a statistical theory of birth *and* growth, as we discuss in Section X. At the moment a first principles field theory of nucleation and growth has not been developed.

We now outline the basic ideas involved in the field theory calculation of the nucleation rate. To do this we first note that the stationary state equilibrium solutions of the Fokker–Planck equations (3.1) and (3.2) are given by

$$\rho_{eq}\{\psi\} \propto e^{-\tilde{F}\{\psi\}/kT} \tag{4.1}$$

(where for simplicity we omit the subscript i in $\{\psi_i\}$), where $\tilde{F}$ is equal to the coarse-grained free energy functional F plus certain constants of the motion. For example, for the binary alloy or binary fluid,

$$\tilde{F}\{c\} \equiv F_\mu\{c\} = F - \mu \int c(\vec{r})\, d\vec{r}\,, \tag{4.2}$$

where μ is the chemical potential. For solutions given by (4.1) the current J is zero. The underlying idea concerning the field theoretic characterization of nucleation is that the states of metastable and stable equilibrium lie in the vicinity of configurations $\{\psi\}$ which minimize $\tilde{F}$ and therefore maximize ρ_{eq}. For example, imagine that a system such as a binary alloy is in a stable one-phase state very near its coexistence curve. This equilibrium state corresponds to a minimum of $\tilde{F}$ which is a spatially uniform solution of the Euler–Lagrange equation, $\delta\tilde{F}/\delta c = 0$. It is clear, however, that there should be another spatially uniform solution of this equation which represents the metastable state at the same chemical potential. Thus the distribution function is a doubly peaked function of the concentration, with its maxima at the stable and metastable values of the concentration. The larger peak corresponds, of course, to the stable phase, while the smaller peak corresponds to the metastable phase. The contribution of this second peak to the partition function (given by the trace of ρ_{eq}) is, however, negligible in the thermodynamic limit, since it is not the absolute maximum of the distribution function. Now slowly change the chemical potential to prepare the system in a metastable state at a point just on the other side of the condensation point. Then the two maxima of the distribution function change roles. What was the stable extremum becomes the metastable extremum and vice versa. It is the decay of the system from this metastable state which we wish to describe in nucleation theory.

The field theoretic description of nucleation is based on the following assumptions of Langer. The decay of a metastable state occurs when a configuration $\{\psi\}$ located in the vicinity of a metastable extremum, say $\{\psi_0\}$, moves to the vicinity of another minimum of lower $\tilde{F}$. (In the simplest

cases this will be the stable state.) The most likely trajectories are those which pass near the lowest intervening saddle point of $\tilde{F}$, say $\{\bar{\psi}\}$. The rate of probability flow across this saddle point $\{\bar{\psi}\}$ then determines the nucleation rate I. As we will show in Section IV.B, this saddle point describes a configuration in which a single, critical droplet of the more stable phase is located somewhere in a spatially homogeneous metastable background which is everywhere the same as the metastable configuration $\{\bar{\psi}_0\}$. It is in this sense that only a single length scale, the size R_c of the critical droplet, enters the field theoretic formulation of nucleation theory. The steady state solution of interest is one with a constant probability flow across $\{\bar{\psi}\}$ from the metastable to the stable extremum (Fig. 9). To find

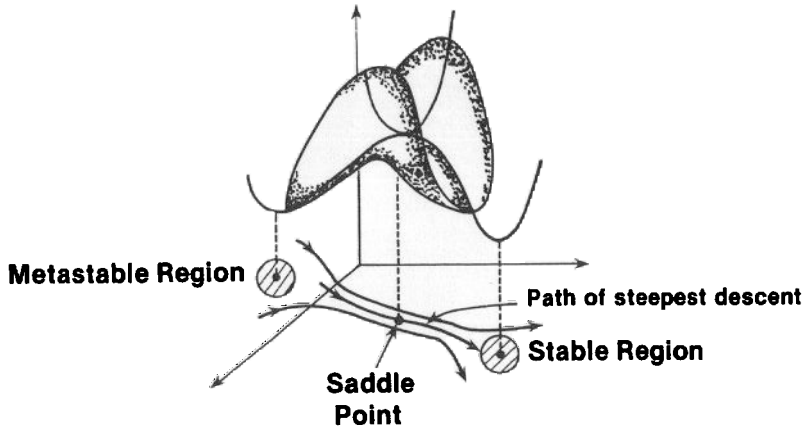

FIG. 9. Schematic illustration of the probability current flowing from a metastable state to a stable state across a saddle point.

this current J, we obtain the steady state solution of (3.1) in the neighborhood of $\{\bar{\psi}\}$. This is done by expanding $\tilde{F}\{\psi\}$ around $\{\bar{\psi}\}$, which leads to a functional linear Fokker–Planck equation with boundary conditions analogous to the ones used in the Becker–Döring theory. The nucleation rate is finally obtained as the integral over the plane perpendicular to the current J in the above described steady state solution, as we discuss in more detail in Section IV.C.

B. A critical droplet solution of the saddle point equation

Before outlining the general results of the nucleation theory, we discuss some properties of the Ginzburg–Landau model which will be useful for

our discussion in Sections IV.D and IV.E. As noted earlier, this model is relevant for the discussion of systems such as simple fluids, binary fluids and binary alloys. In particular, we will be interested in obtaining a solution of the equation for the saddle point which describes the profile of the critical droplet associated with nucleation phenomena in such systems. The prototype free energy functional $\tilde{F}(\psi)$ for these systems is the Ginzburg–Landau free energy for a "ψ^4" model,

$$\tilde{F}(\psi) = \int d\vec{r} \left\{ \tfrac{1}{2}|\nabla\psi|^2 - \tfrac{1}{2}r\psi^2 + \frac{u}{4}\psi^4 - H\psi \right\}. \tag{4.3}$$

This is of the form (3.12), where ψ denotes the order parameter, H denotes a small magnetic field for magnetic systems or a chemical potential in the case of fluids, binary fluids or binary alloys (e.g. (4.2)). The partition function $Z(H)$ is defined by the functional integral

$$Z(H) = \int \delta\psi \, e^{-\tilde{F}(\psi)/k_B T} \tag{4.4}$$

and the expectation value of the order parameter is defined by

$$\langle\psi\rangle = Z^{-1} \int \delta\psi \, \psi(\vec{r}) \, e^{-\tilde{F}/k_B T}. \tag{4.5}$$

We are interested in the case $r > 0$ in (4.3), so that we are dealing with a double well potential

$$V(\psi) \equiv f(\psi) - H\psi \tag{4.6}$$

$$= -\tfrac{1}{2}r\psi^2 + \frac{u}{4}\psi^4 - H\psi. \tag{4.7}$$

There are two minima of $V(\psi)$, $\psi_\pm(H)$. For $H > 0$, ψ_+ describes the stable phase and ψ_- the metastable phase, whereas for $H < 0$ the roles of ψ_+ and ψ_- are reversed.

The maxima and minima of the integrand in (4.4) are solutions of the Euler–Lagrange equation

$$\frac{\delta\tilde{F}}{\delta\psi(\vec{r})} = -\nabla^2\psi(\vec{r}) + \frac{\partial V(\psi)}{\partial\psi(\vec{r})} = 0; \tag{4.8}$$

i.e.

$$\nabla^2\psi(\vec{r}) = -r\psi(\vec{r}) + u\psi^3(\vec{r}) - H. \tag{4.9}$$

The spatially uniform solutions of (4.9) are $\psi_\pm(H)$. In the limit $H \to 0^\pm$, these tend to the limits $\pm\psi_s$ where $\psi_s = \sqrt{r/u}$. This is the mean field theory prediction for the coexistence curve.

A solution of the one-dimensional form of (4.9) which is of particular interest describes the planar interface between the two equilibrium phases

($H = 0$). This is the well known profile

$$\psi_c(z) = \sqrt{r/u} \tanh \sqrt{2}(z - z_0)/\xi \tag{4.10}$$

for an obvious choice of boundary conditions. In (4.10) z denotes the direction normal to the planar interface, z_0 denotes the centre of the interface and ξ is the classical correlation length $\xi = (2r)^{-1/2}$. (This solution has many names in the literature, including kink, soliton and instanton, depending on the context in which it is used.) More accurate theories exist for the interface profile, including renormalization group theories by Ohta and Kawasaki (1977), Rudnick and Jasnow (1978) and Jasnow and Rudnick (1978). Current theories of nucleation only use the approximation (4.10), however.

To understand the role of solutions of (4.9) in nucleation theory, we first consider the problem of obtaining a systematic, mean-field-like evaluation of the free energy of a stable one-phase state at a point near the coexistence curve. Consider, for example, a small field $H > 0$, with a corresponding average value $\psi_+ = \langle\psi\rangle > 0$ which describes the stable phase. Then the integrand in (4.4) has an absolute maximum at the spatially uniform value $\psi(\vec{r}) = \psi_+$. A systematic evaluation of $Z(H)$ may be carried out by expanding $\tilde{F}(\psi)$ around ψ_+:

$$\tilde{F}\{\psi(\vec{r})\} = V[f(\psi_+) - H\psi_+] + \tfrac{1}{2}\iint d\vec{r}\, d\vec{r}\,' \nu(\vec{r}) \mathcal{M}_0 \nu(\vec{r}\,') + \ldots. \tag{4.11}$$

Her V is the volume of the system (not to be confused with the potential $V(\psi)$) and $f(\psi)$ is defined by (4.6) and (4.7). The operator

$$\mathcal{M}_0 = \left.\frac{\delta^2\tilde{F}}{\delta\psi(\vec{r})\delta\psi(\vec{r}\,')}\right|_{\psi_+}. \tag{4.12}$$

Upon inserting (4.11) in (4.4) and performing the resulting Gaussian integrals one obtains

$$Z(H) \cong Z_0(H) = e^{-V[f(\psi_+) - H\psi_+]/k_B T} \left[\det\left(\frac{\mathcal{M}_0}{2\pi k_B T}\right) \right]^{-1/2}. \tag{4.13}$$

If the eigenvalues of $\mathcal{M}_0$ are denoted as $\{\lambda_j^{(0)}\}$ we obtain the formal result

$$Z(H) \cong Z_0(H) = e^{-V[f(\psi_+) - H\psi_+]/k_B T} \prod_j \left(\frac{2\pi k_B T}{\lambda_j^{(0)}}\right)^{1/2}. \tag{4.14}$$

This is the standard mean-field approximation for the partition function which could be extended by a systematic perturbation expansion which we do not discuss here.

This expression is in itself not of particular interest to us. What is relevant to note is that the integrand in (4.4) has another maximum at a spatially

uniform $\psi(\vec{r}) = \psi_-$ which corresponds to the metastable solution of (4.9) for $H > 0$ (Fig. 10). The contribution of this relative maximum to (4.4) could be obtained by precisely the same procedure as above. One would perform a Gaussian expansion around ψ_-. The result would be of the form (4.14) (with ψ_+ replaced by ψ_-) and is thermodynamically negligible in

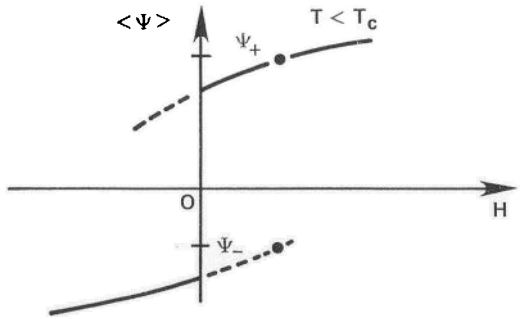

FIG. 10. The stable and metastable values, ψ_+ and ψ_-, of the order parameter. For a binary fluid the order parameter is the concentration and H is the difference of the chemical potential from its condensation value.

comparison with the contribution from the absolute maximum. Now, however, imagine smoothly changing the field H from its original small positive value to a small negative value, such that the average value of ψ remains positive. This corresponds to changing the system from its original stable state to a new metastable state. Then, as described earlier, the roles of the two maxima interchange. It is therefore natural to identify the metastable free energy corresponding to this analytic continuation of the free energy of the stable phase as the logarithm of $Z_0(H)$, given by (4.14). (It is understood that $\psi_+ > 0$ in (4.14) now means the metastable value of $\langle\psi\rangle$ for $H < 0$). Equation (4.14) is the field theoretic analog of the classical droplet model result, eqn (2.7), for the metastable free energy.

The next, essential observation in the field theoretic formulation is that there is another extremum solution of (4.9) which is near the metastable extremum ψ_+. This spatially nonuniform, saddle point solution is a maximum of $\tilde{F}$ which describes a critical droplet. The analysis of this saddle point solution was originally carried out in considerable detail by Cahn and Hilliard (1959). Langer (1967, 1969) then analyzed the nature of the fluctuations about this saddle point, as we summarize in Section IV.E. We briefly outline here the form of this saddle point solution. When $|H|$ is sufficiently small, one finds a solution that one might guess from physical arguments. Namely, the saddle point solution $\bar{\psi}(r)$ describes a radially

symmetric droplet of the nucleating phase embedded in a spatially uniform, metastable background. Its profile is accurately approximated by the profile of the planar interface (4.10). Its form is thus

$$\bar{\psi}(r) \simeq \tfrac{1}{2}(\psi_+ + \psi_-) + \tfrac{1}{2}(\psi_+ - \psi_-)\tanh[(r - R)/\sqrt{2}\xi], \tag{4.15}$$

where R is the droplet radius. The droplet interface thickness is given by the classical correlation length ξ. This solution describes a droplet configuration in which $\bar{\psi}(r = 0) = \psi_-$ and $\bar{\psi}(r \to \infty) = \psi_+$, i.e. a droplet of the stable phase in the metastable background. This is an approximate solution of (4.9) for sufficiently large droplets such that $R \gg \xi$. To determine the critical droplet size R_c, one maximizes the free energy of formation of such a droplet by varying R. Since this free energy is just $\Delta\tilde{F}(R) = \tilde{F}\{\bar{\psi}\} - \tilde{F}\{\psi_+\}$, one easily finds that

$$\Delta\tilde{F}(R) \simeq -\frac{4\pi}{3}R^3 H\Delta\psi + 4\pi R^2\sigma, \tag{4.16}$$

where $\Delta\psi = (\psi_+ - \psi_-)$ and σ is a surface energy

$$\sigma = \int_{-\infty}^{\infty}\left|\frac{d\psi_c(z)}{dz}\right|^2 dz. \tag{4.17}$$

Thus the usual competition between a bulk and surface energy yields the expression for R_c:

$$R_c = \frac{2\sigma}{|H|\Delta\psi}. \tag{4.18}$$

The corresponding activation energy is

$$\Delta F = \Delta\tilde{F}(R_c) = \frac{16\pi\sigma^3}{3(\Delta\psi)^2H^2}. \tag{4.19}$$

For the binary fluid which we discuss in Section IV.D, $\Delta\psi \to \Delta c = c_B - c_A$ (see Fig. 1) and $H \to \delta\mu = \mu - \mu_c$, where μ_c is the condensation value of the chemical potential. We will consider the consequences of this critical droplet and its fluctuations in the next two subsections.

C. Nucleation rates

We now consider the main goal of this section, which is to outline the formal calculation of the nucleation rate for a given model. The basic idea, as noted in Section IV.A, is to find a steady state solution of (3.1) which describes a constant current from the metastable minimum across the saddle point to the more stable minimum (Fig. 9). To do this one imposes

boundary conditions in which the stationary distribution function coincides with the equilibrium solution on the metastable side and is zero on the stable side. This requires a continuous removal of droplets larger than the critical size R_c and a continuous replenishment of the metastable phase. A generalization of the Becker–Döring method was made by Landauer and Swanson (1961) who showed how to use it for a system of arbitrarily many degrees of freedom. Langer extended the Landauer–Swanson approach to the field theories discussed here. Since his 1969 paper is a model of clarity, we simply sketch the solution and indicate the origin of each of the terms in the final expression for the nucleation rate. The first point is to restrict the calculation to the vicinity of the saddle point $\bar{\psi}$, since the surface integral of the current which crosses this point yields the nucleation rate. As a consequence it is natural to write the desired steady state distribution function as

$$\rho\{\psi\} = E\{\psi\}\, e^{-\tilde{F}\{\psi\}/k_B T} \tag{4.20}$$

where one must obtain a solution for $E\{\psi\}$, which we do not discuss. It is natural to expand $\tilde{F}\{\psi\}$ around the saddle point $\bar{\psi}$. Thus for the general class of models discussed in Section III, one has (using the same notation as in that section)

$$\tilde{F}\{\psi\} = \bar{F} + \tfrac{1}{2}\sum_{ij} u_i \mathcal{M}_{ij} u_j + \ldots, \tag{4.21}$$

where $u_i = \psi_i - \bar{\psi}_i$, $\bar{F} = \tilde{F}\{\bar{\psi}\}$ and

$$\mathcal{M}_{ij} = \left.\frac{\partial^2 \tilde{F}}{\partial\psi_i \partial\psi_j}\right|_{\bar{\psi}}. \tag{4.22}$$

It is again natural to diagonalize the quadratic form in (4.21), which requires finding the eigenvalues $\{\lambda_j\}$ of the matrix $\mathcal{M}$. For the purpose of our subsequent discussion in Sections IV.D. and IV.E. we note that for the single variable, "ψ^4" model defined in (4.3), (4.21) becomes

$$\tilde{F}\{\psi\} = \bar{F} + \tfrac{1}{2}\iint d\vec{r}\, d\vec{r}\,' u(\vec{r})\, \mathcal{M}(\vec{r}, \vec{r}\,') u(\vec{r}\,') + \ldots, \tag{4.23}$$

where

$$\mathcal{M}(\vec{r}, \vec{r}\,') = \left.\frac{\delta^2 F}{\delta\psi(\vec{r})\,\delta\psi(\vec{r}\,')}\right|_{\bar{\psi}} \tag{4.24}$$

and $u(\vec{r}) = \psi(\vec{r}) - \bar{\psi}(\vec{r})$. We will discuss the solution of the eigenvalue problem for the "ψ^4" model in Section IV.E. Here we only note two characteristics of the general eigenvalue spectrum of the matrix $\mathcal{M}_{ij}$ in (4.22). The first is that since $\bar{\psi}$ is a saddle point there is one negative eigenvalue, say $\lambda_1 < 0$. This reflects the instability of the critical droplet.

The second point is that there is a set of zero eigenvalues. These arise from the fact that $\bar{\psi}$ does not possess all of the symmetries of $\tilde{F}\{\psi\}$. For example, changing the physical location of the fluctuation defined by $\bar{\psi}$ leaves $\tilde{F}$ invariant. Thus the d translational modes of the droplet of a d-dimensional system should have zero eigenvalues. Similar situations occur in superfluids and superconductors, due to phase invariance (Langer and Ambegaokar, 1967; Langer and Fisher, 1967; McCumber and Halperin, 1970; San Miguel and Gunton, 1981).

To obtain the nucleation rate we need to determine the probability current whose components are given by (3.2). The steady state solution of (3.1) requires that the divergence of this probability current vanishes, i.e. for the general class of models discussed in Section III

$$\sum_{i,j} \frac{\partial}{\partial\psi_i} M_{ij}\left(\frac{\partial F}{\partial\psi_j}\rho + k_B T \frac{\partial\rho}{\partial\psi_j}\right) = 0. \tag{4.25}$$

A solution of (4.25) for ρ can be obtained in the vicinity of the saddle point, using (4.20) and (4.21). From the solution for ρ one then obtains the probability current from (3.2). The nucleation rate I is calculated by integrating this current across a surface which passes through the saddle point. The final result can be written in the standard form

$$I = I_0\, e^{-\Delta F/k_B T}, \tag{4.26}$$

where

$$\Delta F = \tilde{F}\{\bar{\psi}\} - \tilde{F}\{\psi_0\} \tag{4.27}$$

and where ψ_0 denotes the metastable minimum (which would be ψ_+ for the "ψ^4" model). The quantity I_0 is given by

$$I_0 = \frac{|\kappa|}{2\pi}\Omega_0. \tag{4.28}$$

The quantities κ and Ω_0 are often termed the dynamical and statistical prefactors, respectively. They have a very natural interpretation. The dynamical prefactor $|\kappa|$ describes the initial exponential growth rate of the unstable mode at the saddle point. In general it is the negative eigenvalue of the matrix $\underline{\mathcal{M}}$. This eigenvalue equation for κ is obtained by linearizing the nonlinear Langevin equation (3.5) about the saddle point $\bar{\psi}$ (neglecting the noise term).

The statistical prefactor is

$$\Omega_0 = \mathcal{V}\left(\frac{2\pi k_B T}{|\lambda_1|}\right)^{1/2}\left(\frac{\det(\mathcal{M}_0/2\pi k_B T)}{\det(\mathcal{M}'/2\pi k_B T)}\right)^{1/2} \tag{4.29}$$

where $\mathcal{M}_0$ is the generalization of (4.12), i.e.

$$(\mathcal{M}_0)_{ij} = \frac{\partial^2 \bar{F}}{\partial \psi_i \partial \psi_j}\bigg|_{\psi_0}, \tag{4.30}$$

and $\mathcal{M}$ is defined by (4.22). The prime in (4.29) denotes that the negative eigenvalue λ_1 and all zero eigenvalues are omitted. Equation (4.29) can be written in terms of the eigenvalues $\{\lambda_j^{(0)}\}$ of the matrix $(\mathcal{M}_0)$ defined in (4.30) and the eigenvalues of $\mathcal{M}$ defined in (4.22) as

$$\Omega_0 = \mathcal{V}\left(\frac{2\pi k_B T}{|\lambda_1|}\right)^{1/2} \prod_i{}' \left(\frac{2\pi k_B T}{\lambda_i}\right)^{1/2} \prod_j \left(\frac{\lambda_j^{(0)}}{2\pi k_B T}\right)^{1/2}. \tag{4.31}$$

The prime means the same as in (4.29). The product over the $\{\lambda_j^{(0)}\}$ eigenvalues arises from the partition function for the metastable phase (given by (4.14) for the "ψ^4" model). This partition function arises from normalizing the stady state distribution function ρ (given in (4.20)) such that its integral over the metastable region in function space be unity. This is one of the Becker–Döring boundary conditions mentioned earlier. The remaining factors in (4.30) arises from performing Gaussian integrals of $\exp(-\bar{F}\{\psi\})$ (using (4.21)) in the vicinity of the saddle point. The contribution of the zero eigenvalues is given by $\mathcal{V}$. This is the volume of the subspace of ψ space which is spanned by the set of configurations of $\bar{\psi}$ which leaves $\bar{F}$ invariant. $\mathcal{V}$ is proportional to the volume V of the system, as it must be since the meaningful measure of nucleation is I/V. Finally we note that ΔF in (4.27) is just the excess free energy required to form a nucleating droplet of the critical size R_c (e.g. (4.18)) in a metastable state.

Equations (4.26), (4.27), (4.28) and (4.31) thus provide the basis of a first principles statistical theory of nucleation for any system described by the Fokker–Planck equations (3.1) and (3.2). It should be noted that this derivation assumes that the degree of supersaturation is small (e.g. H is small). As well, dynamics enters the calculation of the nucleation rate only through κ in (4.28). We discuss the calculation of κ for fluids and fluid mixtures in the next section.

D. Simple models of nucleation in binary fluids and liquid–gas transitions

We now illustrate these formal ideas for the case of the liquid–gas and binary fluid transitions, to obtain the nucleation rate near their critical points. A hydrodynamic model of the liquid–gas transition was first studied by Langer and Turski (1973), to discuss supercooling and condensation near a critical point. Kawasaki (1975b) considered the same problem, as

well as nucleation in a binary fluid, using similar hydrodynamic models but a somewhat different calculational scheme. The Langer–Turski and Kawasaki theories are equivalent if one corrects a small error made in the original Langer–Turski analysis (J. S. Langer and L. A. Turski, private communication; Kawasaki, 1975b; Turski and Langer, 1980). Since there is a close parallel between the liquid–gas and binary fluid transitions, we will treat both cases simultaneously below, using the notation for the binary fluid. At the end of this discussion we compare the field theoretic predictions with the appropriate form of the Becker–Döring theory. We will see that although in principle the two theories make different predictions for the nucleation rate, the difference is quite small unless one studies nucleation extremely close to the critical point. We will discuss the agreement between these theories and the experimental measurements on critical fluids in Section X.

We begin by discussing a suitable dynamical model for the binary fluid. As noted in Section III this is given by the analog of model H, eqns (3.23)–(3.26), with the order parameter being the local concentration $c(\vec{r})$. Kawasaki (1975b) has, however, shown that the nucleation rate which one obtains from this model is the same as that obtained from a simplified model. In this latter model one neglects the transverse velocity modes, but replaces the bare mobility which enters (3.23) by a renormalized mobility M. Correspondingly, one replaces the bare diffusion constant by a renormalized diffusion constant D. Thus, to keep our discussion as simple as possible, we will consider only this simplified diffusion model for the binary fluid. Similar arguments apply to the gas–liquid system. Here the important slow variables are the entropy density and the transverse velocity modes. Therefore, if one begins with model H, which consists of an order parameter ψ and transverse velocity modes for the ψ_i, one can simultaneously treat the binary fluid and liquid–gas systems, identifying ψ as the local concentration in the former case and as the local entropy density in the latter case (Kawasaki, 1975b). For the gas–liquid system the simplified model includes only the order parameter, with the kinetic coefficient being taken as the renormalized thermal conductivity (i.e. $\lambda_0 \to \lambda$ in (3.23)).

We first sketch a calculation of the dynamical prefactor κ, using the simplified diffusion model of the binary fluid. Rather than giving a formal analysis of the eigenvalue problem for κ (Langer and Turski, 1973; Turski and Langer, 1980), we present an equivalent, heuristic derivation which reveals the basic physics involved (Langer, 1980; Langer and Schwartz, 1980). We restrict ourselves to the situation of small supersaturation, in which case the initial growth rate of the unstable droplet will be small. Thus we can use a quasi-stationary solution of the linearized diffusion equations obtained from (3.8) and (3.9). This means that we look for a steady state solution of the diffusion equation, $\nabla^2 c \simeq 0$. This gives a well

known result for the instantaneous diffusion field (Reghavan and Cohen, 1975) in the neighborhood of a spherical droplet of radius R:

$$c(r) \simeq c_0 - R\frac{\delta c}{r}\left(1 - \frac{R_c}{R}\right). \tag{4.32}$$

Here δc is the supersaturation $c - c_A$ and c_0 is the initial concentration, as shown in Fig. 1. The term which involves R_c/R is a reduction in supersaturation due to the Gibbs–Thomson effect at the curved surface of the droplet. The diffusion flux into the droplet is

$$j = D\left.\frac{\partial c}{\partial r}\right|_{r=R}. \tag{4.33}$$

Since this gives the growth rate of the droplet, $\Delta c(\mathrm{d}R/\mathrm{d}t)$, we obtain the equation of motion:

$$\frac{\mathrm{d}R}{\mathrm{d}t} = \frac{D}{R}\frac{\delta c}{\Delta c}\left(1 - \frac{R_c}{R}\right). \tag{4.34}$$

To obtain the growth rate we linearize this equation around the critical droplet size. Thus from $\delta\dot{R} = -\kappa\delta R$, with $\delta R = R - R_c$, we obtain

$$|\kappa| = \frac{D\delta c}{R_c^2 \Delta c}. \tag{4.35}$$

It is convenient to express κ and the nucleation rate in terms of a dimensionless variable,

$$x = \frac{2}{\beta g_0 \Delta c_0}\frac{\delta\mu}{\epsilon^{\beta\delta}} \tag{4.36}$$

$$\simeq \frac{2}{\beta}\frac{\delta c}{\Delta c}, \tag{4.37}$$

where the critical amplitudes Δc_0 and g_0 are defined in (10.3) and (10.4), and β is about 1/3. The usefulness of the variable x is that for a constant composition quench (4.37) becomes

$$x = \delta T/\varepsilon T_c, \tag{4.38}$$

where δT denotes the undercooling. One can express (4.35) in terms of x and ξ by noting that in the "ψ^4" model the critical radius (4.18) can be approximated (Langer, 1980) by

$$R_c \simeq 2\xi/x. \tag{4.39}$$

Thus we can write κ in (4.35) as

$$|\kappa| \simeq \frac{1}{24}\frac{Dx^3}{\xi^2}. \tag{4.40}$$

An analogous argument can be used to obtain the initial growth rate of a droplet of liquid in a supercooled vapor (Langer and Turski, 1973; Turski and Langer, 1980). In this case the rate of growth is determined by the rate at which the latent heat produced in the formation of a droplet of the nucleating phase can be dissipated. This so-called thermal nonaccommodation effect (Langer and Turski, 1973; Turski and Langer, 1980) clearly involves the thermal conductivity λ. Their analysis leads to an equation similar to (4.34), but with the right-hand side replaced by

$$(2\lambda\sigma T/l^2 n_l)(R - R_c)/R_c R^2.$$

Here σ, l and n_l are the surface tension, latent heat and liquid density, respectively. Thus

$$|\kappa| = \frac{2\lambda\sigma T}{l^2 n_l R_c^3} \tag{4.41}$$

where $R_c = 2\sigma/(\Delta n \delta\mu)$, with $\delta\mu$ being the difference in chemical potential between the supersaturated vapor and the two-phase equilibrium state at the given average density. The quantity $\Delta n \equiv n_l - n_v$, where n_v is the density in the gas phase. For both the binary fluid and gas–liquid transitions it can be shown that the growth rate of critical nuclei satisfies dynamical scaling. That is, both (4.40) and (4.41) can be written in the form

$$\kappa \propto \xi^{-3}(\xi/R_c)^3, \tag{4.42}$$

where ξ is the interface thickness or, equivalently, the bulk correlation length. Dynamical scaling implies that $\kappa = \xi^{-3} f(R_c/\xi)$, where $f(x)$ is some unspecified scaling function

To complete the calculation of the nucleation rate for these fluid systems, one must evaluate the activation free energy ΔF and the statistical prefactor Ω_0 which are given by (4.27) and (4.31) respectively. The activation energy ΔF of a critical droplet is given by (4.19). This can be rewritten as

$$\Delta F = \frac{4\pi}{3}\sigma R_c^2 \tag{4.43}$$

by using (4.18) to eliminate the field. The evaluation of Ω_0 (which is a generalization of the Zeldovitch (1943) factor) involves a calculation of the eigenvalues $\{\lambda_j^{(0)}\}$ and $\{\lambda_j\}$, which describe fluctuations with respect to the metastable minimum and saddle point extremum respectively. This has been done by Langer and Turski (1973) and Günther *et al.* (1980) (see also Affleck, 1980). For a binary fluid near its critical point the final result is

$$\Omega_0 \, \mathrm{e}^{-\Delta F/k_B T} = \frac{C}{\xi^3}\left(\frac{x_0}{x}\right)^{7/3} \mathrm{e}^{-(x_0/x)^2}, \tag{4.44}$$

where x is given by (4.38), C is a constant, and x_0 is a dimensionless number

defined in (10.2). The value of x_0 is of order unity for all the systems so far studied experimentally. It should be noted that the expression (4.44) involves interpreting σ in (4.42) as the true surface tension. Similarly, the eigenvalues have been interpreted in terms of thermodynamic quantities. This has not been justified in a self-consistent fashion, as pointed out by Langer and Turski (1973). It should be noted that (4.44) also holds for the liquid–gas transition, with an appropriate redefinition of x.

The nucleation rate per unit volume, I/V, for the binary fluid then follows from (4.26)–(4.28), (4.31), (4.40) and (4.44) as

$$I/V = C_1 x_0^6 \left(\frac{D}{\xi^5}\right)\left(\frac{x}{x_0}\right)^{2/3} \exp(-x_0/x)^2, \tag{4.45}$$

where $C_1 \simeq 1/(288\pi\sqrt{3})$. it should be noted that this continuum theory makes precise predictions about the prefactors, D/ξ^5 and $(x/x_0)^{2/3}$. The $x^{2/3}$ behavior in particular differs from a detailed droplet model theory of Binder and Stauffer (1976) (Section VII), which is an improved version of the Becker–Döring theory. In principle this difference in the prefactor could be measured, thereby clarifying the theoretical situation. In practice, however, this distinction is so far unobservable. As a final remark about the binary fluid expression (4.44) we observe that its validity is for small values of x. However, Langer and Schwartz (1980) have suggested an *ad hoc* scaling extension of this to large values of x, namely

$$\Omega_0 \, e^{-\Delta F/k_B T} \cong \frac{C}{\xi^3}\left(\frac{x_0}{x}\right)^{7/3}\left(1 + \frac{x}{x_0}\right)^{\phi} e^{-(x_0/x)^2}, \tag{4.46}$$

where $\phi = 10/3 + 1/\delta$ and δ is the exponent which describes the shape of the critical isotherm. Equation (4.46) reduces to (4.44) for small x and is used by Langer and Schwartz in their late time completion theory (see eqn (10.13)).

An expression analogous to (4.44) can also be obtained for the liquid–gas transition, using (4.40). A convenient way to write this for purposes of comparison with the Becker–Döring theory, as well as with experimental measurements, is

$$\frac{I}{V} = J_0\left(\frac{T_c}{\delta T}\right)\varepsilon^{\theta} e^{-(\tau_0 \varepsilon/\delta T)^2}. \tag{4.47}$$

Here J_0 and τ_0 are numbers which involve various critical point amplitudes and $\theta = 9\nu' - 2\beta - \gamma' + 1$, using standard notation for critical exponents. The Becker–Döring prediction (2.19), written in terms appropriate near the critical point (Langer and Turski, 1973), is

$$\frac{I^{BD}}{V} = (J^{BD})\varepsilon^{\nu} e^{-(\tau_0 \varepsilon/\delta T)^2} \tag{4.48}$$

where J^{BD} also involves critical amplitudes.

The usual test of nucleation theory is a prediction for the cloud point, as discussed in detail in Section X. This requires obtaining an expression for the degree of supercooling, δT_c, as a function of the nucleation rate. This δT_c can be obtained from (4.47) by noting that a given nucleation rate, I_c/V, will occur for $\delta T = \delta T_c$, so that

$$I_c/V = J_0 \varepsilon^{\phi}(T_c/\delta T_c) \, e^{-(\tau_0 \varepsilon/\delta T_c)^2}. \tag{4.49}$$

This equation can then be solved for δT_c to yield

$$\frac{\delta T_c}{\varepsilon} = \frac{a}{(1 + b \ln \varepsilon)^{1/2}}, \tag{4.50}$$

where a and b are given in terms of the quantities τ_0, J_0, V/I_c and $\delta T_c/T_c$. A similar expression for $\delta T_c/\varepsilon$ can be obtained from the Becker–Döring form (4.48), but with different values of a and b. It should be noted that the ratio $\delta T_c/\varepsilon$ is only weakly dependent on ε, with the dependence being somewhat stronger in the Langer–Turski theory than in the Becker–Döring formulation. An explicit comparison of these two theories was made by Langer and Turski (1973, and private communication) for Xe and CO_2, for two different nucleation rates $I_c/V = 1$ and $10^5\,\mathrm{cm^3\,s^{-1}}$, using the best available estimates of the various parameters which determine a and b. The results are shown in Table II. The rather disappointing conclusion is

TABLE II. Values of the parameters a and b which appear in the critical supercooling equation $\delta T_c/\varepsilon = a/(1 + b \ln \varepsilon)^{1/2}$ (Langer and Turski, 1973, and private communication).

	Xe		CO_2	
	$I_c/V = 1$	$I_c/V = 10^5$	$I_c/V = 1$	$I_c/V = 10^5$
Becker–Döring equation (4.48)				
a (K)	36.41	39.49	28.47	31.39
b	7.43×10^{-3}	8.74×10^{-3}	7.34×10^{-3}	8.62×10^{-3}
Langer–Turski equation (4.47)				
a (K)	35.75	38.68	28.25	30.50
b	4.08×10^{-3}	4.78×10^{-3}	3.99×10^{-3}	4.65×10^{-3}

that despite all the statistical and hydrodynamic corrections which are taken into account in the continuum theory, the nucleation rate differs only slightly from the Becker–Döring theory. These differences would be observable only for extremely small ε. Thus, although from a theoretical point of view there is no doubt that the continuum theory is a considerably more accurate treatment of nucleation than the classical version, the numerical results do not reflect this fact. We return to this subject again

when we compare the existing theories with experimental measurements on critical fluids in Section X.

E. The essential singularity at a first-order phase transition

Langer (1967) discussed the nature of the singularity to be expected at a first-order phase transition, using the field theoretic model discussed here. For simplicity we restrict our attention to the "ψ^4" model, but it is straightforward to generalize the discussion to models discussed in Section III. Consider the problem posed in Section IV.B of obtaining the analytic continuation of the free energy of the stable phase with $H > 0$ and $\langle \psi \rangle > 0$ to the metastable phase with $H < 0$ and $\langle \psi \rangle = \psi_+ > 0$. From what we have said in Section IV.B, the leading contribution to the partition function $Z(H)$, eqn (4.4), is given by the partition function $Z_0(H)$, eqn (4.14), for the metastable phase. However, there is an additional saddle point contribution $Z_1(H)$, so that

$$Z(H) \cong Z_0(H)\left\{1 + \frac{Z_1(H)}{Z_0(H)} + \dots\right\}, \tag{4.51}$$

where from (4.23)

$$Z_1(H) \cong e^{-\bar{F}/k_B T} \int \delta u \, e^{-1/2k_B T \int\int d\vec{r} d\vec{r}' u(\vec{r}') \mathcal{M}(\vec{r}', \vec{r}) u(\vec{r}) + \dots} \tag{4.52}$$

Care must be taken in evaluating those Gaussian integrals in (4.52) which involve the modes for the negative eigenvalue λ_1 and the d zero eigenvalues. Formally one can write

$$\frac{Z_1(H)}{Z_0(H)} = \mathcal{V} \, e^{-\Delta F/k_B T} \left(\frac{\det(\mathcal{M}_0/2\pi k_B T)}{\det \mathcal{M}''/2\pi k_B T}\right)^{1/2} \tag{4.53}$$

where the double prime denotes that the zero modes are excluded and $\mathcal{V}$ denotes the contribution of the zero modes. It is clear from (4.53) that Z_1/Z_0 is imaginary, due to the factor $i|\lambda_1|^{1/2}$ which characterizes the critical droplet instability. (A more detailed discussion of the integral over the unstable mode in (4.52) corresponding to λ_1 has been given by Langer (1967).) Since $\mathcal{V}$ is proportional to the system volume V, so is Z_1/Z_0. Therefore to obtain the analytic continuation of the free energy of the stable phase, defined as $-\mathcal{F}/k_B T = \ln Z$, one must sum the series

$$\sum \frac{1}{n!}\left(\frac{Z_1}{Z_2}\right)^n$$

implicit in (4.51) to obtain a well defined thermodynamic limit $V \to \infty$. The result is that the imaginary part of $\mathcal{F}$ for this gas of critical droplets is given by

$$\frac{\operatorname{Im} \mathcal{F}(H)}{k_B T} = \mathcal{V}\left(\frac{2k_B T}{|\lambda_1|}\right)^{1/2} e^{-\Delta F/k_B T}\left(\frac{\det(\mathcal{M}_0/2\pi k_B T)}{\det(\mathcal{M}'/2\pi k_B T)}\right)^{1/2} \tag{4.54}$$

where the prime denotes that the contributions from the negative and zero eigenvalues is excluded. Although (4.54) has been obtained for the "ψ^4" model, it should be clear that it is also valid for the cases discussed in Section III and Section IV.D, where $\mathcal{M}_0$ and $\mathcal{M}$ are matrices defined by (4.30) and (4.22). If one now compares (4.54) with the result for I obtained from (4.26)–(4.28) and (4.31), one obtains the interesting result (Langer, 1969; Affleck, 1981)

$$I = \frac{|\kappa|}{\pi} \frac{\operatorname{Im} \mathcal{F}(H)}{k_B T} \tag{4.55}$$

which we mentioned earlier.

To proceed further one needs to determine the eigenvalues of $\mathcal{M}_0$ and $\mathcal{M}$. This has been done by Langer (1967) and subsequently by Günther *et al.* (1980). The latter authors extended the analysis of Langer from three dimensions to d dimensions. As well, they corrected a small error in the Langer paper. The eigenvalues of $\mathcal{M}$ are of particular interest and can be obtained by a perturbation calculation. This makes use of the fact that $(x_\mu/r)\partial\bar{\psi}(r)/\partial r$ $(\mu = 1, 2, \dots, d)$ is an exact eigenfunction of $\mathcal{M}$ with eigenvalue zero, since this eigenfunction describes the translation of the critical droplet. One can then show that $Y_l^\mu(\vec{\eta})\, d\bar{\psi}(r)/dr$ are approximate eigenfunctions of $\mathcal{M}$, with eigenvalues

$$\lambda_{l+1} = \frac{(l-1)(l+d-1)}{R_c^2}\left\{1 + O\left(\frac{l^2\xi^2}{R_c^2}\right)\right\}, \qquad l = 0, 1, 2, \dots. \tag{4.56}$$

The $Y_l^\mu(\vec{\eta})$ are the spherical harmonic functions in d dimensions, with the angles denoted by $\vec{\eta}$. The mode $l = 0$ yields the negative eigenvalue λ_1, while the d-fold degenerate zero eigenvalue corresponds to $l = 1$.

The physical significance of this subset of eigenfunctions of $\mathcal{M}$ is that in the case of interest ($H \to 0$, $R_c \to \infty$) they become a band of soft modes which describe the surface excitations of the spherical critical droplet. Indeed, the $l = 1$ eigenfunction of $\mathcal{M}$ is the Goldstone mode associated with the spontaneous breaking of translation invariance by the center of the droplet. A more detailed discussion of these modes is given by Günther *et al.* (1980).

The result of the calculation for the free energy (Günther *et al.*, 1980) is that

$$\operatorname{Im}_{|H|\to 0} \frac{\mathcal{F}(H)}{k_B T} \simeq A r^{d/2} \left(\frac{r^{4-d/2}}{u}\right)^{d/2} \left(\frac{r^{3/2}}{|H|\sqrt{u}}\right)^{(d-3)d/2} \times \exp\left\{ -\frac{r^{4-d/2}}{u}\left[B\left(\frac{r^{3/2}}{|H|u^{1/2}}\right)^{d-1} + \dots\right]\right\}, \quad 1 < d < 5,\ d \neq 3, \tag{4.57}$$

and

$$\operatorname{Im}_{|H|\to 0} \frac{\mathcal{F}(H)}{k_B T} = A r^{3/2} \left(\frac{\sqrt{r}}{u}\right)^{3/2} \left(\frac{r^{3/2}}{|H|\sqrt{u}}\right)^{7/3} \times \exp\left\{ -\frac{r^{1/2}}{u}\left[B\left(\frac{r^{3/2}}{|H|\sqrt{u}}\right)^{2} + \dots\right]\right\}, \quad d = 3, \tag{4.58}$$

where A and B are dimensionless constants.

Equation (4.58) is the result of Langer (1967), which, however, erroneously had a factor of 8/3 instead of 7/3. Günther *et al.* stress the universality of (4.57) and (4.58). The factors depend only on the geometrical properties of the critical droplet and not on the detailed nature of the double well potential.

Although an imaginary free energy is repugnant to some physicists, it should be noted that this particular prediction is of considerable interest. Namely, as can be seen from (4.55), an important, non-dynamical contribution to the nucleation rate is given by (4.57) or (4.58). Thus a partial test of Langer's formal theory of nucleation can be made by examining the validity of these equations. It should be noted that other predictions for an essential singularity in $\mathcal{F}(H)$ have been made from various droplet models (Sections II and VII) which differ from (4.58). The issue is controversial and remains unsettled. Nevertheless, existing evidence seems to support the validity of Langer's theory. In particular, Lowe and Wallace (1980) have shown that the numerical results of Baker and Kim (1980) for the $d = 2$ Ising model are in excellent agreement with the $|H|$ dependence predicted in (4.57). An additional investigation of this singularity and the "spinodal curve" has been made by Privman and Schulman (1982a, b), using transfer matrix methods.

We conclude by noting several other features of this theory. First, if one uses the explicit form of (4.58) for the three-dimensional binary fluid, one obtains the result (4.44). Second, Günther *et al.* (1980) have shown that the effective Hamiltonian for the surface fluctuations of the critical droplet is

$$\mathcal{H}_{\text{eff}} = \mathcal{H}_v + \mathcal{H}_s. \tag{4.59}$$

The term $\mathcal{H}_v$ describes the bulk free energy of the droplet,

$$\mathcal{H}_v = -\frac{|H|}{d}\int d\Omega (R_c + f)^d. \tag{4.60}$$

The second term describes the surface energy of the interface:

$$\mathcal{H}_s = \int d\Omega (R_c + f)^{d-1}[1 + \tfrac{1}{2}(R_c + f)^{-1}(L_{ij}f)^2]^{1/2}. \tag{4.61}$$

Here $f(\vec{\eta})$ is a field which gives the radial displacement of the critical droplet from its spherical form, where $\vec{\eta}$ denotes the angles or unit vectors (with $\vec{\eta}^2 = 1$). The term $L_{ij} = x_i(\partial/\partial x_j) - x_i(\partial/\partial x_i)$ is the angular momentum generator of rotation in the (i, j) plane. The Hamiltonian $\mathcal{H}_{\text{eff}}$, (4.59), can be shown to be invariant under a nonlinear action of the Euclidean group on the field $f(\vec{\eta})$.

V. Theories of Spinodal Decomposition

A. Thermodynamic theory: linear stability analysis

The first successful qualitative theory of the structure now thought to characterize spinodal decomposition was developed by Hillert (1956, 1961). He derived and solved numerically a nonlinear generalized diffusion equation for one-dimensional diffusion on a lattice. This equation is a one-dimensional lattice analog of model B, eqns (3.8)–(3.11), without the noise term ζ. Cahn (1961, 1962, 1966, 1968) subsequently developed a continuum version of Hillert's model and analyzed the early stages of spinodal decomposition by a linearized theory which we summarize below. The theories of Hillert and Cahn are deterministic in nature, in that the noise term which occurs in (3.7) is not included. Also, the parameters which occur in Cahn's theory are interpreted in terms of measured thermodynamic quantities. We postpone until the next section a more complete statistical theory based on equations such as are discussed in Section III.

The validity of Cahn's linearized theory is now considered by many authors to be at best limited to very short times following the quench. Nevertheless, this theory provides a very useful intuitive understanding of the long wavelength instability. Cahn's model is the generalized diffusion equation (often called the Cahn–Hilliard equation) which results from dropping the noise term ζ in (3.8) for model B and using (3.11) for the free energy functional. The resulting continuity equation,

$$\frac{\partial c(\vec{r})}{\partial t} = -\nabla \cdot \vec{j}, \tag{5.1}$$

is then given by eqn (3.14) for model B, but without the noise:

$$\frac{\partial c(\vec{r})}{\partial t} = M\nabla^2\left[-K\nabla^2 c + \frac{\partial f}{\partial c}\right]. \tag{5.2}$$

Cahn linearized this nonlinear equation about the average concentration c_0, to obtain

$$\frac{\partial u(\vec{r})}{\partial t} = M\nabla^2\left\{-K\nabla^2 + \left(\frac{\partial^2 f}{\partial c^2}\right)_{c_0}\right\} u(\vec{r}), \tag{5.3}$$

where

$$u(\vec{r}) = c(\vec{r}) - c_0. \tag{5.4}$$

For very short times following a quench, one would expect this linearization to be valid, since the concentration fluctuations should be small. Note that if one considers long wavelength fluctuations for which one can neglect $K\nabla^2$ in (5.3), one recovers a diffusion equation, but with a diffusion constant

$$D = M\left(\frac{\partial^2 f}{\partial c^2}\right)_{c_0}. \tag{5.5}$$

This diffusion constant is negative inside the classical spinodal region. For this reason Cahn termed the initial stages of spinodal decomposition "uphill diffusion".

The Fourier transform of (5.3) yields

$$\frac{\partial \hat{u}(k)}{\partial t} = -\omega(k)\hat{u}(k), \tag{5.6}$$

where $\hat{u}(k)$ is the Fourier transform of $u(\vec{r})$ and

$$\omega(k) = MKk^2(k^2 + K^{-1}(\partial^2 f/\partial c^2)_{c_0}). \tag{5.7}$$

Thus inside the classical spinodal region, where $(\partial^2 f/\partial c^2)_{c_0} < 0$, $\omega(k)$ is negative for $k < k_c$ (as shown in Fig. 11), where

$$k_c^2 = +K^{-1}|(\partial^2 f/\partial c^2)_{c_0}|. \tag{5.8}$$

Therefore such long wavelength fluctuations will grow exponentially with time. This is the instability against infinitesimal, long wavelength fluctuations mentioned earlier.

A quantity of experimental interest is the structure function $\hat{S}(k,t) = \langle|\hat{u}(k)|^2\rangle$, discussed in the next section. As is well known, this structure function is proportional to the small angle, diffuse scattering intensity (Rundman and Hilliard, 1967). The Cahn prediction is that

$$\hat{S}(k,t) = \hat{S}(k,0)\, e^{-2\omega(k)t}. \tag{5.9}$$

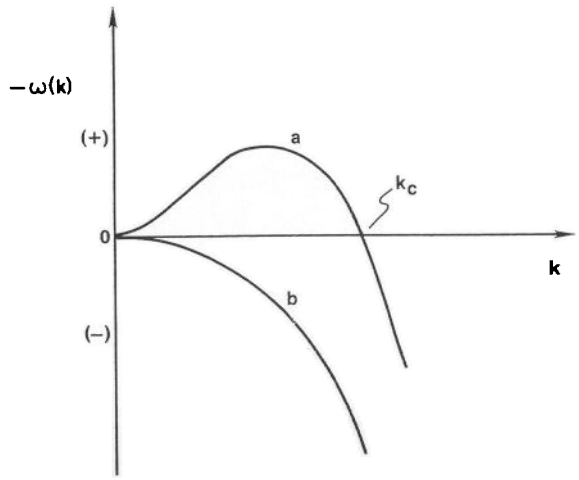

FIG. 11. The behavior of the initial growth rate as predicted by the linear theory for both a metastable and unstable quench.

Thus the initial stages of spinodal decomposition should produce an exponential growth in the scattering intensity for $k < k_c$, with a peak at a (time-independent) wavenumber $k_m = k_c/\sqrt{2}$. Cahn interpreted this k_m as the wavenumber which characterizes the fine, uniformly dispersed precipitate seen in spinodal decomposition studies (Fig. 3).

As we will discuss in Sections VIII and XI, the behaviour predicted by the linear theory, eqn (5.9), is usually not observed in Monte Carlo studies nor in experimental studies of alloys and fluids. However, Marro and Vallés (1983) have recently argued that the very early time Monte Carlo results are consistent with Cook's linear theory discussed below. Also, the linear theory has been claimed to be verified in molecular dynamics studies of fluids during a very short time following a quench (Abraham, 1979). This time scale is, unfortunately, probably too short to be experimentally observable (Goldburg, 1981). In general it is clear that it is necessary to improve the linear theory in order to explain most of the observed experimental results. In the next section, we will discuss several attempts to treat the nonlinear problem including the noise term. (A study of the deterministic model, eqn (5.2), has been made (Novick-Cohen, 1981; Novick-Cohen and Segal, 1982) which deals in particular with the one-dimensional case.) An estimate of the region of validity of the linear theory is given by Skripov and Skripov (1979).

Before discussing the nonlinear theories for the stochastic model B, we summarize several developments related to the Cahn theory. First of all, Cahn (1961) has used it to take into account elastic effects associated with

strains which occur in alloys undergoing composition fluctuations. The result of including the elastic energy in (5.2) is to depress the classical spinodal curve to a new curve known as the coherent spinodal. Thus coherency stress can stabilize a solid solution against infinitesimal composition fluctuations for a significant undercooling below the classical spinodal. This seems to occur in alloys such as Au–Ni. Cahn has also extended the theory to take into account anisotropy (Cahn, 1962) and the effects of an applied magnetic field (Cahn, 1964, 1968) and an applied stress (Cahn, 1963). An excellent summary of the linearized theory, as well as an interesting historical introduction, is given by Cahn (1968) in a review lecture. Another very good review of this theory is given by Hilliard (1970).

Other important contributions by Cahn (1966) have to do with the role of the nonlinear terms which were neglected in going from (5.2) to (5.3). The first point has to do with the necessity of including the higher order terms in the later stages of spinodal decomposition. This is clearly crucial, since the linearized theory predicts an exponential growth of the fluctuations which cannot continue indefinitely if the system is to reach two-phase equilibrium. The second point is that near the classical spinodal the term $(\partial^2 f/\partial c^2)_{c_0}$ is small and the third order term, $(\partial^3 f/\partial c^3)_{c_0}$, characterizes the decomposition process. As Cahn noted, the fluctuations in u are not at all symmetric about $u = 0$ and it is imperative to develop a calculational scheme which can handle this asymmetry. So far the most successful attempt to deal with these nonlinearities is that of Langer *et al.* (1975). As we discuss in the next section this theory provides, however, only a partial solution of the problem.

Finally, we note that Cook (1970) made an important contribution to the theoretical development by observing that it is necessary to add a noise term ζ, to Cahn's equation (5.2), to have a correct statistical description of the alloy dynamics. This, of course, leads to our original model equation of motion (3.8). Cook's observation was that, in addition to a flux produced by the gradient of a local chemical potential, there is an additional flux arising from the random thermal motion of the atoms. This is modeled by the noise term ζ, in (3.8). Although Cook considered the effect of this random force only within the context of the linearized theory, his introduction of noise led to the stochastic model which Langer and others have subsequently used.

B. Statistical theories: the Langer, Bar-on, Miller approximation

Many attempts have been made to develop a theory of spinodal decomposition which is sufficiently powerful to handle the nonlinear effects contained in the equation of motion (3.8). Since most of these attempts

proved rather unsatisfactory, we describe here only the theory of Langer Bar-on and Miller (1975), which is the best of the various calculational schemes proposed so far. We begin by deriving an equation for the non-equilibrium time correlation function,

$$S(|\vec{r} - \vec{r}_0|, t) = \langle u(\vec{r}, t)u(\vec{r}_0, t)\rangle, \tag{5.10}$$

where u is defined in (5.4). The brackets in (5.10) denote an average with respect to the probability distribution functional, $\rho(\{u\}, t)$, which satisfies the Fokker–Planck equation given by (3.3) and (3.4). The reason for considering $S(|\vec{r} - \vec{r}_0|, t)$ is that its Fourier transform,

$$\hat{S}(\vec{k}, t) = \int e^{i\vec{k}\cdot\vec{r}} S(\vec{r}, t)\, d\vec{r}, \tag{5.11}$$

is directly proportional to the X-ray or neutron scattering intensity at a wavenumber transfer $\vec{k}$, as noted earlier.

The equation of motion for S can be obtained by multiplying (3.3) by $u(\vec{r})u(\vec{r}_0)$ and integrating over the function space of the variables u. We assume that the free energy functional F is given by (3.15) and expand $f(c)$ about the average composition c_0. After some straightforward manipulation one obtains the equation

$$\frac{\partial \hat{S}(k)}{\partial t} = -2Mk^2\left[\left(Kk^2 + \left(\frac{\partial^2 f}{\partial c^2}\right)_0\right)\hat{S}(k) + \sum_{n=3}^{\infty}\frac{1}{(n-1)!}\left(\frac{\partial^n f}{\partial c^n}\right)_0 \hat{S}_n(k)\right] + 2Mk_B T k^2, \tag{5.12}$$

where the subscript zero denotes the derivatives of f, evaluated at c_0. The higher order structure functions which appear in (5.12) are the Fourier transforms of the higher order two-point correlations

$$S_n(|\vec{r} - \vec{r}\,'|, t) = \langle u^{n-1}(\vec{r}, t)u(\vec{r}\,', t)\rangle, \tag{5.13}$$

with $S(r, t) = S_2(r, t)$.

To complete this description of $\hat{S}(k)$ we would need to write down the corresponding equations of motion for the higher order correlation functions $\hat{S}_n(k)$. This would lead to a typical hierarchy of coupled equations of motion whose solution would require some approximate truncation scheme. This is a problem that arises in many areas of many-body physics, the difference here being that one is dealing with two-phase phenomena, far from equilibrium. Thus standard many-body techniques involving single peaked Gaussian approximations are not useful since they cannot describe the two-phase equilibration process.

Before discussing the particular truncation scheme proposed by Langer, Bar-on and Miller (LBM), it is convenient to summarize earlier approximations to (5.12). First, the Cahn theory is obtained by neglecting all the

$\hat{S}_n(k)$ $(n > 2)$ as well as the noise term $(2Mk_BTk^2)$ in (5.12). Second, the Cook theory is recovered by neglecting the $\hat{S}_n(k)$ $(n > 2)$ but keeping the noise term in (5.12). Third, a conventional single Gaussian approximation can be made (Langer, 1973). This is of some interest in that it leads to a prediction of coarsening, in contrast to the Cahn and Cook theories. In this approximation one assumes that the distribution functional is a Gaussian, centered at $u = 0$. As a consequence all $\hat{S}_n(k)$ for odd n are zero. If one keeps only the first higher order correlation function, given in this approximation by

$$\hat{S}_4(k) = 3\langle u^2\rangle \hat{S}(k), \tag{5.14}$$

with

$$\langle u^2\rangle = \frac{1}{(2\pi)^3}\int d\vec{k} S(k), \tag{5.15}$$

one replaces $(\partial^2 f/\partial c^2)_0$ in the linear theory by

$$[(\partial^2 f/\partial c^2)_0 + \tfrac{1}{2}(\partial^4 f/\partial c^4)_0\langle u^2(t)\rangle].$$

As a consequence, the characteristic wavenumber k_c now decreases with time, since $\langle u^2\rangle$ is a positive, increasing function of time. Thus this single Gaussian theory predicts coarsening, but clearly is of limited usefulness, as noted above.

The LBM truncation scheme is an improvement over previous theories in that it predicts coarsening, accounts for the absence of exponential growth in observable systems and is qualitatitively accurate for early times throughout the classical spinodal region. It has, however, several shortcomings which we summarize later. The basic physical approximation in the LBM scheme is that the spatial dependence of the higher order correlation functions is the same as that of the two-point correlation function $S(r)$. Specifically, the approximation leads to

$$S_n(r) \simeq \frac{\langle u^n\rangle}{\langle u^2\rangle} S(r). \tag{5.16}$$

This results from assuming that the two-point distribution functional $\rho_2[u(\vec{r}), u(\vec{r}')]$ which determines the $S_n(r)$ has a functional Taylor series expansion

$$\rho_2[u(\vec{r}), u(\vec{r}')] \simeq \rho_1[u(\vec{r})]\,\rho_1[u(\vec{r}')]$$
$$\{1 + g(|\vec{r} - \vec{r}'|)u(\vec{r})u(\vec{r}') + \ldots\}. \tag{5.17}$$

Here ρ_1 is the one-point distribution. (In general, an n-point distribution functional ρ_n is obtained from the original $\rho\{u\}$ by integrating $\rho\{u\}$ over the space of functions u, holding the values of $u(\vec{r}_1), u(\vec{r}_2), \ldots, u(\vec{r}_n)$ constant.) It is straightforward to show from normalization conditions on ρ_1

and ρ_2 that $g(r) = \langle u^2\rangle^{-2}S(r)$, so that (5.13) and (5.17) yield (5.16). While the approximation (5.16) (or (5.17)) seems reasonable for large distances, it is clearly less accurate for short distances. Further improvement of (5.17) would be quite useful.

Using (5.16) one obtains from (5.12) the approximate equation of motion

$$\frac{\partial \hat{S}(k)}{\partial t} = -2Mk^2(Kk^2 + A(t))\hat{S}(k) + 2Mk_BTk^2, \tag{5.18}$$

where

$$A(t) = \sum_{n=2}^{\infty} \frac{1}{(n-1)!}\left(\frac{\partial^n f}{\partial c^n}\right)_0 \frac{\langle u^n\rangle}{\langle u^2\rangle}. \tag{5.19}$$

It should be noted that in the LBM approximation the nonlinearity of (5.12) is approximated by a single k-independent length, $A^{-1/2}(t)$, given by (5.19). The evaluation of $\langle u^n\rangle$ in (5.19) requires ρ_1, whose equation of motion can be determined from the Fokker–Planck equation (3.3) and the use of (5.17). This equation is then solved by parametrizing ρ_1 in terms of a sum of two Gaussians, whose parameters include the peak positions and half-widths. By this process one then obtains a numerical solution of (5.18) and (5.19) for $\hat{S}(k, t)$. An analytical form for $\hat{S}(k, t)$ is thus unavailable.

The solution of (5.18) and (5.19) also requires approximations for M and $f(c)$ which are discussed in the LBM paper (Langer *et al.*, 1975). The free energy $f(c)$ is taken to be of the Ginzburg–Landau form (3.12), with f_0 being the only system-dependent parameter. It is determined in terms of known constants for the three-dimensional Ising model, by use of a mean field approximation. It should also be noted that the coarse-graining size is chosen to be a certain constant times the correlation length.

The calculation of LBM is limited to the critical region, so that they can make use of known critical properties of the Ising model and achieve a certain degree of generality in their analysis. Their results are therefore expressed in terms of scaled variables, such as $q \propto k\xi$, $\tau \propto \xi^{-z}t$ and $\mathcal{S}(q, \tau) \propto \xi^{-\gamma/\nu}\hat{S}(k, t)$. We use conventional notation for the critical exponents (Table I), with the dynamical exponent $z = 2 + \gamma/\nu$. The results of the LBM calculation are shown in Fig. 12 for a critical quench and are qualitatively very similar to Monte Carlo and experimental studies. In fact, the LBM theory is in quite good agreement with Monte Carlo results (Marro *et al.*, 1975) at the critical quench composition and $T \simeq 0.8\,T_c$. This good agreement is in fact rather surprising, since this temperature would appear to be too low for the LBM critical region description to be accurate. Langer *et al.* also evaluated the structure function at a quench composition corresponding to the classical spinodal value. In contrast to the linearized theory (which predicts the physically unreasonable absence of decomposition), the LBM theory yields a behavior quite similar to the behavior

shown in Fig. 12 for a critical quench. This is in qualitative agreement with Monte Carlo and experimental studies, which reveal a gradual change in $\hat{S}(k, t)$ as one moves across the classical spinodal region (Sections IX and XI).

The agreement between the LBM theory and Monte Carlo data is, however, less satisfactory for the off-critical quench than for the critical quench, as is discussed by Sur *et al.* (1977). Nevertheless, it is clear that the LBM theory is the most successful early time description of binary alloy spinodal decomposition available.

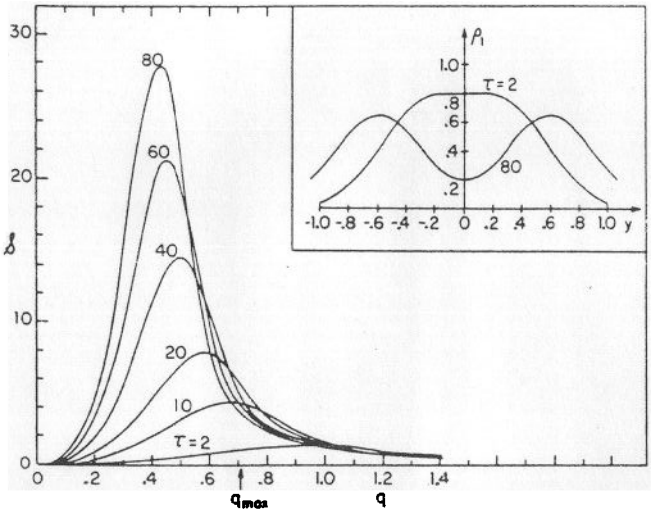

FIG. 12. The scaled structure factor $\mathcal{S}(q)$ for a quench at critical composition at various scaled times τ. The inset depicts the distribution function $\rho_1(y)$ at two of these times. (From Langer *et al.*, 1975.)

It should be noted that versions of the LBM theory have also been applied to a model in which the order parameter is not conserved (Billotet and Binder, 1979) and to a model of tricritical spinodal decomposition (Dee *et al*, 1981). As well, an alternative calculation scheme based on a "mean spherical" model approach has been proposed by Tomita (1978) which yields results reminiscent of the LBM calculation.

The works of Billotet and Binder (1979) and of Binder *et al.* (1978) point out some of the difficulties associated with the LBM study. First, there is an unfortunate dependence of certain results on the (arbitrary) choice of the cell size L used in the LBM calculation. Namely, different choices of the ratio L/ξ give different results, which should not be the case. Second, there is in fact a spinodal curve implicit in the LBM theory, although its

location is shifted from the classical curve and also depends on the choice of cell size. Third and perhaps most important, Binder *et al.* conclude that the LBM theory does not describe fluctuations due to nucleation and growth. Nor does it really describe the expected transition from spinodal decomposition to nucleation. These conclusions are based on the observation by Binder *et al.* that the LBM theory exhibits metastable states with *infinite* lifetime in the region between the coexistence curve and the spinodal curve. Finally, Binder (1977) has argued that the late time behavior of the LBM equation is inconsistent with the Lifshitz–Slyozov $t^{1/3}$ law which we discuss in the next section. In fact, it appears that the LBM theory becomes inaccurate for domain sizes which are a few times the correlation length. It is thus an early time theory. The above objections all serve to demonstrate the intrinsic difficulty of developing a theory which correctly describes the early time spinodal decomposition, the late stage coarsening and the gradual crossover to nucleation. The LBM theory would seem to be an important step in the right direction, but clearly much still remains to be done.

C. Hydrodynamic effects in binary fluids

The experimental observations of spinodal decomposition in binary fluids near the critical point (Huang *et al.*, 1974a, and additional references given in Section X) opened the door to a rich area of experimental and theoretical research. Careful experiments near a critical point are particularly appealing to a theorist because the continuum model discussed in Section III is most valid there. As well, one can make use of known results from critical phenomena, including the concept of universality classes (Wilson and Kogut, 1974). Binary fluids also offer an advantage over alloys in that one does not have to worry about anisotropic and elastic effects. On the other hand, hydrodynamic effects related to fluid flow raise important new issues and present new modes for phase separation. Since one does not yet have a successful theory of spinodal decomposition even for the simplest model of a binary alloy, it is rather clear that theoretical progress in fluids will require considerable effort.

In this section we review some of the theoretical attempts to understand the effects of hydrodynamics on binary fluids. We begin with the work of Kawasaki and Ohta (1978a, b), who calculated the structure function for a spinodally decomposing binary fluid. In principle the starting point is given by the model H of a binary fluid discussed in Section III. However, Kawasaki (1977) has argued that a simplified stochastic model can be used to describe the dynamics of the order parameter $c(r)$. His arguments lead to a model (mentioned in Section IV.D) in which eqn (3.1) for the probability distribution function $\rho(\{c\}, t)$ takes the form (3.3) and (3.4) for a

binary alloy, but with an additional term representing the hydrodynamic effects in the binary fluid. Namely,

$$\frac{\partial \rho(\{c\}, t)}{\partial t} = \mathcal{L}\{c\}\rho(\{c\}, t), \tag{5.20}$$

where

$$\mathcal{L} = \mathcal{L}_A\{c\} + \mathcal{L}_{HD}\{c\}. \tag{5.21}$$

The operator $\mathcal{L}_A$ is the one treated by Langer *et al.* (1975) in their model of an alloy,

$$\mathcal{L}_A = -M \int d\vec{r}\, \frac{\delta}{\delta c(\vec{r})} \nabla^2 \left[\frac{\delta}{\delta c(r)} + \frac{\delta F}{\delta c(r)} \right], \tag{5.22}$$

which follows from (3.3) and (3.4). The second term on the right-hand side of (5.21) is given by

$$\mathcal{L}_{HD}\{c\} = 2 \iint d\vec{r}\, d\vec{r}\,' \frac{\delta}{\delta c(\vec{r})} \nabla c(\vec{r}) \cdot T(\vec{r} - \vec{r}\,') \cdot \nabla' c(\vec{r}\,') \times \left[\frac{\delta}{\delta c(\vec{r}\,')} + \frac{\delta F}{\delta c(\vec{r}\,')} \right]. \tag{5.23}$$

This operator $\mathcal{L}_{HD}$, is an approximate representation of the hydrodynamic effects and involves the Oseen tensor T. The components of this tensor are

$$T_{\alpha\beta} = \frac{1}{8\pi\eta} \left[\frac{1}{r} \delta_{\alpha\beta} + \frac{1}{r^3} r_\alpha r_\beta \right], \tag{5.24}$$

where η is the shear viscosity. The operator $\mathcal{L}_{HD}$ describes the long-range interactions of the order parameter, mediated by the velocity field. The velocity fluctuations are assumed to be Gaussian and in equilibrium. Kawasaki and Ohta (KO) then proceeded as in the LBM calculation to obtain an approximate equation of motion for the binary fluid structure function. This equation is identical to (5.18), apart from an additional term which describes the hydrodynamic interaction. This new equation is then solved numerically to obtain $\hat{S}(k, t)$. The qualitative conclusion that emerges from their analysis is that the hydrodynamic corrections are of substantial importance and significantly modify the LBM results. A more detailed comparison of their theory with experiment is given in Section X.

We should also note two additional points concerning the Kawasaki–Ohta calculation. First, since it is based on the LBM theory, its validity is limited to early times. Siggia (1979) has in fact estimated that the validities of both the LBM and KO theories are at best limited to times of the order

of $100\xi^2/D$, where D is the approximate diffusion constant. Second, and perhaps more important, is a possible inconsistency in the KO theory noted by Binder (1980b). Their theory purports to take into account hydrodynamic effects, which should be important for $k\xi \ll 1$. However, the use of the LBM theory restricts their calculation to the region $k_m \xi \gtrsim 0.3$, where k_m denotes the position of the maximum in $\hat{S}(k, t)$. Thus it is not obvious that their calculation properly treats the hydrodynamic interactions on the desired length scale. In spite of this reservation, it should be noted that their results are in reasonable agreement with the early time binary fluid decomposition experiments.

An important paper by Siggia (1979) deals with the later stages of spinodal decomposition in binary fluids, in which $k_m(t)\,\xi \lesssim 0.1$. In this time regime the system should consist of well defined regions in which the average order parameter is near one of its equilibrium values. In this late stage of coarsening, one can conceive of regions of coexisting phases, separated by sharp interfaces. In the case of binary alloys, for example, this is the domain in which the Lifshitz–Slyozov growth theory, discussed in the next section, should be valid. Siggia does not attempt to calculate $\hat{S}(k, t)$ for the binary fluid in this late time region, but rather examines the influence of hydrodynamics on the coarsening rate. The paper is rich in ideas and a *tour de force* in dimensional analysis. We limit ourselves to summarizing the major conclusions and physical consequences.

Siggia has estimated the effects of several different coarsening mechanisms that can be exhibited in the late stages of phase separation in a binary fluid. These mechanisms depend on the volume fraction v, of the new phase. The simplest possibility for growth is the coalescence of spherical droplets of radius R. The resulting growth law is

$$R^3 = 12DRvt. \tag{5.25}$$

As we will discuss in Section XI, Wong and Knobler (1981) have interpreted their light scattering experiments in terms of Siggia's theory. For this purpose they use the estimate $R = k_m^{-1}$, where k_m denotes the maximum in the intensity of the scattering light. In this case (5.25) can be written approximately as

$$q_m^{-3} \cong 12v\tau \tag{5.26}$$

where q and τ are the scaled variables

$$q = k\xi \tag{5.27}$$

and

$$\tau = Dt/\xi^2. \tag{5.28}$$

One effect of hydrodynamics is to modify (5.26). Namely, as the spheres diffuse toward each other, fluid must be squeezed out from between them.

An estimate of this effect leads to changing (5.26) to

$$q_m^{-3} = \frac{16\pi v\tau}{\ln(0.55/q_m)}. \tag{5.29}$$

Another growth mechanism, which we discuss for the alloy in the next section, is due to evaporation and condensation. This occurs for small supersaturations, when v is small, and leads to the Lifshitz–Slyozov law

$$q_m^{-3} = 0.053\tau. \tag{5.30}$$

It should be noted that the amplitude of this $\tau^{1/3}$ growth law is independent of v, unlike (5.26) and (5.29). The value of the constant, 0.053, is obtained by invoking universality and using data for xenon (given in Langer and Turski, 1973).

The most novel growth mechanism discussed by Siggia occurs if the volume fraction exceeds the percolation limit. A rough estimate of this value is $v_p \simeq 0.15$. In this case, one has connected droplets and can have growth driven by surface tension. The basic idea is to imagine a long wavelength disturbance along the axis of a tube of radius R of the fluid. This variation in the radius of the tube leads to a pressure gradient along the axis. The net effect of this gradient is to drive fluid from the necks to the bulges. An estimate of the growth rate leads to the relation

$$R \simeq 0.1\,\sigma t/\eta, \tag{5.31}$$

where σ and η are the surface tension and shear viscosity, respectively. This then leads to the approximate result

$$q_m^{-1} \simeq 0.3\,\tau \tag{5.32}$$

(Wong and Knobler, 1981). This linear growth rate was also proposed by J. W. Cahn and M. R. Moldover (unpublished). It should be noted that the estimate of the amplitude in (5.31) is very crude (Siggia, 1979).

To summarize, for concentrated mixtures one should first see diffusive growth, with $q_m \propto \tau^{-1/3}$, followed by a crossover to the τ^{-1} behavior given by (5.32). An estimate of the crossover point can be made by equating the two growth rates. A second crossover can also occur, in which gravity dominates at later times. This effect has recently been seen in tricritical ^{3}He–^{4}He mixtures (Benda *et al.*, 1982). A comparison of Siggia's predictions with the experiments of Wong and Knobler is given in Section XI.

Finally, we mention some recent work on spinodal decomposition in one-component fluids. Koch *et al.* (1982) have solved the linearized hydrodynamic equations for the density, velocity and temperature fields, taking into account the random fluctuations in the stress tensor and heat flux.

They find good agreement between the resulting structure factor for the density fluctuations and the molecular dynamics simulation study of the one-component fluid (Mruzik *et al.*, 1978; Abraham, 1979). However, as noted earlier, these molecular dynamics studies involve times which are probably too short to be observed experimentally.

D. Power law approximations

One method which has been used to analyze the behavior of $\hat{S}(k,t)$ as well as of cluster growth involves power law approximations. We summarize here various quantities whose behavior has been analyzed in this way. First, for the structure function it is natural to examine the behavior of the peak position, $k_m(t)$, the peak height $\hat{S}(k_m(t),t)$ and the first moment $k_1(t)$ of $\hat{S}(k,t)$ (eqn (8.7)). These have often been parametrized as

$$k_1(t) \simeq A_1(t + B_1)^{-a}, \tag{5.33}$$

$$k_m(t) \simeq A_m(t + B_m)^{-a'}, \tag{5.34}$$

and

$$\hat{S}(k_m(t),t) \simeq A_s(t + B_s)^{a''}. \tag{5.35}$$

The various constants $A_1, A_m, \ldots$, as well as exponents a, a' and a'', are determined by fitting the quantities of interest over some interval of time. Quite typically, the exponents display a time dependence if the time interval is chosen sufficiently large. In some cases, as for the behavior of $k_m(t)$ for binary fluids (Sections V.C and X), this time dependence has some physical origin. For example, for a binary fluid which is quenched at a critical composition, one expects to find $a'(t) \simeq 1/3$ for early times (diffusive behavior) with an eventual crossover to $a' \simeq 1$ for late times (hydrodynamic percolation effects). In such a case a time-dependent exponent seems sensible. In other cases, however, such as where no one growth mechanism is dominant, a time-dependent exponent might well signal that a power law approximation is simply a poor representation of the time behavior. It would seem appropriate at this relatively early stage of theoretical understanding of such dynamical phenomena that power law approximations such as (5.33)–(5.35) be treated with some caution. In some cases it is possible that they might conceal more physics than they reveal (Langer and Schwartz, 1980).

Another approximation similar to (5.33) has been used by Lebowitz *et al.* (1982) in attempting to analyze their data in terms of Lifshitz–Slyozov behavior. Namely,

$$k_1^{-3}(t) = A + Bt, \qquad t \geq t_0. \tag{5.36}$$

We should also note that in some cases constants such as B_1 or B_m in (5.33) or (5.34) are set equal to zero.

We will discuss in Sections VII and IX the first and second moments ($l_1(t)$ and $l_2(t)$) of the cluster distribution function $n_l(t)$. These also have been analyzed in terms of power law behavior. For example,

$$l_1(t) \sim t^{a_1}, \tag{5.37}$$

$$l_2(t) \sim t^{a_2}, \tag{5.38}$$

where $l_1(t)$ and $l_2(t)$ are defined in (7.37) and (7.38). A scaling form for the distribution function $n_l(t)$ has been proposed which is characterized by another exponent x defined in (7.25). Finally, one often discusses a characteristic domain size $\bar{R}(t)$,

$$\bar{R}(t) \sim t^m. \tag{5.39}$$

This quantity is not always precisely defined. Nevertheless, since $\bar{R}$ is a characteristic linear dimension one expects that $\bar{R} \sim k_1^{-1} \sim k_m^{-1}$. Also, for a characteristic size l, one expects $l \sim \bar{R}^d$. Therefore, one would expect that the exponents a, a', a_1, a_2 and x yield the same physical information as m. Therefore, to a first approximation

$$m \simeq a \simeq a' \tag{5.40}$$

and

$$dm \simeq a_1 \simeq a_2 \simeq x. \tag{5.41}$$

The exponents introduced above are summarized in Table III. This table also includes exponents for the excess free energy $\Delta u(t)$ associated with domain surfaces and for the cluster diffusion coefficient D_l discussed in Section VII.

TABLE III. Table of exponents which characterize the assumed power law behaviour of various quantities defined in the text.

	Exponent	Defining equation
$k_1(t)$	a	(5.33)
$k_m(t)$	a'	(5.34)
$\hat{S}(k_m(t), t)$	a''	(5.35)
l_1	a_1	(5.37)
l_2	a_2	(5.38)
$n_l(t)$	x	(7.25)
$\bar{R}$	m	(5.39)
$\Delta u(t)$	b'	(7.27)
D_l	α	(7.29)

VI. Late Stage Growth Theories

A. Lifshitz–Slyozov theory

The Lifshitz–Slyozov theory (Lifshitz and Slyozov, 1961; Wagner, 1961) is one of the few reasonably well established results in the dynamics of first-order phase transitions. In its original form the theory describes the asymptotic ($t \to \infty$) growth of droplets of a minority phase in a supersaturated phase of a solid solution. (These droplets are often called grains, domains or particles in the literature.) The theory can be used, however, to describe corresponding problems in other systems, such as binary fluids, as discussed in Section V. The theory is derived for the limiting case of small supersaturation, in which the volume fraction of the second phase of, say, B atoms is small. A study of the effect of increasing the volume fraction on the growth rate has been made by Weins and Cahn (1973), which we discuss later.

Lifshitz and Slyozov calculate the asymptotic behavior of the droplet distribution function, $f(R, t)$, where R denotes the radius of a given droplet of the minority phase. In particular, they show that the average droplet size obeys the growth law, $\bar{R} \propto t^{1/3}$. The physics of this late stage growth (or coarsening process) is that larger droplets grow at the expense of smaller droplets. This results from an evaporation–condensation mechanism in which B atoms diffuse through an A-rich matrix from smaller droplets that are dissolving to larger droplets that are growing. The late stage growth is often called Ostwald ripening. An extensive discussion of the Lifshitz–Slyozov theory is given by Lifshitz and Pitaevskii (1981).

The theoretical analysis is based on three coupled equations. These describe the growth rate of a given droplet, the time rate of change of the distribution function $f(R, t)$ and the conservation of solute atoms, respectively. The first equation is (4.20) and arises from the following consideration. Since coarsening occurs only after a nearly equilibrium volume fraction of the second phase has formed, diffusion gradients are quite small. Thus changes in concentration occur quite slowly. As a first approximation one can consider the change in composition with time to be zero. This means that the time-dependent diffusion equation

$$\frac{\partial c}{\partial t} = D\nabla^2 c, \tag{6.1}$$

which can be obtained from (3.8) and (3.9), can be approximated by the steady state diffusion equation

$$\nabla^2 c \cong 0. \tag{6.2}$$

The solution of (6.2) which satisfies the appropriate boundary conditions is given by (4.18). From this equation and the discussion subsequent to it, one obtains the droplet growth rate equation

$$\frac{dR}{dt} = \frac{D}{R}\frac{\delta c}{\Delta c}\left(1 - \frac{R_c}{R}\right). \tag{4.34}$$

For every value of the supersaturation $\delta c(t)$ there is a critical radius $R_c(t)$ for which a droplet is in equilibrium with the background phase. Droplets grow or dissolve, depending on whether their radius R is greater than or less than $R_c(t)$. This is the mechanism by which large grains consume small grains.

The equation for $f(R, t)$ is just the continuity equation

$$\frac{\partial f(R)}{\partial t} = -\frac{\partial}{\partial R}[v(R)f(R)], \tag{6.3}$$

where $v(R)$ is the radial velocity, given by (4.34). The final equation expresses the conservation of solute atoms. Given some initial supersaturation δc_1 (Fig. 1), the volume fraction occupied by the minority phase droplets at the reduced supersaturation $\delta c(t)$ is given by

$$\frac{\delta c_1 - \delta c}{\Delta c - \delta c} \simeq \frac{4\pi}{3}\bar{R}^3 N. \tag{6.4}$$

This equation, in which N is the number of droplets per unit volume and $(4\pi/3)\bar{R}^3$ is their average volume, follows from the lever rule. It should be noted that the time-dependent critical radius $R_c(t)$ is related to the supersaturation $\delta c(t)$ by

$$R_c(t) = \alpha/\delta c(t), \tag{6.5}$$

where for binary fluids (Langer and Schwartz, 1980)

$$\alpha = \frac{2\sigma}{\Delta c(\partial\mu/\partial c)_A}. \tag{6.6}$$

The subscript A in (6.6) denotes the equilibrium concentration c_A is the surface tension.

The asymptotic solutions of eqns (4.20), (6.3) and (6.4) are shown (Lifshitz and Slyozov, 1961; Wagner, 1961) to be

$$f(R, t) \simeq \frac{A}{2D\alpha}\bar{R}^{-6}p(R/\bar{R}) \tag{6.7}$$

and

$$\bar{R}^3(t) = \frac{4}{9}D\alpha t, \tag{6.8}$$

where A is a constant. The scaling function $p(x)$ which appears in (6.7) is given explicitly in the Lifshitz–Slyozov paper. The Lifshitz–Slyozov–Wagner growth law given in (6.8) has been expressed in a scaled form for the binary fluid near its critical point, in (5.30). As we discuss in Sections VIII and XI, there is now reasonable confirmation of (6.8) from Monte Carlo studies of the Ising model of a binary alloy and from experimental studies of binary alloys and binary fluids. (The study of binary fluids (Wong and Knobler, 1981) seems to be the most definitive confirmation of the LS growth rate prediction.)

Two further points should be made concerning the effect of increasing volume fraction on the growth law (6.8). First, Weins and Cahn (1973) studied such effects, within the context of the steady state diffusion equation (6.2). Their solution reduces to the LS growth rate only when the droplets are very far apart. Otherwise they obtain deviations from the LS theory which are significant even at moderate volume fraction. Other theoretical studies of this dependence of "Ostwald" ripening on the volume fraction include Ardell (1972) and Brailsford and Wynblatt (1979). These articles also contain reviews of experimental studies of such effects in metallurgical systems. The second point considers the possible effect of percolated clusters in concentrated systems. Such an effect has not been studied theoretically in binary alloys (in contrast to the work of Siggia for binary fluids). Binder (1980c) has noted, however, that the growth rate of such clusters need not be the same as for isolated droplets. Monte Carlo studies (Section IX) have also considered such clusters.

B. Interface dynamics for models with nonconserved order parameter

The late stage growth of droplets in systems such as binary alloys and binary fluids is only one of many interesting examples of the dynamics of unstable interfaces. A second case concerns the motion of curved antiphase boundaries (APB), which arises in order–disorder transitions in alloys and in paramagnetic–antiferromagnetic transitions in Ising-like systems. An APB is an interface separating domains with identical properties in systems with long-range order. The domains in crystals differ by some relative displacement which is not a superlattice translation (Allen and Cahn, 1979a, b). The local order parameter ψ is not conserved and as a consequence the motion of APBs is not described by the Lifshitz–Slyozov theory. Rather, the average radius of domains satisfies a $t^{1/2}$ growth rate, as we will explain below. Experimental studies involving the dynamics of a nonconserved order parameter have been carried out in temperature quenches in alloys such as Cu_3Au and Ni_3Mn (Collins and Teh, 1973; Hashimoto *et al.*,

1976, 1978; Sato and Hirakawa, 1977). Allen and Cahn (1979a, b) have also analyzed the time dependence of antiphase domain coarsening in Fe–Al. In addition, Monte Carlo simulations have been carried out at low temperatures in a kinetic antiferromagnetic Ising model (Phani *et al.*, 1980; Sahni *et al.* 1981).

The theory of antiphase boundary motion has been most extensively developed by Allen and Cahn (1979a, b). The starting point is a Ginzburg–Landau model without noise for a nonconserved order parameter ψ. This is model A, equation (3.16), so that the deterministic equation of motion is

$$\dot{\psi} = -M\frac{\delta F}{\delta \psi} = -M\left\{-K\nabla^2 + \frac{\partial f(\psi)}{\partial \psi}\right\}, \tag{6.9}$$

where M is a mobility. The free energy $f(\psi)$ is an even function of ψ. The physical picture which underlies the Allen–Cahn theory was originally formulated by Lifshitz (1962). Namely, since the order parameter is not conserved, local equilibrium is established rather quickly. Thus, in a rather

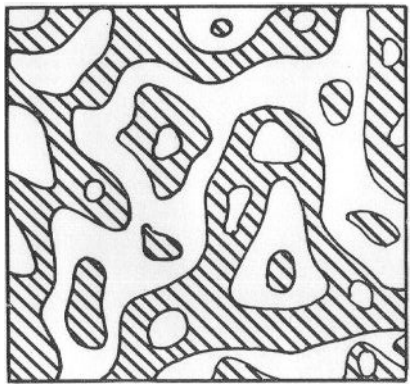

FIG. 13. Schematic evolution of domains and antiphase boundaries. (From Lifshitz, 1962.)

short time following a quench into an unstable state, the system develops local ordered regions or domains, inside which the order parameter takes on one of its possible equilibrium values (Fig. 13). Allen and Cahn considered the case in which the ground state is only doubly degenerate, so that the equilibrium value of the order parameter is either $\pm\psi_e$. (Lifshitz (1962) and Safran (1981) have discussed the case in which the degeneracy is greater than two.) Since the free energy is an even function of ψ, these domains are thermodynamically equivalent. Growth proceeds through the

motion of the interface (APB) between two domains. Within this interface there is a spatial variation of the order parameter, which produces a local diffusion. This diffusion mechanism is, however, entirely different from the Lifshitz–Slyozov long-range diffusion between droplets.

Allen and Cahn obtained an equation of motion for the velocity of a gently curved interface. Their equation predicts that the diffusion which results from gradients in the inhomogeneous interface region leads to a translation velocity for the boundary which is proportional to its mean curvature and independent of the interface free energy. Earlier theories (Smoluchowski, 1951; Turnbull, 1951; Lifshitz 1962) had predicted that the translation was proportional to the product of the mean curvature and the interface free energy. The first step in obtaining the Allen–Cahn result is to rewrite (6.9) in terms of the rate of change of ψ in the direction of $\hat{g}$, where $\hat{g}$ is a unit vector normal to the surfaces of constant ψ. This yields from (6.9)

$$\frac{\partial \psi}{\partial t} = -M\left\{\frac{\partial f}{\partial \psi} - K\left[\frac{\partial^2 \psi}{\partial g^2} - (K_1 + K_2)_\psi \frac{\partial \psi}{\partial g}\right]\right\}, \tag{6.10}$$

where K_1 and K_2 are the principal curvatures of the iso-ψ surfaces. They apply (6.10) to the case in which the interface has a profile given by $\psi_p(g)$ at all normal sections at some particular time. In this situation one can invoke the condition for the equilibrium of planar interfaces, i.e. $\delta F/\delta\psi = 0$. This leads to a cancellation of the first two terms on the right-hand side of (6.10), so that

$$\left(\frac{\partial \psi}{\partial t}\right)_g = -KM(K_1 + K_2)\left(\frac{\partial \psi}{\partial g}\right)_t. \tag{6.11}$$

Since the velocity $v = \partial g/\partial t$ at a constant ψ surface in the interface region is

$$\left(\frac{\partial g}{\partial t}\right)_\psi = -\left(\frac{\partial \psi}{\partial t}\right)_g \Big/ \left(\frac{\partial \psi}{\partial g}\right)_t, \tag{6.12}$$

one then obtains the Allen–Cahn result

$$v = -KM(K_1 + K_2). \tag{6.13}$$

As noted earlier, this expresssion is independent of the surface tension σ. One can immediately show that as a consequence of (6.13) the average size $\bar{R}(t)$ of domains satisfies a $t^{1/2}$ growth law, independent of σ. This growth law was shown by Allen and Cahn (1979a, b) to be obeyed in experiments of domain coarsening in Fe–Al alloys. It has also been indirectly established in Monte Carlo studies of the kinetic Ising model of an

antiferromagnet (Phani *et al.*, 1980; Sahni *et al.*, 1981), although these studies do not examine the issue of the independence of the growth rate on σ. Recently, Sahni *et al.* (1983a) have carried out Monte Carlo simulations in two dimensions to study the temperature behaviour of the prefactor of the $t^{1/2}$ law. The prefactor is observed to depend strongly on temperature for $T = 0.6T_c$, which they explain analytically (Safran *et al.*, 1982) by considering the effect of roughening (or thermal) fluctuations on the domain growth. It should be pointed out that their study is relevant to the problem of domain (or island) growth in surface science. Since the effect of roughening (or thermal) fluctuations is known to be weaker in $d = 3$ than in $d = 2$, a similar study in three dimensions is needed to understand temperature effects on the domain growth dynamics in bulk alloys.

It should also be noted that (6.13), supplemented by a noise term, has been rederived by Bausch *et al.* (1981) and Kawasaki and Ohta (1982a). Bausch *et al.* have used this to discuss the critical dynamics of the Ginzburg–Landau model. Ohta *et al.* (1982) have used it to derive a scaling relation for the structure function $\hat{S}(k, t)$ (Section VIII.C).

Another class of dynamical systems with nonconserved order parameter has also been considered by Chan (1977). This concerns systems which undergo only a first-order phase transition (without an associated second-order critical point). The dynamical problem involves the decay of a metastable state. In contrast to the above situation, the two sides of the interface are not thermodynamically equivalent. Chan has shown by a solitary wave analysis that in this case the growth law is $\bar{R} \propto t$, in agreement with an earlier argument of Lifshitz (1962). Chan's approach can also be applied to the problem considered by Allen and Cahn, in which case one recovers their result. Indeed, eqn (6.13) for a shape-invariant interface profile $\psi_p(g)$ describes a solitary wave solution of (6.9). Kramer (1981a, b) has also used such interface dynamics ideas in an analysis of relative stability for dynamical systems whose equations of motion cannot be derived from a potential.

Other systems with nonconserved order parameter for which the results reviewed here are of relevance include displacive transformations in solids, first-order phase transitions in liquid crystals, uniaxial ferroelectrics, order–disorder structural transitions, anisotropic ferromagnets, transitions in layers of adsorbed gas atoms, helix–coil transitions of polypeptides (Schwartz, 1965) and the helix transition of polynucleotides (Poland and Scheraga, 1970). Section XIII.A on nonlinear relaxation also discusses features relevant to these systems.

We conclude this section by noting that Langer (1971) has deveoped a variational procedure which can be used to calculate late stage growth. Although his original work dealt with binary alloys, with a locally conserved order parameter, it can also be applied to the case of a nonconserved order parameter (San Miguel *et al.*, 1981). This latter work also contains a discussion of model C, as mentioned in Section XII.

VII. Cluster Dynamics

A. Introduction

The theoretical description of first-order phase transitions in terms of cluster models is a major area of research activity. In this section we outline some of the important features of theories of cluster dynamics, which deal with nucleation, spinodal decomposition, and growth mechanisms in systems far from equilibrium. One important approach to cluster dynamics has been developed by Binder, in collaboration with Stauffer, Müller-Krumbhaar and others, which we review in this chapter. A second, closely related, approach to cluster dynamics has been developed by Penrose, Lebowitz and collaborators. This work has focused primarily on cluster growth and is discussed in Section IX. Good reviews which cover various aspects of the use of cluster models in theories of first-order phase transitions include Binder and Stauffer (1976), Penrose (1978), Müller-Krumbhaar (1979), Penrose and Lebowitz (1979) and Binder (1980a, c).

Theories of cluster dynamics are a natural extension of the Becker–Döring theory (Section II). They involve a much more detailed description of clusters than contained in the more macroscopic, field theory models discussed in Sections III and IV. These theories deal with a wide range of cluster sizes, which include very small as well as very large clusters. A fundamental problem in such theories involves giving a definition of clusters which is both precise and useful, as we discuss later. This problem has so far impeded the development of a quantitatively successful dynamical theory. In spite of this difficulty, cluster models have yielded many important qualitative results in the theory of phase separation. These include a scaling theory of nucleation (Section VII.D), an approximate understanding of the smooth transition between nucleation and spinodal decomposition (Section VII.G), dynamical scaling theories for the structure function (Section VIII) and a qualitative explanation of the apparent breakdown of classical nucleation theory (Section X).

Theories of cluster dynamics are based on kinetic equations which model the detailed mechanisms that lead to the formation and evolution of clusters of the different phases in phase separation processes. For example, a binary alloy is described in terms of the average concentration $n_l(t)$ of clusters of the minority phase, of "size" l. Atomic exchanges lead to the evolution of the clusters. This evolution is modeled by a stochastic process which does

not take into account the complications of real systems, such as grains, boundaries and vacancies. Nevertheless, the model is thought to contain the essential physics of phase separation on the same microscopic level as Monte Carlo simulations. (Indeed, this cluster pattern evolution is what is "seen" in the computer experiments.) A major difficulty with these kinetic equations is the lack of knowledge of the equilibrium cluster distribution which occurs in them. This difficulty is closely related to the problem of defining a cluster (Furukawa and Binder, 1982). In this respect it is important to note that the word "cluster" means different things in different contexts. At least three definitions of clusters are discussed in the literature:

(1) *Contour clusters* (Binder and Stauffer, 1976). This is the simplest definition of a cluster for a lattice with nearest neighbor interactions. Namely, a contour cluster is a group of l atoms of the same species such that each atom is a nearest neighbor of at least one other atom of the cluster. These clusters represent order parameter fluctuations on the length scale of the lattice spacing and are appropriate to the study of phenomena at low concentrations and low temperatures (Fig. 14).

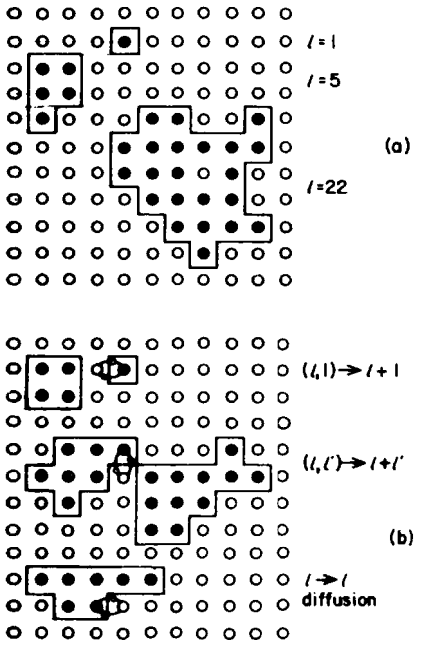

FIG. 14. (a) Clusters of size l in the contour picture. (b) Stochastic interchange of atoms leading to evolution of the cluster pattern. Condensation, dissociation and diffusion processes are shown. (From Binder, 1977.)

(2) *Fluctuation clusters* (Kadanoff, 1971; Stauffer *et al.*, 1971; Binder *et al.*, 1975; Binder, 1976; Kretschmer *et al.*, 1976). At larger concentrations, or near T_c, the contour picture becomes invalid because of percolation effects (Stauffer, 1979; Essam, 1980). Namely, a cluster containing an infinite number of atoms appears. This clearly requires giving a different definition of a cluster (Fig. 15). This can be achieved by redefining l to measure the excess local order parameter. Such "fluctuation clusters" are to be thought of as representing independent fluctuations of the local order parameter on a length scale of the correlation length ξ. A cluster represents a typical fluctuation in a volume of order ξ^d. These are clearly not very precise statements. However, they make clear the fact that a spatial coarse graining is needed to describe critical properties.

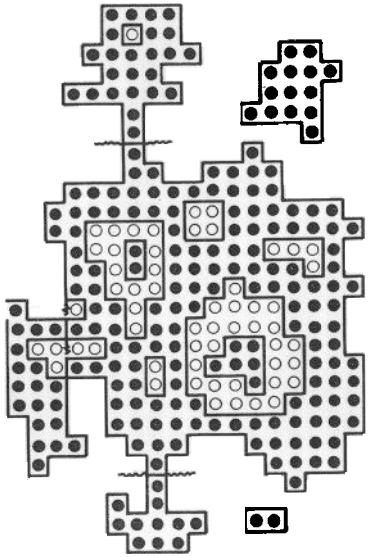

FIG. 15. Clusters of down spins as defined in the contour picture, showing "bubbles" and clusters inside clusters. At positions marked by wavy lines, an additional prescription is used which cuts contours into parts to avoid the occurrence of percolating clusters. (From Binder, 1976.)

(3) *Mathematical clusters* (Domb, 1976; Penrose *et al.*, 1978). These are defined via the low temperature expansion coefficients for the equation of state (Mayer and Mayer, 1940). It should be noted that comparisons between cluster theories and Monte Carlo studies usually use "contour clusters".

Due to the problem of defining clusters, the most significant results of the cluster dynamics approach have been obtained for those regions of the phase diagram in which well defined clusters exist; that is, for low concentrations and low temperatures. This approach, therefore, does not seem to be as appropriate in the critical region, since long-range correlations are difficult to handle in the cluster picture. In this sense, the cluster dynamics approach seems more useful in the region where field theories are less reliable.

The outline of this chapter is as follows. Section VII.B summarizes the most relevant models proposed for the equilibrium cluster distribution needed to deal with the kinetic equations. Section VII.C presents the possible mechanisms for cluster evolution and their representation in terms of kinetic equations. Section VII.D discusses nucleation from the cluster dynamics point of view. We discuss the relation with the Becker–Döring theory and summarize a scaling theory for the nucleation rate. Sections VII.E and VII.F deal with cluster growth. We discuss how two different mechanisms of cluster growth are included in the general kinetic equations. In Section VII.E we show that the predictions of the Lifshitz–Slyozov theory (Section VI) can be obtained from the kinetic equations. In Section VII.F we summarize the Binder–Stauffer theory of cluster growth. Finally in Section VII.G we present a very simplified model calculation which exhibits a smooth transition from nucleation to spinodal decomposition. We also compare the classical Cahn–Hilliard theory with a generalized nucleation theory.

B. Cluster models

An important quantity in theories of cluster dynamics is the equilibrium cluster distribution function n_l. This is in general an unknown quantity for systems of interest. In this section we discuss two phenomenological models for this distribution function which have been used in existing theories of cluster dynamics. One is the classical droplet model discussed in Section II and briefly mentioned again here. The second is the Fisher droplet model (Fisher, 1967a, b, c). In addition we summarize a more general phenomenological scaling theory for n_l which has been used to obtain a scaling theory of the nucleation rate near a critical point. Although our primary aim in this section is to sketch the above theories in view of their use in dynamical theories, we also briefly mention at the end some recent developments concerning clusters and cluster distribution functions. These new results may well be of use in improving our current understanding of cluster dynamics.

The classical droplet model predicts that the equilibrium cluster distribution function is given by (2.1) and (2.2). (Equation (2.2) is often called the capillarity approximation.) Although one expects that the classical theory becomes valid asymptotically for very large clusters at least at low temperatures and small supersaturations (Binder, 1980a), it has several inherent difficulties. One practical difficulty is that the surface energy σ which appears in (2.2) should have l-dependent corrections to the true equilibrium surface tension for planar interfaces. Such corrections are not included in (2.2) and are particularly important for small droplets. Second, the separation of ε_l into a bulk and a surface term is ambiguous for small droplets. For these and other reasons (Binder, 1980a) many attempts have been made to obtain more accurate droplet models. At the time when the cluster dynamics work which we review here was being developed, the Fisher droplet model was often used. Even though this model is now known to be incorrect (from rigorous results such as those of Delyon (1979) and Aizenman *et al.* (1980); D. Stauffer (private communication)), we review it here due to its early use in cluster dynamics. Fisher attempted to obtain a more accurate description of droplets, taking into account their different sizes and shapes. By making an estimate of the entropy of droplets as a function of their surface area, he obtained

$$n_l = q_0 l^{-\tau} \exp - \{[2Hl + b(1 - T/T_c)l^p]/k_B T\}, \tag{7.1}$$

where q_0 and b are constants. The main differences between (7.1) and the classical result arise from the two exponents τ and p. The exponent p specifies the shape of droplets for a given l. Namely, the mean surface area S is parametrized as $S \simeq Al^p$, where $(d-1)/d \leq p \leq 1$. (Individual clusters for which $p < 1$ are called compact, while those for which $p = 1$ are termed ramified. Fisher considered only compact droplets.) Although the model is meant to be valid for low temperatures and small concentration, Fisher also analyzed its behavior near the critical point. He found that p and τ are related to two critical exponents, β and δ, via

$$p = (\beta\delta)^{-1}, \tag{7.2}$$

$$\tau = 2 + \delta^{-1}. \tag{7.3}$$

For the two- and three-dimensional Ising models one then obtains $p = 8/15$ and $p \cong 16/25$, respectively, as compared with the classical model values of $1/2$ and $2/3$ respectively. The Fisher model has many defects, including the obvious one noted by Fisher that the value of p obtained from (7.2) violates the inequality $p \geq (d-1)/d$ for $d = 3$. Thus one must be careful when reading the cluster dynamics literature not to take this model too seriously. Many attempts have been made to improve the Fisher model (Kiang and Stauffer, 1970; Reatto, 1970; Stauffer *et al.*, 1971; Stauffer and Kiang, 1971; Reatto and Rastelli, 1972). An interesting modification

was also proposed by Domb (1976) who estimated the effects of (a) excluded volume interactions between clusters and (b) the contribution of ramified droplets.

Another *ansatz* for n_l is a scaling form developed by Binder (1976), which is based on scaling ideas of Kadanoff (1971). Binder argued that near a critical point the contour definition of clusters is not useful. Instead he used a variable $l' = l^y$ which is a measure of the fluctuations in the order parameter of droplets whose length scale is ξ. The exponent y is an additional, unknown exponent. He argued that the cluster distribution function $n_{l'}$ satisfied a scaling form

$$n_{l'} = (l')^{-(2+\delta^{-1})}\tilde{n}_{l'}(Hl', \varepsilon l'^{1/\beta\delta}). \tag{7.4}$$

The above definition of l' corresponds to the "fluctuation clusters" mentioned in Section VII.A. Binder also argued that (7.4) should agree with the classical droplet model results (2.1) and (2.2) for very large droplets. He thus found that a cluster of l atoms occupies a volume $V_l \sim l^{y(1+\delta^{-1})}$ and contains an excess "mass" l^y. Binder has also discussed the interpretation of the Fisher model within this scaling theory.

Equations (7.1) and (7.4) are the only results from cluster models which we will need in our discussion of cluster dynamics. Nevertheless, it is important to realize that there have been many significant developments in cluster theory in the past few years. Much of this progress has come from ideas developed in the study of percolation. An excellent summary of clusters in the context of percolation is given by Stauffer (1979). His review also contains discussions of the Fisher and Domb models and related work. Since these recent developments should eventually be useful in cluster dynamics, we review them very briefly below.

Recently, rigorous inequalities for the equilibrium cluster distribution function for the Ising model have been obtained (Delyon, 1979; Aizenman *et al.*, 1980). These give upper and lower bounds on n_l in various regions of the thermodynamic domain. Although these results do not in themselves provide a theory for n_l, they are of use in ruling out various phenomenological models. A second interesting area of research has been in the development of better cluster models. The work by Domb on ramified droplets has led to many subsequent studies and refinements of his original ideas (Stauffer, 1979). These include a model proposed by Coniglio and Klein (1980) in which a microscopic definition is given for "fluctuation" clusters for the Ising model. Stauffer (1981) has shown in Monte Carlo studies that this model gives a more accurate description of the critical behaviour of Ising systems than earlier cluster models. Also, Bruce and Wallace (1981) have constructed a droplet theory of Ising systems which is valid near $d = 1$. Their starting point is (4.62), with R_c replaced by R. By renormalization group arguments they are able explicitly to calculate

the droplet distribution function and thereby provide a unified description of droplets of *all* scale sizes near $d = 1$. Their explicit scaling form for n_l disagrees with the phenomenological form (7.4). This disagreement arises from a sum rule which is satisfied by the Bruce–Wallace n_l, but not taken into account in the derivation of (7.4). The work by Bruce and Wallace seems to be the most significant development in recent research on droplet models. It should be very interesting to improve existing cluster dynamics theories (Section VII.D) by incorporating their results, even if this would be limited to d near 1.

It should also be noted that the Fisher and Domb models imply singularities in the free energy which are different from that proposed by Langer ((4.57) and (4.58)). We do not discuss these here, but refer the reader to a lucid summary by Domb (1976) of the predictions of both models. As noted in Section IV, existing evidence supports Langer's form for the essential singularity. In view of the subtlety of this problem, the subject will quite likely remain controversial and unsettled until rigorous results are obtained. It should also be noted that attempts have been made by Klein (1980, 1981) to incorporate both compact fluctuations and ramified fluctuations in a renormalization group description of first order phase transitions. Klein's 1981 paper contains a discussion of both the Langer singularity and spinodal singularities. Additional references dealing with the essential singularity include Binder (1976) and Zia (1981). Binder (1976) discusses a crossover from Fisher to classical droplet behavior as the droplet size increases, as well as the relevance of this to the problem of the essential singularity.

We conclude by noting that several Monte Carlo studies of various aspects of cluster models exist. The relationship between the surface area S and the size l (i.e. the Fisher parameter p) has been studied by Binder and Stauffer (1972) and Binder and Müller-Krumbhaar (1974). Related questions such as the difference between a droplet interface and bulk interfaces (Binder and Kalos, 1980) and the validity of using a mean surface (rather than a distribution of surface areas) in cluster theories (Binder and Stauffer, 1972; Binder, 1976) have been investigated. A recent study of the interface free energy of clusters is due to Furukawa and Binder (1982). Domb and Stoll (1977) have also examined the relative importance of ramified clusters. Several studies of the validity of the Fisher model have also been carried out (Stoll *et al.*, 1972; Binder and Müller-Krumbhaar, 1974; Müller-Krumbhaar, 1974a; Müller-Krumbhaar and Stoll, 1976; Kalos *et al.*, 1978). It should be noted that the original conclusions concerning the validity of the Fisher model for $d = 2$ (Stoll *et al.*, 1972; Binder and Müller-Krumbhaar, 1974) are now thought to be incorrect (D. Stauffer, private communication). Recent Monte Carlo studies of metastability have been carried out on the Glauber model with "long-range" interactions

(Heermann *et al.*, 1982; Heermann and Klein, 1983). The latter study reveals an interesting crossover from a classical to lattice animal behavior associated with a percolation transition. Other interesting Monte Carlo calculations have been carried out on spinodal decomposition for 50:50 mixtures on d-dimensional hypercubes at zero temperature (Levy *et al.*, 1982; Meakin and Reich, 1982). We finally remark that the discussion in this section has been restricted to lattice clusters. We do not consider the more difficult problem of characterizing clusters in fluids, such as occur in molecular dynamics studies (Lee *et al.*, 1973; Abraham, 1974b; Binder, 1975b; Abraham and Barker, 1975; Miyazaki *et al.*, 1977; Binder and Kalos, 1980).

C. Kinetic equations

We now summarize the dynamical theory of cluster formation as developed by Binder and collaborators. One can envisage three different processes that change a given cluster pattern: evaporation–condensation, dissociation–coagulation and diffusion (Fig. 14). The evaporation–condensation and dissociation–coagulation mechanisms are caused by "cluster reactions" and imply a change of the size l of the cluster. Diffusion refers to processes in which the size of the cluster does not change but the center of gravity of the cluster does change. It is important to note that the condensation process is a special case of coagulation of a cluster of size l with a monomer ($l' = 1$). If we ignore cluster diffusion, we can write an equation for the evolution of the number of clusters of size l, $n_l(t)$, which takes into account the processes of cluster reaction:

$$\frac{\mathrm{d}}{\mathrm{d}t}[n_l(t)] = \sum_{l'=1}^{\infty} S_{l+l',l'} n_{l+l'}(t) - \tfrac{1}{2} \sum_{l'=1}^{l-1} S_{l,l'} n_l(t) + \tfrac{1}{2} \sum_{l'=1}^{l-1} C_{l-l',l'} n_{l'}(t) n_{l-l'}(t) - \sum_{l'=1}^{\infty} C_{l,l'} n_l(t) n_{l'}(t). \qquad (7.5)$$

The different terms of this equation can be understood as follows. The first term gives the increase in the number of l-clusters due to dissociation reactions $(l + l') \rightarrow (l, l')$. This is assumed to be proportional to the number of clusters of size $(l + l')$ which are present, where $S_{l+l',l'}$ is the appropriate proportionality coefficient. The second term represents the decrease of l-clusters caused by dissociation reactions $l \rightarrow (l - l', l')$ and is again assumed to be proportional to the number n_l of l-clusters. The factor of 1/2 accounts for overcounting pairs in the summation. The third term represents the increase of l-clusters by coagulation of clusters of size l' and $l - l'$. This is

the reverse process of that represented by the second term. The fourth term represents the decrease of l-clusters by coalescence reactions $(l, l') \rightarrow (l + l')$. This interpretation of eqn (7.5) is phenomenological and is very similar to the law of mass action for chemical reactions. A "derivation" of (7.5) can be given by interpreting $n_l(t)$ as the probability density of having a cluster of size l at time t. One then postulates a Markovian stochastic process in l-space governed by a master equation

$$\frac{\partial n_l(t)}{\partial t} = -\sum_{l'} \omega(l \rightarrow l') n_l(t) + \sum_{l'} \omega(l' \rightarrow l) n_{l'}(t), \qquad (7.6)$$

where $\omega(l \rightarrow l')$ is the transition probability for the state l changing to a state l'. By an appropriate choice of transition probabilities $\omega(l \rightarrow l')$ and $\omega(l' \rightarrow l)$ one can obtain (7.5) from (7.6). It is important to note that the underlying physics in (7.5) requires a specification of the coefficients S and C. A more ambitious justification of (7.5) has been given elsewhere (Binder *et al.*, 1975; Binder and Stauffer, 1976). The underlying idea is to derive (7.5) by appropriate approximations from a master equation (eqn (9.6)) which defines the kinetic Ising model. If one includes enough variables to describe a cluster, one can, in principle, get information as detailed as that given by the microscopic spin configuration. This may be thought of as a change of variables. The quantity $n_l(t)$ is then interpreted as the average number of clusters of size l, with the average taken over all variables (other than l) which are necessary to specify the cluster completely. To obtain eqn (7.5) two main assumptions are then made. The first is a mean field treatment of the "irrelevant" variables. This involves a factorization of the averages with respect to these variables. The second is the assumption that the effective reaction rates in the restricted l-space are Markovian. This is clearly an approximation, since generally speaking the elimination of variables leads to non-Markovian effects.

It is worth noting that if one considers Glauber dynamics (Glauber, 1963) instead of the Kawasaki exchange dynamics (Kawasaki, 1972) appropriate for binary alloys, an equation essentially identical to (7.5) still holds. The main mechanisms that lead to pattern evolution are still dissociation–coagulation processes. In this case, however, the number of particles in the clusters is not conserved by the cluster reaction (Binder *et al.*, 1975). Typical cluster evolutions for the conserved and nonconserved (Kawasaki and Glauber) models are shown in Figs 16 and 17.

The next step in treating (7.5) is to assume detailed balance. This means that the equilibrium cluster distribution n_l is a solution of (7.5), with inverse processes having equal rates. We assume these rates to be the ones governing the nonequilibrium process. The detailed balance condition is thus

$$S_{l+l',l'} n_{l+l'} = C_{l,l'} n_l n_{l'} \equiv W(l, l'). \qquad (7.7)$$

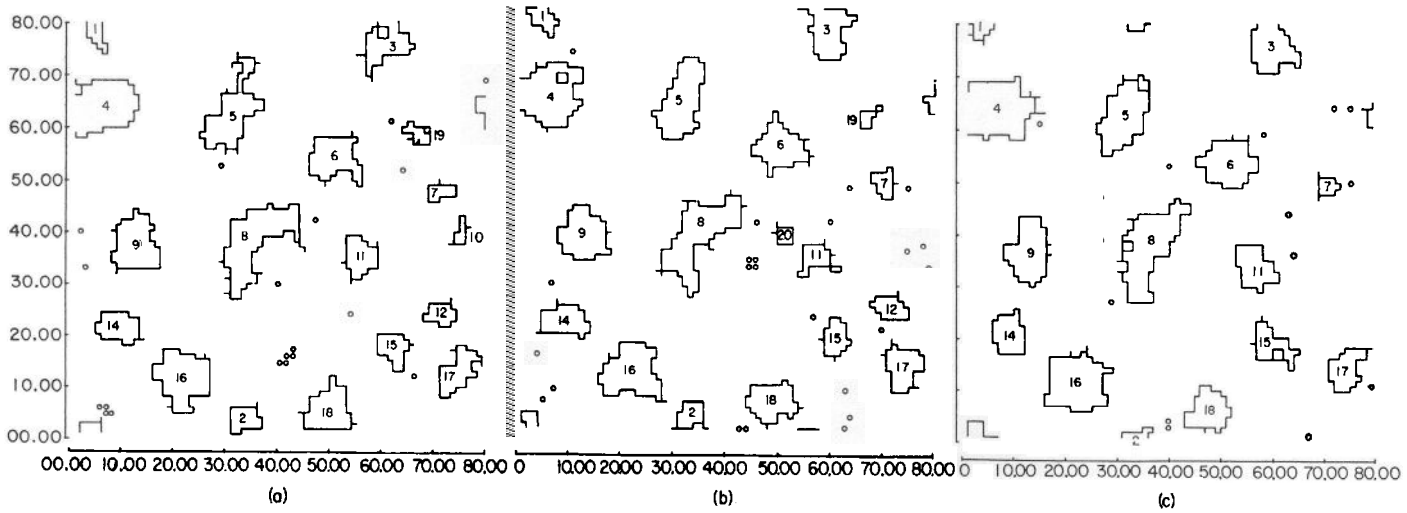

FIG. 16. Snapshots of the atomic configurations evolving with Kawasaki dynamics on an 80×80 lattice at 20% concentration of A atoms and $T = 0.59T_c$. The configurations displayed are at times (a) $t = 11222$; (b) $t = 12494$; (c) $t = 17098$. All clusters of size greater than 10 are labeled. Open circles correspond to monomers. (From Rao *et al.*, 1976.)

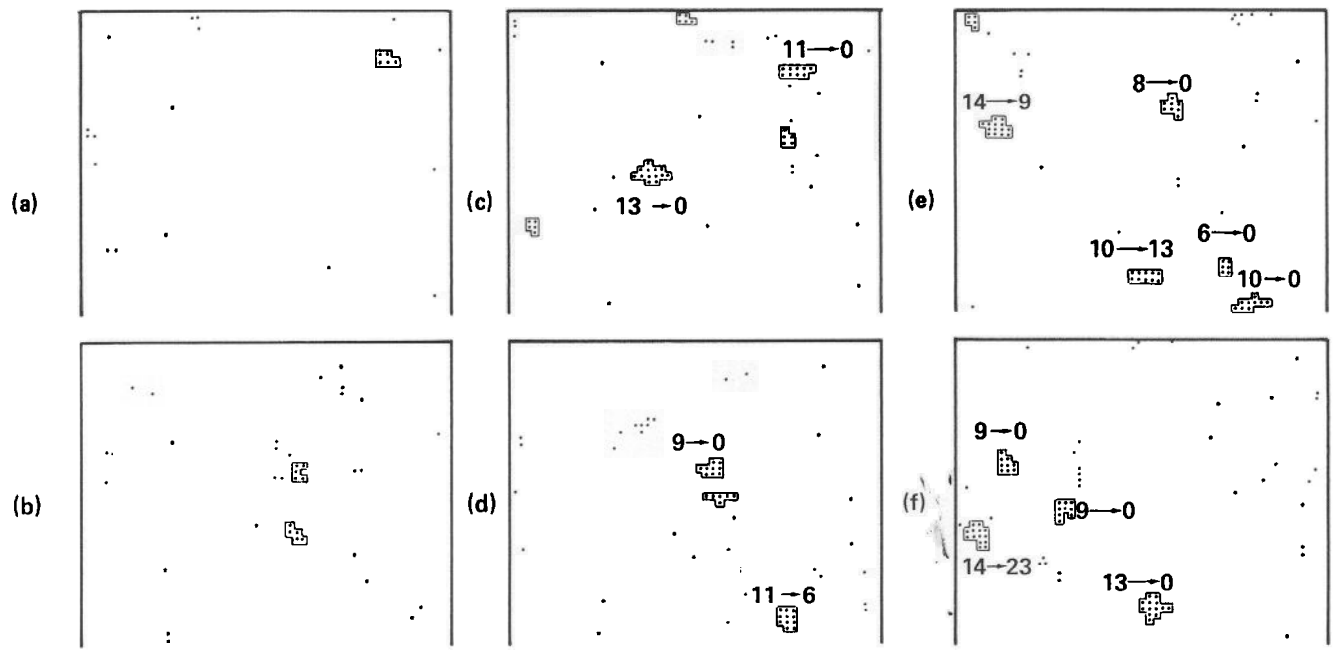

FIG. 17. Snapshot pictures from a Monte Carlo simulation (Glauber dynamics) of the evolution of a 55×55 square Ising lattice, in thermal equilibrium at $T/T_c \simeq 0.7$ (first picture) after switching the magnetic field from zero to $\mu_B H/k_B T = -0.16$. The time interval between two successive snapshots is five Monte Carlo step/spins (MCS) (see Section IX.A). Reversed spins are indicated by black dots while up spins are not shown. Clusters with $l > 5$ are set off by contours. The reaction $(l \rightarrow l')$ indicates the development of a cluster with l spins from the present (l) to the next (l') configuration. Later on the two largest clusters (with $l = 42$ in the last picture) form stable domains of the new phase. (From Binder and Stauffer, 1976.)

This assumption is completely analogous to the one made in Monte Carlo simulations (Section IX). Its validity is an open issue. It automatically yields the correct equilibrium solution and also allows one to replace the set of rates C and S by the single rate W and the equilibrium distribution n_l. We then have

$$\frac{dn_l(t)}{dt} = \sum_{l'=1}^{\infty} \frac{n_{l+l'}(t)}{n_{l+l'}} W(l, l') - \tfrac{1}{2} \sum_{l'=1}^{l-1} \frac{n_l(t)}{n_l} W(l-l', l') + \tfrac{1}{2} \sum_{l'=1}^{l-1} \frac{n_{l'}(t)}{n_{l'}} \frac{n_{l-l'}(t)}{n_{l-l'}} W(l-l', l') - \sum_{l'=1}^{\infty} \frac{n_l(t)}{n_l} \frac{n_{l'}(t)}{n_{l'}} W(l, l'). \quad (7.8)$$

(We use the same notation as in Section II, with n_l denoting the equilibrium cluster distribution and $n_l(t)$ the time-dependent distribution.) Equation (7.8) does not include cluster diffusion. The above treatment can be generalized to include the center of mass $\vec{x}$ of the cluster as another coordinate, so that with an appropriate diffusion constant D_l

$$\frac{\partial}{\partial t} n_l(\vec{x}, t) = D_l \nabla^2 n_l(\vec{x}, t) + \quad (7.9)$$

where on the right-hand side one would include terms similar to those in (7.8). By integrating over $\vec{x}$ in (7.9) one recovers (7.8). A discussion of diffusion processes is postponed until Section VII.E. We note that (7.8) only includes the processes shown in Fig. 14. Thus, for example, reactions which involve three or more clusters are excluded.

Also, as mentioned above, the whole treatment makes no sense when the concentration of the minority phase is large enough for percolation to occur. To avoid this difficulty one must interpret l in a sense different from the strict contour picture that we are using here. Finally, it should be kept in mind that (7.8) can also be applied to systems like liquid mixtures by appropriate choices of $W(l, l')$.

Equation (7.8) is the starting point for the different developments of the cluster theory. An important thing to notice is that (7.8) contains information about all the processes of evaporation–condensation and coagulation. Therefore one can formally rearrange it (given some approximations) so that it displays explicitly a term corresponding to the classical nucleation equation and another corresponding to the classical coagulation equation. The equation one obtains is

$$\frac{\partial n_l(t)}{\partial t} = \frac{\partial}{\partial l}\left(R_l n_l \frac{\partial}{\partial l} \frac{n_l(t)}{n_l}\right) + \tfrac{1}{2} \int_{l_c}^{l} dl' W(l-l', l') \frac{n_{l'}(t)}{n_{l'}} \frac{n_{l-l'}(t)}{n_{l-l'}} - \frac{n_l(t)}{n_l} \int_{l_c}^{\infty} dl' W(l, l') \frac{n_{l'}(t)}{n_{l'}}, \quad (7.10)$$

where the kinetic coefficient R_l is

$$R_l = \frac{1}{n_l} \sum_{l'=1}^{l_c} (l')^2 W(l-l'). \quad (7.11)$$

The first term in (7.10) is the Becker–Döring nucleation equation (Section II). The last two terms correspond to the standard coagulation equation (Friedlander and Wang, 1966; Dunning, 1973; Drake, 1973). To obtain equation (7.10) from (7.8) one considers separately clusters of size $l' < l_c$ and $l' > l_c$, where l_c is a cut-off such that the volume V_{l_c} associated with a cluster of size l_c is $V_{l_c} \sim \xi^d$. The classical picture of nucleation considers large clusters of size $l \gg 1$ reacting with small clusters of size $l' < l_c$. The density of these small clusters $n_{l'}(t)$ is taken as the equilibrium concentration of the one-phase supersaturated metastable state. Thus the first term in (7.10) follows by expanding $W(l-l', l')$ and $n_{l\pm l'}(t)/n_{l\pm l'}$ around $l' = 0$, with $n_{l'}(t) = n_{l'}$. For clusters with $l' > l_c$, dissociation processes can be neglected and sums can be replaced by integrals. These assumptions lead to the coagulation terms of (7.10).

At this point it is necessary to consider the conservation law for the number of particles. This can be written as

$$\frac{d}{dt} \sum_{l=1}^{\infty} l n_l(t) = 0. \quad (7.12)$$

This conservation law is satisfied by (7.8) when the symmetry relation $W(l, l') = W(l', l)$ is fulfilled, but it is not satisfied by (7.10). In fact, in classical nucleation theory the conservation law is not imposed. This is so because there one considers an equilibrium metastable phase at a given supersaturation in which the droplets are formed. Obviously the formation of droplets decreases the supersaturation (a depletion effect). Although this may not be important at earlier times, it becomes crucial at later times when the conservation law dominates the dynamics. This occurs in the Lifshitz–Slyozov theory discussed in Sections VI and VII.E. One can formally include the conservation law in eqn (7.10) by assuming a time-dependent supersaturation through which n_l and $W(l, l')$ depend implicitly on time. The same eqn (7.10) is then valid, but with a time-dependent supersaturation which must be determined self-consistently (Binder, 1977). Finally it is worth stressing that any information to be extracted from (7.10) is based on some *a priori* knowledge or assumption about the functions $W(l, l')$, R_l and n_l. In particular, an important quantity is the equilibrium droplet distribution n_l, as noted in Section VII.B.

D. Nucleation theory

In this section we present a cluster dynamics theory of nucleation. At least two main results have emerged from the theoretical study. One is the concept that an experimentally significant quantity in nucleation is the completion time (Binder and Müller-Krumbhaar, 1974; Binder *et al.*, 1975; Binder and Stauffer, 1976). This is a measure of the time it takes the phase separation process initiated by nucleation to reach completion. We postpone our discussion of completion time to Section X, where we show its usefulness in understanding nucleation experiments in binary fluids. A second result is a scaling law for the nucleation rate near a critical point. This prediction does not rely on a specific choice for n_l, but does involve scaling assumptions for n_l and the cluster reaction rate R_l. (The scaling of the nucleation rate also implies a scaling form for the completion time.) To obtain a specific form for the nucleation rate requires further, model-dependent approximations for n_l and R_l. As we discuss below, the current cluster theory for the nucleation rate per unit volume disagrees with the field theoretic prediction, as given by (4.45). This disagreement is due to the difference between the field theoretic and cluster dynamics descriptions of droplets.

The starting point for the cluster theory of nucleation is the nucleation–coagulation equation (7.10). The first step is to neglect the coagulation terms in (7.10), which leads to the equation

$$\frac{\partial n_l(t)}{\partial t} = \frac{\partial}{\partial l}\left\{R_l n_l \frac{\partial}{\partial l}\left[\frac{n_l(t)}{n_l}\right]\right\}, \tag{7.13}$$

This is formally the same as the Becker–Döring equation (2.14). However, at this point one need not make the Becker–Döring approximations (2.1), (2.2) and (2.15) for n_l and R_l. Rather, one can use (7.13) to obtain a general scaling theory for the nucleation rate per unit volume, I/V, in the vicinity of a critical point. One first assumes that l in (7.13) is to be interpreted in the "fluctuation cluster" sense as the measure of excess order parameter in the cluster. (This means that l is to be identified with $l' = l^y$, mentioned in Section VII.B.) Second, one assumes that n_l has the scaling form (7.4). Third, one assume that the dynamic coefficient R_l satisfies a dynamic scaling form

$$R_l = l^r \tilde{R}(\varepsilon l^{1/\beta\delta}, Hl), \tag{7.14}$$

where

$$r = (2 - \nu z)/\beta\delta \tag{7.15}$$

and z is the usual dynamical exponent. A scaling form for I then follows by substituting (7.4) and (7.14) into the steady state solution (2.17), which

yields (Binder and Müller-Krumbhaar, 1974; Binder *et al.*, 1975; Binder and Stauffer, 1976)

$$\frac{I}{V} = A\,\varepsilon^j \tilde{J}(H/\varepsilon^{\beta\delta}) \tag{7.16}$$

with

$$j = \beta(\delta + 1) + \nu z. \tag{7.17}$$

The constant A is system-dependent, but $\tilde{J}$ is a universal function for systems which belong to the same dynamic universality class. Note that the Langer–Turski and Langer–Schwartz forms (4.45) and (4.46) for the binary fluid are examples of (7.16), but with specific predictions for $\tilde{J}(x)$, with $H/\varepsilon^{\beta\delta} \to x$. (Their D/ξ^5 factor corresponds to ε^j in (7.16).)

To obtain a specific form for $\tilde{J}$ in (7.16) one needs to introduce a particular cluster model. As noted in Section VII.B two different choice have been made for n_l. If one uses the classical model (2.1) and (2.2) and evaluates (2.17) by the same procedure as used in obtaining (2.19), one obtains for the scaling function

$$\tilde{J}_c \sim \exp\{-(x_1/x)^{d-1}\}. \tag{7.18}$$

(We have omitted pre-exponential factors.) If one uses the Fisher model, ((7.1)–(7.3)), one finds by a similar method

$$\tilde{J}_F = Bx^{-(j-1/2)/(\beta\delta-1)} \exp\{-(x_2/x)^{1/(\beta\delta-1)}\}, \tag{7.19}$$

where x_1 and x_2 are constants (Binder and Stauffer, 1976). Since (7.18) and (7.19) are derived from (2.17) by "saddle point" approximations, they are only valid for small supersaturation, $x \ll 1$. (In this domain $x = H/\varepsilon^{\beta\delta}$ is proportional to the undercooling ratio $\delta T/\varepsilon T_c$, as in (4.38).) It should be noted that very near the coexistence curve, with $x \to 0$, it is expected that (a) the classical droplet model should be correct and (b) the prefactor in (7.18) would contain contributions from R_l and from logarithmic corrections to the activation energy ε_l which are difficult to assess (Binder and Stauffer, 1976). (Recently Furukawa and Binder (1982) have performed Monte Carlo studies of the free energy of cluster formation. They have found that the activation energy is appreciably different from that given by classical theory. A better analytical understanding of these results should lead to an improved calculation of the nucleation rate.)

A modified classical model has also been proposed, whose prefactor is such as to satisfy scaling (Binder, 1980a). The universal function for this model is

$$\tilde{J}(x) = x^{-(j-1/2)/(\beta\delta-1)} \exp\{-(x_1/x)^{d-1}\}. \tag{7.20}$$

Thus the cluster theory prediction for the nucleation rate is (from (7.16) and (7.20))

$$\frac{I}{V} = A\varepsilon^{j} x^{-(j-1/2)/(\beta\delta-1)} \exp\{-(x_1/x)^{d-1}\}. \tag{7.21}$$

If one compares (7.21) with the field theory prediction for the binary fluid, (4.45), one sees that the exponential terms are the same (within some multiplicative constant). Since $(j - 1/2) \simeq 5/2$ and $(\beta\delta - 1) \simeq 9/16$ for the binary fluid, the prefactors in (4.45) and (7.21) are different. Although this is a small numerical difference, the two theoretical predictions are nevertheless different. A resolution of this discrepancy has yet to be given. It should also be remarked that the Bruce–Wallace equilibrium results for n_l presumably modify Binder's pre-exponential exponent in (7.21), at least near $d = 1$ (Bruce and Wallace, 1981).

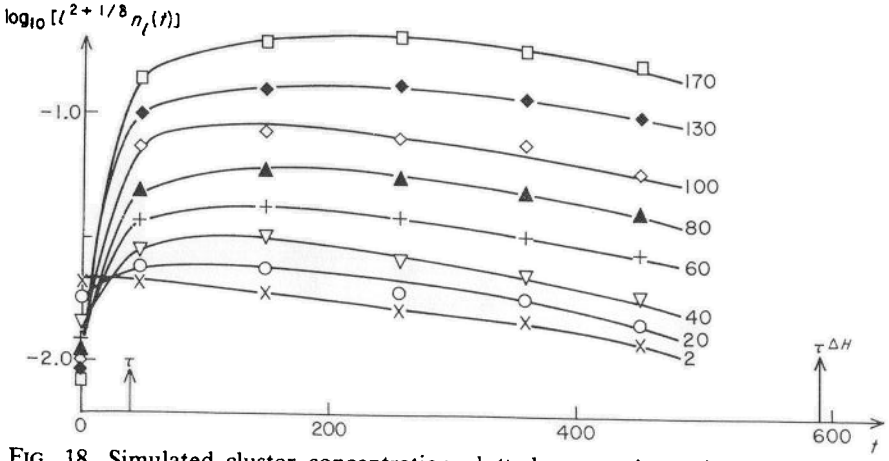

FIG. 18. Simulated cluster concentration plotted versus time t in Monte Carlo step/spins (MCS) for a $d = 2$ square Ising model at $T/T_c \simeq 0.96$ and $\mu_B H/k_B T = -0.015$. The parameter of the curve is l. The variables τ and $\tau^{\Delta H}$ indicate the equilibrium relaxation time and the nonlinear relaxation time respectively, discussed in Section XIII. (From Binder and Stauffer, 1976.)

It should be observed that this discussion of nucleation theory based on (7.13) has assumed that a single variable, l, is sufficient to characterize the cluster. A generalization of (7.13) to a multi-coordinate description of clusters has been given by Binder and Stauffer (1976). The resulting saddle point calculation for I/V is very analogous to the Langer field theory calculation (Section IV). Although a formal expression was obtained for I/V, no explicit evolution (such as given by (7.21)) was carried out. We should also note one particular attempt which has been made to determine

the validity of a single-coordinate cluster equation such as (2.18) (Binder and Stauffer, 1976). This consisted of a numerical investigation of the two-dimensional Glauber model. Although the results were in quite reasonable agreement with such a description, an unequivocal answer cannot yet be given. However, it is interesting to note the behaviour of $n_l(t)$ obtained in the above study, which is shown in Fig. 18. It can be seen that after a certain time (of the order of the equilibrium relaxation time), a plateau is reached which corresponds to the quasi-stationary state n_l^s, on which (2.18) (together with the boundary condition (2.16)) is based. A true steady state solution does not exist. Eventually $n_l(t)$ departs from its plateau value when droplet growth of macroscopic domains becomes important. The resultant decrease in $n_l(t)$ is due to the effects of coagulation and decrease in supersaturation which are not included in the approximate equation (7.13) (see also Section IX.E).

E. Lifshitz–Slyozov theory

In the following we sketch a derivation (Binder, 1977) of the Lifshitz–Slyozov prediction for domain growth, based on (7.10). This complements the discussion of Section VI. We recall that the Lifshitz–Slyozov theory consists of an asymptotic, $t \to \infty$, solution of a continuity equation for the cluster distribution, supplemented by a conservation law. The drift velocity in such an equation is obtained by considering a diffusive growth of large spherical droplets. With these ideas in mind it is clear how to obtain the Lifshitz–Slyozov result from a cluster dynamics theory. We first neglect the coagulation events in (7.10) which are not considered in the Lifshitz–Slyozov theory. This yields (7.13). We also neglect the diffusion part $(\partial^2/\partial l^2)$ of (7.13) with respect to the drift part $(\partial/\partial l)$. This last assumption makes sense for late times. The resultant equation is a continuity equation, in which the equilibrium distribution n_l is taken to be given by the classical droplet model appropriate for large droplets. In addition we introduce a time-dependent field H in order to satisfy the conservation law for the number of particles. We then have

$$\frac{\partial n_l(t)}{\partial t} = -\frac{\partial}{\partial l}(v_l n_l(t)), \tag{7.22}$$

$$v_l = R_l[2H(t) + \sigma]/k_B T. \tag{7.23}$$

We must now specify R_l to determine the drift velocity. The appropriate choice for diffusive growth is $R_l \sim l^{1-2/d}$ (Chandrasekhar, 1943; Penrose

and Lebowitz, 1979). Then for $d = 3$ one has

$$v_l \sim \left[\left(\frac{l}{l_c}\right)^{1/3} - 1\right]. \tag{7.24}$$

The critical size $l_c^{1/3}$ is, from (7.23), inversely proportional to the field $H(t)$, in the same way that R_c is inversely proportional to H in (4.18). The form (7.24) is the LSW velocity (4.34), while (7.22) is the continuity equation (6.3), The LSW result for the growth rate can then be obtained from introducing a time-dependent scaling solution of (7.22),

$$n_l(t) = t^y \tilde{n}(lt^{-x}), \qquad l \to \infty, t \to \infty. \tag{7.25}$$

From (7.25) and the conservation law (7.12) one obtains $y = -2x$. Equation (7.25) is a solution of (7.22) if $x = d/3$, which is the LSW growth law. Equation (7.25) is the scaling solution (6.7). In Section IX we discuss the $t^{1/3}$ growth law and the scaling function $\tilde{n}$ in the context of Monte Carlo studies.

The solution (7.25) can also be used to obtain the asymptotic time dependence of the excess energy associated with the surface of a droplet, using the relation

$$\Delta u(t) = u(t) - u(\infty) = \sum_l u_l n_l(t). \tag{7.26}$$

If one assumes that the droplets are spherical, then $u_l \propto S_l \propto l^{1-1/d}$. Thus from (7.25) one obtains

$$\Delta u(t) \sim t^{-b'}, \qquad b' = 1/3. \tag{7.27}$$

We conclude by summarizing the differences between the LS theory of diffusive droplet growth and the Becker–Döring theory of nucleation. The LS theory neglects the diffusion term, satisfies the conservation law (through the introduction of a time-dependent field $H(t)$), and assumes that $R_l \sim l^{1-2/d}$, rather than the Becker–Döring assumption $R_l \sim S_l \sim l^{(d-1)/d}$.

F. Binder–Stauffer theory of cluster growth

We now discuss an approximate solution of (7.10) which yields the phenomenological Binder–Stauffer (1974) theory for cluster growth at intermediate times. As we discuss below, the validity of the detailed Binder–Stauffer predictions for finite temperatures is unclear. Nevertheless, it is evident that the mechanism of cluster growth considered in their theory is important. What is not clear at the moment is its relative importance as compared to other mechanisms. Since the Binder–Stauffer theory has often been

used in analyzing Monte Carlo and experimental results, we discuss it here in some detail. We begin by summarizing the physical ideas involved.

Their basic assumption is that there exists an intermediate time domain in which clusters of intermediate size diffuse without changing size, until eventually two such clusters coalesce. This coagulation is the Binder–Stauffer growth mechanism and results from the diffusion of clusters. There are at least four mechanisms for diffusion, as shown in Fig. 19. In Fig. 19(a) an atom moves at the surface without any cost of energy. In Fig. 19(b) a

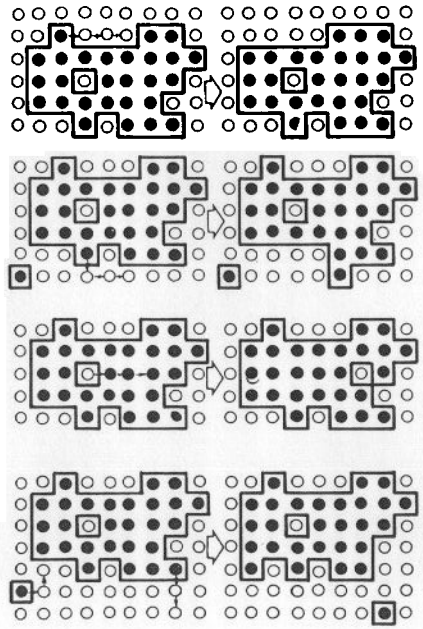

FIG. 19. Schematic illustration of four different mechanics of cluster diffusion. (From Binder and Kalos, 1980.)

monomer evaporates and condenses again in the cluster. The clusters are considered to be diffusing, free Brownian particles. Thus the diffusion constant can be estimated to be $D_l \simeq \omega(\Delta x_G)^2$, where Δx_G is the shift in the center of mass position produced by a given process and ω is the rate at which such processes occur. The center of mass is defined as

$$\vec{x}_G = \frac{1}{l}\sum_i \vec{x}_i, \tag{7.28}$$

where the sum runs over the atoms of the cluster. (We have used the fact that the total mass of the cluster is proportional to its volume V_l, with

$V_l \sim l$ for low temperatures.) The net effect in each of these two processes is that an atom changes its position by a few lattice constants, so that $\Delta x_G \sim l^{-1}$. The rate of these processes is proportional to the number of surface sites, which for low temperatures is given by $S_l \sim l^{1-1/d}$. Therefore

$$D_l \sim l^{-\alpha}, \qquad \alpha = 1 + 1/d. \tag{7.29}$$

In Fig. 19(c) diffusion results from an interior displacement of one of the atoms of the species forming the matrix in which clusters diffuse. These "bubbles" inside the cluster of course become more important at higher temperatures. By a reasoning similar to that given above, one obtains

$$D_l \sim l^{-1}. \tag{7.30}$$

The difference between (7.29) and (7.30) arises from the fact that the number of sites that can participate in the process is proportional to $V_l \sim l$. Finally, in Fig. 19(d) diffusion occurs by condensation of one monomer and evaporation of a second monomer on the other side of the cluster. In this case the displacement of the center of gravity is of order $l^{-1+1/d}$, due to the fact that the change in the coordinate x_i of the atom that has changed position is of the order of the linear dimension of the cluster, $l^{1/d}$. The number of possible participating sites is proportional to S_l, so that

$$D_l \sim l^{-1+1/d}. \tag{7.31}$$

For large l this particular mechanism therefore would appear to dominate those illustrated in Fig. 19(a), (b) and (c). However, one also has to take into account the fact that for low temperatures it is much more probable that the configuration for the processes illustrated in Fig. 19(a) and (b) occurs than the configuration illustrated in Fig. 19(d), which involves monomers. As a consequence, one expects (7.29) to hold at very low temperatures. At larger temperatures D_l will behave as in (7.29) for small l, but for larger l it will cross over to the behaviour given by (7.31). The effective exponent of D_l will therefore vary with temperature. This crossover behaviour seems to be in agreement with Monte Carlo data (Binder and Kalos 1980; Fig. 20).

We now return to a discussion of the Binder–Stauffer theory of cluster growth, which considers a diffusion constant given by (7.29). The cluster size evolution can be obtained from this form of D_l by noting that coalescence of two clusters will produce a change in size of order Δ^d, where Δ is the mean distance between clusters. If one estimates the time needed for a cluster to diffuse (with a diffusion constant given by (7. 29)) over a distance Δ (the only characteristic length in the problem), one easily obtains that the characteristic size l is proportional to $t^{d/(3+d)}$. It is interesting to note that, in contrast to the Lifshitz–Slyozov mechanism, this mechanism

is of local character. It is due to the cluster diffusion which results from evaporation and condensation of monomers as dictated by the local geometry and not by global diffusion currents. Since the $t^{d/(3+d)}$ growth law is based on the estimate (7.29) for the diffusion constant, the theory neglects the other possible processes leading to diffusion shown in Fig. 19. Since it is not at all clear that (7.29) represents the dominant diffusion mechansim, the validity of this growth law remains unclear. In fact, it could very well be incorrect to try to describe growth by a single power law behavior in a regime where there are several competing mechanisms for growth.

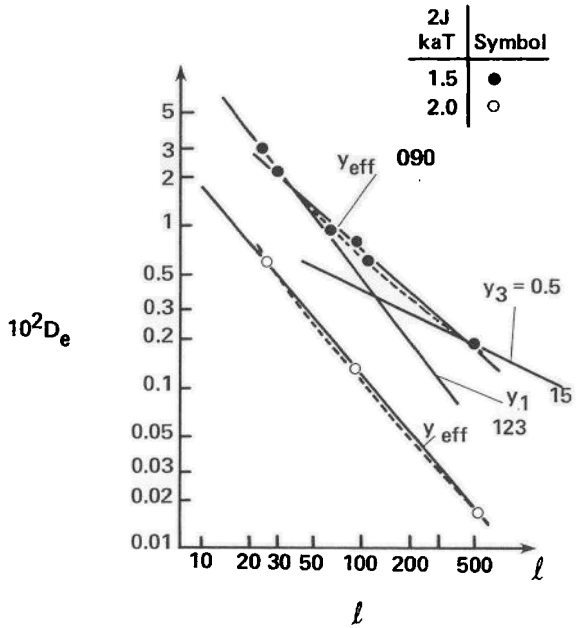

FIG. 20. Log–log plot of cluster diffusivity D_l versus l. Straight lines indicate various estimates for the exponent $\alpha(D_l \sim l^{-\alpha})$. The dashed curves represent the crossover behavior discussed in the text. (From Binder and Kalos, 1980.)

We now turn to the derivation of the Binder–Stauffer theory from the basic equation (7.10). This is done by using the basic assumptions discussed above. Namely, we first neglect the evaporation–condensation term in (7.10) (the first term) and keep the coagulation terms. The underlying picture is that the evaporation–condensation processes are taken into account via a diffusion constant for free clusters and the cluster "collisions" are taken into account by the coagulation terms. A scaling form for the

rate $W(l, l')$ is then assumed for the coagulation terms in (7.10),

$$W(l, l') = n_l n_{l'} l'^{v} \tilde{W}(l/l'). \tag{7.32}$$

This scaling assumption presumably reflects the existence of a single characteristic length in the problem. With this form of W the equation for $n_l(t)$ is now solved by (7.25) with

$$x = -2/y = (1 - v)^{-1}. \tag{7.33}$$

The remaining task is the determination of the exponent v (Binder, 1977). This is done by relating v to the behavior of D_l (as a function of l) by the two following obvious identifications:

$$\frac{\Delta m}{\Delta t} = l' (D_{l'}/\Delta^2) n_{l'}(t) \tag{7.34}$$

$$\frac{\Delta m}{\Delta t} n_l(t) \equiv W(l, l') \frac{n_l(t)}{n_l} \frac{n_{l'}(t)}{n_{l'}}. \tag{7.35}$$

Here Δm is the mass incorporated per unit time Δt into a cluster l by coalescence with clusters l' whose average distance from the cluster l is Δ.

From eqns (7.32), (7.34) and (7.35) one obtains different values of v for the different diffusion mechanisms described by (7.29)–(7.31). From (7.33) one then obtains x. For $T \to 0$ (7.29) leads to $x = d/(d + 3)$, which is the original Binder–Stauffer (1974) prediction. For intermediate temperatures below T_c, (7.30) and (7.31) lead to $x = d/(d + 2)$ and $x = d/(d + 1)$. (These predictions were not in the original Binder–Stauffer theory.) Each of these three values of x is for intermediate times, with the late time behavior given by the Lifshitz–Slyozov value of $x = d/3$. An estimate of the crossover time corresponding to the transition from the intermediate time behavior to the late time behavior is given by Binder (1977).

One can also obtain the exponent b' which characterizes the energy $\Delta u(t)$ in (7.27). One finds that for $T \to 0$, $b = 1/(d + 3)$, whereas for finite T one again has at least three possibilities, $b' = 1/(d + 1)$. $1/(d + 2)$ or $1/(d + 3)$, corresponding to the three diffusion mechanisms described above. Finally, we note that Binder and Stauffer also proposed a scaling form for the structure factor which follows from (7.25). We discuss this in Section VIII, but note here that their $T \to 0$ predictions for the exponents a' and a'' (eqns (5.34) and (5.35)) are $a' = 1/(d + 3)$ and $a'' = d/(d + 3)$.

G. Spinodal decomposition as a generalized nucleation theory

We now summarize some results for $n_l(t)$ that have been obtained by a numerical integration of the general kinetic equation (7.8). The validity

of some of the assumptions involved in this calculation is quite difficult to assess. As well, the quantitative results are probably not very accurate. However, a qualitative picture emerges which is quite interesting. For example, the cluster distribution function $n_l(t)$ changes smoothly as one varies the quench composition from the coexistence curve to the critical composition. There is thus no evidence of any sharp distinction between metastable and unstable states. In fact, one could imagine the process of spinodal decomposition as being a generalized nucleation phenomenon, as we indicate in more detail later.

To integrate (7.8) one needs *a priori* knowledge of three quantities: (1) the initial condition $n_l(0)$; (2) the equilibrium droplet distribution n_l; (3) the reaction rate $W(l, l')$. The choices given by Mirold and Binder (1977) and Binder *et al.* (1978) are the following. First, the initial condition is determined from data for the "site percolation problem" (Coey 1972; Sykes and Glen 1976; Sykes *et al.*, 1976; Stauffer, 1976; Quinn *et al.*, 1976). (This is reasonable, since the initial condition chosen corresponds to a high temperature, disordered phase in which the distribution of B atoms is completely random. This is site percolation.) One also sets $n_l(0) = 0$ for clusters larger than some cut-off size. Second, the equilibrium droplet distribution n_l is the Fisher form (7.1). This is in principle an incorrect choice (Section VII.B) but in practice probably does not qualitatively alter the results. Third, $W(l, l')$ is chosen to be

$$W(l, l') = \hat{c} n_l n_{l'} (l')^{v} \left[\left(\frac{l}{l'} \right)^{1-2/d} + \left(\frac{l}{l'} \right)^{-(1-1/d)} \right]. \tag{7.36}$$

$\hat{c}$ is a proportionality constant that sets the time scale. This form of W is based on the scaling *ansatz* (7.32) and is a simple interpolation between the asymptotic behavior for large and small values of l. (The former is given by the $(l/l')^{1-2/d}$ term and follows from the assumption $R_l \sim l^{1-2/d}$ used in the LS theory. The latter term then follows from the symmetry condition $W(l, l') = W(l', l)$.)

For the case of binary alloys at low temperatures, one chooses $v = -3/d$, as discussed in Section VII.F. (Although liquids have also been considered (Binder *et al.*, 1978), we do not discuss this case here.) Results for the binary alloy were obtained for a $d = 2$ square lattice at the concentration $c_B = 0.1$ and the temperatures $T = 0.6T_c$, $0.7T_c$ and $0.8T_c$, and also at $c_B = 0.2$ and $T = 0.8T_c$. Results were also obtained for the $d = 3$ simple cubic lattice for $c_B = 0.1$ and $T = 0.6T_c$. The qualitative behavior is similar in all these cases. Figure 21 shows a representative example. Both a minimum and a maximum are observed whose positions are shifted to larger values of l as time goes on. The minimum occurs at the critical droplet size, l_c, for nucleation. (Droplets smaller than l_c belong to the supersaturated, A-rich phase.) Droplets larger than l_c are nucleated droplets

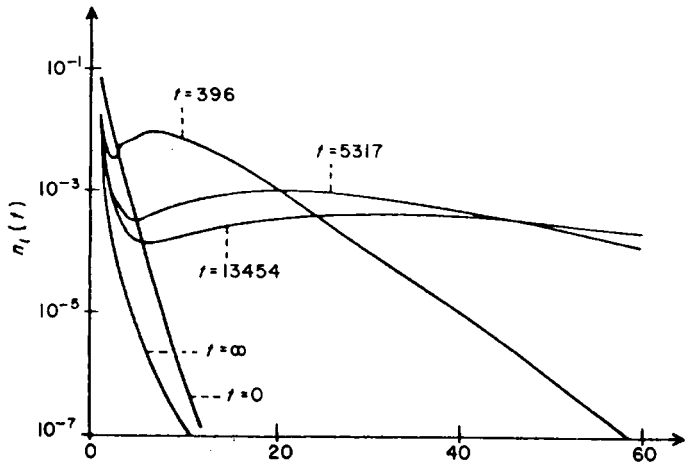

FIG. 21. Cluster size distribution for solids at $c_B = 10\%$ and $T/T_c = 0.6$. (From Mirold and Binder, 1977.)

which are undergoing growth. They have a rather broad distribution in size.

One can also obtain information from $n_l(t)$ about the approximate behavior of the time evolution of (a) the typical cluster size and (b) the excess energy of a cluster of size l. The typical cluster size can be defined in terms of the first or second moments of $n_l(t)$:

$$l_1(t) = \sum_{l>l_0} l n_l(t) / \sum_{l>l_0} n_l(t), \tag{7.37}$$

$$l_2(t) = \sum_{l>l_0} l^2 n_l(t) / \sum_{l>l_0} n_l(t) \tag{7.38}$$

(where the cut-off l_0 essentially excludes equilibrium droplets). The excess energy $\Delta u(t)$ follows from (7.26). These quantities were analyzed in terms of power law approximations, eqns (5.37), (5.38) and (7.27).

The values which were obtained for $T = 0.6T_c$ and a concentration of 10% are $a_1 = 0.35$, $a_2 = 0.38$, $b' = 0.20$ for $d = 2$ and $a_1 = 0.28$, $a_2 = 0.17$, $b' = 0.08$ for $d = 3$. These results are roughly consistent with the Binder–Stauffer predictions of Section VII.F, as well as with the Monte Carlo results discussed in Section IX. The results for higher temperatures and larger concentrations are in less satisfactory agreement with theory, particularly for $d = 3$.

We now turn to a numerical evaluation of the structure factor defined in Section IV. Since the probability that $\vec{r}\,'$ is a site of an l-cluster is by

definition $l n_2(t)$, the correlation function $\langle c(\vec{r}\,')c(\vec{r}\,'+\vec{r})\rangle$ is related to the cluster distribution by

$$\langle c(\vec{r}\,')c(\vec{r}\,'+\vec{r})\rangle = \sum_{l=1}^{\infty} l n_l(t) g_l(\vec{r}), \tag{7.39}$$

where $g_l(\vec{r})$ is the conditional probability that the site $\vec{r}\,'+\vec{r}$ is occupied by a B atom if $\vec{r}\,'$ is within an l-cluster. Therefore, one needs to know $g_l(\vec{r})$ in addition to $n_l(t)$. Binder *et al.* (1978) made a very simple approximation for $g_l(\vec{r})$, shown in Fig. 22. This assumption leads to the correct

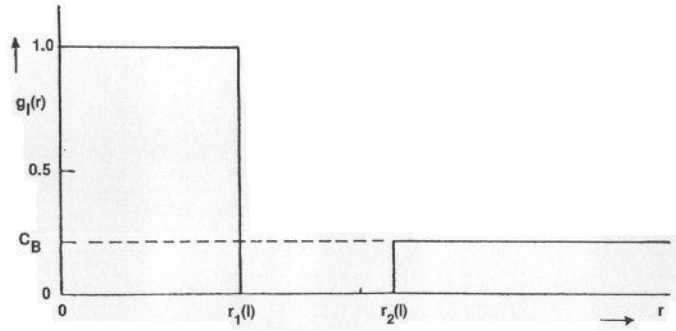

FIG. 22. A simple model of the conditional probability $g_l(r)$. Here $r_1(l)$ denotes an effective cluster radius and $r_2(l)$ an effective radius of its boundary region. (From Binder *et al.*, 1978.)

behavior $\langle c(\vec{r}\,')c(\vec{r}\,'+\vec{r})\rangle \to c_B^2$ for large r. The values of $r_1(l)$ and $r_2(l)$ are fixed such that $\hat{S}(k=0, t=0) = 0$ independently of $n_l(t)$. This satisfies the local concentration conservation for the initial random phase. The clusters are assumed to be spherical and of volume $V_0 l$. This choice of $g_l(r)$ implies also that

$$\hat{S}(k,t) \underset{k\to 0}{\to} k^2, \qquad S(k,t) \underset{k\to\infty}{\to} k^{-2}. \tag{7.40}$$

Using the $n_l(t)$ discussed previously, numerical data for $\hat{S}(k,t)$ have been obtained both for solids (Fig. 23) and fluids. The behavior of the structure factor at $c_B = 0.1$ is qualitatively the same as the one discussed in Section IX for symmetrical quenches. In spite of the crude approximation involved in this calculation, the results very clearly show the smooth transition between the nucleation and spinodal decomposition regimes. In particular, the form of the structure factor displayed is qualitatively similar to that obtained from Monte Carlo simulations in the spinodal region.

We conclude by presenting a physical picture for the gradual transition from the metastable to the unstable domain described above. We first

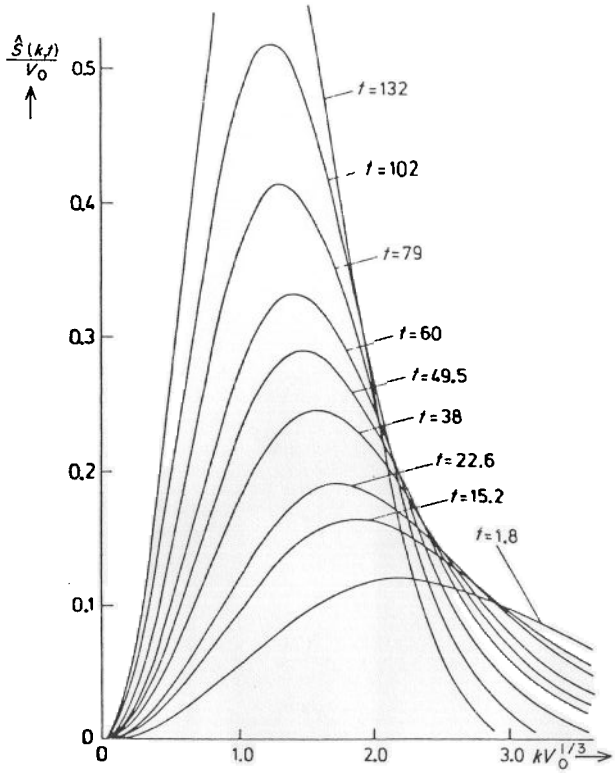

FIG. 23. Structure factor $\hat{S}(k, t)$ plotted versus k for various times after the quench from infinite temperature to $T = 0.6T_c$ for a $d = 3$ Ising model at $c_B = 0.1$. (From Binder *et al.*, 1978.)

recall the classical Cahn–Hilliard (1958, 1959) theory, which assumes the existence of a classical spinodal curve. Their analysis predicts that in the metastable region the activation energy barrier for droplet formation decreases monotonically from infinity to zero as the concentration of the minority species increases from zero to the classical spinodal value (Fig. 24). In addition the radius of the critical droplet, R_c, is predicted to diverge both at the coexistence curve and at the classical spinodal. In the Cahn linear theory of spinodal decomposition, the characteristic length k_c^{-1} (eqn (5.8)) also diverges as one approaches the classical spinodal from the unstable region. Thus in the classical pictures of nucleation and of spinodal decomposition, there is a sharp transition between metastable and unstable states as characterized by the classical spinodal curve. On the other hand, more recent work (Binder and Stauffer, 1976; Binder, 1977; Mirold and Binder, 1977) suggests a considerably different picture. First, the activation

energy never becomes zero, but rather becomes of the order k_BT at the classical spinodal curve and throughout the unstable region. Secondly, the critical radius, R_c, smoothly decreases as the concentration increases to a finite value (of the order of the correlation length ξ) at the classical spinodal and throughout the unstable region. (The critical droplet of course becomes more diffuse as the concentration increases.) Finally, the length which characterizes the instability against long wavelength fluctuations in the unstable region remains finite at the classical spinodal. These two different pictures are shown in Fig. 24. We note that this work of Binder and

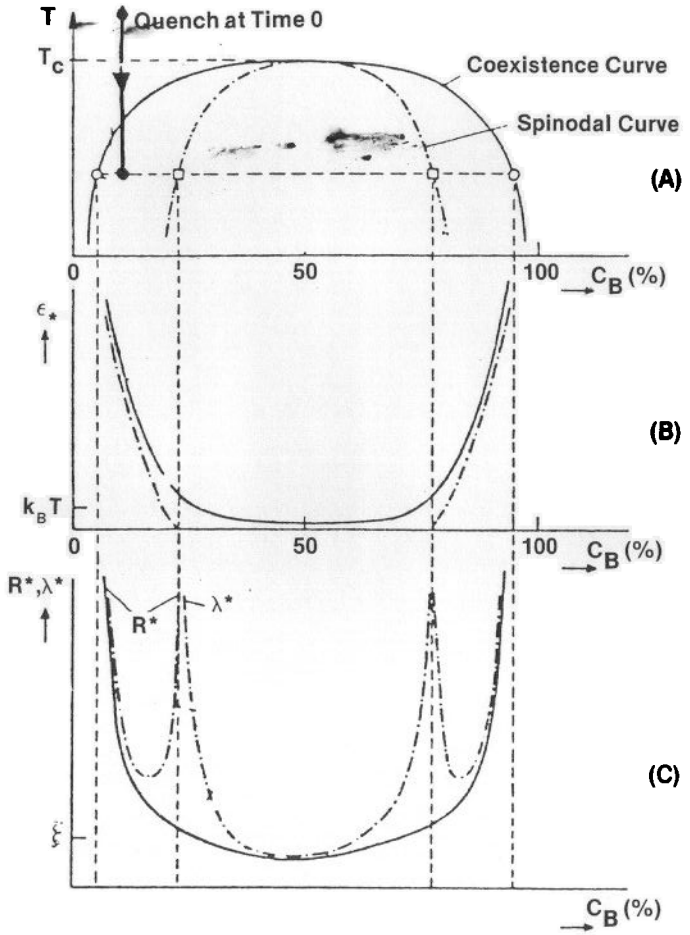

FIG. 24. (a) The schematic phase diagram of a binary mixture; (b) the behavior of the activation energy ε_{l_c} and (c) two characteristic lengths R_c and $\lambda_c \simeq 2\pi k_c^{-1}$. In (c) the broken lines correspond to the Cahn–Hilliard theory and the full line to the theory discussed in the text. (From Binder *et al.*, 1978.)

collaborators suggests that spinodal decomposition could be viewed as a generalized nucleation, in the following sense. In the metastable region the density of critical droplets is very small, due to the larger energy barrier. When this energy barrier becomes very small (of the order $k_B T$), a high density of unstable fluctuations develops. These fluctuations are limited only by the conservation of concentration. Namely, in the vicinity of a localized fluctuation, the formation of other clusters is prevented by the depletion effect (decrease of supersaturation). In this sense, these large clusters form a nearly periodic variation of concentration. Thus the long wavelength fluctuations which characterize spinodal decomposition can be considered as an extreme version of nucleation, involving a very low activation energy. It should be remarked that existing evidence discussed in this review strongly supports the validity of this qualitative picture, rather than the classical Cahn–Hilliard theory. This picture is also completely consistent with the renormalization group results discussed in Section III. Namely, no unique coarse-grained spinodal curve exists. Therefore, there is no reason to expect a sharp distinction between metastable and unstable states.

VIII. Scaling Theories for Structure Functions

A. Introduction

The structure function $\hat{S}(\vec{k}, t)$ as defined in (5.10) and (5.11) for the binary alloy is a fundamental measure of the nonequilibrium properties of the system. Analogous nonequilibrium order parameter correlation functions can also be defined for other systems in which phase separation is observed, such as binary fluids, glasses and antiferromagnets. It is therefore of considerable interest that these order parameter structure functions seem to exhibit a simple scaling behavior somewhat reminiscent of the scaling behavior observed in critical phenomena. Although some theoretical attention has been given to this nonequilibrium scaling, the subject is not as yet well understood. Renormalization group theory may be useful here.

The basic idea underlying the scaling of $\hat{S}(\vec{k}, t)$ is that after some initial transient time following a quench, a characteristic, time-dependent length scale, $\kappa^{-1}(t)$, is established. Various choices of definition of this length exist. For example, one could define $\kappa(t)$ as $k_1(t)$, the first moment of $\hat{S}(k, t)$. Alternatively, one could choose $\kappa(t)$ as $k_m(t)$, the position of the maximum in $\hat{S}(k, t)$. If there is only one time-dependent characteristic length for the system, either choice will suffice. In Monte Carlo studies it is convenient to use $k_1(t)$, partly because it is difficult to determine k_m accurately. In other cases, such as binary fluids, it is common to use $k_m(t)$,

since its position can be determined rather accurately. For systems in which the order parameter is not conserved, as in antiferromagnets and order–disorder transitions, $k_m = k_1 = 0$, but one can choose $\kappa(t) = \sqrt{k_2(t)}$, where k_2 is the second moment of $\hat{S}(k, t)$. In all cases it is assumed that $\kappa^{-1}(t)$ is a measure of the size of the ordered regions which are developing in the system.

It is convenient to introduce a normalized structure function (Marro *et al.*, 1979)

$$\tilde{S}(k, t) = \frac{\hat{S}(k, t)}{\Sigma_k k^2 \hat{S}(k, t)} \tag{8.1}$$

such that

$$\sum_k k^2 \tilde{S}(k, t)$$

is independent of time. The sum on k is over the first Brillouin zone for a binary alloy. One then introduces a function

$$F(x; t) = \kappa^d(t)\, \tilde{S}(k, t), \tag{8.2}$$

for a given $\kappa(t)$, where

$$x = k/\kappa(t). \tag{8.3}$$

The scaling *ansatz* is that after some transient time t_0

$$F(x; t) = F(x), \qquad t \geq t_0, \tag{8.4}$$

so that from (8.2)

$$\tilde{S}(k, t) = \kappa^{-d}(t) F(x), \qquad t \geq t_0, \tag{8.5}$$

where the "scaling function" $F(x)$ is independent of time. It should be noted that recent Monte Carlo studies of the Ising model use a slightly different definition of $\tilde{S}(k, t)$ in (8.1). Namely, the function $\tilde{S}(k, t)$ which appears in (8.1) is replaced by a structure function $S_1(k, t) = A[S(k, t) - S_c(k)]$, where A is a normalization constant and $S_c(k)$ is the equilibrium structure function on the coexistence curve. The motivation for such a background subtraction is discussed by Lebowitz *et al.* (1982). We will neglect this subtraction in our subsequent discussion, since in many cases it makes no practical difference.

The scaling *ansatz* (8.5) is certainly quite plausible. Nevertheless, it should be noted that the existence of a single dominant length scale does not necessarily imply that $F(x; t)$ is time-independent. (See, for example a theory of the quenched time-dependent Ginsburg–Landau model: Kawasaki *et al.* (1978).) One could expect that there are "corrections to scaling" such that $F(x; t)$ is weakly time-dependent. In this case one might consider (8.5) as a first approximation, in which correction terms should

also appear. Such effects have not been studied to date. What has been investigated in Monte Carlo and experimental studies is the behavior of the ratio

$$r(t) = \frac{k_2(t)}{k_1^2(t)}, \tag{8.6}$$

where the nth moment of $\tilde{S}(k, t)$ is defined as

$$k_n(t) = \frac{\Sigma k^n \tilde{S}(k, t)}{\Sigma \tilde{S}(k, t)} = \frac{\Sigma k^n \hat{S}(k, t)}{\Sigma \hat{S}(k, t)}. \tag{8.7}$$

If (8.5) is correct, then $r(t)$ should be strictly independent of time for $t \geq t_0$. Monte Carlo studies of the three-dimensional Ising model (Lebowitz *et al.*, 1982), two-dimensional tricritical model (Sahni *et al.*, 1982c) and experimental studies of binary fluids (Knobler and Wong, 1981) all reveal a very slow time dependence of $r(t)$ in their scaling regimes. Although this appears to be a rather small effect, it does suggest that there are weak corrections to (8.5), or possibly that the asymptotic scaling regime has not yet been attained. This point certainly requires further experimental and theoretical study.

The apparent validity of (8.5) as a good first approximation for the structure function in the "late time" region of the phase separation poses an interesting challenge to theoreticians. There is clearly a need for a theory which predicts the form of $F(x)$ as well as the dynamical behavior of $\kappa(t)$. This scaling function is not a universal function, in that it seems to depend on the thermodynamic variables which characterize the quench position. For example, the scaling functions for binary alloys and binary fluids depend on the temperature and the concentration, albeit somewhat weakly. It should also be noted that if (8.5) is correct, then various quantities such as the peak position $k_m(t)$ and peak height $\tilde{S}(k_m(t), t)$ are related. For example, if one chooses $\kappa(t) = k_m(t)$, then (8.5) implies that

$$\tilde{S}(k_m(t), t) = k_m^{-d}(t) F(1). \tag{8.8}$$

If one assumes that the peak height and the peak position are parametrized by power law behavior with exponents a'' and a', as discussed in Section V, then (8.8) implies that $a'' = da'$.

B. Scaling for systems with a conserved order parameter

The first theoretical prediction that the structure function should scale was made by Binder and Stauffer (1974) who considered phase separation in alloys and liquid mixtures. Their work primarily dealt with predicting the

growth rate of clusters in terms of the cluster-reaction model summarized in Section VII. In addition, an explicit scaling form was given for $\hat{S}(k, t)$ for a model of binary alloys in which phase separation proceeds by the diffusion and coalescence of large clusters. Sufficiently long after a quench, ordered regions of typical size $\bar{R}(t)$ have formed. Assume that the dominant dynamics governing the growth of such clusters is diffusive, with a time-dependent diffusion constant $D(t)$ which depends on the average cluster size. Binder and Stauffer then approximate the long wavelength behavior of $\hat{S}(k, t)$ by

$$\hat{S}(k, t) = \frac{A_1 \bar{R}(t)^{d-2}}{k^2 + \bar{R}^{-2}(t)} \{1 - e^{-A_2 D(t) k^2 t}\}, \qquad k \leq \bar{R}^{-1} \ll \xi, \tag{8.9}$$

where A_1 and A_2 are constants which depend on the average concentration of B atoms. The origin of the various terms in (8.9) is the following. The prefactor on the right-hand side of (8.9) is an Ornstein–Zernike-like description of the coexistence of two phases. The factor $\bar{R}(t)^{d-2}$ is necessary to satisfy the sum rule

$$\sum_k \hat{S}(k, t) = 1,$$

assuming that the contribution from small k gives a dominant term to the sum. The other factor in (8.9) describes a diffusive relaxation toward equilibrium. The behavior of $D(t)$ can be estimated by arguments given in Section VII, which we do not reproduce here. To obtain an explicit scaling function from (8.9) one need only note that the maximum in $\hat{S}(k, t)$ should occur at $k_m(t) \propto \bar{R}^{-1}$, so that

$$\bar{R}^{-2} D(t) = A_3 t^{-1}, \tag{8.10}$$

where A_3 is a constant. Thus from (8.5), (8.9) and (8.10) one has

$$F_{BS}(x) = \frac{A_1}{1 + x^2} \{1 - e^{-A_3 x^2}\}, \qquad x \leq 1 \ll \bar{R}/\xi, \tag{8.11}$$

where we have neglected the normalization factor in (8.1). The low temperature ($T \to 0$) growth law for $\bar{R}(t)$ is, from Section VII, $\bar{R} \sim t^{a'}$, $a' = 1/(3 + d)$. To our knowledge no test of this scaling function has been made in the Monte Carlo or experimental studies. Binder and Stauffer did not predict the concentration dependence of A_1 and A_3, so there would be two adjustable parameters. However, it seems likely that this scaling theory is too simplified to be accurate.

Binder *et al.* (1978) subsequently gave a more fundamental discussion of $\hat{S}(k, t)$ based on the cluster model approach discussed in Section VII. Their starting point is eqn (7.49), which expresses $\hat{S}(k, t)$ in terms of the cluster distribution function $n_l(t)$ and the conditional probability $g_l(\vec{r})$. As

noted in Section VII, this equation can be used to obtain a qualitatively successful, generalized nucleation theory of spinodal decomposition. It can also be used to obtain a general scaling expression for $\hat{S}(k, t)$. This formal expression for $\hat{S}(k, t)$ is the sum of two terms, the first being a Lorentzian (Ornstein–Zernike) expression which approaches the equilibrium correlation function as $t \to \infty$. The second term represents the effects of droplet formation and has a scaling form (8.5). The scaling function F is given in terms of an integral involving the product of the scaling function for the droplet distribution and the conditional probability function $g_l(r)$. Since no analytical expression is given for $g_l(r)$ or for F, we do not discuss this approach further. It does seem, however, to provide a useful starting point for a cluster model calculation of the scaling function.

Another interesting, more detailed phenomenological scaling theory for binary alloys and fluid mixtures is due to Furukawa (1978, 1979, 1981). This work also deals with the growth of clusters that occurs after the early time spinodal decomposition process. Furukawa discusses a phenomenological model for the structure function $\hat{S}(k, t)$ in which he incorporates certain of the cluster growth ideas of Binder and Stauffer within the framework of nonlinear Langevin equations. The results are numerical predictions for the structure functions of binary alloys and binary fluids. These predictions agree reasonably well with experiments. However, the theory involves three adjustable parameters.

Both the formalism and details of his theory are somewhat complicated. However, the basic ideas and approximations are relatively simple, as we summarize below for the case of the binary alloy. The extension of his approach to binary fluids is given at the end of this discussion. Furukawa begins with a nonlinear Langevin equation of the form (3.16) (Furukawa, 1981, eqn (3.19)). He approximates this equation by a renormalized, linear Langevin equation which is assumed to describe the late stage growth of a gas of free clusters. The effects of the linearization are included in a renormalization of the random force, mobility and free energy functional which appear in the Langevin equation. The major assumption in this linearized model is that the free energy functional which describes the gas of free clusters is not the Ginzburg–Landau form (3.15). Rather, it is taken to be

$$F \cong \tfrac{1}{2} \sum_k \chi_k^{-1} |c_k|^2 + O(c_k^3), \tag{8.12}$$

where c_k is the Fourier transform of the local concentration and χ_k is a positive "susceptibility". This susceptibility is supposed to be determined by the cluster shape and cluster configuration. Thus there is no vestige in (8.12) of the negative susceptibility, $(\partial^2 f/\partial c^2)$, which is crucial for the early

stage decomposition. The equation for the structure function then takes the form

$$\frac{\partial \hat{S}(k, t)}{\partial t} = -2Mk_B T k^2 \chi_k^{-1} \hat{S}(k, t) + 2k_B T M k^2. \tag{8.13}$$

Furukawa argues that the mobility which appears in the above equation can be taken as the bare mobility which enters the original nonlinear equation. Given this approximate equation of motion, the remaining task is to determine χ_k. He assumes that $\hat{S}(k, t)$ has the scaling form (8.5) (neglecting the normalization in (8.1)), with the scaling length being the average cluster size, $\bar{R}$. This requires that χ_k scales. Furukawa then takes

$$\chi_k^{-1} = \alpha k_m^d [(k/k_m)^\gamma + \beta], \tag{8.14}$$

where $k_m \cong \pi/\bar{R}$ denotes the peak position of $\hat{S}(k, t)$. This form, in which α, β and γ are three adjustable parameters, is suggested by a mean field calculation (Furukawa, 1977). (The mean field calculation yields $\chi_k^{-1} = O(\bar{R}^d)$ for $k < k_m$ and $\chi_k^{-1} = \infty$ for $k > k_m$.) Estimates of γ can be obtained by assuming, as Furukawa does, that $\hat{S}(k, t) \simeq \chi_k$ for $k \gtrsim k_m$. At low temperatures and small supersaturations one obtains $\gamma = d + 1$. This reflects the expected behavior of $\hat{S}(k, t)$ for large k, which arises from the form factor of compact droplets. For this reason any sensible theory for the scaling function $F(x)$ should predict that $F(x) \sim x^{-4}$ for $x \gg 1$, in the low temperature, small supersaturation domain. Away from the coexistence curve the clusters become less compact and γ should differ from $d + 1$. Furukawa estimates that $\gamma = 2d$ for extremely entangled surfaces, near the center of the miscibility gap.

The behavior of $\bar{R}$ is assumed to be governed by the Binder–Stauffer diffusion–reaction mechanism, with $\bar{R} \sim t^{1/d+2}$. The three parameters in (8.14) are determined from experimental data and have different values at different quench points. The resultant form for $\hat{S}(k, t)$ is found to be in good agreement with Monte Carlo data for the three-dimensional Ising model of a binary alloy at $T \simeq 0.59 T_c$ and one-to-one composition (Marro *et al.*, 1975) and at $T \simeq 0.59 T_c$ and one-to-four composition (Sur *et al.*, 1977), with the best fits occurring for $\gamma = 6$. Furukawa also found reasonable agreement with the results of an off-critical quench of Au–Pt (Singhal *et al.*, 1978).

The same ideas can also be applied to binary fluids. In this case the renormalized mobility which enters (8.13) is estimated to be proportional to $\bar{R}^2$, with $\bar{R} \sim t^{1/d}$. These differences between fluids and alloys arise from hydrodynamic effects. A parametrization of χ_k^{-1} which takes into account hydrodynamic effects is employed for the binary fluids. The agreement between theory and experiment is shown to be reasonable for an off-critical quench in isobutyric acid plus water (Wong and Knobler, 1978).

Two final remarks should be made regarding Furukawa's analysis. The first is that the theory does not describe the asymptotic time domain in which the Lifshitz–Slyozov–Wagner growth law is correct. The second is that it is difficult to judge the significance of Furukawa's scaling theory, due to the various approximations and adjustable parameters which are involved. In particular, the agreement between the theory and experiment seems somewhat forced. Furukawa basically requires that $\hat{S}(k, t)$ be fit by (8.14) for $k \geq k_m$. Since the correct behavior of $\hat{S}(k, t)$ at $k = 0$ is guaranteed by the local conservation law implicit in (8.13), there is not too much room left for disagreement. On the other hand, his observation that the Ginzburg–Landau free energy functional does not provide a useful starting point for the description of the late stage behavior of $\hat{S}(k, t)$ seems a useful insight. The same point has also been made by Siggia (1979).

Finally, we note that a simple phenomenological theory for the scaling function also has been given by Rikvold and Gunton (1982). Their theory assumes scaling and is based on a model which describes a gas of spherical droplets of the minority phase, surrounded by depletion zones. A simple approximation is made for the pair correlation function for droplets, somewhat similar to the approximation of Binder *et al.* (1978) discussed in Section VII.G. The scaling function is obtained by averaging over a distribution of droplet sizes assumed to be given by the Lifshitz–Slyozov distribution function (Section VI). The only parameter which enters this theory is the volume fraction v of the minority phase. The agreement with the results for the kinetic Ising model (Section IX), and binary alloys and binary fluids (Section XI) for $v \leq 0.2$ is quite reasonable. The approaches of Furukawa (1981) and Rikvold and Gunton (1982) are somewhat complementary, in that Furukawa obtains dynamical information, but no explicit analytical form for the scaling function, whereas Rikvold and Gunton obtain an explicit scaling function, but no dynamical information (since they do not determine the time dependence of the scaling length).

We conclude this section by remarking that the best first principles starting point for a theory of scaling in binary alloys and binary fluids seems to be provided by the recent theory of interface dynamics developed by Kawasaki and Ohta (1982a). Also, the physical basis for scaling is obvious from Fig. 3. One can imagine that by a suitable scale transformation a given configuration, e.g. (e) can be reduced to a preceding one (e.g. (d)).

C. Scaling in systems with a nonconserved order parameter

Scaling is perhaps better understood in systems with a nonconserved order parameter than for systems such as binary alloys and binary fluids. Indeed, there is a recent derivation (Ohta *et al.*, 1982) of a scaling function $F(x)$

which seems to explain the scaling results found in Monte Carlo studies of the two- and three-dimensional Ising antiferromagnet (Phani *et al.*, 1980; Sahni *et al.*, 1981). In addition, two other theoretical treatments of the time-dependent Ginzburg–Landau model described by eqn (6.9) (with a "ψ^4" free energy and supplemented by a noise term) have predicted a scaling of $\hat{S}(k, t)$. Each of these three theories predicts that the time dependence of the characteristic length is $\kappa^{-1}(t) \sim t^{1/2}$, in agreement with the Monte Carlo results. Each theory yields a scaling function, but only the recent work by Ohta *et al.* (1982) has been compared with the Monte Carlo results.

One study is an adaptation of the LBM theory to the nonconserved case by Billotet and Binder (1979). Since the main ideas of such an approach have been summarized in Section V, we do not discuss this work here. Billotet and Binder obtain a numerical solution for a scaling function from their theory. This function is clearly in qualitative agreement with the Monte Carlo results. A second study by Kawasaki *et al.* (1978) involves a solution of (6.9) which is based on a singular perturbation theory. In this calculation a certain weak coupling ($u \to 0$), long time ($t \to \infty$), large distance limit is taken, such that a natural time variable $y(t)$ remains finite. (This variable y is proportional to $ut^{-d/2}e^{M\xi^{-2}t}$, where u is the coefficient of the "ψ^4" term in the Ginzburg–Landau free energy functional.) Closed form scaling solutions are obtained for the probability distribution functional and the structure function $\hat{S}(k, t)$. The scaling function, however, has an explicit time dependence. The limitations of this calculation are twofold, the first being the restriction to the weak coupling limit. The second is that the short wavelength fluctuations (ψ_k; $k > \xi^{-1}$) are included in (6.9) only via the renormalization of various coefficients which enter the equation. As a result, the theory seems incapable of describing the short wavelength fluctuations appropriate for the interface dynamics.

The most recent studies of the time-dependent Ginzburg–Landau model are by Kawasaki and Ohta (1982a) and Ohta *et al.* (1982). The work of Kawasaki and Ohta is complementary to that of the singular perturbation theory in that an explicit discussion of the interface dynamics is given. A derivation of a Euclidean invariant Langevin equation is presented which describes the random displacement of an interface. This equation reduces to the Allen–Cahn equation (6.13) if one neglects noise. An equivalent formulation is also given in terms of a Fokker–Planck equation for the probability distribution functional for the interface displacement. Kawasaki and Ohta (1982b) extended this treatment to other models. Ohta *et al.* (1982) have subsequently succeeded in obtaining an approximate solution for the scaling function for the Allen–Cahn equation which is in satisfactory agreement with the Monte Carlo results of Phani *et al.* (1980) and Sahni *et al.* (1981). It also appears that there is a very close relationship between

the scaling functions of Kawasaki *et al.* (1978) and Ohta *et al.* (1982) (Kawasaki *et al.*, 1983).

IX. Monte Carlo Studies

A. Introduction

In this section we will discuss the Monte Carlo methods which have been used quite successfully to study the kinetics of various model systems of first-order phase transitions. The most extensive work has been done on simple models of binary alloys by Lebowitz, Kalos and their collaborators (Bortz *et al.*, 1974; Marro *et al.*, 1975; Rao *et al.*, 1976; Sur *et al.*, 1977; Kalos *et al.*, 1978; Penrose *et al.*, 1978; Lebowitz *et al.*, 1982). Some work has also been carried out on magnetic binary alloys by Kawasaki (1978, 1979), mainly to understand the effects of magnetic interactions on the phase separation process. In this section we will review only the work on simple models of nonmagnetic binary alloys. The most comprehensive summary of this work is contained in the recent scaling studies by Lebowitz *et al.* (1982). It is worth pointing out that one of the distinct advantages of Monte Carlo computer simulations is that in contrast to real experiments one can work with simple systems and avoid the complexities that are usually present in real systems.

For studying the phase separation process in a binary A–B alloy, we consider a lattice where each site may be occupied by either an A atom ($C_i^A = 1, C_i^B = 0$) or a B atom ($C_i^B = 1, C_i^A = 0$), where C_i^A and C_i^B are local concentration variables. The Hamiltonian describing this binary alloy system is given by

$$\mathcal{H} = \sum_{i \neq j} [C_i^A C_j^A \phi_{AA}(\vec{r}_{ij}) + 2C_i^A C_j^B \phi_{AB}(\vec{r}_{ij}) + C_i^B C_j^B \phi_{BB}(\vec{r}_{ij})] - \sum_i C_i^A \mu_A(\vec{r}_i) + \sum_i C_i^B \mu_B(\vec{r}_i) + \mathcal{H}_0, \tag{9.1}$$

where $\mu_A(\vec{r})$ and $\mu_B(\vec{r})$ are the local chemical potentials. The pair potentials, $\phi_{AA}(\vec{r}_{ij})$, depend only on the relative distance $\vec{r}_{ij} = \vec{r}_i - \vec{r}_j$ between the atoms. The background term $\mathcal{H}_0$ contains the kinetic energy of the atoms. One assumes a perfect rigid lattice without vacancies. The rigidity of the lattice eliminates elastic distortions which are generally present in real binary alloys and affect the morphology of A-rich and B-rich clusters. It is convenient to introduce a spin representation in terms of the variable $\sigma_i = \pm 1$ using the relations

$$C_i^A = (1 + \sigma_i)/2, \qquad C_i^B = (1 - \sigma_i)/2, \tag{9.2}$$

which leads to the Ising model Hamiltonian

$$\mathcal{H} = -\sum_{i \neq j} J(\vec{r}_{ij}) \sigma_i \sigma_j - \sum_i H_i \sigma_i + \mathcal{H}_0', \tag{9.3}$$

where the "exchange constant" is given by

$$2J(\vec{r}_{ij}) = \phi_{AB}(\vec{r}_{ij}) - \tfrac{1}{2}[\phi_{AA}(\vec{r}_{ij}) + \phi_{BB}(\vec{r}_{ij})] \tag{9.4}$$

and the "magnetic field" is

$$2H_i = \sum_{j \neq i} [\phi_{BB}(\vec{r}_{ij}) - \phi_{AA}(\vec{r}_{ij})] + \mu_A(\vec{r}_i) - \mu_B(\vec{r}_i). \tag{9.5}$$

One usually considers nearest neighbor interactions, with $J(\vec{r}_{ij}) = J =$ constant. The term $\mathcal{H}_0'$ in (9.3) is the renormalized background which includes $\mathcal{H}_0$.

The Ising Hamiltonian defined above does not have any dynamics of its own. The microscopic description of the time evolution of a given configuration of atoms $\{c(\vec{r})\}$ (or spins $\{\sigma_i\}$) is based on the fact that the atoms (or spins) have to overcome potential barriers to exchange positions (or exchange spins). The energy for this exchange is supplied by the thermal vibrations or phonons which are assumed to be in equilibrium at a temperature T to which the system is quenched. The phonons thus act as a thermal reservoir or heat bath which brings the system to equilibrium at a temperature T by inducing random exchanges between neighboring atoms (or spins). Since the strength of the phonons depends upon the temperature, it determines a time scale for the evolution. Furthermore, "memory effects" are only important on the time scale of lattice vibrations. Thus one may ignore them as far as the evolution of a configuration is concerned, since this occurs on a much slower time scale. In that case the evolution of a state is described in terms of a Markovian equation for the probability distribution function $P(\{\sigma\}, t)$ (where from now on we use spin language):

$$\frac{d}{dt}[P(\{\sigma\}, t)] = -P(\{\sigma\}, t) \sum_{\{\sigma'\}} W(\{\sigma\} \to \{\sigma'\}) + \sum_{\{\sigma'\}} W(\{\sigma'\} \to \{\sigma\}) P(\{\sigma'\}, t) \tag{9.6}$$

where $W(\{\sigma\} \to \{\sigma'\})$ is the transition probability from a configuration $\{\sigma\}$ to a new configuration $\{\sigma'\}$. We consider only those transitions which permit the interchange of a spin σ_i with a neighboring spin σ_j (Kawasaki dynamics: see Kawasaki, 1972). It is worth pointing out that in real binary alloys the exchange of any two atoms occurs indirectly via vacancies rather than directly as has been assumed in the above discussion. Despite the above oversimplification of the model, the agreement between computer simulation studies of this model and experiments on real binary alloys is quite good. We discuss this point further in Section XI.A.

When the system is in equilibrium at a given temperature T, the detailed balance condition for the transition probabilities implies

$$\frac{W(\{\sigma\}\rightarrow\{\sigma'\})}{W(\{\sigma'\}\rightarrow\{\sigma\})} = \exp(-\Delta\mathcal{H}/k_BT), \tag{9.7}$$

where $\Delta\mathcal{H}$ is the change in energy produced by an exchange $\{\sigma\}\rightarrow\{\sigma'\}$. This relation does not specify W uniquely. One simple choice consistent with eqn (9.7) is

$$W(\{\sigma\}\rightarrow\{\sigma'\}) = \frac{1}{2\tau}\left[1 - \tanh\frac{\Delta\mathcal{H}}{2k_BT}\right]. \tag{9.8}$$

The arbitrary time constant τ sets the time scale in the problem. τ is a strongly temperature-dependent function. In principle, it can be estimated by considering the thermally activated diffusion process of an A atom in a sea of B atoms (Lebowitz *et al.*, 1982). Generally, one sets $\tau = 1$, thus measuring time in units of "one Monte Carlo step/spin" (MCS).

In computer simulations, one quenches a high temperature, uniform state of a given magnetization to a point inside the two-phase coexistence region and carries out the spin exchanges using standard Monte Carlo procedures (Metropolis *et al.*, 1953; Binder, 1979). At suitable time intervals, one records the spin configurations and computes the various physical quantities of interest. When this procedure is repeated for "many" runs with different initial configurations, then the average of a physical quantity at a given time over different runs corresponds to its ensemble average. Sometimes, in order to minimize the scatter in data, one carries out a "time averaging" at a given time t by averaging over all the data in the time interval between $(t - \Delta t)$ and $(t + \Delta t)$, where Δt is generally chosen to be less than 10 Monte Carlo steps.

The size N of the lattice is generally restricted by practical computational limitations, even though one would like to have as large a lattice as possible so that it simulates a real macroscopic system. The actual simulations have been performed on square lattices by Flinn (1974), Bortz *et al.* (1974) and Rao *et al.* (1976) with $N = 55 \times 55$, 80×80 and 200×200 sites. Similar studies have also been carried out by Marro *et al.* (1975) and Sur *et al.* (1977) on a simple cubic lattice, with $N = 30 \times 30 \times 30$ and $50 \times 50 \times 50$ sites. Periodic boundary conditions are used in order to avoid edge effects due to free surfaces. Nevertheless, one has to worry about finite size effects, especially when some characteristic physical length such as a domain size is comparable to the linear dimension of the system.

In Fig. 25 we display the phase diagram of the three-dimensional Ising model of a binary alloy which is obtained using the low temperature series expansion by Essam and Fisher (1963). The value of the critical temperature T_c is known accurately for this system ($4J/k_BT_c = 0.88686$). The dotted

curve corresponds to the classical spinodal curve. This is shown for convenience to allow one to distinguish in a loose sense between metastable and unstable regions. The points P_i for which Monte Carlo simulations have been carried out by Marro *et al.* (1975) and Sur *et al.* (1977) are depicted by black dots in Fig. 25. The points P_1–P_5 correspond to $T = 0.59T_c$ and concentrations $\bar{c} = 0.05, 0.075, 0.1, 0.2, 0.5$, respectively. The

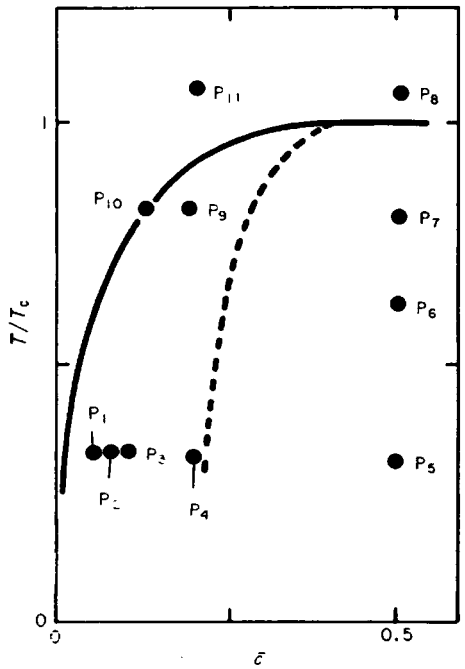

FIG. 25. The phase diagram (T versus $\bar{c}$) of the three-dimensional Ising model of a binary alloy. The solid line corresponds to the coexistence curve (drawn according to low temperature series expansion) and the broken line is the classical spinodal line. The quenches from very high temperatures to the phase points P_j ($j = 1, \ldots, 11$) are discussed in this review (From Lebowitz *et al.*, 1982.)

points P_6–P_8 to $\bar{c} = 0.5$ and $T/T_c = 0.78, 0.89, 1.07$, respectively, and P_9 to $\bar{c} = 0.2$ and $T = 0.89T_c$. In the following two sections we will discuss the results for the structure factor and energy per site. We will present the results in detail for three-dimensional simulations and only briefly point out the qualitative differences between the two- and three-dimensional studies, since most of the qualitative features remain the same for these two cases. We should also add a caveat concerning the data analysis done

in these Monte Carlo simulations. Most of the data has been fitted to simple power laws (Section V.D) and estimates for the exponents have been obtained. It is, however, possible to fit the same data with other functional forms (Lebowitz *et al.*, 1982), thus making it difficult to draw definitive conclusions. Further theoretical progress is necessary before one can be confident about the interpretation of Monte Carlo or experimental data. In spite of this note of caution, however, the power law approximations have led to a reasonably consistent description of the observed phenomena.

Finally, we note that Monte Carlo methods suffer from one major limitation in that usually one cannot study the very late stage behavior of a system due to limited computer time. Therefore most Monte Carlo simulations carried out to study the dynamics of phase separation so far provide information for times much before final equilibrium is reached.

B. Structure function

A quantity which is of primary physical interest is the structure factor $\hat{S}(\vec{k}, t)$ which has been discussed in Section V. This is the Fourier transform of the pair correlation function $G(\vec{r}, t)$:

$$G(\vec{r}, t) = \frac{1}{N}\sum_{\vec{r}_i} \langle [c(\vec{r}_i, t) - \bar{c}][c(\vec{r}_i + \vec{r}, t) - \bar{c}] \rangle, \tag{9.9}$$

$$\hat{S}(\vec{k}, t) = \sum_{\vec{r}} e^{i\vec{k}\cdot\vec{r}} G(\vec{r}, t) = \frac{1}{N}\left\langle \left| \sum_{\vec{r}_i} e^{i\vec{k}\cdot\vec{r}_i} (c(\vec{r}_i, t) - \bar{c}) \right|^2 \right\rangle. \tag{9.10}$$

Here $\bar{c}$ is the average concentration which remains constant during the evolution, $\vec{r}$ and $\vec{r}_i$ run over the N lattice sites, and $\vec{k}$ ranges over the first Brillouin zone. The angle brackets $\langle\,\rangle$ denote the ensemble average which is realized in the computer simulations by making several independent runs. According to this definition we have the sum rules

$$\frac{1}{N}\sum_{\vec{k}} \hat{S}(\vec{k}, t) = 1 - \bar{c}^2; \tag{9.11}$$

$$\hat{S}(\vec{k} = 0, t) = 0. \tag{9.12}$$

In addition, corresponding to the random initial configuration present at $t = 0$ (immediately following quenching), one has

$$\hat{S}(\vec{k} \neq 0, 0) \simeq 1 - \bar{c}^2. \tag{9.13}$$

In order to improve the accuracy and the presentation of data, one deals with a spherical average of $\hat{S}(\vec{k}, t)$ over a number of shells,

$$\hat{S}(k, t) = \sum{}' \hat{S}(\vec{k}, t) \Big/ \sum{}' 1, \qquad k = \frac{2\pi n}{N^{1/3}}, \tag{9.14}$$

where $n = 0, 1, 2, \ldots, (\sqrt{3}/2)N^{1/3}$. Each sum Σ' in eqn (9.14) for a given value of n is over a spherical shell defined by

$$n - \tfrac{1}{2} \leq \left(\frac{N^{1/3}}{2\pi}\right)|k| < n + \tfrac{1}{2}.$$

Generally, one truncates n at some convenient integer $n_c < (\sqrt{3}/2)N^{1/3}$, beyond which the structure factor is so small that it is hard to distinguish its value from the typical errors encountered in the Monte Carlo experiment.

Before we discuss the behavior of the structure factor in detail at various points of the phase diagram for both two- and three-dimensional models, we summarize a few of its very general features. First, at all points studied so far within the coexistence region, the structure factor $\hat{S}(k, t)$ develops a peak at a finite value of the wavenumber $k_m(t)$ which decreases with time. Also the intensity of the peak increases with time. Second, the original papers reported that there is no observed time regime in which $\hat{S}(k, t)$ grows exponentially, in contrast to the linear theory. (This conclusion may be incorrect, however, since Marro and Vallés (1983) have recently argued that the very early time Monte Carlo results are in agreement with Cook's extension of the linear theory (Section V.A).) Third, $\hat{S}(k, t)$ exhibits a "late time" scaling behavior which is of both experimental and theoretical interest. Thus the kinetic Ising model displays the same qualitative features as other systems discussed throughout this article.

We now discuss some of the detailed results. The behavior of the structure factor $\hat{S}(k, t)$ at P_4 (Fig. 26(a)), which lies close to the classical spinodal curve just inside the nucleation regime, is quite similar to that observed at P_5 (Fig. 26(b)), which lies in the middle of the spinodal region. The behavior at P_4 is contrary to the linear Cahn theory, which predicts no decomposition at all for this case, as noted in Section V. Langer *et al.* (1975), on the other hand, predict a broad but well defined peak at P_4 for $\hat{S}(k, t)$, of lesser intensity as compared to that at the point P_5. They also predict a "common tail" for large k which is not seen at P_4. Both at P_4 and P_5, a "crossover" phenomenon for $k > k_m(t)$ has been observed as predicted by LBM theory for the symmetric case P_5. The qualitative behavior of the structure factor $\hat{S}(k, t)$ is the same for the points P_6 and P_7 as that of P_5, except that the intensity of the peak at a given time decreases with increasing temperature.

The point P_9 lies well inside the classical metastable region of the phase diagram. The observed $\hat{S}(k, t)$ for this point as shown in Fig. 27(a)) is rather similar to that displayed in Fig. 27(b) for P_8. The latter point lies

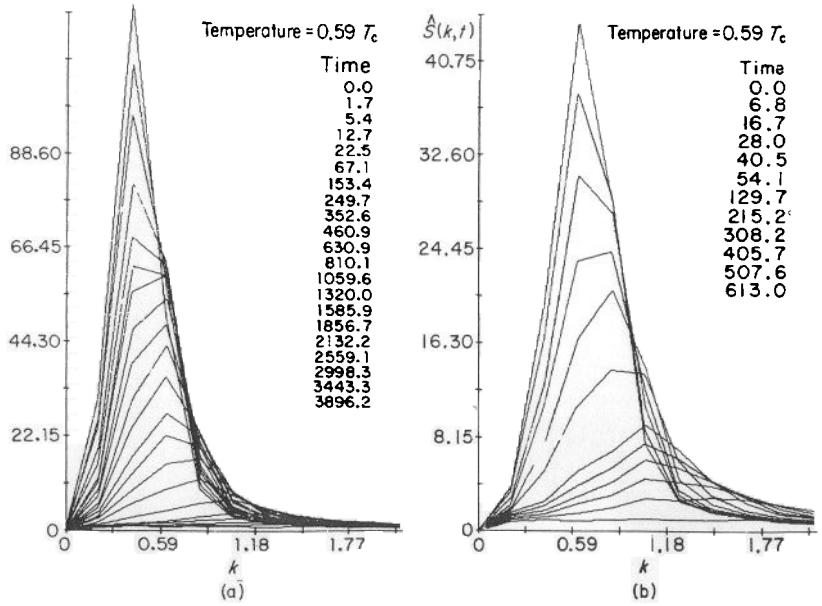

FIG. 26. Time evolution of the spherical averaged structure function $\hat{S}(k, t)$ versus k at (a) P_4 ($T = 0.59T_c$, $\bar{c} = 0.2$) and (b) P_5 ($T = 0.59T_c$, $\bar{c} = 0.5$). The times listed in each figure correspond to different curves from the bottom of the picture to the top. Due to the finite sizes of the lattices used in these simulations, the data for $\hat{S}(k, t)$ is obtained at discrete values of k and is connected by straight lines. Time is measured in MCS units. ((a) From Sur *et al.*, 1977; (b) from Marro *et al.*, 1975.)

just outside the coexistence curve in the one-phase region, where significant "local ordering" can still take place. Here one finds that after an initial growth for large values of k, $\hat{S}(k, t)$ quickly decays to a steady value, giving rise to a common tail for $k > k_{max}$ which can be approximately represented by an Ornstein–Zernike form. The behavior of $\hat{S}(k, t)$ at P_1–P_3 (in the classical metastable regime) is also qualitatively similar to the one discussed above for P_8 and P_9 except that one observes larger fluctuations for the points closer to the coexistence curve. This is particularly true at $\bar{c} \leq 0.03$ and $T = 0.59T_c$, where it is difficult to express the data in any useful manner. Short runs have also been carried out at the point P_{10} ($\bar{c} = 0.127$, $T = 0.84T_c$), very close to the coexistence curve, where the system reaches a stationary state quite soon. Also the early time behavior of the structure factor $\hat{S}(k, t)$ at P_{11} ($\bar{c} = 0.2$, $T = 1.07T_c$) shown in Fig. 27(c) is qualitatively similar to that for P_8 (Fig. 27(b)), but the intensity is lower and more comparable to that observed for $\bar{c} = 0.5$ and $T = 1.5T_c$ (Marro *et al.*, 1975). It is believed that at points outside the coexistence curve, the late time values of $\hat{S}(k, t)$ are those of the equilibrium system.

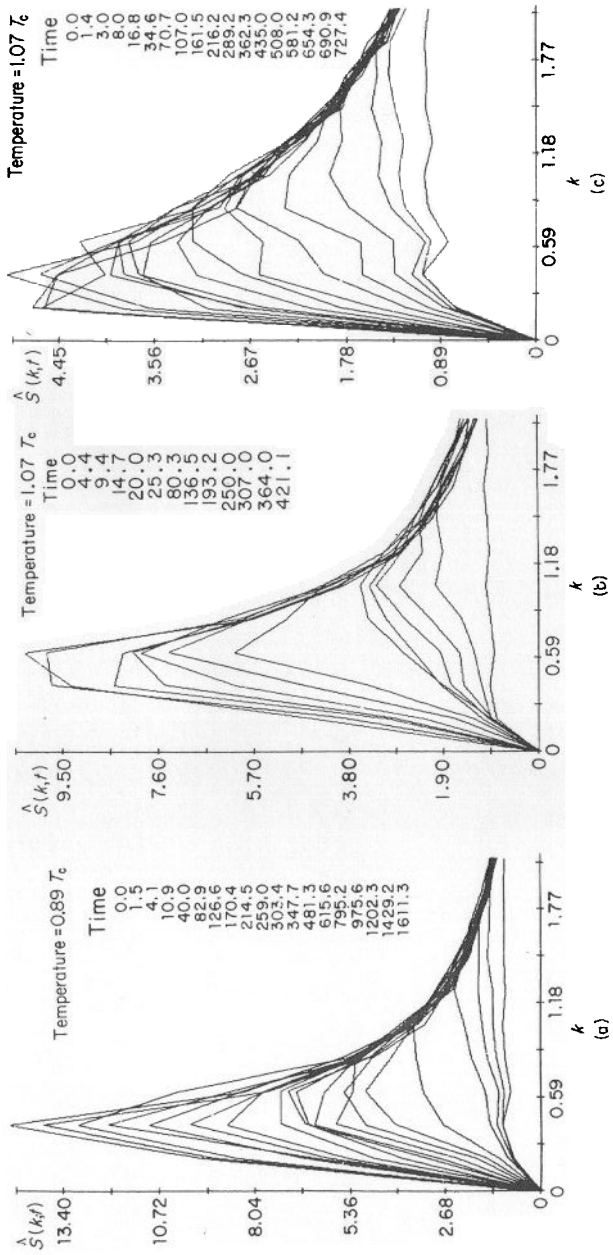

FIG. 27. Time evolution of the spherical averaged structure function $\hat{S}(k, t)$ versus k at (a) P_9 ($T = 0.89T_c$, $\bar{c} = 0.2$), (b) P_8 ($T = 1.07T_c$, $\bar{c} = 0.5$) and (c) P_{11} ($T = 1.07T_c$, $\bar{c} = 0.2$), respectively. The times listed in each figure correspond to different curves from the bottom of the figure to the top. ((a) From Sur *et al.*, 1977; (b) from Marro *et al.*, 1975; (c) from Sur *et al.*, 1977.)

In Fig. 28(a), (b) and (c) $\hat{S}(k,t)$ is plotted as a function of time for different values of k for the points P_5, P_8 and P_9, respectively. A study of these figures shows that there is no time regime where $\hat{S}(k,t)$ grows exponentially. We see that at P_5 $\hat{S}(k,t)$ initially grows with time, reaches a peak, and then decays at successively earlier times as k increases. This leads to the crossover phenomenon discussed earlier. For very small k values, the peak is never reached during the course of the simulations. On the other hand, at the points P_8 and P_9, $\hat{S}(k,t)$ continues to grow as time increases until it reaches a maximum value at t', and then appears to remain stationary. This maximum value as well as the value of t' decreases as k increases. This explains the common tail seen in Fig. 27(b) and (c).

In two dimensions, the evolution of the structure factor was studied in detail by Bortz *et al.* (1974) and Rao *et al.* (1976) at $T = 0.586T_c$ and $\bar{c} = 0.5$ and 0.2 respectively, on an 80×80 lattice. The behavior at these points is qualitatively similar to P_5 and the crossover phenomenon is observed at both points. Another point at $\bar{c} = 0.5$ and $T = 1.1T_c$ was also studied and found to exhibit behavior similar to P_8. For large k, the common tail of $\hat{S}(k,t)$ quickly equilibrates to a simple functional form $S(k) \sim k^{-2}$. This is consistent with the calculations of Fisher and Burford (1967) of the equilibrium $\hat{S}(k)$ for the two-dimensional Ising model above T_c.

One important difference between the different quenches is the time it takes (in units of τ) for the system to achieve a certain amount of segregation as reflected in the development of $\hat{S}(k,t)$. Comparison of the structure functions at P_1 and P_5 suggests that the speed of segregation increases as one moves from near the coexistence line towards the middle of the spinodal region. The same is true as one moves down from P_7 to P_5. Very close to T_c the system will be in the region of critical slowing down. This results in an extremely slow segregation rate which cannot be seen in computer simulations.

Two important parameters which characterize the time evolution of $\hat{S}(k,t)$ are the location of the peak $k_m(t)$ and the height of the peak $\hat{S}(k_m(t),t)$, as mentioned in Section V.D. Due to the finite (small) size of the systems studied in computer simulations, one can only measure wavenumbers k which are widely spaced. This leads to a difficulty in determining these parameters precisely. Using a parabolic fit to three values of k around

FIG. 28. The development of the spherical averaged structure function $\hat{S}(k,t)$ as a function of time (measured in Monte Carlo steps) for different values of wavenumbers k at P_5, P_8 and P_9, respectively. The corresponding $n = N^{1/3}k/2\pi$ is shown at the end of each curve. ((a), (b) From Marro *et al.*, 1975; (c) from Sur *et al.*, 1977.)

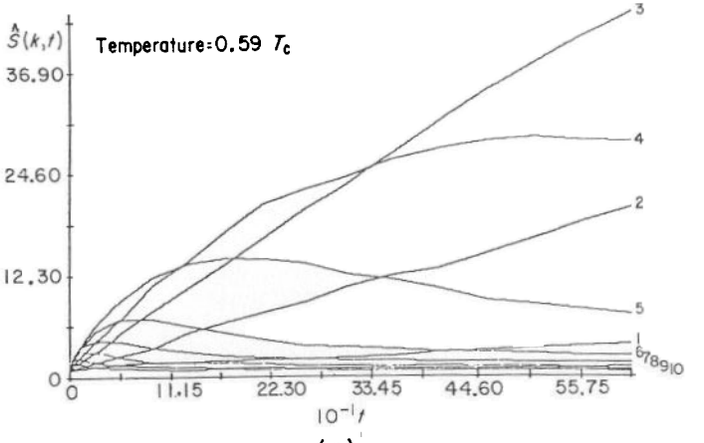

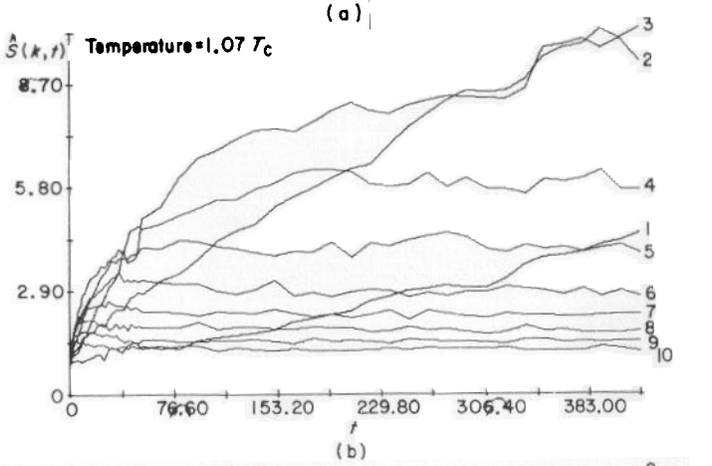

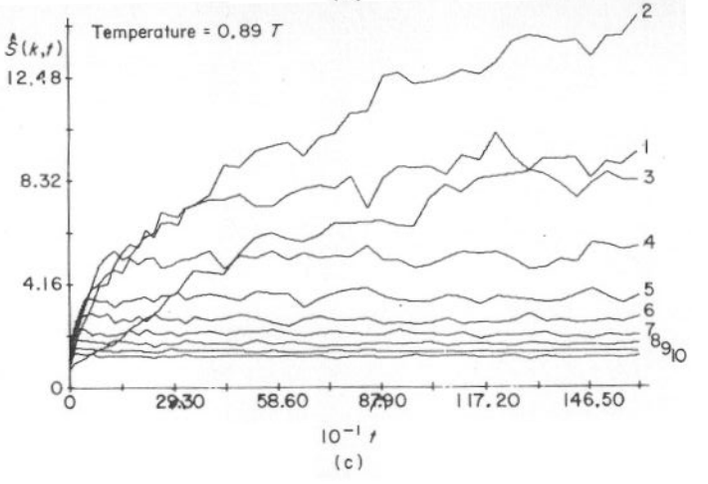

k_m, one finds an approximate fit with the following formulas (see eqns (5.34) and (5.35)):

$$k_m(t) \sim (t + 10)^{-a'}, \tag{9.15}$$

$$\hat{S}(k_m(t), t) \sim (t + 10)^{a''}. \tag{9.16}$$

The arbitrary additive constant 10 is simply included to display the early time behavior of the system properly on a log–log plot and is irrelevant for the determination of asymptotic power laws and hence exponents. The exponents a' and a'' have been shown to be approximately equal to 0.2 and 0.7 for points P_4–P_8, respectively, but their values for P_9 are somewhat smaller, being 0.16 and 0.4, respectively.

However, the more reliable and smooth quantities are the first and the second moments $k_i(t)$ $(i = 1, 2)$ of $\hat{S}(k, t)$, defined as

$$k_i(t) = \sum_{k=0}^{k_c} k^i \hat{S}(k, t) \Big/ \sum_{k=0}^{k_c} \hat{S}(k, t), \tag{8.7}$$

where $k_c = 2\pi n_c / N^{1/3}$. Different values of the upper cut-off n_c have been used for different sizes of the lattices. For example, for $d = 3$, $n_c = 10$ for $N^{1/3} = 30$ and $n_c = 14$ for $N^{1/3} = 50$. The first moment $k_1(t)$ behaves more smoothly than $k_m(t)$ and its asymptotic behavior is well described (see eqn (5.33)) by

$$k_1(t) \sim t^{-a}. \tag{9.17}$$

After the very early transient times, the value of the exponent a is reported by Marro *et al.* (1979) to change from $a \simeq 0.2$ near the center of the spinodal region to $a \simeq 0.33$ at low concentrations of one component. Recently, the data has been reanalyzed by Lebowitz *et al.* (1982) for very late times and a good fit has been obtained with the form eqn (5.36), in agreement with the Lifshitz–Slyozov theory. In Table IV, the values of A and B for eqn (5.36) are listed for different points P_i. Our guess is that the latter is indeed the correct description of the phenomena for "late stages". It is worth pointing out that very close to the coexistence curve, at $T = 0.59T_c$ and $\bar{c} = 0.035$, short evolutions gave extremely small values of $a \leqslant 0.04$ but one should not attach any significance to them. We should also mention that the exponent a is influenced by the value of the cut-off n_c used. For example, at P_3, $a \simeq 0.22$ for $n_c = 14$, $a \sim 0.19$ for $n_c = 10$ and $a \simeq 0.18$ for $n_c = 7$. As a rule, one should go on increasing the value of n_c until one finds that the exponent does not change significantly by increasing n_c any further.

On the basis of cluster dynamics ideas discussed in Section VII, Binder and Stauffer (1974) have predicted that $a'' = 3a'$ and $a' = 1/6$ at low temperatures, $a' = 1/4$ for $T \simeq T_c$ and $a' = 1/2$ for $T > T_c$, $d = 3$. Only the first

TABLE IV. The exponent a defined by a simple power law ($k_1 \sim t^a$) and the adjustable parameters A and B of the linear fit of k_1^{-3} with time at different points P_1–P_7. Here t_0 is the approximate time beyond which the data is analyzed and scaling of the structure function is observed according to eqn (9.20).

Phase point	Maximum duration of run (MCS)	$k_1 \sim t^{-a}$	$k_1^{-3} = A + Bt/10^3$, $t \geqslant t_0$		
		a	A	B	t_0
$P_1\{0.59T_c, 5\%\}$	14000	0.35	8.8	1.5	6800
$P_2\{0.59T_c, 7.5\%\}$	10200	0.23	7.5	1.5	4000
$P_3\{0.59T_c, 10\%\}$	7300	0.21	3.6	1.5	2500
$P_4\{0.59T_c, 20\%\}$	3900	0.19	2.3	1.7	1500
$P_5\{0.59T_c, 50\%\}$	650	0.19	1.2	3.0	350
$P_6\{0.78T_c, 50\%\}$	1700	0.23	1.4	3.9	1000
$P_7\{0.89T_c, 50\%\}$	6600	0.25	3.5	3.9	1000

one of these predictions is in reasonable agreement with the results of P_4, P_5 and P_6. Also the result of the LBM theory (Langer *et al.*, 1975), $a' \simeq 0.21$, is consistent with the Monte Carlo results at P_5–P_7. In two dimensions, simulations on an 80×80 lattice at $T = 0.586T_c$ and $\bar{c} = 0.5$ give $a' \simeq 0.2$ and $a'' \simeq 0.6$. The Binder–Stauffer theory predicts $a' = 0.2$ and $a'' = 0.4$ for $d = 2$, for $T \to 0$. (Note that $a'' = da'$ is a scaling relation, as discussed in Section VIII.A.) It should be stressed that in view of the current uncertainty concerning both theoretical and numerical results, meaningful comparisons between theory and "experiment" are difficult to make at the moment.

C. Scaling results

Experiments and theory always deal with systems of macroscopic size which correspond to the limit $N \to \infty$. In this limit k becomes a continuous variable and $\hat{S}(k, t)$ becomes a continuous function of k. The sum rule (eqn (9.11)) goes over to the integral

$$\frac{1}{2\pi^2} \int_0^{k_{max}} k^2 \hat{S}(k, t)\, dk = 1 - \bar{c}^2, \tag{9.18}$$

where k_{max} denotes the maximum wavevector within the first Brillouin zone and $\tilde{S}(k, t)$ is the sphericalized "macroscopic" structure factor, about which one would like to obtain information from the computer simulations. To understand the late time behavior of $\tilde{S}(k, t)$, one considers the quantity

$$\tilde{S}_1(k, t) = \tilde{S}(k, t) - \tilde{S}_{eq}(k). \tag{9.19}$$

where $\tilde{S}_{eq}(k)$ denotes the equilibrium structure factor for a macroscopic, fully segregated, two-phase system. Correspondingly, one defines an analogous quantity $S_1(k, t)$ for finite systems by subtracting $\hat{S}_{eq}(k, T)$ from $\hat{S}(k, t)$. The value of the equilibrium structure function $\hat{S}_{eq}(k, T)$ is obtained by quenching to a point at a temperature T on the coexistence curve and waiting for the system to reach equilibrium. At low temperature $S_{eq}(k, T)$ is negligible compared to $\hat{S}(k, t)$ for small values of k, after some initial time, so that $S_1(k, t) \simeq \hat{S}(k, t)$. However, at high temperatures (e.g. at P_7), $\hat{S}_{eq}(k, T)$ is large at relevant k values and should not be neglected. Next, one looks for those features of the discrete structure factor $S_1(k, t)$ which will smoothly go over to the "macroscopic" structure factor $\tilde{S}_1(k, t)$. For example, one considers the first and second moments which are obtained using eqn (9.16), replacing $\hat{S}(k, t)$ with $S_1(k, t)$. In Table V, the ratio $r(t) = k_2/k_1^2$(eqn (8.6)) is listed at selected values of time for several points, as obtained by Lebowitz *et al.* (1982). This table indicates that $r(t)$ is to a good first approximation independent of time. This suggests that the discrete structure factor $S_1(k, t)$ is related to a scaled function such that (as in eqn (8.5))

$$S_1(k, t) = \kappa^{-3}(t) F(k/\kappa(t)), \tag{9.20}$$

where $F(x)$ is a continuous function describing $S_1(k, t)$ and κ(t) is some characteristic wavenumber. In order to check the validity of the scaling hypothesis and to find the smooth function F from the computer simulations, Lebowitz *et al.* (1982) define a function of two variables $x = k/k_1(t)$ and time t (as in eqns (8.1) and (8.2))

$$F(x, t) = \frac{L}{\pi} k_1^3(t) \tilde{S}_1(k, t), \tag{9.21a}$$

$$\tilde{S}_1(k, t) = S_1(k, t) \Big/ \sum_{k=0}^{k_c} k^2 S_1(k, t) \tag{9.21b}$$

and see whether for late times $F(x, t) \simeq F(x)$, a smooth function of x independent of time. The normalized structure factor $\tilde{S}_1(k, t)$ defined in eqn (9.21b) is used so that the sum rule for the function $F(x)$ is

$$\int_0^\infty x^2 F(x)\, dx = 1. \tag{9.22}$$

TABLE V. The ratio of the second moment to the square of the first moment as the function of time for points P_1–P_7.

													Tend	L	NR
P_1	t (MCS)	151	536	1340	2593	3899	5304	6834	8458	10299	12576		14000	50	1
	k_1	0.897	0.789	0.719	0.613	0.496	0.413	0.378	0.360	0.344	0.333				
	k_2/k_1^2	1.28	1.33	1.32	1.36	1.35	1.39	1.36	1.35	1.34	1.35				
P_2	t (MCS)	86	331	595	1159	2437	3870	5431	6633	7861	9266		10200	50	1
	k_1	0.931	0.802	0.725	0.590	0.474	0.421	0.403	0.382	0.372	0.365				
	k_2/k_1^2	1.23	1.26	1.29	1.33	1.32	1.29	1.28	1.29	1.30	1.30				
P_3	t (MCS)	55	227	630	1313	2062	3010	3720	4807	5836	6970		7300	50	1
	k_1	0.973	0.846	0.706	0.587	0.543	0.501	0.481	0.447	0.438	0.415				
	k_2/k_1^2	1.19	1.22	1.23	1.24	1.24	1.24	1.24	1.26	1.25	1.26				
P_4	t (MCS)	28	110	250	574	934	1320	1721	2132	2705	3593		3900	30	8
	k_1	1.048	0.908	0.799	0.694	0.634	0.601	0.576	0.552	0.528	0.491				
	k_2/k_1^2	1.15	1.16	1.17	1.17	1.17	1.17	1.17	1.17	1.18	1.18				
P_5	t (MCS)	12	28	41	64	130	216	309	406	508	560		650	30	8
	k_1	1.107	1.065	1.038	0.983	0.895	0.831	0.783	0.747	0.717	0.705				
	k_2/k_1^2	1.14	1.14	1.13	1.13	1.13	1.13	1.13	1.13	1.13	1.13				
P_6	t (MCS)	16	56	190	409	795	955	1117	1281	1446	1614		1700	30	8
	k_1	1.091	0.950	0.787	0.685	0.603	0.578	0.555	0.538	0.520	0.504				
	k_2/k_1^2	1.13	1.14	1.16	1.17	1.18	1.18	1.19	1.19	1.19	1.19				
P_7	t (MCS)	117	301	586	1144	1773	2589	3415	4245	5085	6357		6600	30	8
	k_1	0.849	0.690	0.584	0.502	0.448	0.418	0.393	0.369	0.349	0.327				
	k_2/k_1^2	1.13	1.18	1.23	1.25	1.26	1.27	1.27	1.29	1.29	1.31				
Au–60%Pt, $T \simeq 0.6T_c$	t(s)	0(?)	30	60	120	360	600	900	—	—	—	—	—	∞	—
	$k_1 \times 10^6$	11.5	11.93	11.56	11.26	10.49	10.15	9.74							
	k_2/k_1^2	1.20	1.12	1.12	1.12	1.12	1.12	1.12							

The function $F(x, t)$ obtained from computer simulation by Lebowitz *et al.* (1982) is shown in Figs. 29–31 for "deep", "intermediate" and "shallow" quenches, respectively. There is reasonable evidence that the scaling hypothesis is correct. While these curves appear somewhat similar, one can notice, nevertheless, differences between the scaling function $F(x)$ at different quenches.

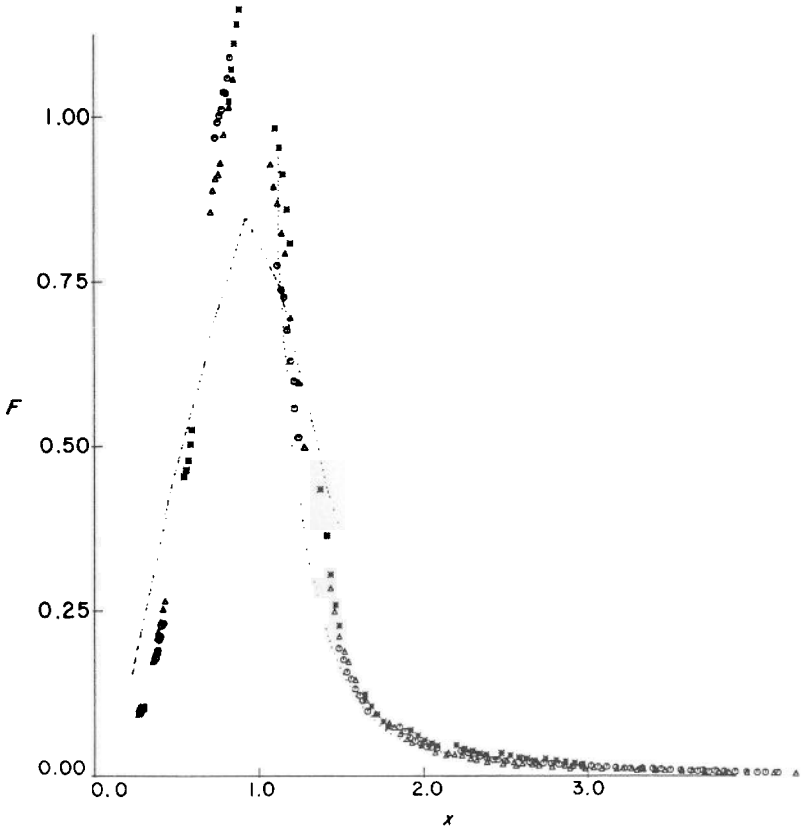

FIG. 29. The scaling function $F(x)$ versus x in the case of "deep" quenches. The triangles (Δ) correspond to a quench to P_4 ($T = 0.59T_c$, $\bar{c} = 0.2$) for times $t \geq 1500$, the asterisks (*) to P_5 ($T = 0.59T_c$, $\bar{c} = 0.5$) and $t \geq 350$ and the circles ($\bigcirc$) to P_6 ($T = 0.78T_c$, $\bar{c} = 0.5$) and $t \geq 1000$. The dashed line represents the shape of the function at an early time ($t = 110$ in the case of P_4) when scaling does not hold. The dotted line corresponds to a fit with a function $F^{-1} = \alpha_1 + \alpha_2 x^4$ for the data in the interval $x_m < x < x_0(t)$, suggested by the work of Furukawa (1979, 1981). (From Lebowitz *et al.*, 1982.)

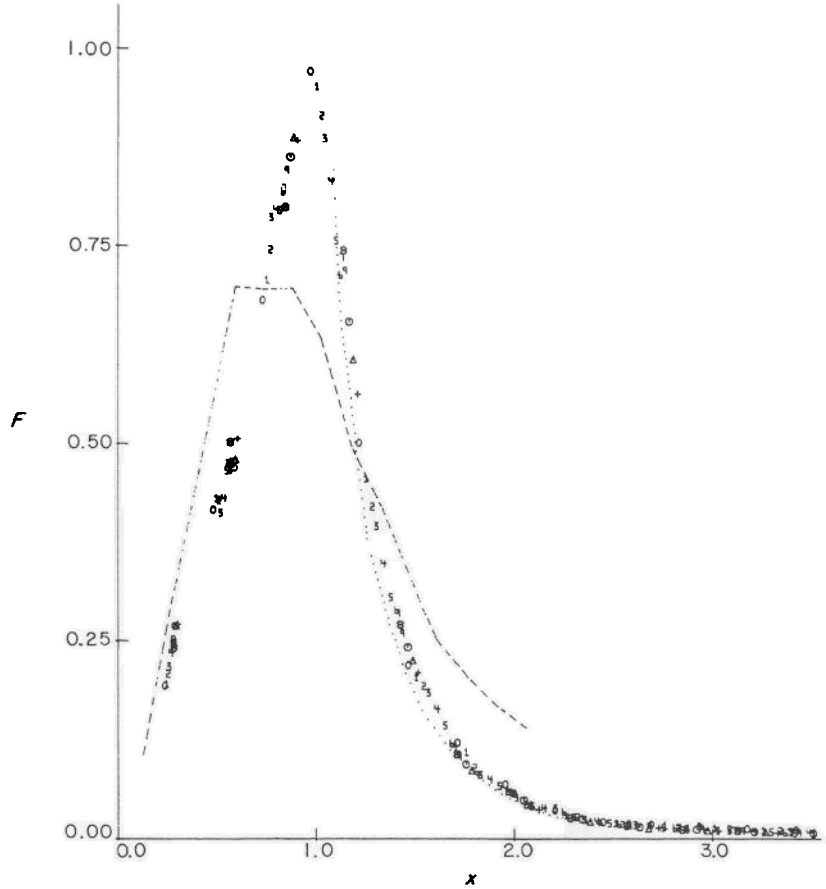

FIG. 30. The scaling function $F(x)$ versus x in the case of "intermediate" quenches to P_3 ($T = 0.59T_c$, $\bar{c} = 0.1$). The data in the time interval $2500 \leq t \leq 7300$ is denoted by different symbols (0, 1, 2, 3, . . .), where circles ($\bigcirc$) corresponds to an early time $t \simeq 2500$ and crosses ($\times$) correspond to the late times $t \simeq 7300$. The dashed curve is the behavior of $F(x)$ at an early time ($t \simeq 228$) where scaling does not hold. The dotted line is a fit $F^{-1} = \alpha_1 + \alpha_2 x^4$ to the data of $F(x)$ for $x > x_m$. (From Lebowitz *et al.*, 1982.)

D. Surface energy

Another quantity which is monitored in these computer simulations is $u = N_{AB}/N$, the number of A—B bonds per lattice site. This is related to the total energy U of the system through the simple relation $U = NJ(2u - 3)$. At $t = 0$, the quantity $u \simeq 6\bar{c}(1 - \bar{c})$ and decreases rapidly

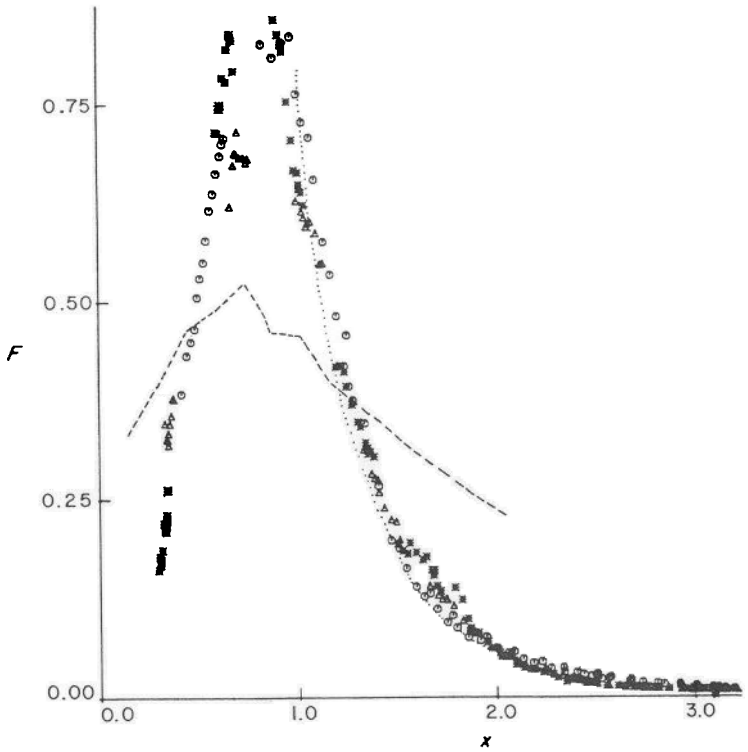

FIG. 31. Same as in Figs 29 and 30 in the case of "shallow" quenches to P_1 ($T = 0.59T_c$, $\bar{c} = 0.05$), P_2 ($T = 0.59T_c$, $\bar{c} = 0.075$) and P_7 ($T = 0.89T_c$, $\bar{c} = 0.5$). The data included in the scaling analysis at P_1 (triangles), P_2 (asterisks) and P_7 (circles) is beyond t_0 where t_0 is equal to 6800, 4000 and 1000, respectively. The dashed line is for P_1 at $t = 209$. (From Lebowitz *et al.*, 1982.)

(after a quench in the two-phase region) to approach asymptotically the finite equilibrium value $u_\infty(\bar{c}, T)$. Unfortunately, there exists no reliable estimates of $u_\infty(\bar{c}, t)$ for $T < T_c$, since the interfacial energy gives a non-vanishing contribution to $u_\infty(\bar{c}, T)$ for the finite systems studied in computer simulations. Marro *et al.* (1975) have estimated an approximate value of $u_\infty(\bar{c}, T)$ for $T < T_c$ by setting

$$u_\infty(\bar{c}, T) = u_\infty(\bar{c}, 0)\sigma(T) + u_p(T), \tag{9.23}$$

where $\sigma(T)$ is the surface tension (with $\sigma(0) = 1$ and $\sigma(T > T_c) = 0$). They used the value of $\sigma(T)$ for $0 < T < T_c$ obtained from Monte Carlo computations by Leamy *et al.* (1973). The quantity $u_p(T)$ is the equilibrium energy in the pure phase. It satisfies $u_p(0) = 0$ and has been estimated theoretically by Baker (1963) and Binder (1972).

Assuming an asymptotic behavior for $u(t)$ of the form

$$u(t) \sim t^{-b}, \tag{9.24a}$$

$$(u(t) - u_\infty(T)) \sim t^{-b'}, \tag{9.24b}$$

$$(u(t) - u_p(T)) \sim t^{-b''}, \tag{9.24c}$$

Marro *et al.* (1975) and Sur *et al.* (1977) have obtained estimates of b, b' and b'' which are listed in Table VI. It should be noted that the exponents for some points are in approximate agreement with the predictions of the Binder–Stauffer (1974) theory which gives $b' \simeq 1/6$ for $d = 3$ (Section VII.F). At other points, deviations from this theoretical value are very large. Studies of $u(t)$ for the two-dimensional case have also been made by Rao *et al.* (1976). Values for the exponents are given in this paper. It should be noted, however, that definitive statements about $u(t)$ cannot be made at the moment in either two or three dimensions. Existing estimates for exponents such as b, b' and b'' should therefore be viewed with considerable caution.

TABLE VI. The exponents b, b' and b'' as defined in eqn (9.24) for different phase points.

$\bar{c}$	T/T_c	Phase point	b	b'	b''
0.5	0.59	P_5	0.16	0.22	0.18
	0.78	P_6	0.10	0.22	0.16
	0.89	P_7	0.06	0.21	0.13
	1.07	P_8	0.02	0.79	0.79
0.2	0.59	P_4	0.16	0.28	–
	0.89	P_9	0.02	0.14	–
	1.07	P_{11}		1.0–1.1	–
0.1	0.59	P_3		0.33	

E. Cluster growth

We next present some results for cluster growth, to shed some more light on the dynamical evolution of a system undergoing a phase separation process. This cluster approach is especially useful in helping to understand the transmission electron microscope (TEM) experiments on real alloys.

Kalos *et al.* (1978) and Penrose *et al.* (1978) have carried out extensive computer simulations and have monitored the growth of clusters at low concentrations. In their Monte Carlo simulations they have characterized a cluster by two parameters (or cluster coordinates). These are the size l, defined as the total number of A (or B) atoms in a given cluster, and the surface area s, defined as the total number of A—B bonds. This is an example of the cluster picture discussed in Section VII. It is quite easy to monitor the above two parameters in computer simulation studies. They have also monitored the cluster distribution $n_l(t)$ from which they have obtained the average cluster size $\bar{l}$, the average surface size $\bar{s}$ and the energy per site u as a function of time. We first discuss some qualitative features of the cluster growth at different points on the phase diagram (Kalos *et al.*, 1978). We then summarize a quantitative analysis of the cluster growth due to Penrose *et al.* (1978).

Kalos *et al.* (1978) and Sur *et al.* (1977) have studied the cluster distribution function $n_l(t)$ at points very close to the coexistence curve and at P_1–P_4. These simulations were performed on simple cubic lattices of $50 \times 50 \times 50$ and $30 \times 30 \times 30$ sites using periodic boundary conditions. For values of concentrations close to the saturated vapor density $c_5 \simeq 0.0146$, but less than $\bar{c} \simeq 0.035$ at $T = 0.59T_c$, the cluster distribution function $n_l(t)$ rapidly ($t \leqslant 100$) settles down to a stationary value characteristic of a metastable state. Between the points P_1 and P_3, the distribution of small clusters still rapidly approaches a quasistationary distribution which corresponds to metastable states. However, there is now a measurable rate at which larger clusters develop (i.e. there is a finite nucleation rate). A detailed quantitative analysis of cluster growth and its distribution at point P_2 ($\bar{c} = 0.075$, $T = 0.59T_c$) based on the ideas of the Becker–Döring (1935) and Lifshitz–Slyozov (1961) and Wagner (1961) theories is summarized in the concluding part of this section. The results of this analysis are also applicable to all points between P_1 and P_3.

As the concentration $\bar{c}$ is increased further to the region $0.1 \leqslant \bar{c} \leqslant 0.2$ at $T = 0.59T_c$, Kalos *et al.* (1978) observed an early appearance of relatively large, loose clusters which coexist with very small clusters ($l \leqslant 10$). The number of A atoms and their relative distribution in small clusters is close to what is observed in the A-poor ("gas") phase in a system existing in the two-phase equilibrium state and becomes time independent. However, the system shows a slow process of coagulation of the larger clusters into still larger compact clusters which will eventually lead to a fully segragated A-rich ("liquid") phase.

On further increasing the concentration $\bar{c}$ beyond P_4, the system undergoes percolation, i.e. an "infinite" size cluster appears. This happens in the Ising model at approximately $\bar{c} \simeq 0.31$ at $T = \infty$ (the value of the uncorrelated percolation threshold for a simple cubic lattice). As the temperature is lowered, the correlation between atoms become important and results in decreasing the percolation threshold value. The percolated clusters have been noticed by Sur *et al.* (1977) at concentrations as low as $\bar{c} = 0.2$ at $T = 0.59T_c$.

A detailed quantitative analysis of the cluster growth at P_2 has been given by Penrose *et al.* (1978). The time evolution of the clusters following quench can be divided into three stages. In the first stage, which lasts for about 10 MCS ($t \leqslant 10$), the distribution of clusters changes rapidly. The initial distribution in which nearly all the atoms are in monomers evolves toward one with many more large clusters ($l \geqslant 2$) and fewer monomers. During the second stage ($10 \leqslant t \leqslant 100$), the number of large clusters ($l > 30$) continues to grow, but the distribution of small clusters ($l \leqslant 10$) has more or less stabilized. In the third stage ($t \geqslant 100$) the number of large clusters decreases slowly, whereas the individual clusters increase in size. It should be noted that even at the latest times studied, however, the system is never near equilibrium. There are about 20 large clusters present (of variable size 25–750), rather than one single large equilibrium cluster of $l \simeq 7500$.

Penrose *et al.* (1978) base their quantitative analysis of the cluster growth at P_2 on the ideas of the Becker–Döring and Lifshitz–Slyozov theories discussed in Sections II, VI and VII. In particular, their discussion is based on the formal Becker–Döring equation (7.13), together with the conservation law

$$\sum_{l=1}^{\infty} l n_l(t) = \bar{c} = \text{constant}. \tag{9.25}$$

They discuss their analysis in terms of an adjustable parameter ω which physically corresponds to the instantaneous "vapor pressure", which changes with time as the cluster distribution changes. For a cluster of size l, this parameter is given by an approximate empirical formula

$$\omega_l = \omega_s \left[1 + \frac{C}{(l-2)^{1/3}}\right]. \tag{9.26}$$

In (9.26) C acts as a surface tension and depends upon the temperature (Buhagiar, 1980) and the saturated vapor pressure

$$\omega_s = \lim_{l \to \infty} \omega_l = 0.010526 \quad \text{for} \quad T = 0.59T_c.$$

The physical basis for writing eqn (9.26) is that the "vapor pressure" of a spherical droplet of size l exceeds that over a plane surface by an amount proportional to the curvature ($l^{-1/3}$) of the surface of the droplet. Using eqns (9.25) and (9.26), Penrose *et al.* obtain a cluster distribution $n_l(t)$

TABLE VII. Comparison of steady state distribution of small clusters obtained from (a) computer simulations, (b) empirical formula (9.26) and (c) numerical solution of Becker–Döring equation (third row) at P_3 ($T = 0.59T_c$, $\bar{c} = 0.1$) for different times. Also the ratio ω/ω_s is listed as a function of time. The factor ω_s (the equilibrium value of ω) is equal to 0.010526 at $T = 0.59T_c$.

t	ω/ω_s	l_c		$n_1(t)$	$n_2(t)$	$n_3(t)$	$n_4(t)$	$n_5(t)$	$n_6(t)$	$n_7(t)$	$n_8(t)$	$n_9(t)$	$n_{10}(t)$	$\sum_1^{10} ln_l(t)$
75.67	2.0160	15.43	(a)	2134	546	248	145	97	69	53	44	34	29	6764
			(b)	1934	497	237	144	100	75	60	50	44	39	6771
			(c)	1923	497	241	152	110	85	69	59	51	45	7172
550.88	1.7007	42.94	(a)	1621	368	139	72	39	27	18	14	9	9	3818
			(b)	1631	353	142	73	43	27	18	13	9	7	3813
			(c)	1631	354	142	74	44	29	20	14	11	9	3896
1105.72	1.6211	60.78	(a)	1545	333	123	59	32	18	13	9	6	5	3358
			(b)	1554	321	123	60	34	20	13	9	6	4	3352
			(c)	1555	322	123	61	34	21	14	10	7	5	3399
2358.4	1.5063	110.51	(a)	1465	282	100	42	23	12	8	4	3	2	2813
			(b)	1445	277	98	45	23	13	8	5	3	2	2809
			(c)	1443	277	98	45	23	13	8	5	3	2	2807
4118.24	1.4292	180.18	(a)	1397	260	83	33	16	8	5	3	2	1	2508
			(b)	1371	250	84	36	18	10	5	3	2	1	2504
			(c)	1371	250	84	36	18	10	5	3	2	1	2504
5570.5	1.4310	177.90	(a)	1420	266	77	32	16	9	4	3	2	1	2515
			(b)	1373	250	84	37	18	10	5	3	2	1	2510
			(c)	1373	250	84	37	18	10	5	3	2	1	2510

which is in reasonable agreement with the results of Monte Carlo simulation. Furthermore, they show that the critical size of the cluster, l_c, increases linearly with time as predicted by the LS theory. However, we should point out that their analysis and the computer simulation results are not in the asymptotic time domain of the LS theory. A discussion of this fact is given by Penrose *et al.* (1978).

Finally, we note that Buhagiar (1980) has solved the Becker–Döring kinetic equation (7.13) numerically at P_3 ($T = 0.59T_c$, $\bar{c} = 0.1$). The initial data for $T = \infty$ was provided by computer simulations. He obtained both the cluster distribution $n_l(t)$ and the parameter $\omega(t)$ at different times. These results are shown in Table VII, together with the results of the Monte Carlo study at P_3 (Marro *et al.*, 1975). As can be seen, his results agree quite well with the simulation results.

X. Studies of Nucleation in Near-critical Fluids

A. Experimental results

In 1962 Sundquist and Oriani found that the binary fluid perfluoromethylcyclohexane (PMCH) plus methylcyclohexane (MCH) could be supercooled in the vicinity of its critical point to an extent very much greater than predicted by classical nucleation theories of the Becker–Döring (1935) or Langer–Turski (1973) type. This result attracted considerable attention in the field, since it seemed to signal a major breakdown in our theoretical understanding of nucleation. Subsequent experiments on a variety of binary mixtures and one-component systems confirmed that near the critical point metastable fluids seemed unusually stable (Dahl and Moldover, 1971; Heady and Cahn 1973; Huang *et al.*, 1974b, 1975); Schwartz *et al.*, 1980; Howland *et al.*, 1980). These experiments were originally interpreted as implying that the nucleation rate, of the form (4.14), was much smaller near a critical point than the existing theories predicted. Furthermore, the effect seemed dramatic, since the rate seemed smaller by a factor of about 10^{20} (Langer, 1980). Thus, several theories were proposed which tried to explain the experimental results in terms of effects which would significantly decrease the nucleation rate, either by increasing the activation energy or decreasing the kinetic prefactor in (4.14) (Mou and Lovett, 1975; Sarkies and Frankel, 1975; McGraw and Reiss 1979). Such theories, however, proved to be unsuccessful (Howland *et al.*, 1980). It now appears that these experiments have not observed a breakdown of nucleation theory, but rather an effect of the critical slowing down of droplet growth. An account of this theoretical explanation, which involves both the nucleation and growth of droplets, is given in Section X.B.

Before discussing this theory, we summarize the experimental results. These experiments do *not* measure the nucleation rate I. Rather they determine the cloud point temperature. As noted in Section I, this is the temperature at which, on the time scale of the experiment, there is a sudden clouding of the system due to the appearance of droplets. One technique for determining this cloud point involves temperature quenches at constant pressure. In this case one lowers the temperature by constant increments of 1–5 mK, say, waiting for some period of time between each step, say 1 min. The cloud point is then taken to be the lowest temperature determined before the intensity of transmitted light dramatically decreases. An alternative quench method in binary mixtures involves altering the pressure at constant temperature. This produces both a change in the coexistence curve and in T_c, with $\Delta T_c = (dT_c/dp)\Delta p$, where $T_c(p)$ is a pressure-dependent line of critical points (Wong and Knobler, 1978). A typical estimate of the cloud point is shown in Fig. 32 (Howland *et al.*,

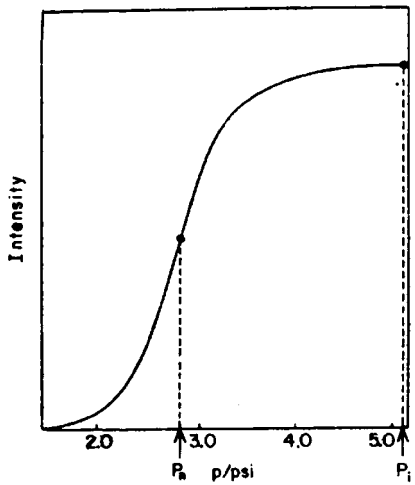

FIG. 32. Transmitted intensity in arbitrary units versus pressure for a quench from $\Delta T = 7$ mK. The quench was begun at P_i and P_n is taken as the cloud point. (From Howland *et al.*, 1980.)

1980). It should be noted that in these pressure quenches the speed of the quench is limited only by the velocity of sound and the size of the sample. Thus an effective temperature shift can be attained in only a few milliseconds. This is several orders of magnitude faster than a conventional bath quench.

The location of the cloud point is rather precisely predicted by classical nucleation theory. Thus experimental measurements of the cloud point can

be used to test nucleation theory. The theoretical determination of the cloud point is based on the fact that the nucleation rate has a sharp dependence on the degree of supercooling. This supercooling is expressed in terms of the natural variable x defined in (4.36). For a constant composition quench it is given by

$$x = \delta T/\varepsilon T_c, \tag{4.37}$$

where we use the notation indicated in Fig. 1. The natural variable which enters in the Langer–Turski expression (4.45) is

$$y = x/x_0, \tag{10.1}$$

where

$$x_0 = \frac{8}{\beta}\left(\frac{\pi}{3}\right)^{1/2}\left(\frac{\sigma_0^3}{k_B T}\right)^{1/2} \Big/ (\Delta c_0)^2 g_0. \tag{10.2}$$

To estimate I/V in (4.45) one needs to determine x_0 and other quantities whose asymptotic behaviour near the critical point is given by the following set of relations (as in Table I):

$$\Delta c = \Delta c_0 \varepsilon^{\beta}; \tag{10.3}$$

$$\frac{\partial^2 G}{\partial c^2} = g_0 \varepsilon^{\gamma}; \tag{10.4}$$

$$\xi = \xi_0 \varepsilon^{-\nu}; \tag{10.5}$$

$$\sigma = \sigma_0 \varepsilon^{\mu}; \tag{10.6}$$

$$D = D_0 \varepsilon^{\nu}; \tag{10.7}$$

where G is the Gibbs free energy. Experimental estimates of these quantities for two mixtures, PMCH + MCH, and isobutyric acid plus water (IW), are given in Table VIII (Howland *et al.*, 1980). Using these values one can then estimate from (4.31) that I/V changes from 1 cm^{-3} s^{-1} to 10^5 cm^{-3} s^{-1} as the supercooling is increased from $y \cong 0.13$ to $y \cong 0.15$. Thus the Langer–Turski theory gives a quite precise prediction for the location of the cloud point. (A very similar prediction follows from the Becker–Döring theory, eqn (4.35).) As noted in Section IV, the general prediction for the critical supercooling is of the form (4.36). However, as can be seen in Fig. 33 (Howland *et al.*, 1980), one sees strong deviations from this relation as the critical point is approached. It is this deviation that was originally interpreted as implying a failure of classical Becker–Döring or Langer–Turski type theories.

TABLE VIII. Critical parameters.

	IW	PMCH + MCH
T_c (K)	299	399
σ_0 (dyn cm^{-1})	26	21.9
Δc_0 (cm^{-3})	3.06×10^{22}	3.12×10^{21}
D_0 (cm^2 s^{-1})	1.51×10^{-6}	1.6×10^{-5}
ξ_0 (cm)	1.8×10^{-8}	2.2×10^{-8}
g_0 (erg cm^3)	1.5×10^{-35}	1.0×10^{-33}
x_0	1.2	1.3
ν	0.62	0.62
β	0.31	0.33

However, it now appears that the correct explanation of this phenomenon is one originally proposed by Binder and Stauffer (1976). They first observed that a cloud point is not an intrinsic, time-independent property of a system. It in fact involves time, since it is the temperature at which, on the *time scale of the experiment*, the sample becomes cloudy. They suggested, therefore, that a more meaningful quantity in these experiments is the "completion time", which is the time required for the reaction to go to completion. This completion time clearly involves not only the rate at which droplets are born, but also the rate at which they grow. Binder and

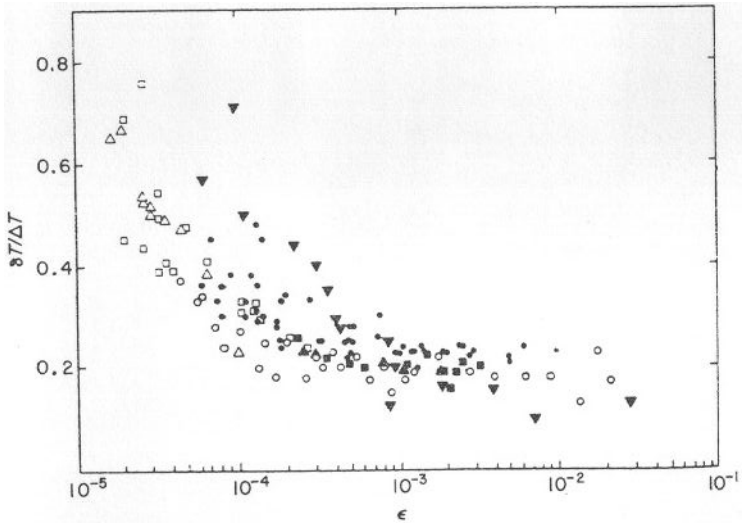

FIG. 33. Comparison of several supercooling experiments. Squares and triangles, IW; closed circles, PMCH + MCH; open circles, methanol + cyclohexane; inverted triangles, LW. (From Howland *et al.*, 1980.)

Stauffer thus suggested that effects of critical slowing down were responsible for the apparent deviations from classical theory. The slowing down of the growth rate is a consequence of the fact that in fluid mixtures growth is controlled by diffusion, but the diffusion constant vanishes as $T \to T_c$ (eqn (10.7)). Therefore experimentalists were unable to see clouding of the system simply because the droplets had not grown to an observable size, rather than because they had not formed. A detailed version of this simple idea is summarized and compared with experimental results in the next section.

Before concluding this discussion of experimental results, it should be noted that these experiments are quite difficult and involve a choice of several different experimental procedures. Although all the experiments measure cloud points, there are significant differences in the details among the various experiments. A nice discussion of these differences and their significance in the interpretation of results is given by Howland *et al.* (1980).

B. Theory of completion time

Langer and Schwartz (1980) have developed a detailed theory which describes the nucleation and growth of droplets in metastable, near-critical fluids. Their work is an extension of the original calculation of Binder and Stauffer (1976) which we summarize later. The Langer–Schwartz theory is not a first principles theory of nucleation and growth, due to the difficulty of extending the field theoretic formalism of nucleation theory (Section IV) to the late-stage growth regime. Nevertheless, their simplified model seems to describe reasonably well the present experimental results. No definitive test of their theory exists as yet, however.

The basic equations of the Langer–Schwartz theory are those of Lifshitz and Slyozov (Section VI), supplemented by a source of droplets which describe the nucleation events. The droplet growth rate equation is

$$\frac{dR}{dt} = \frac{D}{R}\left(\frac{\delta c}{\Delta c} - \frac{2d_0}{R}\right), \tag{10.8}$$

which is (4.20), rewritten in terms of a capillary length d_0,

$$d_0 = \frac{\sigma}{(\Delta c)^2 (\partial\mu/\partial c)_A}. \tag{10.9}$$

If one uses a Ginzburg–Landau "c^4" model for the free energy, one can estimate d_0 to be

$$d_0 = \xi/6. \tag{10.10}$$

The second equation is (6.4), which expresses the conservation of solute molecules. The third equation is the continuity equation for the droplet distribution function $f(R, t)$, modified by a term $j(R)$ which describes a source distribution of droplets:

$$\frac{\partial f(R,t)}{\partial t} = -\frac{\partial}{\partial R}[f(R)v(R)] + j(R). \tag{10.11}$$

The nucleation rate per unit volume, $J = I/V$, is given by

$$J = \int_{R_c}^{\infty} j(R)\, dR. \tag{10.12}$$

Since the experiments on critical fluids involve relatively large supersaturations for which no field theory yet exists, Langer and Schwartz assume that J can be described in terms of the imaginary free energy, via eqn (4.55). They approximate this (unknown) free energy (see (4.46)) by

$$\frac{1}{kT}\,\mathrm{Im}\,\mathcal{F}(x) = \frac{A}{\xi^3}\left(\frac{x_0}{x}\right)^{7/3}\left(1+\frac{x}{x_0}\right)^{\phi}\exp-\left(\frac{x_0}{x}\right)^2, \tag{10.13}$$

where $\phi = (10/3 + 1/\delta) \simeq 3.55$. This form for Im $\mathcal{F}$ reduces to (4.44) for small supersaturation, $x \ll 1$, and satisfies the scaling form

$$\mathcal{F} = \varepsilon^{3\nu}(-x)^{1+1/\delta}, \qquad x \gg 1. \tag{10.14}$$

The nucleation rate is then determined from (4.55) and (10.13).

Equations of motion for dN/dt and $d\bar{R}/dt$ are then obtained by taking the time derivative of

$$N = \int_{R_c}^{\infty} f(R)\, dR \tag{10.15}$$

and

$$\bar{R} = N^{-1}\int_{R_c}^{\infty} f(R)R\, dR, \tag{10.16}$$

using (10.11). (It should be noted that (10.15) differs from that of Lifshitz and Slyozov in that only droplets with $R > R_c$ are considered as part of the B phase.) The equations of motion which Langer and Schwartz thus use are the conservation law (6.4), (10.15) and (10.16).

Their theory is based on a truncation of these equations of motion which involves some rather *ad hoc* approximations which we do not discuss. They also impose a boundary condition that the late stage growth agrees with the Lifshitz–Slyozov result (6.8). The resulting equations are then solved

numerically for the relative supersaturation y, given by (10.1), as a function of the scaled time τ,

$$\tau = \frac{Dx_0^3}{24\xi^2}t, \tag{10.17}$$

for different initial supersaturations $y_1 = x_1/x_0$. One quantity of interest is the scaled completion time τ_c, defined as the time at which the reaction has gone half-way to completion, i.e.

$$y(\tau_c) = \tfrac{1}{2}y_1. \tag{10.18}$$

Their results are shown in Fig. 34. A Binder–Stauffer estimate of τ_c as well as a scaled version τ_N, of the conventional nucleation time t_N, are also shown in this figure. This latter quantity is defined as $1/J$, where J is the nucleation rate obtained from (4.45) and (10.13). Then τ_N is defined through (10.17), with $t = t_N$.

Before discussing Fig. 34, we briefly summarize a version of the Binder–Stauffer theory, using the nucleation and scaling forms assumed by Langer and Schwarz. The first approximation in the Binder–Stauffer

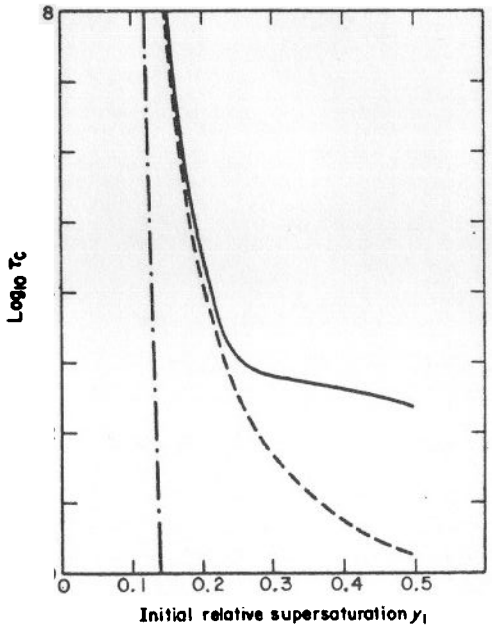

FIG. 34. Half-completion time τ_c as a function of initial relative supersaturation. The solid line is the Langer–Schwartz theory. The dashed curve has been computed using the Binder–Stauffer approximation and the dash–dot curve is the conventional nucleation time. (From Howland *et al.*, 1980.)

theory is that one can neglect the capillary corrections to the growth rate, given by $2d_0/R$ in (10.8). This is reasonable as the reaction goes to completion because the droplets become very large. The other approximation is to neglect the time dependence of the supersaturation in the equations for $d\bar{R}/dt$ and dN/dt. In this approximation new droplets are formed at a constant rate during the process. The prediction of this theory for τ_c is shown in Fig. 34. We can see from this figure that the Langer–Schwartz and Binder–Stauffer theories are in reasonable agreement for small supersaturation $y_1 \leqslant 0.2$, as should be the case. The other significant point is that the nucleation curve shown in Fig. 34 is distinctly to the left of the completion curves for the physically accessible values of τ_c. The location of this nucleation curve is very nearly independent of temperature and relatively insensitive to the choice of t_N.

An interesting prediction of the Langer–Schwartz theory which can be compared with the experimental results is that if one chooses a fixed completion time t_c (e.g. 1 min) typical of a given experiment, then the dynamical scaling relation

$$\tau_c(y_1) = \frac{Dx_0^3 t_c}{24\xi^2} = \frac{D_0 x_0^3 t_c}{24\xi_0^2}\varepsilon^\nu \tag{10.19}$$

yields a relation between the initial (relative) supersaturation y_1 and the rescaled temperature, where

$$\varepsilon_c = \left(\frac{D_0 x_0^3}{24\xi_0^2}\right)^{1/3\nu}\varepsilon. \tag{10.20}$$

Thus

$$\varepsilon_c^{3\nu} = \tau_c(y_1)/t_c. \tag{10.21}$$

The only system-dependent parameter which occurs in (10.21) is x_0, but the dependence of τ_c on this parameter should be relatively weak. Therefore, if a given group of experiments on different systems has a fixed observation time t_c, all the measurements of the maximum relative supersaturation y_1 should lie on a single curve $y_1(\varepsilon_c)$. This curve is given implicitly by (10.21).

We can now compare the experimental work on critical fluids with the Langer–Schwartz theory. This is done in Fig. 35, where it can be seen that the agreement between theory and experiment is quite reasonable, given the relative uncertainty in experimental determination of t_c and other parameters which enter the theory (Langer and Schwartz, 1980; Howland *et al.*, 1980). Therefore the deviations from the classical cloud point curve seem to be due to the effects of critical slowing down on the droplet growth.

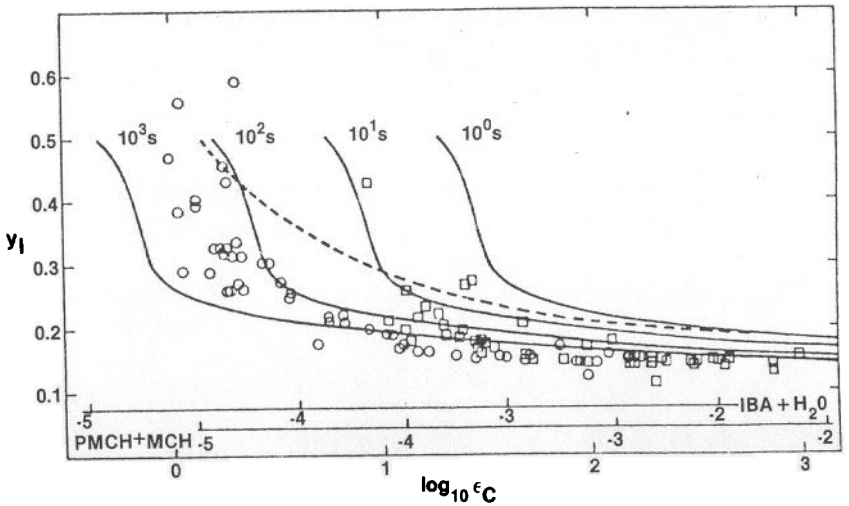

FIG. 35. Completion time curves for 1, 10, 100 and 1000 s. The ordinate is the relative initial supersaturation $y_1 = x_1/x_0$ and the abscissa is defined by eqn (10.20). Dashed curve represents simplified theory for $t_c = 15$. (From Howland *et al.*, 1980.)

However, a corollary of this conclusion is that one still has no direct test of nucleation theory itself.

An ambitious experimental program, aimed at examining in more detail nucleation and growth in critical fluids, has been initiated by Khrishnamurthy and Goldburg (1980). They studied with a microscope the formation and growth of nuclei in metastable 2,6-lutidine and water close to its critical point. They were able to confirm quite convincingly the simultaneous occurrence of nucleation and growth, and thereby establish that the basic idea of Binder and Stauffer is correct. In addition, they measured the droplet size distribution function, density of droplets and average droplet size as a function of time. Unfortunately the rate of droplet formation depends so strongly on the supercooling that their results were only reproducible within an order of magnitude from one quench to another. Therefore they were unable to test quantitatively the predictions of the Langer–Schwartz theory. Nevertheless, this work clearly establishes the direction of future research in this area, in that a detailed experimental determination of the phase separation of a fluid now seems feasible.

Finally, we should note that not all experimental results are in agreement with the Langer–Schwartz theory. In particular, in a measurement of metastability in CO_2 (Huang *et al.*, 1975) at a reduced temperature, $\varepsilon = 3.15 \times 10^{-3}$ and supersaturation $x_1 = 0.16$, the system remained stable for 4 h without showing any detectable latent heat. Thus the system showed

no detectable nucleation, in disagreement with theory. Also the work of Krishnamurthy and Goldburg (1980) revealed a considerably greater number of droplets at the relative supersaturation $y_1 = 0.1$ than the theory would predict. A satisfactory explanation of such phenomena remains to be given. Thus one should still consider the issue of anomalous undercooling in near-critical fluids as only partially resolved. Further experimental and theoretical studies of this phenomenon seem necessary. However, at the moment there is no convincing evidence to suggest that homogeneous nucleation theory needs major revision.

XI. Experimental Studies of Spinodal Decomposition

A. Binary alloys

As mentioned earlier, the first experimental and theoretical studies of spinodal decomposition were carried out on alloys. This field is now a major area of research and several excellent reviews of the experimental work exist. In particular, a review of recent X-ray and neutron small angle scattering (SAS) experiments (Gerold and Kostorz, 1978) contains a detailed summary of experimental work since the pioneering X-ray SAS experiments on an Al–Zn alloy. Also, de Fontaine (1979) has reviewed the thermodynamics of phase separation as it relates to aotmic ordering. Tiapkin (1977) has discussed the microstructural aspects of decomposition and given an extensive list of the experimental studies. Ditchek and Schwartz (1979) have surveyed the experimental and theoretical work and in particular have discussed various applications of alloys undergoing spinodal decomposition. Another review which includes a discussion of other systems such as mixed oxides and geological systems has been written by Jantzen and Herman (1978). In view of the existence of such comprehensive reviews of the metallurgical literature, we primarily will content ourselves with discussing quite recent experimental work which shows the scaling behaviour first observed in Monte Carlo studies.

A classical example of phase separation in binary alloys is Al–Zn. This system has been extensively investigated, beginning with the original X-ray, SAS studies of Rundman and Hilliard (1967). They originally interpreted their results as a verification of the linear Cahn theory (Section IV). However, Gerold and Merz (1967) argued that this interpretation was incorrect. Further experiments were performed, which have led to a general consensus that the observed early time behavior of Al–Zn is not described by the linear theory. (This is reviewed by Gerold and Kostorz (1978).) Rather, the behavior is in qualitative agreement with the LBM theory. Exponential growth of $\hat{S}(k,t)$ is not observed. Instead, a peak in the

scattering intensity develops and grows with time. Coarsening is manifested by a continual decrease in the position of the peak height, $k_m(t)$. A partial list of these experimental studies of Al–Zn inlcudes Agarwal and Herman (1973), Junqua *et al.* (1974), Bartel and Rundman (1975), Laslaz *et al.* (1977a, b) and Laslaz (1978). It should also be noted that in addition to diffraction studies, other experimental methods exist for studying the process of phase separation in a less direct way. These are described by Ditchek and Schwartz (1979) and include measurements of electrical resistivity, thermoelectric power and magnetic measurements. Since these do not give information about $\hat{S}(k,t)$ directly, we do not discuss them here.

The most definitive study of Al–Zn seems to be the recent transmission electron microscope (TEM) and neutron SAS experiments by Hennion *et al.* (1982) and Guyot and Simon (1982). The SAS studies are the first phase separation experiments performed on single crystals. The use of single crystals allowed these authors to study certain anisotropic effects and to avoid discontinuous precipitation phenomena which occur at grain boundaries. The simultaneous use of TEM and SAS methods allowed them to compare cluster growth and structure function measurements.

The experiments have been carried out for several points in the slightly supersaturated region of the Al–Zn phase diagram, as shown in Fig. 36. Measurements of the coherent scattering cross-section per unit volume, $d\Sigma(\vec{k},t)/d\Omega$, directly yield the structure function via the standard expression (Hennion *et al.*, 1982)

$$\frac{d\Sigma(\vec{k},t)}{d\Omega} = \frac{1}{v_a}(b_{Al} - b_{Zn})^2 \hat{S}(k,t), \tag{11.1}$$

where v_a is the average atomic volume, b_{Al} and b_{Zn} are the scattering lengths for Al and Zn, respectively, and $\vec{k}$ is the scattering vector. The magnitude of $\vec{k}$ is related to the scattering angle θ by

$$k = 4\pi \sin\left(\frac{\theta}{2}\right)/\lambda, \tag{11.2}$$

where λ is the neutron wavelength. The use of long wavelength neutrons allows one to reach small k values not attainable in X-ray studies. (Neutron wavelengths in the range 0.67–1.86 nm were employed.) Results for the average scattering cross-section are shown in Fig. 37. These exhibit the qualitative behavior which has already been described.

The moments of $\hat{S}(k,t)$ can be obtained from the measured $d\Sigma/d\Omega$, using (11.1) and the definition

$$k_n(t) = \sum_{k_a}^{k_b} k^n \hat{S}(k,t) \Big/ \sum_{k_a}^{k_b} \hat{S}(k,t), \qquad n = 1, 2, \tag{11.3}$$

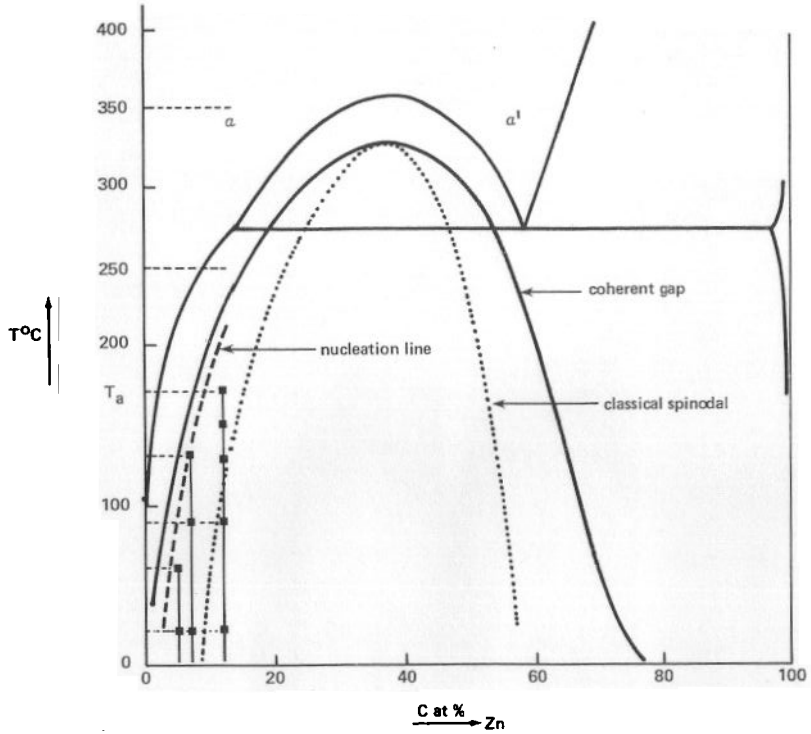

FIG. 36. Phase diagram for Al–Zn, showing the various quench points investigated (Hennion *et al.*, 1982; Guyot and Simon, 1982). The classical spinodal curve is shown as a dotted line.

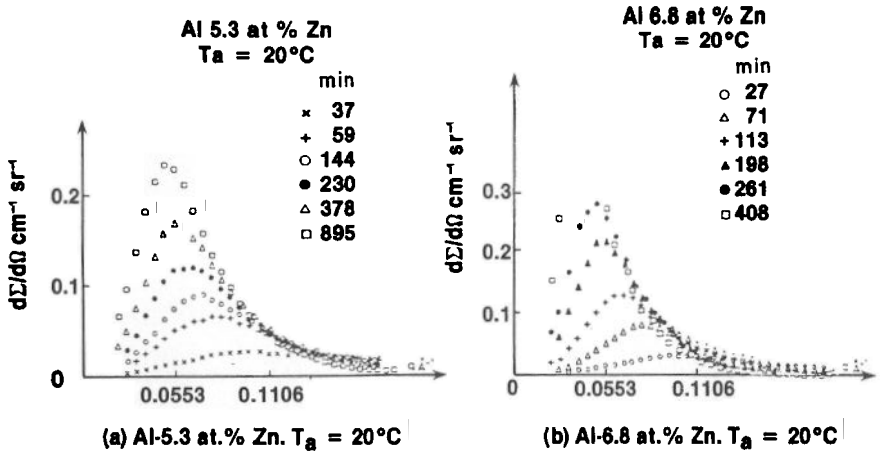

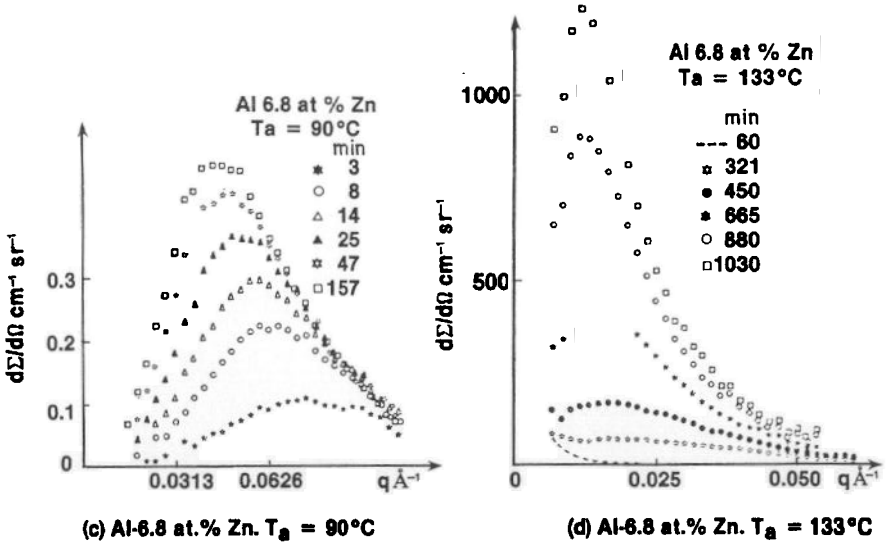

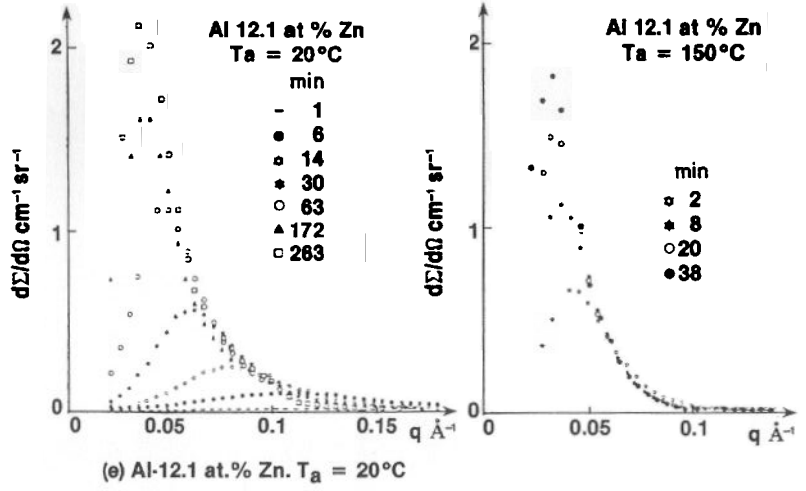

FIG. 37. The average scattering cross-section for Al–Zn for different aging temperatures T_a and concentrations. (a) Al 5.3 at% Zn, $T_a = 20\,°C$; (b) Al 6.8 at% Zn, $T_a = 20\,°C$; (c) Al 6.8 at% Zn, $T_a = 90\,°C$; (d) Al 6.8 at% Zn, $T_a = 133\,°C$; (e) Al 12.1 at% Zn, $T_a = 20\,°C$; (f) Al 12.1 at% Zn, $T_a = 150\,°C$. (From Guyot and Simon, 1982.)

where k_a and k_b are the minimum and maximum observable values of k. These cut-off wavenumbers occur in all numerical and experimental studies of $\hat{S}(k, t)$ and introduce an error in the determination of the moments. In particular, the existence of an upper cut-off, k_b, makes any precise determination of the moments for $n > 2$ difficult.

An analysis of $\hat{S}(k, t)$ and its scaling behavior has been given by Hennion *et al.* (1982) and Guyot and Simon (1982). To begin with, an attempt was made to model the time dependence of $k_m(t)$, $k_1(t)$ and $\hat{S}(k_m, t)$ by power law approximations. Typical results are shown in Table IX. These must be

TABLE IX. Power law approximation.

Alloy concentration	T (°C)	a	a''	m
5.3 at% Zn	20	0.2–0.3	0.9–1.0	0.3
6.8 at% Zn	20	0.25–0.3	1.0	0.3
	90	0.3	0.6	0.15–0.3
	110	0.1–0.3	—	—
	133	0.25–0.3	1.0	0.2–0.3
12.1 at% Zn	20	0.3	1.0	0.15–0.3
	130	0.15	0.45	0.15
	150	0.15	0.45	0.15
	169	0.15	0.45	—

viewed with caution, given the ambiguity involved in such fits. The possibility that $\hat{S}(k, t)$ might scale after some initial transient time is studied by first determining the behavior of $r(t)$, defined by (8.6) and (11.3). It was found (Hennion *et al.*, 1982) that this ratio is a slowly varying function of time for the different quenches studied. Typical variations are shown in Fig. 38. Since to a first approximation this ratio is constant, one can try a scaling analysis, as discussed in Section VIII. The results of this for the different quenches are shown in Fig. 39. The agreement with a scaling form after a certain transient time seems quite reasonable. The authors also claim that the scaling function $F(x)$ shows no significant variation with either temperature or alloy composition. A more conservative viewpoint would be that a weak dependence on these variables is observed. The latter conclusion would be more in accord with the results of the analysis of data from Monte Carlo and binary fluid experiments. The overall agreement of the binary alloy experiments with Monte Carlo results is in fact quite good, as we discuss later.

Several qualitative features of the Al–Zn study should be noted. The first is that the phase separation process depends on the degree of super-

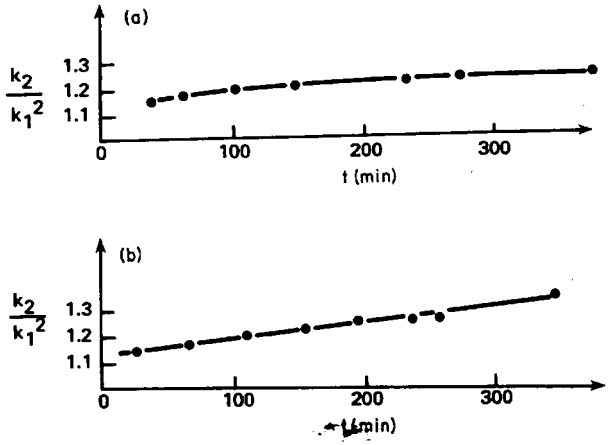

FIG. 38. The quantity $r(t) = k_2(t)/k_1^2(t)$ as a function of time for (a) Al 5.3 at% Zn, $T_a = 20$ °C; (b) Al 6.8 at% Zn, $T_a = 20$ °C.

saturation, as one would expect. In particular, both $k_m(t)$ and $\hat{S}(k, t)$ decrease as one decreases the supersaturation. Secondly, the late stage growth rate seems to satisfy the Lifshitz–Slyozov $t^{1/3}$ law for small supersaturation, as can be seen from Table IX. (To our knowledge, however, no experimental confirmation of the amplitude predicted by this theory, eqn (6.8), has been made.) The growth rate at Al 12.1 at% Zn does not seem to satisfy the Lifshitz–Slyozov law. Guyot and Simon (1982) interpret this as possibly indicating a coagulation growth mechanism, of the type proposed by Binder and Stauffer (1974, 1976). Thirdly, the study shows no evidence of any sharp distinction between metastable and unstable states in the region of the phase diagram which has been studied so far. The authors also note that the TEM studies of polycrystalline samples are consistent with their SAS results. (This comparison involved invoking a modeling of $\hat{S}(k, t)$ in terms of a cluster distribution which involves a hard sphere correlation function.) In addition, Guyot and Simon (1982) report that the time dependence of the number of droplets per unit volume which is observed in the Al–Zn studies is in good agreement with the Langer–Schwartz theory of nucleation and growth discussed in Section X. It should be noted, however, that this comparison involves using the theory at temperatures considerably below the critical point, where the Langer–Schwartz scaling approximations are presumably invalid (P. Guyot, private communication).

An interesting theoretical problem which has been raised by the Al–Zn experiments is the important role played by vacancies in real alloys. In alloys such as Al–Zn, the interchange of A and B atoms occurs through

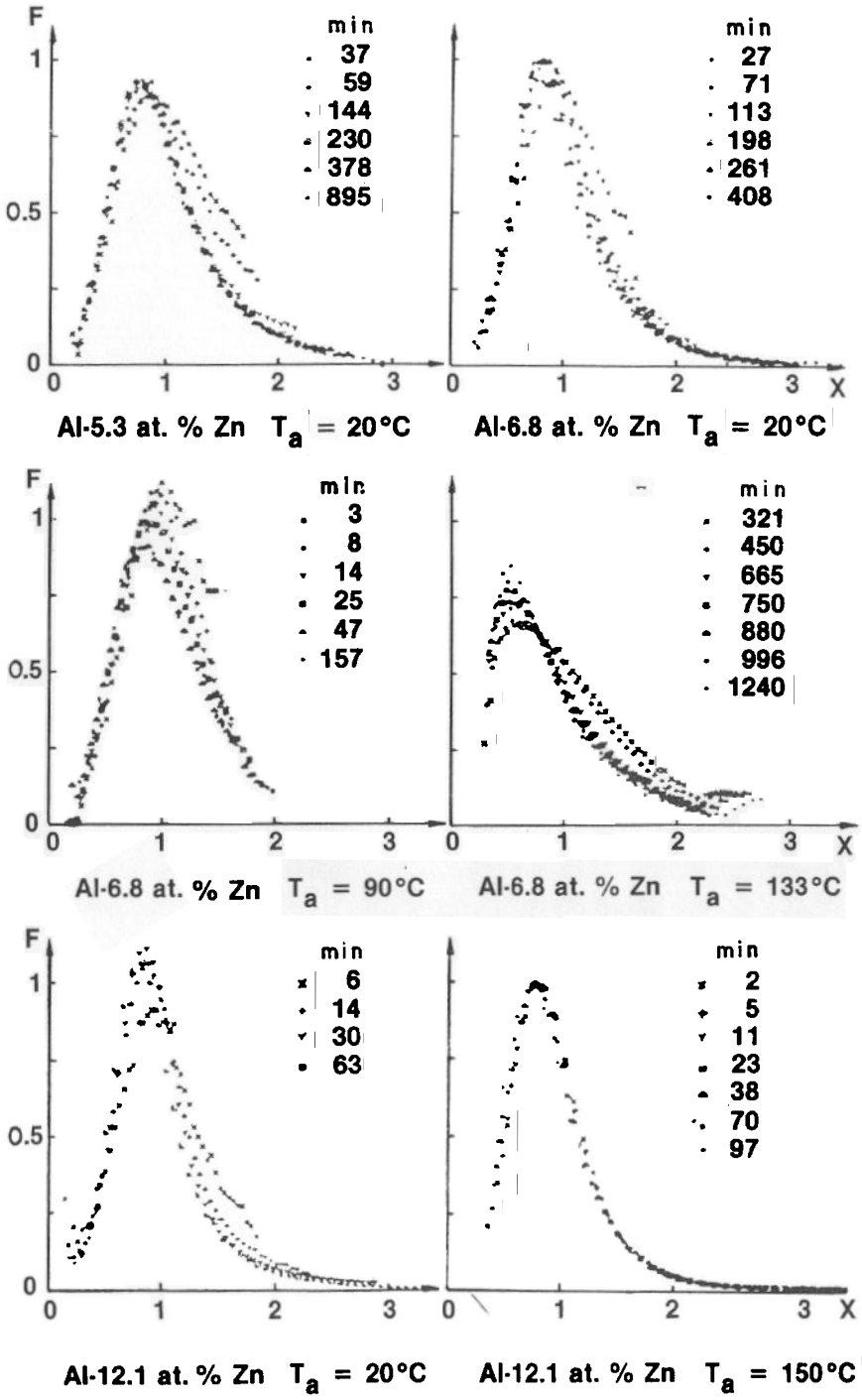

vacancies, rather than through the direct exchange employed in the Kawasaki exchange dynamics model used in Monte Carlo studies. There are two kinds of vacancies in the Al–Zn experiment: quench vacancies, which are present in the initial high temperature, disordered state, and thermal vacancies, which are in equilibrium at the quenched (aging) temperature. Hennion *et al.* (1982) have observed that it is the quench vacancies which are responsible for the initial stages of phase separation in their experiments, since these have a much larger diffusion constant than thermal vacancies. These quench vacancies are gradually eliminated from the system by being trapped at zone interfaces or removed at sinks. Thermal vacancies then take over. Thus the time unit, which is the time separating two successive interchanges of A and B atoms, changes during the experiment. When quench vacancies are important, the time unit is proportional to $\exp(U_m/k_BT)$, where U_m is the migration energy of the vacancy. When thermal vacancies take over, however, the time unit is proportional to $\exp((U_m + U_f)/k_BT)$, where u_f is the formation energy. A simple estimate (Hennion *et al.*, 1982) of these two time scales for Al–Zn at 20°C is 10^{-6} s and 10^6 s respectively. Such an effect has not been taken into account in theoretical or Monte Carlo studies.

In spite of this difficulty with making a precise comparison of time scales between Monte Carlo and experimental studies, the scaling functions obtained by these two methods are remarkably similar. Hennion *et al.* (1982) have shown, for example, that their scaling function for Al 5.3 at% Zn, $T/T_c = 0.49$, is very similar to the Monte Carlo data at the points P_1, P_2 and P_6, if they rescale the vertical axis. As well, quite good agreement is also obtained with the results of P_1, P_2 and P_6 for Al 6.8 at% Zn at $T = 0.64$ when both have been rescaled. Lebowitz *et al.* (1982) have also shown that the data for Au 60 at% Pt (Singhal *et al.*, 1978) is in good agreement with the Monte Carlo data at P_4 and P_5 if the vertical axis is rescaled (Fig. 40). Thus the Kawasaki model seems to describe the phase separation process in these binary alloys reasonably well.

B. Binary fluids

Another class of systems in which spinodal decomposition has been extensively studied is binary fluids. It was initially believed that experimental studies of spinodal decomposition in these liquid mixtures were not feasible, since the interdiffusion constant D is normally several orders of magnitude

FIG. 39. The scaling function $F(x)$ for the various concentrations of Zn and different aging temperatures T_a shown in Fig. 37. (From Guyot and Simon, 1982.)

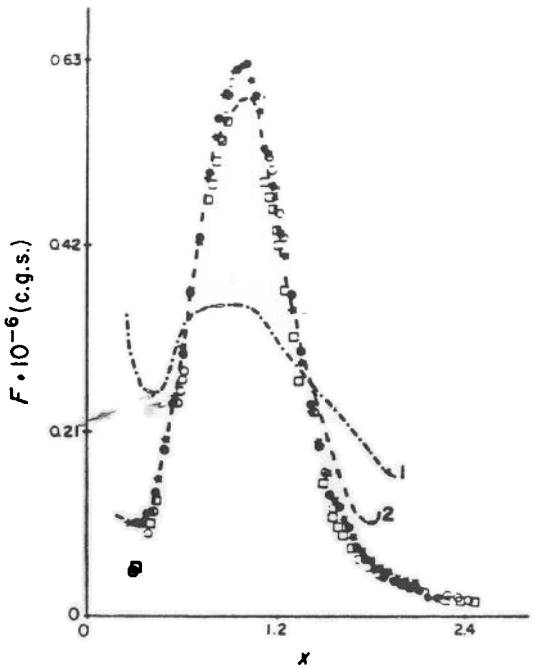

FIG. 40. Comparison of computer simulation data (empty symbols) with the experimental data from Singhal *et al.* (1978), for Au 60 at% Pt alloy quenched to $T \simeq 0.6T_c$. The full circles are for $t = 900$ s and the stars for $t = 360$ s, both lying on the same curve, except perhaps for $x \geq 1.8$. The broken line 1 is for $t = 0$ (the initial sample was already decomposed to some extent) and the broken line 2 is for $t = 30$ s. In both cases scaling does not yet hold. The empty circles correspond to the computer simulation at P_5 while the empty squares are for P_4. Only the vertical scale of the computer simulation results needed to be changed in order to obtain this fit. (From Lebowitz *et al.*, 1982.)

larger than in alloys or glasses. Thus the time scales for spinodal decomposition are typically very small for such fluids. However, Huang *et al.* (1974a) were able to circumvent this difficulty by making measurements very close to the critical point, where D vanishes (eqn (10.7)).

In this critical region spinodal decomposition occurs on an experimentally observable time scale. Since the pioneer work of Huang *et al.* (1974a) on cyclohexanemethanol, several other binary fluids have been investigated. These include 2,6-lutidene plus water (LW) (Schwartz *et al.*, 1975; Goldburg *et al.*, 1978a,b; Chou and Goldburg, 1979, 1981; Goldburg, 1981) and isobutyric acid plus water (IW) (Wong and Knobler 1978, 1979, 1981; Chou and Goldburg 1979, 1981). We discuss these experiments in some

detail below, since they seem to provide some of the most detailed tests of scaling. As well, of course, they reveal interesting hydrodynamic effects.

A typical experiment consists of illuminating the fluid sample with a laser beam, following a temperature or pressure quench of the system to an unstable state. The scattered light forms a ring which brightens and decreases in diameter as the system evolves, as mentioned in Section I. From measurements of the scattering intensity, $I(k, t)$, experimentalists can determine the time dependence of the ring diameter $k_m(t)$ and peak intensity $I(k_m, t)$. (The wavenumber k is related to the scattering angle θ by (11.2), where $\lambda = \lambda_0/n$, with λ_0 and n being the vacuum wavelength and refractive index of the mixture, respectively.) When multiple scattering effects can be ignored $I(k, t)$ is proportional to the structure function $\hat{S}(k, t)$, and a direct test with theory is then possible. The results of a typical scattering experiment are shown in Fig. 41 for an IW mixture quenched at the critical composition (Chou and Goldburg, 1981). It can be seen there that the intensity maximum, $I(k_m, t)$ rapidly increases as the ring collapses. Since such experiments are in the critical region, it is natural to use the scaled variables

$$q = k\xi \tag{5.27}$$

and

$$\tau = Dt/\xi^2, \tag{5.28}$$

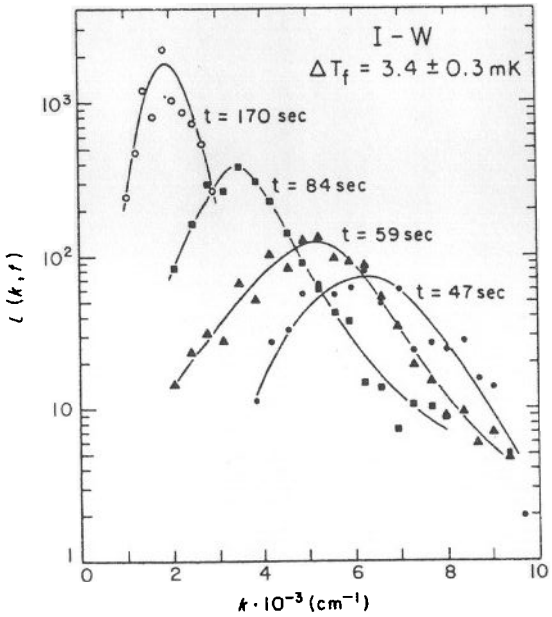

FIG. 41. The scattering intensity $I(k, t)$ versus k at different times in IW. The quench depth $\Delta T_f = 3.4$ mK. (From Chou and Goldburg, 1981.)

where ξ and D are given by (10.5) and (10.7) respectively. (Note that (5.28) differs slightly from the scaled time introduced in (10.17).) It should be observed that these light scattering experiments span several decades in the scaled time τ, for the small values of reduced temperature $\varepsilon = (T_c - T)/T_c$ which are studied. For example, in IW one has $\tau \simeq 4.6 \times 10^9 \varepsilon^{1.8}$ (t/s). The experiments by Chou and Goldburg (1981) explored the regions $3 \times 10^{-6} \leqslant \varepsilon \leqslant 2 \times 10^{-5}$ and $6 \leqslant \tau \leqslant 1000$.

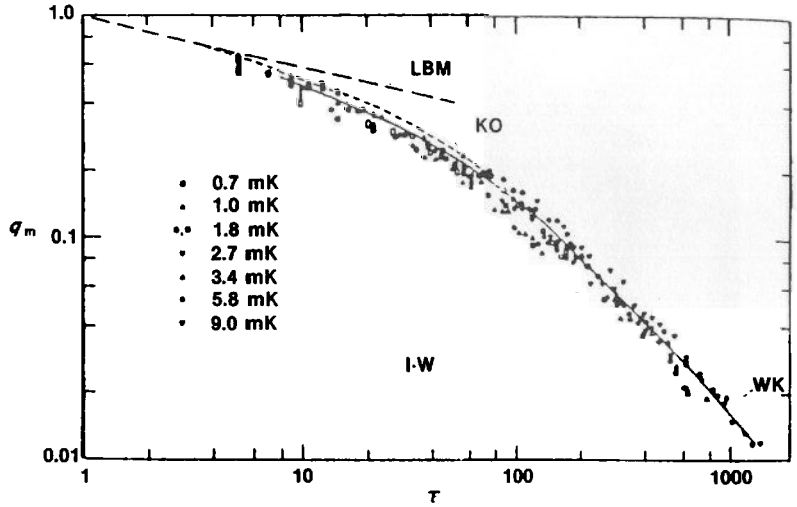

FIG. 42. The scaled peak position q_m as a function of the scaled time τ for a critically quenched IW mixture. (From Chou and Goldburg, 1979.)

The earlier experiments on the binary mixtures IW and LW clearly showed the important effects of hydrodynamics in the spinodal decomposition/coarsening process. For example, Fig. 42 shows the behavior of the scaled peak position, $q_m(\tau)$, as a function of the scaled time τ for a critically quenched mixture of IW (Wong and Knobler, 1978; Chou and Goldburg, 1979). These two experiments yielded almost identical results, even though the temperature quench rates of Chou and Goldburg (of about 10 s) were several orders of magnitude larger than the much more rapid pressure quenches of Wong and Knobler. What is clearly evident in Fig. 42 is the important role played by hydrodynamics in the critical quench. The growth rate $q_m(\tau) \sim \tau^{-a'}$ crosses over from an early stage diffusive behavior of $a' \simeq 1/3$ to a late time behavior of $a' \simeq 1$. The latter behavior is in agreement with the prediction by J. W. Cahn and M. R. Moldover (unpublished) and Siggia (1979) (Section V) that $a' = 1$, where flow in percolated droplets dominates the dynamics. It can also be seen from Fig.

42 that the LBM theory (Section V) for binary alloys is inapplicable for binary fluids, as is to be expected. On the other hand, the Kawasaki–Ohta (KO) theory (Section V), which extends the LBM approach to give an approximate treatment of hydrodynamics, describes rather well the early time behavior of $q_m(\tau)$. It does not, however, yield the crossover to the $a' = 1$ behavior.

A more challenging test of theory is provided by the experimental measurements of the peak height behavior. As shown in Fig. 43, the experimental results for IW cannot be explained by the KO theory. A power law approximation was used to fit $I(q_m, \tau)$ by Wong and Knobler

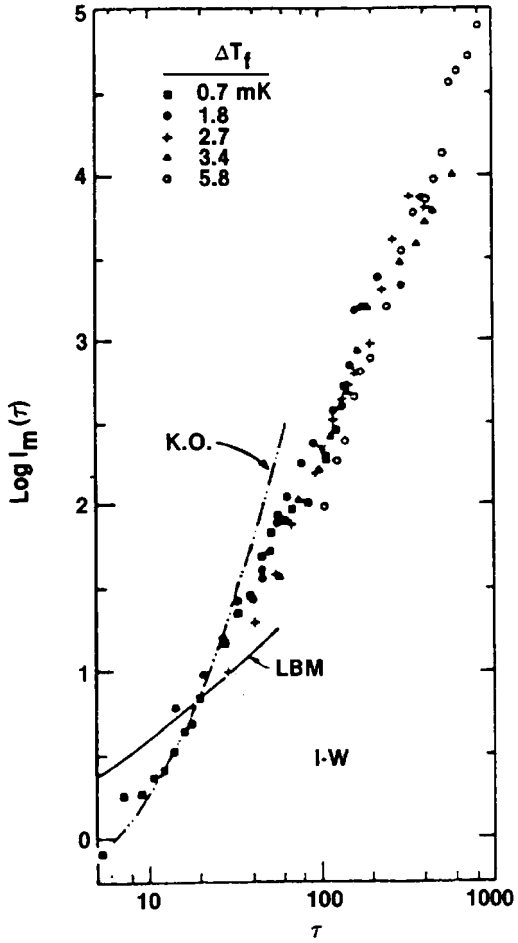

FIG. 43. The scaled ring intensity as a function of the scaled time τ for a critically quenched IW mixture. (From Chou and Goldburg, 1979.)

(1978) and yielded an exponent a'' which increased from $a'' \simeq 1.2$ to $a'' = 2.3$. Chou and Goldburg (1979) noted that the late stage behavior was consistent with an exponent $a'' = 3$, but no definitive determination seems available yet. It should also be noted that experiments on LW by Chou and Goldburg (1979) yielded results for the scattering intensity which are essentially identical to the behavior of $q_m(\tau)$ and $I(q_m, \tau)$ discussed above. This confirms the dynamical universality one might expect near a critical point, even in systems which are far from equilibrium.

The most detailed investigation of droplet growth in binary fluids is the recent work of Wong and Knobler (1981) on IW. They determined the behavior of the peak position $k_m(t)$ by measurements of $I(k_m, t)$ for several critical and off-critical quenches. This allowed them to examine the influence of the volume fraction v of droplets on $k_m(t)$. In particular, they were able to test the predictions of Siggia (eqns (5.26), (5.29), (5.30) and (5.32)) which are based on a consideration of various growth mechanisms possible in binary fluids. Wong and Knobler's analysis is based on 10 sets of quench data, shown in Table X. They determined the volume fraction v from

TABLE X. Initial relative temperatures ΔT_i, temperature jumps δT, and corresponding volume fractions v.

		δT (mK)				
Set	T_i (mK)	1.45	2.89	5.79	11.6	23.2
1	0	0.50	0.50	0.50	0.50	0.50
2	0.01	0.39	0.41	0.43	0.44	0.45
3	0.14	0.26	0.31	0.34	0.37	0.40
4	0.55	0.16	0.22	0.27	0.31	0.34
5	1.5	0.10	0.14	0.20	0.25	0.29
6	3.0	0.06	0.09	0.14	0.19	0.24
7	6.0	0.03	0.06	0.09	0.14	0.19
8	10.2	0.02	0.04	0.06	0.10	0.15
9	17.1	0.01	0.02	0.04	0.07	0.12
10	24.7	0.01	0.02	0.03	0.06	0.09

measurements of the initial and final (quenched) temperatures T_i and T_f. Using the lever rule they obtain the relation

$$v = [1 - (\Delta T_i/\Delta T_f)^{\beta}]/2, \tag{11.4}$$

where β is defined in (10.3) and $\Delta T_i = T_c - T_i$, $\Delta T_f = T - T_f$.

The behavior of the scaled peak position, $q_m(\tau)$, is shown as a function of τ for several typical quenches in Fig. 44. Figure 44(a) shows the crossover from a $\tau^{-1/3}$ to a τ^{-1} behavior predicted by Siggia for large v. This τ^{-1}

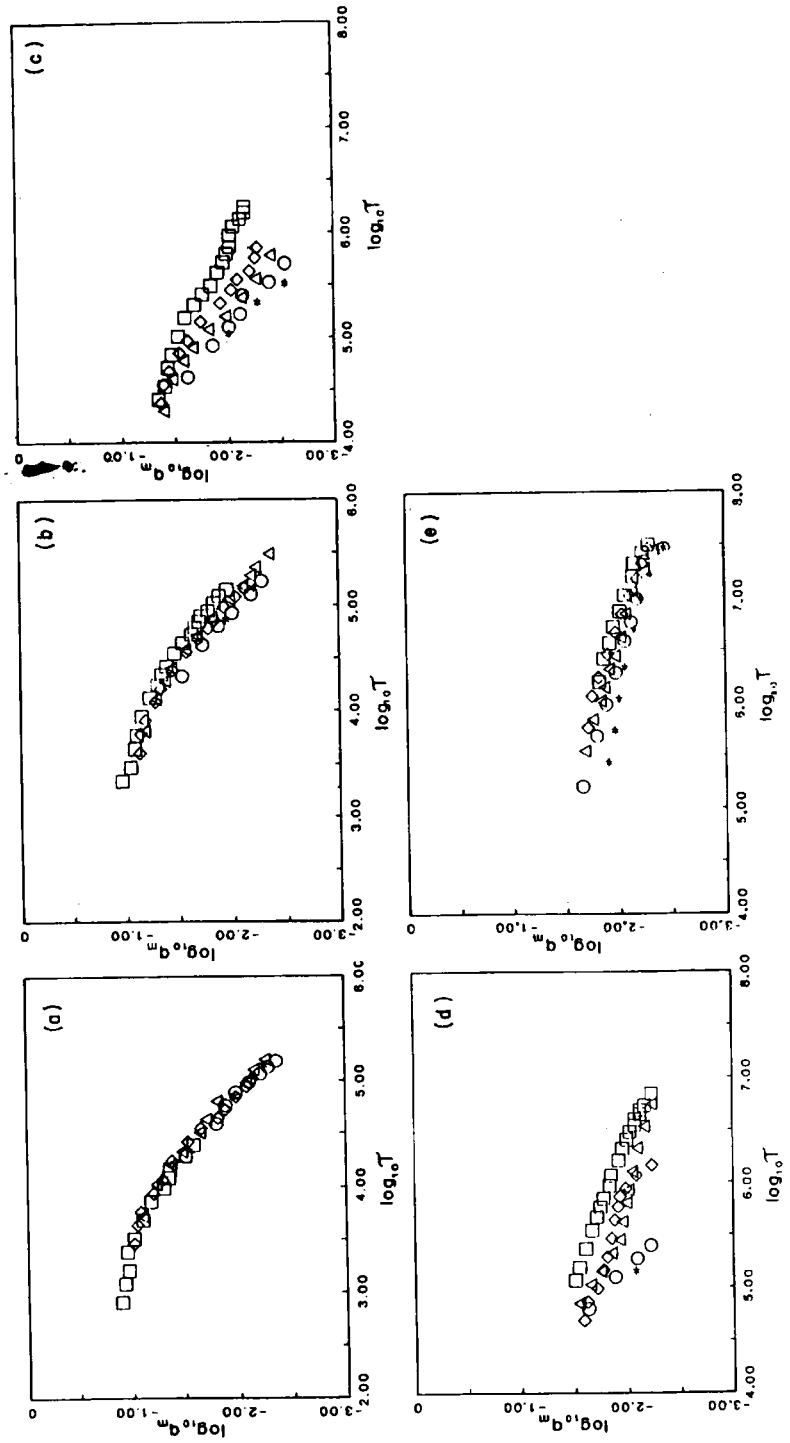

FIG. 44. The dependence of $\log q_m$ on $\log \tau$ for different quenches shown in Table X. Symbols represent different quench depths □, 1.5 mK; ◇, 2.9 mK; △, 5.8 mK; ○, 11.6 mK; *, 23.2 mK. (a) Set 1; (b) set 4; (c) set 7; (d) set 8; (e) set 10. (From Wong and Knobler, 1981.)

behavior seems to be restricted to the region $v \geq 0.10$. For shallower quenches, in which v is small, this crossover to τ^{-1} disappears, as can be seen in Fig. 44(e). This is again in qualitative agreement with Siggia's theory. A detailed comparison of Siggia's predictions for $q_m(\tau)$ was made by Wong and Knobler, in particular (5.26) and (5.30), which we write as

$$q_m^{-3}(\tau) \simeq A\tau. \tag{11.5}$$

The results of their analysis for the sets 8, 9 and 10 of Table X are shown in Table XI. One noteworthy result is the confirmation of the Lifshitz–Slyozov theory for $v \leq 0.02$, eqn (5.30), in which A should be independent of v and approximately equal to 0.053. A second result is a semiquantitative confirmation of the behavior (5.26), in which A should be $12v$. This behavior of A is confirmed only within a factor of two.

TABLE XI. Coefficients of τ for quenches exhibiting $\tau^{-1/3}$ behaviour without crossover.

Set	ΔT_f (mK)	A	A/v
8	1.5	0.055	3
	2.9	0.98	24
	5.8	0.76	13
9	1.5	0.041	4
	2.9	0.016	8
	5.8	0.67	17
	11.6	0.10	1.4
10	1.5	0.052	5
	2.9	0.052	3
	5.8	0.22	7
	11.6	0.85	14

Two concluding remarks should be made about the Wong–Knobler study. The first is that the observed crossover to the τ^{-1} behavior is only in qualitative agreement with (5.32). The observed amplitude differs from that in (5.32) by about two orders of magnitude. The second remark is that a crucial assumption in the Wong–Knobler analysis is that the droplet size R which occurs in Siggia's unscaled equations is taken to be $R = k_m^{-1}$. However, Chou and Goldburg (1979) have found that the ratio of the average droplet size $l(t)$ to $k_m^{-1}(t)$ was in the range 5–10 in the late stage droplet growth. Thus it is not clear (as Wong and Knobler note) that $R = k_m^{-1}$ is an exact identification. They find, however, that the best overall agreement with Siggia's theory is obtained with this particular choice.

Finally, we discuss the issue of the scaling of the structure function in these liquid mixtures. The first observation of scaling in such systems was by Chou and Goldburg (1981). They analyzed the behavior of the scattering intensity $I(k, t)$ for three critical quenches for LW and four critical quenches for IW. After making corrections for the background intensity and multiple scattering effects, they showed that a scaling of the form (8.5) was satisfied. The scaling wavenumber $\kappa(t)$ was chosen to be the peak height position $k_m(t)$. This scaling was shown to hold in the range $6 \leq \tau \leq 1000$, with the scaling function $F(k/k_m(t))$ exhibiting no dependence on time. The absence of any transient region in which $F(x)$ depends on τ is quite different from the Monte Carlo and neutron scattering experiments on binary alloys. As noted earlier, strong transient effects have been observed in these systems. Chou and Goldburg also found that their scaling function was quite similar to that of Lebowitz *et al.* (1982).

A more detailed investigation of this scaling behavior has recently been carried out by Knobler and Wong (1981) for IW. They analyzed the behavior of a normalized structure function $\tilde{S}(k, t)$ which was defined in terms of the scattering intensity as

$$\tilde{S}(k, t) = I(k, t) \Big/ \int_{k_a}^{k_b} k^2 I(k, t)\, dk \tag{11.6}$$

The range of integration extended from $k_a = 0.3\, k_m$ to $k_b = 3.0\, k_m$. The normalization was essentially unaffected by increasing the range of integration. They also evaluated the moments

$$k_n(t) = \int_{k_a}^{k_b} k^n I(k, t) \Big/ \int_{k_b}^{k_b} I(k, t)\, dt, \qquad n = 1, 2, \tag{11.7}$$

to examine the behavior of $r(t)$ defined in (8.6). The scaling wavenumber was chosen as $\kappa(t) = k_m(t)$. The analysis was carried out for six critical quenches (labeled A–F) and 11 off-critical quenches, seven in the water-rich phase (G–M) and four in the isobutyric acid-rich phase (N–Q). Corrections similar to those of Goldburg and Chou were made for multiple scattering and background effects.

Typical results for the scaling function $F(x)$ are shown in Fig. 45 for an off-critical quench K and a critical quench A. The 15 scans included in Fig. 45(a) cover a period of 38–1070 s after the quench. The unnormalized intensities at k_m vary by a factor of approximately 30. Knobler and Wong concluded that within the precision of the data a (time-dependent) scaling behavior is obeyed. In Fig. 45(b), the scaling *ansatz* seems less accurate. In Table XII the behavior of the scaling function $F(x)$ is given in terms of its peak values and full width at half-maximum $\Delta x_{1/2}$ for all the quenches which they analyzed. Table XIII shows the behavior of $r(t)$.

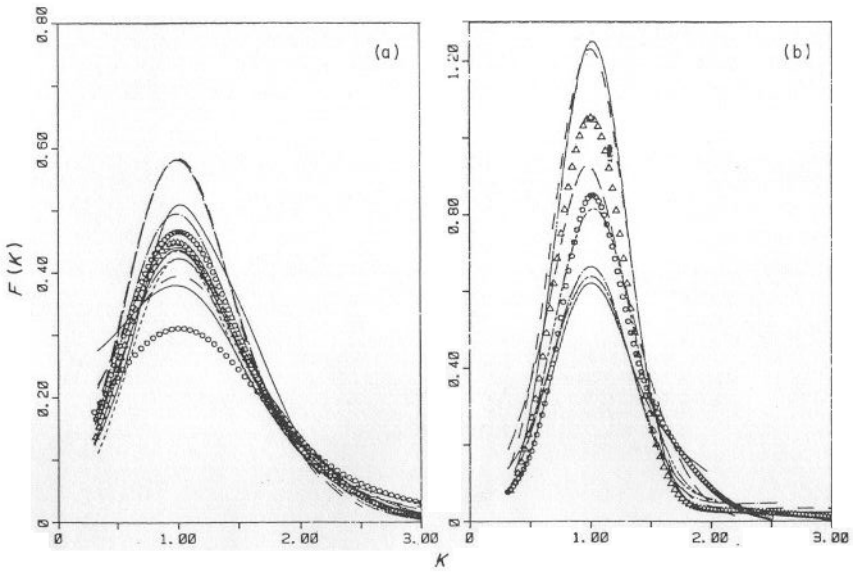

FIG. 45. The scaling function $F(x)$ for two different quenches in IW: (a) an off-quench K for 15 scans; (b) a critical quench A for nine scans. (From Knobler and Wong, 1981.)

TABLE XII. Properties of scaling functions $F(x)$.

Quench	$F(1)$	$\Delta x_{1/2}$	k_2/k_1^2
A	0.87 ± 0.10	0.76	1.13 ± 0.05
B	1.28 ± 0.25	0.55	1.10
C	1.21 ± 0.08	0.49	1.12 ± 0.02
D	0.99 ± 0.10	0.70	1.12
E	0.68 ± 0.13	0.73	1.19 ± 0.07
G	0.46 ± 0.05	1.10	1.18 ± 0.02
H	0.38 ± 0.06	1.56	1.21 ± 0.03
I	0.42 ± 0.06	1.14	1.23 ± 0.02
J	0.60 ± 0.06	0.92	1.19 ± 0.04
K	0.44 ± 0.04	1.12	1.19 ± 0.02
M	0.52 ± 0.06	1.00	1.22 ± 0.03
N	0.69 ± 0.13	0.94	1.14 ± 0.01
O	0.73 ± 0.08	0.88	1.14 ± 0.01
Q	0.60 ± 0.05	1.04	1.17 ± 0.02

TABLE XIII. Variation of $r = k_2/k_1^2$ during a quench.

Quench J		Quench K		Quench N	
$r/10^5$		$r/10^5$		$r/10^3$	
0.69	1.14	0.26	1.15	1.35	1.14
0.97	1.17	0.40	1.16	1.18	1.13
1.25	1.17	0.53	1.16	2.30	1.12
1.54	1.18	0.67	1.16	2.8	1.13
2.04	1.17	0.90	1.17	3.2	1.12
2.6	1.18	1.14	1.19	3.6	1.14
3.1	1.18	1.39	1.19	5.2	1.13
4.3	1.19	1.85	1.18	6.3	1.14
5.3	1.20	2.33	1.19	8.8	1.14
6.3	1.18	2.8	1.19	11.7	1.15
7.3	1.21	3.3	1.20	16.5	1.15
8.3	1.22	3.8	1.21		
10.2	1.23	4.7	1.21		
12.0	1.23	5.5	1.22		
		7-2	1.23		

It is clear from Table XII that the scaling function is much narrower for critical quenches than for off-critical quenches. The values shown there should be compared with the critical quench results of Chou and Goldburg (1981). These are $F(1) = 1.5 \pm 0.1$ and $\Delta x_{1/2} = 0.45 \pm 5\%$ for LW and $F(1) = 1.6 \pm 0.3$ and $\Delta x_{1/2} = 0.5 \pm 10\%$ for IW. It should also be noted that the Monte Carlo results (Lebowitz *et al.*, 1982) are $F(1) = 0.9$ and $\Delta x_{1/2} = 0.7$ for the quenches P_4, P_5 and P_6. The quench P_3 has $F(1) \simeq 1$ and $\Delta x_{1/2} \simeq 0.7$. Therefore, as noted in Section IX, no significant difference between the half-widths was seen in the Monte Carlo work, in contrast to the conclusion of Knobler and Wong for IW.

Glasses

Extensive experimental and theoretical studies have dealt with spinodal decomposition in glass systems. Experiments have involved both TEM and X-ray SAS measurements. A review of spinodal decomposition in glasses has been given by Jantzen and Herman (1978). They cite several prior reviews of phase separation in glasses and give detailed references to the experimental and theoretical literature in this field. We therefore restrict our attention to a recent experiment which shows a scaling of the structure function in the quasi-binary glass B_2O_3–$PbO(Al_2O_3)$ (Craievich and Sanchez, 1981). Before summarizing this work we first note that spinodal

decomposition has been of particular interest in glass-forming systems because of their inherent isotropy. This is an advantage over most crystalline systems such as Al–Zn, whose structure functions exhibit considerable anisotropy. The glass on which the most detailed experimental studies of spinodal decomposition have been carried out is Na_2O–SiO_2, as discussed by Jantzen and Herman (1978).

Recent small angle X-ray scattering studies of B_2O_3–$PbO(Al_2O_3)$ have shown that the structure function $\hat{S}(k,t)$ satisfies a scaling of the form (8.5), with the characteristic wavenumber being $\kappa(t) = k_1(t)$. A quench was carried out at a critical composition of 80:15:5 (wt%) and a temperature $T \simeq 0.65T_c$ (where $T_c \simeq 657\,°C$). The structure factor $\hat{S}(k,t)$ was determined in a time range of about 12–400 min. During that time $r(t) = k_2/k_1^2$ remained approximately constant and equal to $r \simeq 1.39$. The structure factor exhibited a behavior quite similar to that shown in Fig. 37 for Al–Zn. The glass data was shown to be consistent with the scaling form (8.5) in the observed time range. The exponent a which describes the first moment $k_1(t)$ (eqn (5.33)) was determined to be $a \simeq 0.23$, which is in reasonable agreement with the Monte Carlo results for the binary alloy (Section IX). Craievich and Sanchez note that with the increased availability of highly collimated, very intense X-ray sources, more accurate determinations of $\hat{S}(k,t)$ over an interesting range of time and length scales will become possible.

XII. Tricritical systems

A. Theory

Several recent studies consider nucleation and spinodal decomposition phenomena in tricritical systems. In this section we review theoretical investigations of such phenomena. In Sections XII.B and XII.C we discuss Monte Carlo studies of two-dimensional tricritical models and experimental studies of ^{3}He–^{4}He mixtures respectively.

Tricritical systems are characterized by a line of critical points associated with an order–disorder transition, ending at a tricritical point. Below the tricritical point both ordering and phase separation occur simultaneously. Thus two order parameters, ψ and c, are necessary to describe tricritical phenomena. A typical phase diagram for tricritical systems is shown in Fig. 46. In the usual situation ψ is a nonconserved variable (the superfluid order parameter for ^{3}He–^{4}He), while c is a conserved variable (the local concentration of ^{3}He for ^{3}He–^{4}He). These variables are dynamically coupled in the field theoretic equations which describe such systems (Section III.A). This coupling makes it more difficult to obtain a theoretical description of

dynamical phenomena in tricritical systems than in simple critical systems such as an Ising model of a binary alloy. On the other hand, one might expect a richer dynamical structure to exist as a consequence of this additional order parameter. It should also be noted that the upper critical dimension for tricritical models is $d = 3$. Thus, apart from logarithmic corrections, mean field theory gives an accurate description of much of the static tricritical behavior. A comprehensive review of the theory of tricritical points is given by Lawrie and Sarbach (1983, forthcoming article in Vol. 9 of this series).

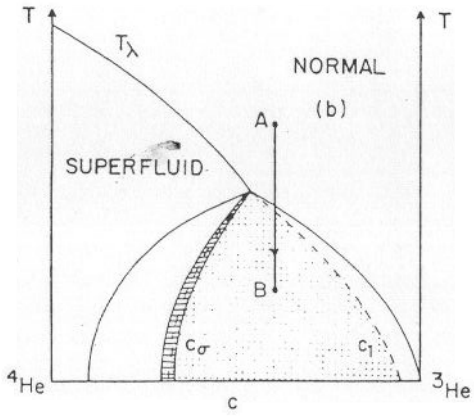

FIG. 46. Schematic temperature–concentration phase diagram for ^{3}He–^{4}He mixtures. The line of critical points T_λ and the tricritical point at temperature T_t are indicated. A quench from the normal phase into the coexistence region is shown. The spinodal lines C_1 and C_σ are also indicated. (From Hohenberg and Nelson, 1979.)

The first theoretical studies of spinodal decomposition in tricritical systems appear to be due to Allen and Cahn (1976, 1979a, b). They discussed the coherent spinodal curve (1976) and aspects of domain growth (1979) for alloys such as Fe–Al. The first detailed theory of spinodal decomposition which dealt with the dynamical coupling of two order parameters is due to Hohenberg and Nelson (1979). They developed a linearized theory of spinodal decomposition for ^{3}He–^{4}He mixtures, based on a dynamical model of Siggia and Nelson (1977) (eqns (3.27)–(3.34)). Their analysis revealed two unusual features associated with "tricritical spinodal decomposition" in ^{3}He–^{4}He mixtures. The first is that the inverse susceptibility $\tilde{\chi}^{-1}$ which is responsible for the initial stages of phase separation of the ^{3}He phase is rather different from that for the binary alloy (i.e. $(\partial^2 f/\partial c^2)_{c_0}$ in the Cahn

equation (5.3)). Namely, as shown in Fig. 47 this "constrained" inverse susceptibility $\bar{\chi}^{-1}$ becomes increasingly negative as one increases the average concentration in the spinodal region. It then discontinuously changes to a positive value as one crosses into the classical metastable domain. (This discontinuity is an artifact of the mean field theory; Hohenberg and Nelson (1979).) To understand how this $\bar{\chi}$ arises and how one defines the spinodal curve for such tricritical systems, one must consider the initial behavior immediately following a quench into the miscibility gap (shown in Fig. 46). Since $|\psi|$ (the amplitude of ψ) and c are nonconserved and conserved variables respectively, $|\psi|$ will immediately relax to some constrained value $\bar{\psi}$ determined by the initial values of c and the temperature. The local concentration c will remain essentially constant during this rapid relaxation of $|\psi|$, since the time scale for its evolution is much longer than for $|\psi|$. One obtains this constrained value $\bar{\psi}$ from the equation of motion for $|\psi|$ (which follows from (3.27) upon neglecting the gradient and noise terms) by setting $\partial|\psi|/\partial t = 0$. Associated with this constrained value $\bar{\psi}$ is a "constrained" susceptibility which is obtained by evaluating the usual mean field concentration susceptibility at $|\psi| = \bar{\psi}$. This analysis yields the function $\bar{\chi}$ shown in Fig. 47 and also yields a definition of the spinodal

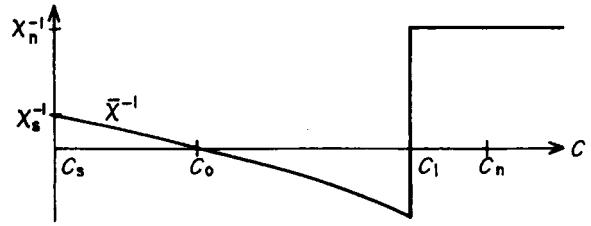

FIG. 47. Constrained susceptibility $\bar{\chi}$ as a function of concentration for fixed temperature. The spinodal values C_1 and C_o of Fig. 46 and the equilibrium values at the "superfluid" (C_s) and "normal" (C_n) side are shown. (From Hohenberg and Nelson, 1979.)

curve which is shown in Fig. 46. Note that these definitions of $\bar{\chi}$ and the spinodal curve follow from the *dynamical* argument given above. This same reasoning is immediately applicable to the relaxational model C (eqns (3.18)–(3.22)), which can be used to describe the tricritical metamagnet model discussed in Section XII.B. A detailed discussion of the above analysis for model C has been given by San Miguel *et al.* (1981).

Hohenberg and Nelson then linearize the equations of motion (3.27)–(3.29) for the conserved variables c, q and θ (where q is the "entropy" and θ is the phase of $\psi = |\psi| e^{i\theta}$) about the point $(\bar{\psi}, c_0)$, where c_0 is the initial quench concentration. This linearization involves three hydrodynamic

modes (when $\bar{\psi}^2 \neq 0$), a diffusion mode and two second sound modes. The result for the nonequilibrium structure factor $\hat{S}(k,t) \equiv \langle c_k(t) c_{-k}(t)\rangle$ is

$$\hat{S}(k,t) = a_1 e^{-2\bar{D}_0 k^2 t} + a_2 e^{-(\bar{D}_0+\bar{D}_2)k^2 t} \cos \bar{u}_2 k t + a_3 e^{-2\bar{D}_2 k^2 t} \cos 2\bar{u}_2 k t + a_0, \tag{12.1}$$

where the a_i are time-independent constants that depend in a complicated way on the hydrodynamic parameters and the initial conditions. The quantities $\bar{u}_2(k)$ and $\bar{D}_2(k)$ are nonequilibrium versions of the second sound velocity and damping rate and are typically positive. The diffusion constant $\bar{D}_0(k)$ is negative for some range of wavenumbers. Thus the first term in (12.1) grows while the third term dies out. (The first term is the analog of (5.9) for the binary alloy.) Since in principle $(\bar{D}_0 + \bar{D}_2)$ could be negative, the second term in (12.1) would yield a "flickering" component in the scattering. This is the second unusual feature of tricritical spinodal decomposition which we mentioned above. However, Hohenberg and Nelson find that $(\bar{D}_0 + \bar{D}_2)$ is typically positive near the tricritical point, so this flickering may be difficult to observe experimentally.

Since it is known that the time domain of applicability of a linear theory is quite limited, it is interesting to see if one can develop an approximate nonlinear theory for tricritical systems. Unfortunately the additional order parameter and hydrodynamic modes makes this even more difficult to do than for binary alloys. However, a LBM-like theory (Section V) has been developed for the relaxational model C (Dee *et al.*, 1981). The most interesting result of this theory is a quite asymmetric behavior of the structure factor $\hat{S}(k,t) = \langle c_k(t) c_{-k}(t)\rangle$ as a function of the average quench concentration c_0. This theoretical result is a reflection of the asymmetry in an effective Hamiltonian which is used in the calculation. This Hamiltonian results from the replacement of $|\psi|$ by $\bar{\psi}$ in the equation of motion (3.19) for c. As mentioned in Section XII.B a similar asymmetric behavior in $\hat{S}(k,t)$ is seen in Monte Carlo simulations.

The nucleation rate and late stage growth law have also been derived for model C (San Miguel and Gunton, 1981; San Miguel *et al.*, 1981). The calculation of the nucleation rate follows the formalism outlined in Section IV and requires determination of the activation energy, the imaginary part of the free energy and the dynamical prefactor κ (i.e. (4.26)–(4.29), (4.55)). This involves first determining the saddle point solution $(\bar{\psi}, \bar{c})$ (the "tricritical droplet") for the Hamiltonian (3.20). This is more difficult than for the "ψ^4" model discussed in Section IV, due to the existence of the second-order parameter c. A perturbation solution of the saddle point equations can be given, however, to lowest order in a perturbation parameter $g = \chi_n^{1/2} l_0/\xi$ (where ξ is the mean field correlation length and χ_n and l_0 are defined in (3.20)). The result which one obtains for the activation

energy is the same as (4.19) when expressed in terms of the corresponding tricritical quantities. An explicit expression for the surface tension σ is obtained which includes a correction term in addition to the expected dominant singularity. The latter is in agreement with previous phenomenological predictions (Papoular, 1974; Widom, 1975). The result for the imaginary part of the free energy for model C is the same (to leading order) as (4.57) and (4.58), with an appropriate change of variables (San Miguel and Gunton, 1981). For example, the magnetic field H is replaced by $\delta\Delta = \Delta - \Delta_0$, which is the variable for model C which is appropriate for the description of metastable states. The result that to leading order the static contribution to the nucleation rate (the imaginary free energy) is identical for model C and the Ising model is due to the fact that this is determined by the geometrical properties of the Hamiltonian which describes the saddle point droplet solution and its deformations (Section IV). To leading order this is the same for the two models. However, since the Ising model possesses a symmetry with respect to H which does not exist for model C with respect to $\delta\Delta$, the higher order contributions to the imaginary free energy will be different.

The calculation of the nucleation rate for model C is completed by determining the dynamical prefactor κ in (4.55). In principle this is done by linearizing eqns (3.18) and (3.19) about the tricritical saddle point solution $(\bar{\psi}, \bar{c})$. The actual calculation was performed by using a variational method due to Langer (1971) (San Miguel *et al.*, 1981). This also allows one to determine the late stage growth law (Langer, 1971, 1975). The result for model C is that κ involves a mixing of two different growth mechanisms (Allen–Cahn and Lifshitz–Slyozov; see Section VI). This seems natural since for this model one is dealing simultaneously with a nonconserved variable ψ and a conserved variable c. For large enough droplets, however, the late stage growth law reduces to the LS $t^{1/3}$ behavior.

The calculations discussed above have also been carried out for ^{3}He–^{4}He mixtures, except that the dynamical prefactor was left undetermined (San Miguel and Gunton, 1981). Thus a complete expression for the nucleation rate has not been given. In this case it is clear, however, that hydrodynamic effects which are included in the Siggia–Nelson (1977) model will give rise to a different dynamical prefactor than obtained for model C. The result for the imaginary free energy for ^{3}He–^{4}He mixtures (and hence for its contribution to the nucleation rate, eqn (4.55)) also differs from model C for a normal ^{4}He fluid metastable state (but not for a superfluid metastable state). This arises from the fact that model C has a discrete symmetry of the Ising type, whereas due to the complex nature of the order parameter ψ, the Hamiltonian for ^{3}He–^{4}He has a continuous symmetry. Namely, the Hamiltonian has a well known invariance under gauge transformations. The result is that when evaluating Ω_0 in (4.29) one

obtains contributions from zero eigenvalues associated with the invariance under a change of phase. This leads to a contribution to the imaginary free energy (4.54) which changes the exponent 7/3 in (4.58) to 23/6 on the normal fluid side of the ^{3}He–^{4}He coexistence curve (San Miguel and Gunton, 1981).

B. Monte Carlo studies

Recently detailed Monte Carlo studies of the ordering and phase separation processes for a two-dimensional model of a metamagnet have been carried out (Sahni and Gunton, 1980; Sahni *et al.*, 1982). The Hamiltonian for this model is

$$H = J \sum_{\text{nn}} \sigma_i \sigma_j - \frac{1}{2} J \sum_{\text{nnn}} \sigma_i \sigma_k + H \sum_i \sigma_i \tag{12.2}$$

where $\sigma_i = \pm 1$, $J > 0$ and the spins are situated on a square lattice. The symbols nn and nnn denote sums over nearest and next nearest neighbors, respectively. The phase diagram for this model is reasonably well known (Landau, 1972; Landau and Swendsen, 1981). In particular the tricritical point is estimated to be at the temperature $T_t \simeq 1.21\, J/k_B$ and magnetization $M_t \simeq 0.37$ (Landau and Swendsen, 1981).

The dynamical studies have been carried out for several different quenches into the miscibility gap below the tricritical point. The dynamics of this system is taken to be Kawasaki spin exchange. This model is the lattice analog of model C. The nonconserved and conserved order parameters ψ and c for this metamagnet are the local sublattice magnetization and local magnetization respectively. It should also be noted that with a standard change of variables (12.2) can also be considered to be a model of a binary alloy (in which ordering and phase separation effects are taken into account) or of a chemisorption system (Section XIII.F). Thus computer simulation studies of ordering and phase separation for this model could give qualitative insight into the behavior of binary alloys or chemisorption systems below their tricritical points.

In the computer simulation studies two structure functions, $\hat{S}_{\psi\psi}(k, t)$ and $\hat{S}_{cc}(k, t)$ have been determined (the notation is obvious). As with other systems discussed in this review, a time domain in which linear theory is valid (Hohenberg and Nelson, 1979) was not observed. Nevertheless, both structure functions exhibit dynamical instabilities, as is implicit in the Hohenberg–Nelson theory. The behavior of $\hat{S}_{cc}(k, t)$ is qualitatively similar to that seen in Monte Carlo studies of a binary alloy (Section IX) for $\hat{S}(k, t)$. That is, the peak height $\hat{S}_{cc}(k_m, t)$ increases while $k_m(t)$ decreases

with time. The other structure factor behaves very similarly to that for a pure antiferromagnet, whose order parameter is nonconserved (Phani *et al.*, 1980; Sahni *et al.*, 1981). Namely, $\hat{S}_{\psi\psi}U(k,t)$ develops a peak at $k = 0$ which increases with time. The first and second moments of each of these structure factors have also been determined. To a first approximation the ratios $r_\psi(t)$ and $r_c(t)$ (analogous to (8.6)) are time-independent after an initial transient behavior. However, a small but definite time dependence was found in several of the quenches. Various power law approximations for the moments were also obtained, which are given in Sahni *et al.* (1982).

As with other systems discussed here, both structure factors were found to exhibit a scaling behavior as given by (8.5) (although no normalization was used). This was the first observation of scaling in tricritical systems (Sahni and Gunton, 1980; Sahni *et al.*, 1982). The best example of this is shown in Fig. 48 for a quench to a temperature $T \simeq 0.6T_t$ and a magnetization $M = 0.5$. The scaling of $\hat{S}_{\psi\psi}(k,t)$ at values of the average magnetization which are less and greater than $M = 0.5$ was much less satisfactory,

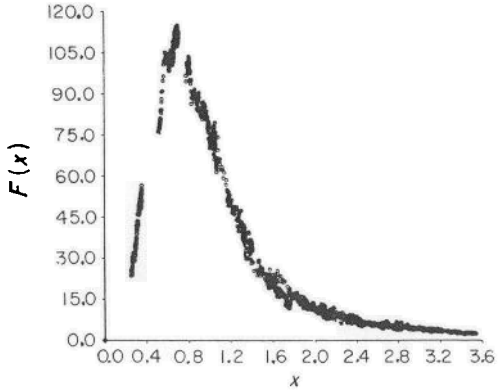

FIG. 48. The scaling function for the conserved variable structure function for the two-dimensional metamagnet at a quench temperature $T \simeq 0.6T_t$ and magnetization $M = 0.5$. (From Sahni *et al.*, 1982.)

however. This is due in part to (a) significant "metastability" problems, (b) scatter in the Monte Carlo data and (c) possible deviations from scaling. It should also be noted that in Fig. 48 the scaling function seems much more peaked than the corresponding scaling functions shown for the Ising model in Section IX. To some extent this is misleading, however, due to the discrete values of wavenumbers sampled in the simulation study. The true scaling function is undoubtedly rounder at the top than the figure suggests.

An interesting feature of the compuer simulation studies is a pronounced asymmetry in $\hat{S}_{cc}(k,t)$ as a function of the average quench magnetization. Namely, at a fixed time the peak height $\hat{S}_{cc}(k,t)$ increases with increasing magnetization (i.e. as one moves from left to right in the metamagnet phase diagram corresponding to Fig. 46). There is no value of the magnetization about which $\hat{S}_{cc}(k,t)$ is symmetric, in contrast to the symmetric Ising model discussed in Section IX. This asymmetric behavior clearly reflects the asymmetry of the tricritical coexistence curve (such as is shown in Fig. 46), in contrast to the symmetric coexistence curve shown in Fig. 25. Eventually a value of the average magnetization ($M \simeq 0.7$) is reached for which this peak height begins to decrease (at fixed time) with increasing M. Detailed studies of this effect show that it is a rather gradual transition (Sahni *et al.*, 1983b). This transition appeared to be rather sharp in preliminary studies reported by Sahni *et al.* (1982). An open theoretical question concerning the observed asymmetry is whether this behavior is related to the constrained susceptibility $\tilde{\chi}$ (Fig. 47). A detailed answer to this question will require a more accurate calculation of $\tilde{\chi}$ than the mean field result (Fig. 47). It seems clear that such a calculation will yield a much more rounded, but nevertheless asymmetric $\tilde{\chi}$. A theory for the nonlinear terms neglected in linear theory (Hohenberg and Nelson, 1979; San Miguel *et al.*, 1981) will also be necessary. The LBM-type calculation of Dee *et al.* (1981) does predict an asymmetry qualitatively similar to the Monte Carlo results, but it was based on a mean-field-type model.

C. ^{3}He–^{4}He mixtures

In this section we discuss several recent light scattering experiments of phase separation in ^{3}He–^{4}He mixtures quenched below the tricritical point. The ^{3}He–^{4}He system has several interesting differences with the organic binary mixtures discussed in Sections X and XI. Its ordered state, for example, is superfluid. As a consequence it has a second sound mode not present in normal binary mixtures. As well, its phase diagram and various thermodynamic and transport properties are well known, as is the case for certain binary fluids. Its thermodynamic properties are, however, mean-field-like. Its coexistence curve is also much more asymmetric near the tricritical point (Fig. 46) than is the case for an organic binary mixture near its critical point, as already noted. So far, the most interesting difference between phase-separating ^{3}He–^{4}He and normal binary fluids which has been observed experimentally is due to gravity, as we mention later.

The first study of phase separation in the ^{3}He–^{4}He liquid mixtures was made by Hoffer *et al.* (1980). They observed the formation of a halo which brightened and rapidly collapsed. This is qualitatively similar to the

behavior observed in the IW and LW mixtures discussed in Section XI. However, the time scale for the collapse was much shorter for ^{3}He–^{4}He than for these mixtures. It should also be remarked that, as noted earlier, the observation of a collapsing ring does not necessarily imply that one is seeing a spinodal decomposition process. A similar phenomenon can arise from scattering from a distribution of nucleated droplets that subsequently grow in size. Indeed, it seems likely that most if not all of the light scattering results discussed in this section are due to such an effect (Alpern *et al.*, 1982b).

A subsequent study (Sinha and Hoffer, 1981) showed that the intensity of scattered light satisfied a scaling of the form (8.5), with the characteristic scaling length being $k_m^{-1}(t)$. However, it is apparent from their results that the scaling function $F(k/k_m)$ could have a weak time dependence. In both of these studies the peak position was fitted to a power law of the form (5.34). The authors found that the exponent a exhibited a strong time dependence, changing from a value of $a' \simeq 1/3$ at early times to $a' \simeq 1$ at later times. This is similar to the observations of Chou and Goldburg and Knobler and Wong (Section XI) and in agreement with Siggia's predictions for ordinary binary mixtures (Section V). Nevertheless, it should be noted that the estimates of the exponent for ^{3}He–^{4}He are not precise and depend to some extent on the choice of the time origin ($t = 0$) (Hoffer *et al.*, 1980). It should also be noted that the scaling function obtained by Sinha and Hoffer is very sharply peaked, in a fashion rather similar to the computer simulation studies (Fig. 48). This extreme sharpness should be viewed with some caution, however, as it seems rather unusual. It could possibly be an artifact of experimental uncertainties in the light scattering data. Further study of this point for both the metamagnet and ^{3}He–^{4}He mixtures clearly seems useful.

Other light scattering studies on ^{3}He–^{4}He mixtures which are pressure quenched into the miscibility gap have been carried out by Benda *et al.* (1981, 1982). In their initial study the angular distribution of scattered light was measured for a wide range of quenches inside the miscibility gap. Halos were observed not only for quenches inside the spinodal region estimated by Hohenberg and Nelson (Fig. 46), but also well outside this region. They also noted an interesting asymmetry in the scattering pattern which they subsequently investigated in much greater detail (Benda *et al.*, 1982), as we discuss below. In both of their studies the time scale of the measurements, in units of $\tau = D\xi^{-2}t$ (eqn (5.28)), corresponded to the domain $\tau \geqslant 10^6$, which is the region of late stage growth. (This estimate is based on extrapolated values for D and ξ on the coexistence curve obtained from Leiderer *et al.* (1974, 1975).) Correspondingly, the region of wave vectors corresponds to $k_m/\xi < 10^{-3}$, where the distance between "clusters" is much greater than the interfacial thickness. On the other hand,

Sinha and Hoffer (1981) estimate that their measurements are in the range $5 < \tau < 10^2$, which are in a much earlier stage of the phase separation process. None of these studies are in a time domain for which the Hohenberg–Nelson theory (Section XII.A) would apply. In addition, none of the experiments observe the "flickering" effect discussed in Section XII.A.

We now summarize the work of Benda *et al.* (1982) in which anisotropic scattering is observed. Their earliest observations of the light scattering data show an isotropic halo, with the intensity of scattered light satisfying the scaling law (5.8). However, in the later stages the angular distribution becomes anisotropic about the direction of the incident beam. This is shown in Fig. 49, in which the structure factors $\hat{S}_v$ and $\hat{S}_h$ are displayed.

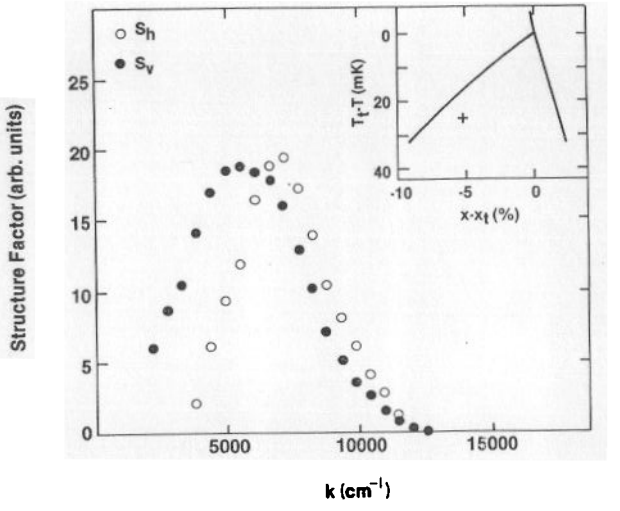

FIG. 49. Structure factors S_h and S_v, determined from the scattered intensity in the horizontal and the vertical scattering phase, respectively. This is for a time $t = 1.3$ s after starting decomposition from $T = 0.830$ K and $p = 0.724$ bar to 0.310 bar. The quenched state is indicated in the insert (+). The error bars are smaller than the symbol size. (From Benda *et al.*, 1982.)

These structure factors are obtained from simultaneous scans in the vertical and horizontal directions. As can be seen from this figure, the position of the peak, $k_{m,v}$, for S_v is smaller than the corresponding $k_{m,h}$ for S_h. As the process continues, $k_{m,v}$ becomes considerably smaller than $k_{m,h}$. As a consequence of this anisotropy, there is a breakdown of the simple scaling relation (5.8).

Benda *et al.* interpret this effect as due to the influence of gravity on the later stages of phase separation. There has been no detailed theoretical

treatment of the effect of gravity in this separation process. However, Siggia (1979) did anticipate the possibility that such an effect could eventually dominate at sufficiently late times. He estimated that gravity should begin to dominate when the droplet size is approximately equal to $(\sigma/g\Delta\rho)^{1/2}$, where σ is the surface tension, $\Delta\rho$ the density difference between the two phases and g the gravitational acceleration. This corresponds to a droplet size of about 10 μm for the quench shown in Fig. 49. This yields a predicted crossover at a value of k_m which is consistent with the experimental results. The effect of gravity also accounts for $k_{m,v} < k_{m,h}$. Namely, since large droplets will rise (or fall) faster than small ones, collisions will occur which will lead to coalescence and hence growth in the vertical direction. The effect in the horizontal direction will be neglible, thus accounting for the difference between $k_{m,v}$ and $k_{m,h}$. It is clear that a detailed theoretical treatment of gravitational effects would be very helpful. The ^{3}He–^{4}He mixtures provide the first example in which such effects seem to be observable.

We conclude by observing that earlier studies of nucleation in ^{3}He–^{4}He mixtures were carried out by Brubaker and Moldover (1974). There appear to be discrepancies between this work and the more recent studies of Benda *et al.* (1982) which are at the moment unexplained.

XIII. Special Topics

In this final section we give brief summaries of experimental and/or theoretical work on the kinetics of first-order phase transitions for a variety of topics not discussed so far in the text. In some cases, such as for superfluids and superconductors, extensive experimental and theoretical work exists on nucleation phenomena, whereas for several other systems research is at a more preliminary level. In general, far less attention has been given to spinodal decomposition than to nucleation phenomena. Our purpose in writing this section is to survey existing work in the field with the aim of suggesting areas for further study.

A. Nonlinear relaxation and metastability

A completely satisfactory characterization of metastable states has not yet been given. This remains as an important fundamental problem of statistical mechanics. From a rigorous point of view attempts have been made to describe metastable states in terms of constrained ensembles (Penrose and Lebowitz, 1979). For the questions considered in this review, however, it is more important to characterize the decay of the metastable state and to

calculate its associated lifetime. Since metastability is essentially a dynamical problem it is useful to give a dynamical description of metastable states. One such characterization has been proposed in terms of a nonlinear relaxation function by Binder and Müller-Krumbhaar (1974).

The general concept of a nonlinear relaxation function and an associated nonlinear relaxation time was introduced by Suzuki (1971) to describe the nonlinear relaxation of a system to equilibrium after a finite change of thermodynamic parameters, such as changes in temperature or applied external fields. We are interested in the particular case in which a phase transition is required for the system to equilibrate. The word "nonlinear" refers to the fact that this is not a case which involves small fluctuations around equilibrium, where linear response theory would be valid. In equilibrium there are two relevant statistical quantities which contain information about "time structure". These are the correlation function and the linear response function, which are related by an appropriate fluctuation dissipation relation. No such relation exists in the nonlinear case. The importance of the nonlinear relaxation becomes particularly dramatic near T_c, where very small deviations from equilibrium can have profound effects on systems. In such situations an expansion around equilibrium necessarily breaks down. The range of validity of linear response theory shrinks to zero as the final state of the system approaches the critical point.

The nonlinear relaxation function is of particular importance for dynamical processes in which the order parameter is not conserved (e.g. model A). We have already given examples of such systems in Section VI. There is also the hope that the understanding of these processes would yield some insight about dynamical processes with conserved order parameter. We should also mention that the experimental information in nonconserved dynamics (Section VI) is not very abundant. No attempt has yet been made to extract experimental information on the nonlinear relaxation time and compare it with the theoretical predictions discussed below.

In general we consider the situation in which a system in equilibrium is described by some Hamiltonian $\mathcal{H}_i$ for $t < 0$. At $t = 0$ the system is abruptly forced into a new condition governed by a new Hamiltonian $\mathcal{H}$. We then study the relaxation of some macroscopic property $A = \langle a \rangle$ to the equilibrium state corresponding to $\mathcal{H}$. The nonlinear relaxation function is then defined by

$$\phi_A(t) = \frac{A(t) - A(\infty)}{A(0) - A(\infty)}, \tag{13.1}$$

where in a "Heisenberg representation" the average defining $A(t)$ is taken with respect to $e^{-\beta\mathcal{H}_i}$. In a "Schrödinger representation" the average is taken with respect to the time-dependent probability distribution $\rho(t)$,

where $\rho(0) \sim e^{-\beta\mathcal{H}_i}$ and $\rho(\infty) \sim e^{-\beta\mathcal{H}}$. The relaxation time is defined by

$$\tau_A = \int_0^\infty dt \phi_A(t). \tag{13.2}$$

Other possible definitions have been given by Suzuki (1969, 1970), Schneider and Stoll (1974) and Ikeda (1977).

If A stands for a particular Fourier mode of a field $\psi(\vec{x}, t)$, then (Binder, 1973)

$$\phi_A(\vec{x}, t) = \frac{\langle \psi_{\vec{k}}(t) \rangle - \langle \psi_{\vec{k}}(\infty) \rangle}{\langle \psi_{\vec{k}}(0) \rangle - \langle \psi_{\vec{k}}(\infty) \rangle}. \tag{13.3}$$

Of particular interest is the $\vec{k} = 0$ mode which corresponds to a homogeneous equilibrium situation. When studying the relaxation of the order parameter to a state above T_c with no symmetry-breaking field applied we have $M(\infty) = 0$, where $M(t) = \langle \psi_0(t) \rangle$. This corresponds to the isothermal process in which a symmetry breaking field is switched off above T_c and also to the process in which the system is heated from below to above T_c at constant vanishing field. We then have

$$\tau_M = \int_0^\infty dt \frac{M(t)}{M(0)}. \tag{13.4}$$

The properties of the nonlinear relaxation time and nonlinear relaxation function in the asymptotic critical region have been studied by scaling arguments (Racz, 1975, 1976; Fisher and Racz, 1976; Kretschmer *et al.*, 1976; Sancho *et al.*, 1980), series expansions (Suzuki, 1971; Ikeda, 1976a, b; Suzuki and Ikeda, 1976; Racz and Collins, 1976; White, 1976; Csepes and Racz, 1978), renormalization group (Kawasaki, 1976; Suzuki, 1976c; Bausch and Janssen, 1976; Bausch *et al.*, 1979; Yamada *et al.*, 1977; Eisenriegler and Schaub, 1980), Monte Carlo simulations (Binder, 1981a; Ogita *et al.*, 1969; Stoll *et al.*, 1973; Binder and Stoll, 1973; Binder and Müller-Krumbhaar, 1974; Racz and Collins, 1975; Kretschmer *et al.*, 1976; Bolton and Johnson, 1976) and cluster dynamics (Binder and Stoll, 1973; Binder and Müller-Krumbhaar, 1974; Binder *et al.*, 1975; Kretschmer *et al.*, 1976).

As noted above, Binder and Müller-Krumbhaar (1974) have proposed a constructive definition of a metastable state according to the behavior of $\phi(t)$. Their point of view is that a metastable state is one which does not evolve appreciably in time on a time scale large compared with the equilibrium relaxation time. Accordingly, the metastable state is associated with the existence of a flat part (plateau) of the nonlinear relaxation function. By its definition, this characterization does not permit a clear-cut distinction between metastable and unstable states. In this interpretation

the nonlinear relaxation time is identified with the lifetime of the metastable state. This suggests then the identification of the nonlinear relaxation time with the completion time of Section X (Binder and Müller-Krumbhaar, 1974). Monte Carlo simulations on a $d = 2$ Ising model with Glauber dynamics (Binder and Müller-Krumbhaar, 1974) substantiate the plateau picture of the nonlinear relaxation after small field reversal for $T < T_c$ (Fig. 50). In fact, the various parts of $\phi(t)$ can be interpreted in terms of the

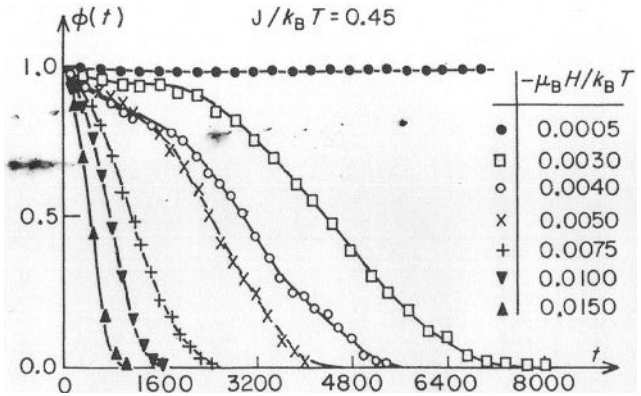

FIG. 50. Monte Carlo results for the nonlinear relaxation function for the two-dimensional Glauber model. The different values of magnetic field at a temperature $J/k_BT = 0.45$ are indicated in the column. (From Binder and Müller–Krumbhaar, 1974.)

processes seen in snap-shots of the Monte Carlo cluster evolution: A first concave part corresponds to the relaxation to the metastable state, with an increase in the number of small clusters. The flat part associated with the metastable state corresponds to the formation of noninteracting clusters of intermediate size which disintegrate. The linear decay of $\phi(t)$ corresponds to the coagulation reactions of intermediate clusters which have become sufficiently stable. Finally, the last exponential decay is associated with the final stage of the process in which the original background phase has been reduced to small clusters in the emerging phase.

The plateau behavior of $\phi(t)$ has been found in a mean field solution of the Ginzburg–Landau model of an Ising ferromagnet with nonconserved order parameter (eqn (3.17) without ζ). One considers a reversal of the magnetic field at $T < T_c$ from $H \geq 0$ to $H' < 0$ and slightly larger (in absolute value) than the spinodal value H^* (Binder, 1973). For values of $|H'|$ for which $|H'| < |H^*|$, $\phi(t)$ does not decay to zero. The system is caught in a mean field "metastable" state, which has an infinite lifetime.

For values of $|H'|$ much larger than $|H^*|$, $\phi(t)$ decays very rapidly to zero, indicating the decay of the unstable state. Billotet and Binder (1979) have attempted to calculate $\phi(t)$ for this same model including fluctuations. The decoupling of the equations for the moments is made following essentially the Langer–Bar-on–Miller scheme (Section V). The numerical solution of the equation yields results for $\phi(t)$ which are qualitatively similar to those of mean field. In particular, infinitely long-lived metastable states exist although the value of H^* is reduced with respect to the mean field value. Billotet and Binder (1979) concluded from this result that the Langer–Bar-on–Miller theory contains a spinodal curve and does not include a description of the mechanism of nucleation and growth believed to be essential in understanding the smooth transition between unstable and metastable states. The comparison of the results of this calculation with the Monte Carlo data mentioned above show that the theory overestimates the lifetime of the metastable state and that it predicts a too rapid decay of $\phi(t)$ from its plateau value. In fact, this decay time is predicted to be essentially independent of H'. This is in disagreement with the identification of this decay time with the nonlinear relaxation time and the lifetime of the state. These deficiencies are less important for larger values of H', that is, going away from the metastable region. On the other hand, the initial time behavior of $\phi(t)$ indicating the decay to the metastable state is in good agreement with the theory. This confirms the validity of the Langer–Bar-on–Miller scheme for early times.

As a final remark we wish to point out that the nonlinear relaxation function seems to be an important "first principles" tool to study some properties of first-order phase transitions which have not yet been extensively used.

B. Relaxation of fluctuations under various quench conditions

Most studies of nucleation and spinodal decomposition assume that the quench from a disordered phase to a point below the coexistence curve is instantaneous. This is clearly an idealization of the actual situation (except in Monte Carlo studies) in which the actual quench rate is finite. Theoretical studies of the effect of such finite quenches have so far not been carried out. In this section we deal with a somewhat different class of quenches in which the dynamical evolution of a system differs from that of usual nucleation or spinodal decomposition experiments. We will consider in particular the behavior of a system under three different quench conditions. The first is a temperature or pressure quench in the stable, one-phase region (Binder, 1977; Wong and Knobler, 1979). The second is a "double quench". The system is first quenched from above to below T_c and then

subsequently "quenched" back to a state above T_c (Wong and Knobler, 1978; Ruiz, 1982). The third considers periodic variations of temperature which brings the system alternatively above and below T_c (Onuki, 1981, 1982a, b, c). The difficulty of dealing with time-dependent quenches, mentioned at the beginning, arises, of course, in the case of this periodic temperature variation. It is worth noting in this regard that finite quench rates have been considered in other dynamical situations than those discussed here. For example, Ahlers *et al.* (1981) have considered the effects of bringing a system through an instability point at a finite rate in interpreting their experiments on the onset of ordered structures in Rayleigh–Benard systems. Caroli *et al.* (1981) have also studied the decay of metastable and unstable states in zero-dimensional models of systems which are driven through a bifurcation point at a finite velocity.

We first consider a quench from one state in a one-phase region to a second point in the same region. Any fluctuation of such a system will decay to the homogeneous equilibrium state. It is obvious that a linear theory such as that of Cook (Section V) should be valid for this quench condition in the limit $k \to 0, t \to \infty$. By considering the eigenvalue spectrum of the time evolution operator which appears in the master equation (9.6), Binder (1977) has shown that in this limit the corresponding structure factor is given by

$$\hat{S}(k,t) = \hat{S}_T(k)\, e^{-2D_{T'}(k)k^2 t} + \hat{S}_{T'}(k)\{1 - e^{-2D_{T'}(k)k^2 t}\}. \qquad (13.5)$$

In eqn (13.5) T and T' denote the initial and final temperatures, respectively while $\hat{S}_T(k)$ and $\hat{S}_{T'}(k)$ denote the corresponding equilibrium structure factors. The mutual diffusion constant at T' is $D_{T'}(k)$. This form is the appropriate solution of Cook's equation (Section V), where $D_T(k) = k^{-2}\omega(k)$ and $\omega(k)$ is defined by eqn (5.7). Scaling arguments can be used to extend the result (13.5) to the critical region. A simple exponential decay for $\hat{S}(k,t)$ is predicted by (13.5) if $T' > T$. If $T' < T$, however, $\hat{S}(k,t)$ is predicted to develop a maximum at $k_m(t)$, where

$$k_m(t) \xrightarrow[t \to \infty]{} 0.$$

This behavior has been confirmed for the binary fluid IW by Wong and Knobler (1979). They studied $\hat{S}(k,t)$ for the two quenches $T = T_c + 70$ mK, $T' = T_c + 10$ mK and $T = T_c + 10$ mK, $T' = T_c + 70$ mK respectively. The same behavior for $\hat{S}(k,t)$ has also been observed in Monte Carlo simulations for the Ising model in quenches from $T = \infty$ to $T' = 1.1T_c$ (Marro *et al.*, 1975). This one-phase quench is, of course, a rather simple dynamical problem.

The second case is the double quench $T \to T' \to T$, with $T' < T_c < T$.

Such an experiment has been performed by Wong and Knobler (1978) in a binary fluid. Although they did not give a detailed analysis of their results, they found that the scattering ring which developed following the first quench to the lower temperature T' continued to collapse after the second quench to the higher temperature T. The rate of collapse, however, is smaller at the temperature T than at the lower temperature T'. Subsequent to this experiment, Ruiz (1982) has developed a theory for such a double quench for fluids. As in the one-phase quench discussed above, Ruiz's analysis is based on linearizing the dynamical equations of motion. He explicitly considers hydrodynamic effects by including a coupling of the local velocity field to the local concentration. He finds that the structure factor obeys a scaling behavior similar to that observed in ordinary spinodal decomposition, as discussed in Section VIII. He obtains a value $a = \frac{1}{2}$ for the exponent (5.33) for $k_1(t)$ which he argues corresponds to the crossover between $a = 1/3$ and $a = 1$ discussed by Siggia (Section V).

The third case of spinodal decomposition due to a periodic temperature variation has been considered by Onuki (1981, 1982a, b, c) in an interesting series of papers. This temperature variation can be produced by a sound wave or more generally by a periodic external force such as a pressure or magnetic field. Onuki has analyzed the behavior of TDGL models for a single component order parameter which is either conserved or nonconserved (models A, B; Section III). He has concluded that in general fluctuations show a strong periodic enhancement when the following two conditions are fulfilled. First, the amplitude of the temperature oscillation must be larger than $|T_0 - T_c|$, where T_0 is the mean temperature. Second, the parameter μ must be much greater than unity, where μ is the ratio of the decay rate of a mode of characteristic length ξ_c to the frequency of oscillation of the temperature. A major difference between the conserved and nonconserved cases is that in the former case the fluctuation enhancement is cutoff at a wavenumber $k_c = \mu^{-1/2}\xi_c^{-1}$ (unless the mean temperature is very close to the shifted critical temperature). In the latter case all fluctuations with wavenumbers less than ξ_c^{-1} exhibit enhancement.

Onuki has evaluated the time dependence of the order parameter for the nonconserved TDGL model by a mean field approximation. The critical temperature is unchanged, so that for $T_0 > T_c$ the system remains in the disordered phase, while for $T_0 < T_c$ the order parameter exhibits a forced oscillation. An analysis of the linearized equation for the structure factor in the disordered phase yields a periodic solution with an enhancement of fluctuations under the two conditions stated above. When $\mu \gg 1$ (as for a large periodic variation of temperature), the nonlinear coupling of the fluctuations cannot be neglected. This case is treated by Onuki generalizing ideas of Suzuki (1976a, b, 1977a, b, 1981) for a system with one degree of freedom and of Kawasaki *et al.* (1978) for the nonconserved TDGL

model. These authors argue that, in the decay of an unstable state, there is first a Gaussian regime in which the nonlinear terms can be neglected. There is also a nonlinear regime in which the noise (the internal fluctuations) can be neglected. Under a periodic oscillation of temperature, the system alternates between the Gaussian and non-Gaussian regimes. One has a sequence of variances of the Gaussian distribution of fluctuations which tends to a limit in which the system reaches a periodic state. (This is true as long as the interval in which $T_c - T_0$ is positive and is large enough for the system to return to the Gaussian regime.) By such arguments Onuki concludes that the nonlinear coupling of fluctuations produces a shift in the critical temperature. This new critical temperature is defined as the mean value of the temperature for which the system first exhibits an ordered state (holding other parameters constant). Furthermore, for $\mu \gg 1$ the transition is shown to be first order. Onuki also evaluates the structure factor in the periodic, disordered state and the order parameter in the periodic, ordered state.

A mean field treatment of the conserved TDGL model does not show any special features for the order parameter. The critical point is unchanged and below T_c the order parameter attains its equilibrium value. Nevertheless, the linearized equation for the structure factor implies a similar behavior for this quantity as in the nonconserved case, for a restricted range of k. Thus there is also a periodic solution in this case, with an enhancement of fluctuations.

Onuki (1982c) has subsequently presented a numerical study of periodic spinodal decomposition in solid and fluid binary mixtures. His analysis is based on the theories of Langer *et al.* (1975) and Kawasaki and Ohta (1978a) for these systems, discussed in Section V. For fluid mixtures the periodic variation in temperature can be achieved experimentally by a periodic change in pressure, whereas in solids it can be realized by a macroscopic change in temperature. He finds that for solid mixtures under appropriate conditions the scattering intensity should display two peaks, implying the existence of two types of clusters. The smaller ones are created and destroyed within each period, but some of them survive to grow into the larger ones after several periods. For fluids, he finds this double peak only in certain time intervals, presumably due to the influence of hydrodynamic interactions. In both cases, the nature of the transition which occurs as the average temperature is lowered with a fixed size of the temperature vibration remains unknown, although it could be a first-order transition. Finally, it is worth mentioning that by making the period of temperature oscillation very small, one effectively reduces the time scale of the decay of the order parameter. Therefore this method of temperature oscillation provides a means for studying spinodal decomposition in systems with rapid time scales.

C. Superfluidity and superconductivity

The basic idea of nucleation as a thermally activated process which requires a critical size fluctuation has been used to calculate the critical velocity of a superfluid flow (Langer and Fisher, 1967; Langer and Reppy, 1970). The underlying concept is that a stable superfluid flow is a nonequilibrium phenomenon, for which many-body equilibrium theories that only consider small fluctuations around equilibrium are incorrect. A nonzero superfluid flow characterized by a velocity v_s is then regarded as a metastable state. There exists a finite probability (per unit time) for homogeneous nucleation to a more stable state with smaller velocity, caused by the appearance of large, localized fluctuations. If v_s is sufficiently small, such a probability is too small to be observed experimentally. The critical velocity has an operational definition quite similar to the cloud point. It is the velocity for which $|dv_s/dt|$ is larger than a characteristic observable value. As in the case of the cloud point, this turns out to be a sharply defined quantity. A nucleation rate of the general form (4.26) can be used to fit the experimental data reasonably well (Langer and Reppy, 1970). It is nevertheless important to note that the main theoretical predictions, such as the logarithmic decay of v_s, are independent of the specific model one uses to calculate the activation energy. The model proposed by Langer and Fisher (1967) identifies the "droplet" or localized fluctuation of the nucleation picture as a vortex ring. The creation of a vortex ring is the mechanism for the dissipation of energy that causes the decay of the superfluid flow. This vortex ring characterizes the saddle point of nucleation theory (Section IV) and connects two superfluid states with a difference of 2π in the phase of the complex order parameter. As for the binary fluid (Section IV), the activation energy or energy of formation of the vortex ring can be calculated phenomenologically using hydrodynamic ideas. The numerical agreement with experiment is rather poor, due to the rough estimates used in the calculation of the activation energy and the prefactor of the nucleation rate. The calculated critical velocity turns out to be an order of magnitude larger than the experimental value (Langer and Reppy, 1970).

An analogous problem that has been studied from the same viewpoint is the transition to resistive states in superconducting channels when a large enough supercurrent occurs (Langer and Ambegaokar, 1967; McCumber and Halperin, 1970). Here again the superconducting state is regarded as a metastable state that decays to a state of lower supercurrent through the appearance of a localized fluctuation. The system can be described by a Ginzburg–Landau functional for the complex order parameter. In the case of thin whiskers the problem becomes essentially one-dimensional. From the mathematical point of view this one-dimensional problem is very interesting, since the different ingredients of the nucleation rate (4.26) can

be explicitly calculated (McCumber and Halperin, 1970). In particular this is the only example for which an explicit evaluation of the different eigenvalues entering in the prefactor Ω_0 has been carried out. Similar to the superfluid case, the saddle point is a configuration connecting two superconducting states with a difference of $2\pi/L$ in wavenumber (L is the length of the system channel). The first calculation by Langer and Ambegaokar (1967) yielded large discrepancies with experimental results which were attributed to the existence of inhomogeneities. A revised calculation (McCumber and Halperin, 1970) of the prefactor of the nucleation rate seems to reconcile theory and experiment. Recently a more powerful approach to the mathematical problems considered by McCumber and Halperin (1970) has been presented (Durn *et al.*, 1981). In particular the method allows one to obtain explicit results for arbitrary values of the current.

D. Electron–hole condensation in semiconductors

As is well known, it is possible to form electron–hole pairs in semiconductors by optical excitation (Wolfe, 1982). At high temperatures these pairs behave like a Bose gas of free excitons. At high density the gas ionizes into a fermionic system (electron–hole plasma) and a metal–insulator transition occurs. Below a critical temperature a first-order phase transition occurs which is analogous to a gas–liquid transition. Two-phase coexistence consists of a low density exciton gas together with a high density fermionic "liquid" phase (an electron–hole plasma). This is a nonequilibrium state, but its phase diagram looks very much like an ordinary gas–liquid system. For example, Thomas *et al.* (1978) have determined the phase diagram for Ge, which has a critical temperature $T_c = 6.7 \pm 0.2$ K and a critical density $n_c = (0.6 \pm 0.1) \times 10^{17}\,\mathrm{cm}^{-3}$. The phase diagram for Si has been determined by Shah *et al.* (1977), with $T_c = 27 \pm 1$ K and $n_c = 1.1 \times 10^{18}\,\mathrm{cm}^{-3}$. Reviews of this subject have been given by Hensel *et al.* (1977) and by Rice (1977).

Nucleation phenomena in this nonequilibrium phase transition have been studied by theorists (Silver, 1975a, b, 1977, 1978; Combescot and Combescot, 1976; Staehli, 1976; Westervelt, 1976a, b; Koch and Haug, 1979; Combescot, 1980) and experimentalists (Bagaev *et al.*, 1976; Etienne *et al.*, 1976; Staehli, 1976; Dite *et al.*, 1977; Shah *et al.*, 1977b; Hammond and Silver, 1979; Voisin *et al.*, 1979). The classical Becker–Döring theory (Section II) has been adapted to this nonequilibrium situation by Silver (1975a, b, 1977) and Westervelt (1976a, b). The main difference between the theory discussed in Section II and that for the electron–hole problem is that it is necessary to supplement the rate equations which contain the

usual evaporation–condensation mechanism (or excitons in a droplet). The additional terms account for the decay of excitons due to their finite lifetime and for the creation of excitons by optical pumping. The finite lifetime of the excitons provides a mechanism for droplets to lose particles at a rate which is proportional to the droplet volume. (This mechanism is of course absent in classical nucleation theory.) As a consequence, droplets cannot grow to form a single macroscopic phase. In the nonequilibrium, steady state situation there exists a characteristic size for which the droplet is stable. For this size, the evaporation–condensation and finite lifetime effects compensate each other. Droplets which are larger or smaller than the characteristic size will shrink or grow, respectively. The nucleation rate is the measure of the flow of droplets across the critical size saddle point to the stable state, which is a droplet of characteristic size. An interesting effect is that the characteristic size grows while the critical size decreases as a function of supersaturation. Therefore, at a given temperature there exists a minimum supersaturation at which both sizes are equal. At lower supersaturations no stable droplet size is reached. The finite lifetime effects become more important at low temperatures because the evaporation and condensation rates decrease strongly with temperature, whereas the recombination rate is practically constant. These facts imply that the minimum supersaturation becomes very small at low temperatures. For instance, the theory predicts a minimum supersaturation for Ge of order unity for $T \simeq 1.5\,\mathrm{K}$ (Silver, 1978). Below this temperature significant deviations from an "equilibrium" liquid–gas behaviour must occur. Sizeable stationary droplet solutions are excluded by these theoretical considerations, so that metastability is ruled out. The main predictions of this finite lifetime nucleation theory seem to be in agreement with experimental observations. These finite lifetime effects are more important in Si than in Ge (Hammond and Silver, 1979), since the lifetime is two orders of magnitude smaller in this case.

Silver (1978) has given a field theoretic generalization of the above Becker–Döring-type theory. This theory is based on the ideas discussed in Section IV. His starting point is a hydrodynamic model which essentially consists of the Langer–Turski (1973) equations for the liquid–gas transition, supplemented by a damping term which simulates the scattering from phonons. There are also additional terms in the continuity equation which model the creation of excitons and the electron–hole recombination. Silver discusses the droplet solution of these equations, but does not give a complete calculation of the nucleation rate. The predictions of his theory are in general similar to the simpler finite lifetime, Becker–Döring-type theory. However, his formulation might allow one to study the case of large supersaturations, for which nucleation theory is not applicable. His theory also predicts properties of the stable droplet which differ substantially from the capillarity approximation. In particular, these droplets are characterized by both a velocity and a concentration profile.

Finally, we note an interesting microscopic calculation by Kirczenow (1982) who analyses the surface and interface structure of the binary electron–hole liquid in ⟨111⟩ stressed Ge at $T = 0$. In this case two different electron species ("hot" and "cold") exist. Phase separation between two different phases (I and II) is predicted to occur without any nucleation process taking place, even though the transition is of first order (as long as the electron–hole liquid has a free surface). Phase I consists of cold electrons and holes, while phase II consists of hot electrons, cold electrons and holes.

E. Coherent metal–hydrogen systems

In certain metal–hydrogen alloys, such as PdH_x and NbH_x a gas–liquid-like phase transition occurs at moderate hydrogen concentrations. In the temperature–density domain which normally corresponds to two-phase coexistence, the density of hydrogen is inhomogeneous. There are in fact two possible phase diagrams which can be discussed and in principle experimentally measured. The first is the true equilibrium state, which is an incoherent state in which a hydrogen-rich "liquid" phase coexists with a hydrogen-poor "gas" phase. Since incoherency implies a mismatch of lattice parameters between the two phases, the interface between the phases by necessity contains localized dislocations. The second, metastable state is a coherent state which, in a certain region of the phase diagram, consists of an inhomogeneous distribution of hydrogen which varies on a macroscopic scale. It is the coherent state with which we will be concerned, since it is experimentally realizable and should exhibit unusual spinodal decomposition. Its unusual characteristics are due in part to the presence of coherency stresses. These prevent rapid density variations of hydrogen and thereby preclude the formation of sharp interfaces.

The theory of the coherent and incoherent phase transitions of hydrogen in alloys has been developed by Wagner and Horner (1974), Horner and Wagner (1974) and Bausch *et al.* (1975). This theory is based on the idea due to Alefeld (1969) that the dominant attractive force between the protons is a long-ranged, elastic interaction. This interaction arises from a deformation of the host lattice by an interstitial proton. This deformation produces a long-range strain field which acts on the other protons. The above theory predicts that the phase transitions of coherent metal–hydrogen systems are of a mean field or Landau type. This prediction seems to be in good agreement with experiment (Buck and Alefeld, 1972; de Ribaupierre and Manchester, 1974a, b, 1975; Manchester, 1976; Zabel

and Peisl, 1979, 1980). A comprehensive review of the experimental and theoretical situation in metal–hydrogen alloys has been given by Wagner (1978). It should be noted that these phase transitions exhibit a strong sensitivity on the sample geometry. This was predicted by Wagner and Horner (1974) and confirmed experimentally by Zabel and Peisl (1979, 1980).

A theory of spinodal decomposition in coherent metal–hydrogen systems has been developed by Janssen (1976). This is a deterministic theory in which noise (internal fluctuations) is neglected and is based on equations of motion similar to those of Cahn (Section V). The physical situation described by these equations is, however, quite different from normal systems such as binary alloys or binary fluids. The reason is that in the coherent state the important density fluctuations only consists of a *few* unstable macroscopic ("surface") modes. Janssen was thus able to give an explicit solution for the time dependence of the dominant unstable mode, which included nonlinear coupling terms ignored in the Cahn theory. Kappus and Horner (1977) extended Janssen's theory to the case of extremely deep quenches where all the surface modes (those which depend upon the surface geometry) are unstable. They treated the noise term in an approximate way and were able to give an explanation of the quasi-periodic precipitation which has been observed on the surface of rapidly quenched NbH_x systems (Pick, 1978). Haus and King (1982) have recently considered coherent spinodal decomposition for an elastically isotropic, spherical sample which undergoes a shallow quench into the unstable region. Their theory treats both the noise and nonlinear terms using ideas originally developed for systems with a discrete set of unstable modes (Arecchi and Degiorgio, 1971; Suzuki, 1976a, b; Haake, 1978). Specific predictions have been made for NbH_x which can in principle be experimentally tested. Their theory seems to be the most complete study to date of coherent spinodal decomposition.

Finally we note that Burkhardt and Wöger (1975) have proposed using X-ray scattering to measure coherent spinodal decomposition in metal–hydrogen alloys. The idea is to determine the time dependence of the order parameter (the macroscopically varying hydrogen density) by measuring the shifts in the Bragg maxima. It should also be noted that all the theories of coherent spinodal decomposition discussed here assume that the system remains coherent during such a process. However, Wagner (1978) has pointed out that this is in general incorrect. Instead, in the later stages one would expect a partially incoherent phase separation to occur, due to the creation and motion of dislocations. Nevertheless, he points out that if one is sufficiently close to T_c one could expect a coherent state to be maintained for several hours. A recent review of experimental studies of metal–hydrogen systems has been given by Manchester (1982).

F. Physisorption and chemisorption systems

There are a number of two-dimensional physisorption (He, Ar and Kr on graphite) and chemisorption systems (O/W (110), H/W (100), N/W (100), O/Pd (110)) (Sinha, 1980), which undergo both an order–disorder phase transition and a phase separation process simultaneously below a certain "multi-critical" temperature. In the case of physiadsorbed systems the adatoms (He, Kr, Ar) sit at the bottom of the potential wells of the graphite atoms and hence are weakly attached to the substrate. This is in contrast to the chemisorption systems where an adatom (O, N) is chemically bonded to the host surface atoms (W, Pd, Ag). At high temperatures, adatoms are randomly distributed on the host surface and the system is in a disordered or "fluid" state. As the temperature is suddenly quenched below a certain "critical" temperature (which depends upon the coverage), islands of a definite symmetry develop and grow in time. The symmetry of the ordered islands depends upon the nature of the adatom–adatom interactions as well as the symmetry of the underlying substrate. The development of the ordered domains can in principle be studied in low energy electron diffraction (LEED) or X-ray scattering experiments (Lagally *et al.*, 1978). Most of the LEED investigations have been directed toward studying the equilibrium properties of these systems. For example, the location of the Laue spots in the diffraction pattern provides information about the symmetry of the ordered regions. Measuring the intensity and width of the Laue spots (Buchholz and Lagally, 1975) determines the total amount of a given order in the system and provides useful information about the phase diagrams of these systems. Monte Carlo studies (Williams *et al.*, 1978) of the model systems have been carried out in conjunction with LEED experiments to estimate the adatom–adatom interactions. Very recently, using Monte Carlo techniques, Sahni and Gunton (1981) have carried out a dynamical study of a simple model of O/W (110). They monitored the growth of islands of $p(2 \times 1)$ and $p(1 \times 2)$ order after the system is quenched from a high temperature "fluid" phase to a temperature below the "multi-critical" temperature. The ordering and phase separation is indicated by the development of the peaks in the order parameter and atomic coverage structure factors, respectively. This system evolves very slowly, so that equilibrium is never attained in this study. This is presumably due to the presence of antiphase boundaries between $p(2 \times 1)$ and $p(1 \times 2)$ domains. Recently, Safran (1981) has argued on analytical grounds that such a system (O/W (110)) with four degenerate ground states will stay metastable forever in two dimensions. However, his argument is limited to very low temperatures and a coverage of 1/2. An extension of his ideas to high temperatures and different coverages is needed for understanding the slow growth seen in computer simulations. Lagally *et al.* (1978) have

also noticed the slow evolution of the O/W (110) system in experimental studies. At present it is not clear whether this is due predominantly to surface heterogeneties (e.g. terraces), the smallness of the diffusion constant or antiphase boundaries as seen in Monte Carlo simulations by Sahni and Gunton (1981).

G. Intercalation compounds

One of the most interesting but at present poorly understood phenomenon in intercalation compounds is the dynamical evolution of the pure stage ordering. This ordering is a periodic sequence of n host layers and one intercalant layer. General reviews of intercalation have been given by Fischer and Thompson (1977, 1978). Although staging has also been observed in a number of transition metal dichalcogenides, the best known systems are graphite intercalation compounds (GICs) where staging has been reported as high as $n \sim 10$. Graphite is a layered compound and consists of parallel planes of graphite atoms stacked up along the c axis. The intercalant atoms (Br_2, C, K, Rb) enter the GICs from the periphery of the interplanar regions. At equilibrium, one observes an ordering along the c-axis as well as an in-plane superlattice arrangement of intercalant atoms. The most striking feature of the c-axis ordering is the staging which is independent of the wide variety of in-plane ordering. The in-plane ordering includes both solid (commensurate and/or incommensurate with the graphite host) and liquid phases.

This universal feature of the staging phenomenon (independent of the in-plane ordering) makes it possible to understand the essential physics of staging by assuming a simple model without any detailed knowledge of the in-plane interactions. Such an attempt has recently been made by Safran (1980), who obtained the phase diagram of intercalation compounds in a mean field approximation by assuming an average attractive in-plane interaction and repulsive interplanar interaction between intercalants. There are regions in the phase diagram where stages n and $(n+1)$ coexist in equilibrium, e.g. at high coverages stages 1 and 2 coexist below a tricritical point. Safran (1980) has also studied the dynamical evolution of the quenched system from a high temperature "fluid" phase to a temperature $T < T_t$ where stage ordering and phase separation occurs simultaneously. This work involved an application of Tomita's approximation (Tomita, 1978) to spinodal decomposition (Section V.B). Safran numerically evaluated both the in-plane ($S_{\parallel}(k, t)$) and interplane ($S_{\perp}(k, t)$) structure factors which exhibit growing peaks. Within the plane, the intercalant atoms form islands which grow in time and their interplanar positions (or staging) changes due to c-axis repulsive interactions. Safran's highly simplified

dynamical model does not take into account explicitly the electrostatic or the elastic interactions which play an important role in the staging phenomenon. No experiments have been done to date on the dynamics of staging and in-plane ordering.

H. Nucleation and spinodal decomposition in polymer blends

An interesting area with potentially important applications of spinodal decomposition is that of polymer blends. A few compatible binary polymer melts of chemically different polymers A and B have been found. Such mixtures are entirely miscible in the one-phase region but undergo phase separation beyond a critical point. A review of the thermodynamic properties of such systems in terms of a Flory–Huggins equation of state has been given by de Gennes (1979). An earlier discussion has been given by McMaster (1973). The metallurgy of such blends has also been discussed (Krause, 1972; Klempner and Frisch, 1977).

A few experimental studies of nucleation and spinodal decomposition phenomena in these blends have already been performed. McMaster (1975) has investigated the binary styrene–acrylonitrile copolymer–poly(methyl methacrylate) system (SAN/PMMA) by TEM methods. He observed the formation of a dispersed two-phase structure for the concentrations 75% SAN:25% PMMA and temperature $T = 265\,^{\circ}C$. Ostwald ripening was seen in which the time dependence of the domain growth was consistent with the Lifshitz–Slyozov theory (Section VI). He also observed the formation of a highly interconnected, two-phase structure characteristic of spinodal decomposition for quenches at 25% SAN:75% PMMA, $T = 180\,^{\circ}C$ and $T = 210\,^{\circ}C$ respectively. This interconnected structure coarsened much more rapidly than the dispersed structure. The size of phase-separated domains in the interconnected morphology grew initially in a linear fashion, quite similar to that found in binary fluids (i.e. to (5.32)). During the later stages the growth was shown to cross over to an exponential behavior. McMaster attributed the coarsening of this interconnected structure to a viscous flow mechanism which was driven by interfacial tension. He presented a simplified analysis of this complex flow based on an earlier theory by Tomotika (1935). (Tomotika considered the break-up of an infinite cylindrical thread of one viscous Newtonian fluid which is immersed in a second viscous Newtonian fluid.) Further theoretical study of this interesting coarsening problem is obviously warranted.

Nishi *et al.* (1975) also studied nucleation and spinodal decomposition in polystyrene–poly(vinyl methyl ether) mixtures, using light transmission, optical microscope and pulsed NMR methods. They observed both the dispersed, two-phase structure and the highly interconnected structure seen

by McMaster. They interpreted these two morphological structures as produced by nucleation and spinodal decomposition, respectively. Large differences in light transmission were found for these two different structures. They also found qualitative differences in the coarsening rates of these two structures, consistent with McMaster's observations. By using Cahn's linear theory (Section V) to analyze their spinodal decomposition data, they were able to obtain estimates of the thermodynamic and dynamical parameters for this polymer–polymer system. The polystryrene–poly(vinyl methyl ether) system has also been studied by several other groups. The most recent work is a light scattering study by Snyder *et al.* (1983) who have analyzed their early time results in terms of a Cahn–Hilliard-like expression. Their paper also gives detailed references to other work on this system. The problem of phase separation in polymer blends in thin films has also been studied by Reich and Cohen (1981) and other authors (additional references are given in Reich and Cohen, 1981).

Another experimental study of spinodal decomposition has been carried out by Gilmer *et al.* (1982). They studied de-mixing in the system atactic polystyrene–atactic poly(*ortho*-chlorostyrene) (aPS/aPOCS) by light scattering techniques. Their data for the wavenumber $k_m(t)$ which locates the maximum in the scattering intensity was analyzed using a power law approximation ((5.34) with $B_m = 0$). They found that the exponent a' varied with temperature, molecular weights and composition of the sample, with the major change being due to temperature. Their values for a' are in the range $a' = 0.8$–1.6, which is similar to the result of McMaster in the initial stages of coarsening. (His observation corresponds to $a' = 1$.) Gilmer *et al.* interpret their results for aPS/aPOCS as indicating that viscous flow is the dominant mechanism for domain growth in their study. They do not see the exponential growth observed by McMaster in the later stages of coarsening, possibly because their study does not include the late time region.

More recently, Pincus (1981) has given a theoretical analysis of the initial stages of spinodal decomposition in polymer blends. He considered a rapidly quenched mixture of two polymers of polymerization N_A and N_B. For simplicity he discussed the symmetric case $N_A = N_B = N$, for long chains $N \gg 1$. His dynamical model assumes that the chain mobility is controlled by reptation (de Gennes, 1971). Reptation is a diffusive motion of a polymer chain in a randomly shaped "tube" formed by a background of obstacles. The original conditions under which reptation was considered valid required that the background be in a fixed (frozen-in) configuration. As such, it was considered unlikely that reptation was a relevant mechanism for polymer melts, since the obstacles themselves are mobile polymer chains. However, subsequent work (Edwards and Grant, 1973; de Gennes, 1976, 1980; Doi and Edwards, 1978a, b, c; Klein, 1978) suggested that reptation is relevant in all dense polymer systems. If reptation is the

dominant dynamical effect in polymer blends, then the very early stage of spinodal decomposition should be qualitatively different from that of binary alloys. This results from the fact that the mobility which occurs in the equations of motion analogous to (5.1) and (5.2) is strongly k-dependent. (Another difference between polymer blends and binary alloys is that the Flory–Huggins free energy is used, rather than a Ginzburg–Landau free energy.) As a consequence, Pincus finds from the linear equation of motion (analogous to Cahn's theory, Section V) that the most unstable mode (immediately after the quench) is molecular weight dependent. The corresponding growth rate is proportional to the melt reptation diffusion constant. These predictions seem to be consistent with the experimental results of Nishi *et al.* (1975) discussed above. However, it is not obvious that a linear theory is applicable in the domain of time which is experimentally studied. In addition, recent neutron spin–echo studies of entangled polymer chains in a melt (Richter *et al.*, 1981) and computer simulation studies of a model of such a melt (Richter *et al.*, 1981; Baumgärtner and Binder, 1981) are in general inconsistent with the reptation model. (A recent Monte Carlo study by Deutsch (1982) yields results which seem consistent with the reptation model, however. Kremer (1983) disagrees with Deutsch's conclusion.) Thus for both reasons further experimental and theoretical studies of spinodal decomposition in polymer blends would seem necessary. Two additional points concerning the theory of Pincus should be made. The first is that his paper corrects an earlier theory (de Gennes, 1980) of spinodal decomposition for the same model. The second is that Pincus concludes that the late stage growth behavior of polymer blends should satisfy a Lifshitz–Slyozov (Section VI) growth law. Namely, the average droplet volume should increase linearly with time. This prediction is consistent with the experimental results of McMaster (1975). Finally, it is worth repeating an observation by de Gennes (1980) that spinodal decomposition and coarsening in polymer blends could lead to new structures which have an excellent linkage between components. This would be of considerable technological importance.

It should also be noted that nucleation and spinodal decomposition phenomena have been studied in polymer–solvent systems (van Aarsten, 1970; Smolders *et al.*, 1971; van Emmerik and Smolders, 1972; van Emmerik *et al.*, 1973). A discussion of the thermodynamic properties of such systems has been given by de Gennes (1979).

I. Essential singularity in percolation problems

It is well known that the cluster generating function $f_p(H)$ in percolation problems plays a role similar to the free energy of a thermodynamic phase

transition as a function of the magnetic field (Stauffer, 1979; Essam, 1980). For the percolation problem H is an "external field" and p is the probability for a site or a bond to be occupied. The percolation transition is characterized by the existence of an infinite cluster for $p > p_c$. (No infinite cluster exists for $p < p_c$.) Kunz and Souillard (1978) have given rigorous proofs of a number of properties concerning the analyticity of the cluster generating function as a function of H, for the interacting and noninteracting site and bond percolation problems. An important result is the proof of the existence of an essential singularity of $f_p(H)$ for $H = 0$ in the percolation regime, that is $p > p_c$. This rigorous result is most interesting because of the analogy with the conjecture of an essential singularity at the coexistence curve of a thermodynamic first-order phase transition discussed in Section IV. The proof shows that for $p \geq p_c$ the clusters have an effective volume and that there exist contours whose volume grows faster than the surface area. These facts are reminiscent of the droplet picture used by Langer (Section IV) to calculate the imaginary part of the free energy for a metastable state which characterizes the essential singularity of Ising-like systems. In fact Harris and Lubensky (1981) and Lubensky and McKane (1981) have shown that the essential singularity of the cluster generating function can be understood from a consideration of instantons (droplets) in a metastable state, in a discussion which precisely follows Langer's calculation of the imaginary part of the free energy. They have also used the general Langer droplet picture to calculate the p-dependence of the cluster size distribution function (the Laplace transform of the cluster generating function) near the percolation threshold. The calculation is based on the fact (Fortuin and Kasteleyn, 1972; Lubensky, 1979) that $f_p(H)$ can be obtained as the limit of the free energy of a q-state ferromagnetic Potts model in the limit $q \to 1$, where H is the magnetic field. In the mean field treatment of this model there exist two spatially uniform local equilibrium states: the first is singly degenerate and the second is $(q-1)$-fold degenerate. For $H > 0$ the first state is stable, but becomes metastable for small $H < 0$ and droplets of the second state will appear. The contribution of these droplets to the free energy of the system gives rise to the essential singularity. The activation energy of the droplets is calculated as outlined in Section IV for the thermodynamic singularity. This activation energy contains a bulk term due to the free energy difference of the two spatially uniform local equilibrium states and a surface term associated with the droplet configuration connecting the two spatially uniform states. The prefactor Ω_0 analogous to (4.29) is calculated in an analogous way to that in Section IV, by considering the effects of small fluctuations. The mean field result is valid for $d > 6$ (the upper critical dimension is 6). The extension to the critical behavior for $d < 6$ is worked out integrating renormalization group recursion relations in the same way that Houghton and Lubensky (1981) extended

Langer's results to the critical region (Section IV). After performing a Laplace transform of the result for $f_p(H)$, the final result for the cluster size distribution $C(n)$ is

$$C(n) = n^{-\theta} \exp(-A[(p - p_c)n^{\zeta}]), \qquad p > p_c, \tag{13.6}$$

where $\zeta = 1 - 1/d$ and

$$\theta' = \begin{cases} (1/2d)[1 + 4d - d^2], & d = 2, 4, 6, \\ -1/9, & d = 3, \\ -449/450, & d = 5. \end{cases} \tag{13.7}$$

The different values of θ' arise from additional logarithmic divergences in the calculation of fluctuation of the critical droplet for different values of d. This is also analogous to the different exponent that appears for $d = 3$ in the Ising model (Section IV).

J. Geological systems

A considerable amount of research has been carried out on phase transitions in complicated, geological silicate systems. A short review of the evidence for spinodal decomposition in systems such as pyroxenes and feldspars has been given by Jantzen and Herman (1978). Experimental studies of spinodal decomposition in such silicates have involved TEM investigations, which explore the microstructures of these minerals (McConnell, 1971; McLaren, 1974).

Another phenomenon of self-organization occurs in rocks, which are polycrystalline aggregates of a variety of minerals. There is considerable geological evidence to suggest that, within a certain range of temperatures and pressures, such a rock can spontaneously reorganize into bands of mineral concentration. This is known as metamorphic layering. One example is that of a random quartz–feldspar–mica aggregate which spontaneously reorganizes into bands which are rich in quartz plus feldspar or mica. Dissolution and precipitation seem to be the basic mechanisms for such a change, rather than a migration of crystals. A theory of this self-organization has been proposed by Ortoleva *et al.* (1982) and Strickholm *et al.* (1983). This theory is based on equations for crystal growth and dissolution and has been rather successful in predicting many aspects of this metamorphic layering. Other spontaneous pattern formations are known to exist in minerals, such as are discussed by Haase *et al.* (1980) and Berner (1980).

K. Pattern formation in chemical reactions

A number of patterns have been observed in chemical reactions whose formation can be explained using concepts which we have discussed in this review. For example, in the classic Liesegang-type experiment (Feinn *et al.*, 1978) coprecipitates such as $Pb(NO_3)_2$ and KI produce a PbI_2 precipitate. This can result in the formation of regular, macroscopic bands for certain concentrations of the coprecipitates. This phenomenon has been attributed to a periodic sequence of supersaturation, nucleation and depletion. More recent experiments show that even a uniform system can evolve into a mottled pattern of precipitate, following an aging process (Feinn *et al.*, 1978). Both the Liesegang banding and this uniform precipitate instability have been explained recently in terms of a Lifshitz–Slyozov-type theory (Feinn *et al.*, 1978; Lovett *et al.*, 1978; Feeney *et al.*, 1983). Namely, "Ostwald ripening" occurs in which large crystals grow at the expense of nearby small crystals. Regions in which the average particle size is larger than for the surrounding regions experience particle growth via accretion of material which is dissolved from nearby crystals.

L. Gels

A gel is a macroscopic, cross-linked polymer network which is generally immersed in a solvent. Gels can be roughly categorized as either weak (where the bond energy is comparable to k_BT) or strong (where the bond energy is much larger than k_BT). Both classes have been extensively studied and shown to exhibit interesting phase transitions. One transition is the sol–gel transition, in which a macroscopic polymer network is formed. Other transitions include phase separation, gel collapse and higher order critical points.

For example, Tanaka *et al.* (1979) have studied critical phenomena and phase separation in weak gels consisting of gelatin polymers in a methanol–water solvent. The qualitative features of the phase diagram have been explained by mean field theory (Tanaka, 1978), as well as by means of percolation models (Coniglio *et al.*, 1982). Tanaka *et al.* (1979) also investigated the temperature dependence of the transmitted and scattered light intensities for this system. As the temperature is lowered the system exhibits what appears to be a sharp transition from a transparent to an opaque state. This was interpreted as locating a spinodal point (where in a mean field theory the concentration fluctuations of the gelatin molecules diverge), but such an interpretation should clearly be viewed with considerable reservation. It seems clear, however, that a detailed study of nucleation and decomposition phenomena in such systems would be useful.

Another type of phase transition has been observed in polyacrylamide gels immersed in acetone–water mixtures. In this case the polymer network in the gel collapses if one either lowers the temperature or increases the acetone concentration (Tanaka, 1978; Tanaka *et al.*, 1980). This is a gel–gel transition in which the two gel phases are distinguished by different gel volumes. This volume discontinuity can be quite large, as gel collapses have been observed in which the volume decreases by a factor of 350. Tanaka *et al.* (1979) have obtained qualitative phase diagrams from a mean field theory. They have also shown that the ionization of the polymer network plays a key role in such phase transitions (Tanaka *et al.*, 1980). A study of dynamical phenomena in such a phase transition, if experimentally feasible, would also merit consideration.

M. Optical instabilities

Two examples of the decay of an unstable state have been extensively studied in quantum optics. The first of these involves the build-up of laser radiation when a laser is switched on. This phenomenon can be described in terms of a Fokker–Planck equation for the probability function of the complex, coherent state amplitude (Risken, 1965; Haken, 1970). This model has been treated by many authors, including Gordon and Aslaksen (1970), Arecchi and Degiorgio (1971), Suzuki (1976a, b) and Haake (1978). The existing theory, which takes into account the nonlinearity of the dynamics, is in good agreement with experiment. This problem is perhaps the best understood of the many dynamical instabilities discussed in this article, primarily because only a few modes become unstable, in contrast to the field theoretic models discussed in Section III.

A second example is the problem of superfluorescence. A macroscopic number of atoms are initially brought to identical excited states and then allowed to radiate spontaneously. Under suitable conditions the atoms will radiate cooperatively, producing short, intense pulses. One can view the initial atomic state of complete inversion as a state of unstable equilibrium (Haake, 1978). The decay of this state is due to the presence of microscopic, random fluctuations of the initial atomic dipole moments. A detailed dynamical study of such superfluorescent pulses has been given by Haake *et al.* (1979, 1980, 1981). In particular, the delay time statistics of superfluorescent pulses has been analyzed in terms of a passage time at which the field intensity reaches a specified value. It turns out that this passage time can be determined quite accurately from the early stage linear dynamics of the radiating system (Haake *et al.*, 1981). Thus for this problem one can obtain most of the interesting observed results without treating the nonlinear terms in the equations of motion.

N. Molecular dynamics

Molecular dynamics provides a very useful technique for studying various aspects of metastability and instability. In this method one solves numerically Newton's equations of motion for a given number of particles, thereby obtaining a detailed microscopic description of the dynamical evolution of the system. This is a well known procedure which has been discussed by Rahman (1964), Verlet (1967), Kushick and Berne (1973) and others. A review of the use of molecular dynamics in studying metastability and instability in fluids has been given by Abraham (1979). Here we summarize some relatively recent developments which seem particularly interesting for the subject of this article. First, the original molecular dynamics study of spinodal decomposition in a Lennard–Jones fluid mentioned in Section V (Mruzik *et al.*, 1978; Abraham, 1979) has been extended in a detailed investigation of phase separation in a two-dimensional, one-component fluid (Abraham *et al.*, 1982; Desai *et al.*, 1983). These studies of a Lennard–Jones fluid extend out to times of the order of several hundred picoseconds, during which the structure function develops in a way similar to that shown in Fig. 41. A corresponding experimental study of real fluids would be very difficult to achieve in this time interval. (Indeed, such numerical and laboratory studies are rather complimentary with respect to the time scales which are probed.) The results of the two-dimensional study include (Koch *et al.*, 1983) a detailed observation of the density morphology and the radial distribution function. The "late time" behavior of the mean cluster size is found to be $t^{1/2}$ and $t^{1/3}$ for constant temperature and constant energy quenches, respectively. Koch *et al.* show that these cluster growth results can be explained by a Lifshitz–Slyozov-type theory. An observed scaling of the structure factor (the Fourier transform of the radial distribution function) is explained by a simple model calculation. This work yields interesting new results which still require greater theoretical understanding. In particular it is clear that one needs a better theory of nonlinear phenomena than presently exists.

A second area in which molecular dynamics seems to provide beautiful results is that of nucleation and crystal growth in supercooled liquids. Although this review has not dealt with this topic, this subject is of fundamental importance in nucleation theory. Recent molecular dynamics studies (Mandell *et al.*, 1976; Hsu and Rahman 1979a, b) have shown that the final ordered structure which a supercooled liquid achieves after homogeneous nucleation is determined by the interaction potential between the atoms. For example, the simulation studies convincingly show that supercooled liquid argon forms a close-packed structure, while supercooled liquid rubidium forms a body-centred cubic structure. This of course agrees with experimental results, but raises the interesting theoretical problem

of explaining how relatively small changes in pairwise atomic interaction energies can lead to the nucleation of very different ordered structures.

Acknowledgements

This work was supported in part by grants from the National Science Foundation (No. DMR-8013700), the Swiss National Foundation and the US–Spanish Committee for Scientific Cooperation. J.D.G. wishes to acknowledge the kind hospitality of the Département de Physique Théorique, Université de Genève, Switzerland, and the Institut für Festkörperforschung der Kernforschungsanlage, Jülich, West Germany, where part of this work was carried out. We wish to thank Mrs Lucille Tucker for her assistance in typing a preliminary version of this manuscript and particularly to thank Miss Francine Nicole for her extraordinary assistance in typing the final manuscript. We also wish to acknowledge the stimulating conversations and assistance of numerous scientific friends. Finally, we wish to thank Professor K. Binder, Dr K. Kaski and Mr P. Rikvold for their constructive criticisms of this article.

References

Abraham, F. F. (1974a). "Homogeneous Nucleation Theory", Academic Press, New York and London.
Abraham, F. F. (1974b). *J. Chem. Phys.* **61**, 1221.
Abraham, F. F. (1979). *Phys. Rep.* **53**, 93.
Abraham, F. F. and Barker, J. A. (1975). *J. Chem. Phys.* **63**, 2266.
Abraham, F. F., Koch, S. W. and Desai, R. C. (1982). *Phys. Rev. Lett.* **49**, 923.
Affleck, I. (1980). PhD thesis, Harvard University.
Affleck, I. (1981). *Phys. Rev. Lett.* **46**, 388.
Agarwal, A. and Herman, H. (1973). *Sci. Metall.* **7**, 503.
Ahlers, G., Cross, M. C., Hohenberg, P. C. and Safran, S. (1981). Preprint.
Aizenmann, M., Delyon, F. and Souillard, B. (1980). *J. Stat. Phys.* **23**, 267.
Alefeld, G. (1969). *Phys. Stat. Sol.* **32**, 67.
Allen, S. M. and Cahn, J. W. (1976). *Acta Metall.* **24**, 425.
Allen, S. M. and Cahn, J. W. (1979a). *Acta Metall.* **27**, 1017.
Allen, S. M. and Cahn, J. W. (1979b). *Acta Metall.* **27**, 1085.
Alpern, P., Benda, Th. and Leiderer, P. (1982). *Phys. Rev. Lett.* **49**, 1267.
Andreev, A. F. (1964). *Sov. Phys. JETP* **18**, 1415.
Ardell, A. J. (1972). *Acta Metall.* **20**, 61.
Arecchi, F. T. and Degiorgio, V. (1971). *Phys. Rev. A* **3**, 1108.
Bagaev, V. S., Zamkovets, N. V., Keldysh, L. V., Sibel'din, N. N. and Tsvetkov, V. A. (1976). *Sov. Phys. JETP* **43**, 783.
Baker, J. A. (1963). *Phys. Rev.* **129**, 99.
Baker, G. A. and Kim, D. (1980). *J. Phys. A* **13**, L103.
Band, W. (1939). *J. Chem. Phys.* **7**, 324, 927.

Bartel, T. L. and Rundman, K. B. (1975). *Metall. Trans* **6A**, 1887.
Baumgärtner, A. and Binder K. (1981). *J. Chem. Phys.* **75**, 2994.
Bausch, R. and Janssen, H. K. (1976). *Z. Phys. B* **25**, 275.
Bausch, R., Horner, H. and Wagner, H. (1975). *J. Phys. C, Solid State Phys.* **8**, 2559.
Bausch, R., Eisenriegler, E. and Janssen, H. K. (1979). *Z. Phys. B* **36**, 179.
Bausch, R., Dohm, V., Janssen, H. K. and Zia, R. K. P. (1981). *Phys. Rev. Lett.* **47**, 1837.
Becker, R. and Döring, W. (1935). *Ann. Phys.* **24**, 719.
Benda, Th., Alpern, P. and Leiderer, P. (1981). *Physica* **107B**, 157.
Benda, Th., Alpern, P. and Leiderer, P. (1982). *Phys. Rev. B* **26**, 1450.
Berner, R. A. (1980). "Early Diagenesis: A Theoretical Approach", Princeton University Press, Princeton, N.J.
Bijl, A. (1938). PhD dissertation, University of Leiden.
Billotet, C. and Binder, K. (1979). *Z. Phys. B* **32**, 195.
Binder, K. (1972). *Physica* **62**, 508.
Binder, K. (1973). *Phys. Rev. B* **8**, 3423.
Binder, K. (1975a). *In* "Fluctuations, Instabilities and Phase Transitions" (T. Riste, ed.), Plenum, New York.
Binder, K. (1975b). *J. Chem. Phys.* **63**, 2265.
Binder, K. (1976). *Ann. Phys.* **98**, 390.
Binder, K. (1977). *Phys. Rev. B* **15**, 4425.
Binder, K. (1979). *In* "Monte Carlo Methods in Statistical Physics" (K. Binder ed.), Springer Verlag, Berlin.
Binder, K. (1980a). *J. Phys. (Paris) C* **4**, 51.
Binder, K. (1980b). *Solid State Commun.* **34**, 191.
Binder, K. (1980c). *In* "Systems far from Equilibrium" (L. Garrido, ed.), Lecture Notes in Physics Vol. 132, Springer Verlag, Heidelberg.
Binder, K. (1981a). *J. Stat. Phys.* **24**, 69.
Binder, K. (1981b). *Z. Phys. B* **43**, 119.
Binder, K. and Kalos, M. H. (1980). *J. Stat. Phys.* **22**, 363.
Binder, K. and Müller-Krumbhaar, H. (1974). *Phys. Rev. B* **9**, 2328.
Binder, K. and Stauffer, D. (1972). *J. Stat. Phys.* **6**, 49.
Binder, K. and Stauffer, D. (1974). *Phys. Rev. Lett.* **33**, 1006.
Binder, K. and Stauffer, D. (1976). *Advanc. Phys.* **25**, 343.
Binder, K. and Stoll, E. (1973). *Phys. Rev. Lett.* **31**, 47.
Binder, K., Stauffer, D. and Müller-Krumbhaar, H. (1975). *Phys. Rev. B* **12**, 5261.
Binder, K., Billotet, C. and Mirold, P. (1978). *Z. Phys. B* **30**, 183.
Binder, K., Kalos, M. H., Lebowitz, J. L. and Marro, J. (1979). *Advanc. Colloid Interface Sci.* **10**, 173.
Bolton, H. C. and Johnson, C. H. J. (1976). *Phys. Rev. B* **13**, 3025.
Bortz, A. B., Kalos, M. H., Lebowitz, J. L. and Zendejas, M. A. (1974). *Phys. Rev. B* **10**, 535.
Bouchard, M. and Thomas, G. (1975). *Acta Metall.* **23**, 1485.
Brailsford, A. D. and Wynblatt, P. (1979). *Acta Metall.* **27**, 489.
Brubaker, N. R. and Moldover, M. R. (1974). *In* "Low Temperature Physics", LT-13, Plenum, New York.
Bruce, A. D. and Wallace, D. J. (1981). *Phys. Rev. Lett.* **47**, 1743.
Buck, H. and Alefeld, G. (1972). *Phys. Stat. Sol.* **49**, 317.
Buchholz, J. C. and Lagally, M. G. (1975). *Phys. Rev. Lett.* **35**, 442.
Buhagiar, A. (1980). PhD thesis, Open University.
Burkhardt, T. W. and Wöger, W. (1975). *Z. Phys. B* **21**, 89.
Cahn, J. W. (1961). *Acta Metall.* **9**, 795.

Cahn, J. W. (1962). *Acta Metall.* **10**, 179.
Cahn, J. W. (1963). *J. Appl. Phys.* **34**, 3581.
Cahn, J. W. (1964). General Electric Research Laboratory Report, RL 3561M.
Cahn, J. W. (1966). *Acta Metall.* **14**, 1685.
Cahn, J. W. (1968). *Trans. Metall. Soc. AIME* **242**, 166.
Cahn, J. W. and Hilliard, J. E. (1958). *J. Chem. Phys.* **28**, 258.
Cahn, J. W. and Hilliard, J. E. (1959). *J. Chem. Phys.* **31**, 688.
Caroli, B., Caroli, C., Roulet, B. and Saint James, D. (1981). *Physica* **108A**, 233.
Chan, S. K. (1977). *J. Chem. Phys.* **67**, 5755.
Chandrasekhar, (1943). *Rev. Mod. Phys.* **15**, 1; reprinted in "Selected Papers on Noise and Stochastic Processes" (N. Wax, ed.), Dover, New York, 1952.
Chou, Y. C. and Goldburg, W. I. (1979). *Phys. Rev. A* **20**, 2105.
Chou, Y. C. and Goldburg, W. I. (1981). *Phys. Rev. A* **23**, 858.
Coey, J. M. D. (1972). *Phys. Rev. B* **6**, 3240.
Coleman, S. (1977). *Phys. Rev. D* **15**, 2929.
Collins, M. T. and Teh, H. C. (1973). *Phys. Rev. Lett.* **30**, 781.
Combescot, M. (1980). *Phys. Rev. B* **21**, 771.
Combescot, M. and Combescot, R. (1976). *Phys. Lett.* **56A**, 228.
Coniglio, A. and Klein, W. (1980). *J. Phys. A* **13**, 2775.
Coniglio, A., Stanley, H. E. and Klein, W. (1982). *Phys. Rev. B* **25**, 6805.
Cook, H. E. (1970). *Acta Metall.* **18**, 297.
Craievich, A. and Sanchez, J. M. (1981). *Phys. Rev. Lett.* **47**, 1308.
Csepes, Z. and Racz, Z. (1978). *J. Phys. A* **11**, 575.
Dahl, D. and Moldover, M. R. (1971). *Phys. Rev. Lett.* **27**, 1421.
Dee, G., Gunton, J. D. and Kawasaki, K. (1981). *Progr. Theoret. Phys.* **65**, 365.
de Fontaine, D. (1967). PhD thesis, Northwestern University.
de Fontaine, D. (1975). *In* "Treatise on Solid State Chemistry", Vol. 5 (N. B. Hannay, ed.), Plenum, New York.
de Fontaine, D. (1979). *Solid State Phys.* **34**, 74.
de Gennes, P. (1971). *J. Chem. Phys.* **55**, 572.
de Gennes, P. (1976). *Macromolecules* **9**, 587.
de Gennes, P. (1979). "Scaling Concepts in Polymer Physics", Cornell University Press, Ithaca, N.Y.
de Gennes, P. (1980). *J. Chem. Phys.* **72**, 4756.
de Ribaupierre, Y. and Manchester, F. D. (1974a). *J. Phys. C* **7**, 2126.
de Ribaupierre, Y. and Manchester, F. D. (1974b). *J. Phys. C* **7**, 2140.
de Ribaupierre, Y. and Manchester, F. D. (1975). *J. Phys. C* **8**, 1339.
Delyon, F. (1979). *J. Stat. Phys.* **21**, 727.
Desai, R. C., Koch, S. W. and Abraham, F. F. (1983). *Physica*, **118A**, 136.
Deutsch, J. M. (1982). *Phys. Rev. Lett.* **49**, 926.
Ditchek, B. and Schwartz, L. H. (1979). *Annu. Rev. Mater. Sci.* **9**, 219.
Dite, A. F., Kulakorski, V. D. and Timofeev, V. B. (1977). *Sov. Phys. JETP* **45**, 604.
Doi, M. and Edwards, S. F. (1978a). *J. Chem. Soc. Faraday Trans. II* **74**, 1789.
Doi, M. and Edwards, S. F. (1978b). *J. Chem. Soc. Faraday Trans. II* **74**, 1802.
Doi, M. and Edwards, S. F. (1978c). *J. Chem. Soc. Faraday Trans. II* **74**, 1818.
Domb, C. (1976). *J. Phys. A* **9**, 283.
Domb, C. and Stoll, E. (1977). *J. Phys. A* **10**, 1141.
Drake, R. L. (1973). *In* "Topics in Current Aerosol Research", Part II (G. M. Hidy and J. R. Brock, eds), Pergamon Press, Oxford.
Droz, M. and Combescot, M. (1975). *Phys. Lett. A* **51**, 473.
Dunning, J. W. (1973). *Faraday Symp. Chem. Soc.* **7**, 7.

Durn, I. H., Kleinert, J. and Unal, N. (1981). *J. Low Temp. Phys.* **42**, 137.
Eckmann, J.-P. (1981). *Rev. Mod. Phys.* **53**, 643.
Edwards, S. F. and Grant, J. W. V. (1973). *J. Phys. A* **6** 1169, 1186.
Eisenriegler, E. and Schaub, B. (1980). *Z. Phys. B* **39**, 65.
Essam, J. W. (1980). *Rept. Progr. Phys.* **43**, 833.
Essam, J. W. and Fisher, M. E. (1963). *J. Chem. Phys.* **38**, 802.
Etienne, B., Benoit a la Guillaume, C. and Voos, M. (1976). *Phys. Rev. B* **14**, 712.
Farkas, L. (1927). *Z. Phys. Chem. (Leipzig) A* **125**, 236.
Feeney, R., Schmidt, S. L., Strickholm, P., Chadam, J. and Ortoleva, P. (1983). *J. Chem. Phys.* **78**, 1293.
Feinn, D., Ortoleva, P., Scalf, W., Schmidt, S. and Wolfe, M. (1978). *J. Chem. Phys.* **69**, 27.
Fischer, J. E. and Thompson, T. E. (1977). *Mater. Sci. Eng.* **31**, 1977.
Fischer, J. E. and Thompson, T. E. (1978). *Phys. Today* **31**, no. 7, 36.
Fisher, M. E. (1967a). *Physics* **3**, 255.
Fisher, M. E. (1967b). *J. Appl. Phys.* **38**, 981.
Fisher, M. E. (1967c). *Rept. Progr. Phys.* **30**, 6161.
Fisher, M. E. and Burford, R. J. (1967). *Phys. Rev.* **156**, 583.
Fisher, M. E. and Racz, Z. (1976). *Phys. Rev. B* **13**, 5039.
Flinn, P. A. (1974). *J. Stat. Phys.* **10**, 89.
Flory, P. (1971). "Principles of Polymer Chemistry", Cornell University Press, Ithaca, N.Y.
Fortuin, C. M. and Kasteleyn, P. W. (1972). *Physica* **57**, 536.
Frenkel, J. (1939). *J. Chem. Phys.* **7**, 200, 538.
Frenkel, J. (1946). "Kinetic Theory of Liquids", reprinted by Dover, New York, Chap. VII.
Friedlander, S. K. and Wang, C. S. (1966). *J. Colloid Interface Sci.* **22**, 126.
Furukawa, H. (1977). *Phys. Lett.* **62A**, 377.
Furukawa, H. (1978). *Prog. Theoret. Phys.* **59**, 1072.
Furukawa, H. (1979). *Phys. Rev. Lett.* **43**, 136.
Furukawa, H. (1981). *Phys. Rev. A* **23**, 1535.
Furukawa, H. and Binder, K. (1982). *Phys. Rev. A* **26**, 556.
Gerold, V. and Kostorz, G. (1978). *J. Appl. Cryst.* **11**, 376.
Gerold, V. and Merz, W. (1967). *Sci. Metall.* **1**, 33.
Gibbs, J. W. (1906). *In* "The Scientific Papers of J. Willard Gibbs", vol. 1, Longmans, Green and Co., New York; reprinted 1961 by Dover, New York.
Gilmer, J., Goldstein, N. and Stein, R. S. (1982). To be published.
Glauber, R. J. (1963). *J. Math. Phys.* **4**, 294.
Goldburg, W. I. (1981). *In* "Scattering Techniques Applied to Supramolecular and Nonequilibrium Systems" (S. H. Chen, B. Chu and R. Nossal, eds), Plenum, New York.
Goldburg, W. I. and Huang, J. S. (1975). *In* "Fluctuations, Instabilities and Phase Transitions" (T. Riste, ed.), Plenum, New York.
Goldburg, W. I., Shaw, C. H., Huang, J. S. and Pilant, M. S. (1978a). *J. Chem. Phys.* **68**, 484.
Goldburg, W. I., Schwartz, A. J. and Kim, M. W. (1978b). *Progr. Theoret. Phys.*, Suppl. 64, 477.
Gordon, J. P. and Aslaksen, E. W. (1970). *IEEE J. Quant. Electron.* **6**, 428.
Graham, R. (1975). *In* "Fluctuations, Instabilities and Phase Transitions" (T. Riste, ed.), Plenum, New York.

Graham, R. (1981). *In* "Stochastic Nonlinear Systems in Physics, Chemistry and Biology" (L. Arnold and R. Lefever, eds), Springer Verlag, Berlin.
Graham, R. (1982). *In* "Scattering Techniques Applied to Supramolecular and Nonequilibrium Systems" (S. H. Chen, ed.), Plenum, New York.
Günther, N. J., Nicole, D. A. and Wallace, D. J. (1980). *J. Phys. A* **13**, 1755.
Gunton, J. D. (1979). *In* "Dynamical Critical Phenomena and Related Topics" (C. P. Enz, ed.), Lecture Notes in Physics no. 104, Springer Verlag, Heidelberg.
Guyot, P. and Simon, J. P. (1982). *In* "Solid–State Phase Transformations" (H. I. Aaronsen *et al.*, eds), AIME, New York, p. 325.
Haake, F. (1978). *Phys. Rev. Lett.* **41**, 1685.
Haake, F., King, H., Schröder, G., Haus, J. and Glauber, R. (1979). *Phys. Rev. A* **20**, 2047.
Haake, F., Haus, J., King, H., Schröder, G. and Glauber, R. (1980). *Phys. Rev. Lett.* **45**, 558.
Haake, F., Haus, J. W., King, H., Schröder, G. and Glauber, R. (1981). *Phys. Rev. A* **23**, 1322.
Haase, C. S., Chadam, J., Feinn, D. and Ortoleva, P. (1980). *Science* **209**, 272.
Haken, H. (1970). *In* "Handbuch der Physik", Vol. XXV/2c (L. Genzel, ed.), Springer-Verlag, Berlin.
Halperin, B. I., Hohenberg, P. C. and Ma, S. K. (1974). *Phys. Rev. B* **13**, 4119.
Halperin, B. I., Hohenberg, P. C. and Siggia, E. D. (1974). *Phys. Rev. Lett.* **32**, 1289.
Hammond, R. B. and Silver, R. N. (1979). *Phys. Rev. Lett.* **42**, 523.
Harris, A. B. and Lubensky, T. C. (1981). *Phys. Rev. B* **24**, 2656.
Hashimoto, T., Miyoshi, T. and Ohtsuka, M. (1976). *Phys. Rev. B* **13**, 1119.
Hashimoto, T., Nishimura, K. and Takeuchi, Y. (1978). *Phys. Lett.* **65A**, 250.
Haus, J. W. and King, H. (1982). *Phys. Rev. B* **25**, 3298.
Heady, R. B. and Cahn, J. W. (1973). *J. Chem. Phys.* **58**, 896.
Heermann, D. W. and Klein, W. (1983). *Phys. Rev. B* **27**, 1732.
Heermann, D. W., Klein, W. and Stauffer, D. (1982). *Phys. Rev. Lett.* **49**, 1262.
Hennion, M., Ronzaud, D. and Guyot, P. (1982). *Acta Metall.* **30**, 599.
Hensel, J. C., Phillips, T. G. and Thomas, G. A. (1977). *In* "Solid State Physics", Vol. 32 (F. Seitz, D. Turnbull and H. Ehrenreich, eds), Academic Press, New York.
Herman, H. and MacCrone, R. K. (1971). *J. Amer. Ceram. Soc.* **55**, 50.
Hillert, M. (1956). ScD thesis, Massachusetts Institute of Technology.
Hillert, M. (1961). *Acta Metall.* **9**, 525.
Hilliard, J. E. (1970). *In* "Phase Transformations" (H. I. Aronson, ed.), American Society for Metals, Metals Park, Ohio.
Hoffer, J. K., Campbell, L. J. and Bartlett, R. J. (1980). *Phys. Rev. Lett.* **45**, 912.
Hohenberg, P. C. and Halperin, B. I. (1977). *Rev. Mod. Phys.* **49**, 435.
Hohenberg, P. C. and Nelson, D. (1979). *Phys. Rev. B* **20**, 2665.
Horner, H. and Wagner, H. (1974). *J. Phys. C, Solid State Phys.* **7**, 3305.
Horner, H. and Jüngling, K. (1979). *Z. Phys. B* **36**, 97.
Houghton, A. and Lubensky, T. C. (1981). *Phys. Lett.* **77A**, 479.
Howland, R. G., Wong, N. C. and Knobler, C. M. (1980). *J. Chem. Phys.* **73**, 522.
Hsu, C. S. and Rahman, A. (1979a). *J. Chem. Phys.* **70**, 5234.
Hsu, C. S. and Rahman, A. (1979b). *J. Chem. Phys.* **71**, 4974.
Huang, J. S., Goldburg, W. I. and Bjerkaas, A. W. (1974a). *Phys. Rev. Lett.* **32**, 921.
Huang, J. S., Vernon, S. and Wong, N. C. (1974b). *Phys. Rev. Lett.* **33**, 140.

Huang, J. S., Goldburg, W. I. and Moldover, M. R. (1975). *Phys. Rev. Lett.* **34**, 639.
Ikeda, H. (1976a). *Progr. Theoret. Phys.* **55**, 1298.
Ikeda, H. (1976b). *Progr. Theoret. Phys.* **55**, 2027.
Ikeda, H. (1977). *Progr. Theoret. Phys.* **57**, 687.
Janssen, H. K. (1976). *Z. Phys. B* **23**, 245.
Jantzen, C. M. F. and Herman, H. (1978). *In* "Phase Diagrams: Material Science and Technology", Vol. 5 (A. A. Alper, ed.), Academic Press, New York, p. 127.
Jasnow, D. and Rudnick, J. (1978). *Phys. Rev. Lett.* **41**, 698.
Jeffries, C. D. (1975). *Science* **189**, 955.
Junqua, A., Delafond, J., Mimault, J. and Grilhé, J. (1974). *Scripta Metall.* **8**, 317.
Kadanoff, L. P. (1971). *In* "Critical Phenomena" (M. S. Green, ed.), Academic Press, New York, p. 118.
Kalos, M., Lebowitz, J. L., Penrose, O. and Sur, A. (1978). *J. Stat. Phys.* **18**, 39.
Kappus, W. and Horner, H. (1977). *Z. Phys. B* **27**, 215.
Kaski, K., Binder, K. and Gunton, J. D. (1983). Submitted for publication.
Katsura, S. and Takizawa, M. (1974). *Progr. Theoret. Phys.* **51**, 82.
Katz, J. L. and Donohue, M. D. (1979). *Advanc. Chem. Phys.* **40**, 137.
Kawabata, C. and Kawasaki, K. (1978). *Phys. Lett.* **65A**, 137.
Kawasaki, K. (1970). *Ann. Phys.* **61**, 1.
Kawasaki, K. (1972). *In* "Phase Transitions and Critical Phenomena", Vol. 2 (C. Domb and M. S. Green, eds), Academic Press, London.
Kawasaki, K. (1973). *J. Phys. A* **6**, 1289.
Kawasaki, K. (1975a). *Phys. Lett.* **53A**, 117.
Kawasaki, K. (1975b). *J. Stat. Phys.* **12**, 365.
Kawasaki, K. (1976). *Progr. Theoret. Phys.* **56**, 1705.
Kawasaki, K. (1977). *Progr. Theoret. Phys.* **57**, 826.
Kawasaki, K. and Gunton, J. D. (1976). *In* "Progress in Liquid Physics" (C. Croxton, ed.), John Wiley and Sons, Chichester.
Kawasaki, K. and Ohta, T. (1978a). *Progr. Theoret. Phys.* **59**, 362.
Kawasaki, K. and Ohta, T. (1978b). *Progr. Theoret. Phys.* **59**, 1406 (addendum to the 1978a reference).
Kawasaki, K. and Ohta, T. (1982a). *Progr. Theoret. Phys.* **67**, 147.
Kawasaki, K. and Ohta, T. (1982b). *Progr. Theoret. Phys.* **68**, 129.
Kawasaki, K., Yalabik, M. C. and Gunton, J. D. (1978). *Phys. Rev. A* **17**, 455.
Kawasaki, T. (1978). *Progr. Theoret. Phys.* **59**, 1812.
Kawasaki, T. (1979). *Progr. Theoret. Phys.* **61**, 384.
Kawasaki, T., Imaeda, T. and Gunton, J. D. (1981). *In* "Perspectives in Statistical Physics", M.S. Green Memorial Volume (H. J. Ravache, ed.), North Holland, Amsterdam.
Kawasaki, K., Ohta, T. and Nagai, T. (1983). *J. Phys. Soc. Jpn* **52**, Suppl., 131.
Kiang, C. S. and Stauffer, D. (1970). *Z. Phys.* **235**, 130.
Kikuchi, R. (1967). *J. Chem. Phys.* **47**, 1664.
Kim, M. W., Schwartz, A. J. and Goldburg, W. I. (1978). *Phys. Rev.* **41**, 657.
Kirczenow, G. (1982). *Phys. Rev. Lett.* **48**, 1125.
Klein, J. (1978). *Macromolecules* **11**, 852.
Klein, W. (1980). *Phys. Rev. B* **21**, 5245.
Klein, W. (1981). *Phys. Rev. Lett.* **22**, 1569.
Klein, W., Wallace, D. J. and Zia, R. K. P. (1976). *Phys. Rev. Lett.* **37**, 639.
Klempner, D. and Frisch, K. (1977). "Polymer Alloys", Plenum, New York.
Knobler, C. M. and Wong, N. C. (1981). *J. Phys. Chem.* **85**, 1972

Koch, S. W. and Haug, H. (1979). *Phys. Stat. Solidi (b)* **95**, 155.
Koch, S. W., Desai, R. C. and Abraham, F. F. (1983). *Phys. Rev.* **27**, 2152.
Kramer, L. (1981a). *Z. Phys. B* **41**, 357.
Kramer, L. (1981b). *Z. Phys. B* **45**, 167.
Kramers, H. (1940). *Physica* **VII**, 284.
Krause, S. (1972). *J. Macromol. Sci. Rev. Macromol. Chem. C* **7**, 251.
Kremer, K. (1983). IFF/KFA preprint.
Kretschmer, R., Binder, K. and Stauffer, D. (1976). *J. Stat. Phys.* **15**, 267.
Krishnamurty, S. and Goldburg, W. I. (1980). *Phys. Rev. A* **22**, 2147.
Kunz, H. and Souillard, B. (1978). *J. Stat. Phys.* **19**, 77.
Kushick, J. and Berne, B. J. (1973). *J. Chem. Phys.* **59**, 3732.
Lagally, M. G., Wang, G. C. and Lu, T. M. (1978). *CRC Crit. Rev. Solid State Mat. Sci.* **7**, 233.
Landau, D. P. (1972). *Phys. Rev. Lett.* **28**, 449.
Landau, D. P. and Swendsen, R. H. (1981). *Phys. Rev. Lett.* **46**, 1437.
Landau, L. D. and Lifshitz, E. M. (1959). "Fluid Mechanics", Pergamon Press, London.
Landauer, R. and Swanson, J. A. (1961). *Phys. Rev.* **121**, 1668.
Langer, J. S. (1967). *Ann. Phys.* **41**, 108.
Langer, J. S. (1969). *Ann. Phys.* **54**, 258.
Langer, J. S. (1971). *Ann. Phys.* **65**, 53.
Langer, J. S. (1973). *Acta Metall.* **21**, 1649.
Langer, J. S. (1974). *Physica* **73**, 61.
Langer, J. S. (1975). *In* "Fluctuations, Instabilities and Phase Transitions" (T. Riste, ed.), Plenum, New York.
Langer, J. S. (1980). *In* "Systems Far From Equilibrium" (L. Garrido, ed.), Lecture Notes on Physics no. 132, Springer Verlag, Heidelberg.
Langer, J. S. and Ambegaokar, V. (1967). *Phys. Rev.* **164**, 498.
Langer, J. S. and Fisher, M. E. (1967). *Phys. Rev. Lett.* **19**, 560.
Langer, J. S. and Reppy, J. D. (1970). *In* "Low Temperature Physics", Vol. 6 (C. J. Gorter, ed.), North Holland, Amsterdam.
Langer, J. S. and Schwartz, A. J. (1980). *Phys. Rev. A* **21**, 948.
Langer, J. S. and Turski, L. A. (1973). *Phys. Rev. A* **8**, 3230.
Langer, J. S. and Turski, L. A. (1980). *Phys. Rev. A* **22**, 2189.
Langer, J. S., Bar-on, M. and Miller, H. D. (1975). *Phys. Rev. A* **11**, 1417.
Laslaz, G. (1978). Thesis, Grenoble, France.
Laslaz, G., Guyot, P. and Kostorz, G. (1977a). *J. Phys. (Paris)* **38**, 406.
Laslaz, G., Kostorz, G., Roth, M., Guyot, P. and Stewart, R. J. (1977b). *Phys. Stat. Sol. (a)* **41**, 577.
Lawrie, I. D. and Sarbach, S. (1983). *In* "Phase Transitions and Critical Phenomena", Vol. 9 (C. Domb and J. L. Lebowitz, eds), Academic Press, London, in preparation.
Leamy, H. J., Gilmer, G. H., Jackson, K. A. and Bennema, P. (1973). *Phys. Rev. Lett.* **30**, 601.
Lebowitz, J. L., Marro, J. and Kalos, M. H. (1982). *Acta Metall.* **30**, 297.
Lee, J. K., Barker, J. A. and Abraham, F. F. (1973). *J. Chem. Phys.* **58**, 3166.
Leiderer, P., Watts, D. R. and Webb, W. W. (1974). *Phys. Rev. Lett.* **33**, 483.
Leiderer, P., Nelson, D. R., Watts, D. R. and Webb, W. W. (1975). *Phys. Rev. Lett.* **34**, 1080.
Levy, A., Reich, S. and Meakin, P. (1982). *Phys. Lett.* **87A**, 248.
Lifshitz, E. M. and Pitaevskii, L. P. (1981). "Course on Theoretical Physics, Vol 10, Physical Kinetics", Pergamon Press, Oxford.

Lifshitz, I. M. (1962). *Sov. Phys. JETP* **15**, 939.
Lifshitz, I. M. and Slyozov, V. V. (1961). *J. Phys. Chem. Solids* **19**, 35.
Lothe, J. and Pound, G. M. (1962). *J. Chem. Phys.* **36**, 2080.
Lovett, R., Ortoleva, P. and Ross, J. (1978). *J. Chem. Phys.* **69**, 947.
Lowe, M. J. and Wallace, D. J. (1980). *J. Phys. A* **13**, L381.
Lubensky, T. C. (1979). *In* "Ill Condensed Matter" (R. Balian and G. Toulouse, eds), North Holland, Amsterdam.
Lubensky, T. C. and McKane, A. J. (1981). *J. Phys. A* **14**, L157.
Ma, S. K. (1976). "Modern Theory of Critical Phenomena", Benjamin Cunningham Inc., Worcester, Mass.
Ma, S. K. and Mazenko, G. (1975). *Phys. Rev. B* **11**, 4077.
McConnell, J. D. C. (1971). *Min. Mag.* **38**, 1.
McCumber, D. E. and Halperin, B. I. (1970). *Phys. Rev. B* **1**, 1054.
McGraw, R. and Reiss, H. (1979). *J. Stat. Phys.* **20**, 385.
McLaren, H. C. (1974). *In* "The Feldspars" (W. S. MacKenzie and J. Zussman eds), Manchester University Press, Manchester, p. 378.
McMaster, L. P. (1973). *Macromolecules* **6**, 760.
McMaster, L. P. (1975). *Advanc. Chem. Ser.* **142**, 43.
Manchester, F. D. (1976). *J. Less Common Metals* **49**, 1.
Manchester, F. D. (1982). *In* "Proceedings of the International Symposium on the Electronic Structure and Properties of Hydrogen in Metals, Richmond, Va".
Mandell, M. J., McTague, J. P. and Rahman, A. (1976). *J. Chem. Phys.* **64**, 3699.
Mandell, M. J., McTague, J. P. and Rahman, A. (1977). *J. Chem. Phys.* **66**, 3070.
Marro, J. and Vallés, J. L. (1983). *Phys. Lett. A*, to be published.
Marro, J., Bortz, A. B., Kalos, M. H. and Lebowitz, J. L. (1975). *Phys. Rev. B* **12**, 2000.
Marro, J., Lebowitz, J. L. and Kalos, M. H. (1979). *Phys. Rev. Lett.* **43**, 282.
Mayer, J. E. and Mayer, M. G. (1940). *In* "Statistical Mechanics", Wiley, New York, Chap. 14.
Meakin P. and Reich, S. (1982). *Phys. Lett. A* **92**, 247.
Metiu, H., Kitahara, K. and Ross, J. (1979). *In* "Fluctuation Phenomena" (E. W. Montroll and J. L. Lebowitz, eds), North Holland, Amsterdam.
Metropolis, N., Rosenbluth, A. W., Rosenbluth, M. N., Teller, A. H. and Teller, E. (1953). *J. Chem. Phys.* **21**, 1087.
Mirold, P. and Binder, K. (1977). *Acta Metall.* **25**, 1435.
Miyazaki, J., Pound, G. M., Abraham, F. F. and Barker, J. A. (1977). *J. Chem. Phys.* **67**, 3851.
Mori, H. (1965). *Progr. Theoret. Phys.* **33**, 423.
Mou, C. Y. and Lovett, R. (1975). *J. Chem. Phys.* **62**, 3298.
Mruzik, M. R., Abraham, F. F. and Pound, G. M. (1978). *J. Chem. Phys.* **69**, 3462.
Müller-Krumbhaar, H. (1974a). *Phys. Lett.* **48A**, 459.
Müller-Krumbhaar, H. (1974b). *Phys. Lett.* **50A**, 27.
Müller-Krumbhaar, H. (1979). *In* "Monte Carlo Methods in Statistical Physics" (K. Binder, ed.), Springer Verlag, Berlin.
Müller-Krumbhaar, H. and Stoll, E. (1976). *J. Chem. Phys.* **65**, 4294.
Nelson, D. and Fisher, M. E. (1975). *Phys. Rev.* B **11**, 1030.
Nicoll, J., Chang, T. and Stanley, H. E. (1976). *Phys. Rev. A* **13**, 1251.
Nishi, T., Wang, T. T. and Kwei, T. K. (1975). *Macromolocules* **8**, 227.
Novick-Cohen, A. (1981). PhD dissertation, Weizmann Institute of Science.
Novick-Cohen, A. and Segal, L. (1982). To be published.
Ogita, N., Ueda, A., Matsubara, T., Matsuda, H. and Yonezawa, F. (1969). *J. Phys. Soc. Jpn* **26**, Suppl. 145.

Ohta, T. and Kawasaki, K. (1977). *Progr. Theoret. Phys.* **58**, 467.
Ohta, T., Jasnow, D. and Kawasaki, K. (1982). *Phys. Rev. Lett.* **49**, 1223.
Oki, K., Sagana, H. and Eguchi, T. (1977). *J. Phys. (Paris) C* **7**, 414.
Onuki, A. (1981). *Progr. Theoret. Phys.* **66**, 1230.
Onuki, A. (1982a). *Progr. Theoret. Phys.* **67**, 768.
Onuki, A. (1982b). *Progr. Theoret. Phys.* **67**, 787.
Onuki, A. (1982c). *Phys. Rev. Lett.* **48**, 753.
Ortoleva, P., Merino, E. and Strickholm, P. (1982). *Amer. J. Sci.* **282**, 617.
Papoular, M.(1974). *Phys. Fluids* **17**, 1038.
Parrinello, M. and Rahman, A. (1980). *Phys. Rev. Lett.* **45**, 1196.
Penrose, O. (1978). *In* "Stochastic Processes in Nonequilibrium Systems" (L. Garrido, P. Seglar and P. J. Shepherd, eds), Lecture Notes in Physics no. 84, Springer Verlag, Heidelberg.
Penrose, O. and Lebowitz, J. L. (1979). *In* "Studies in Statistical Mechanics", Vol. 7 (J. L. Lebowitz and E. W. Montroll, eds), North Holland, Amsterdam.
Penrose, O., Lebowitz, J. L., Marro, J., Kalos, M. H. and Sur, A. (1978). *J. Stat. Phys.* **19**, 243.
Pfeuty, P. and Toulouse, G. (1975). "Introduction to the Renormalization Group and to Critical Phenomena", John Wiley and Sons, London.
Phani, M. K., Lebowitz, J. L., Kalos, M. H. and Penrose, O. (1980). *Phys. Rev. Lett.* **45**, 366.
Phythian, R. (1977). *J. Phys. A* **10**, 777.
Pick, M. A. (1978). Jül-Bericht Jül-951-FF, Kernforschungsanlage Jülich.
Pincus, P. (1981). *J. Chem. Phys.* **75**, 1996.
Poland, D. and Scheraga, H. A. (1970). "Theory of Helix–Coil Transitions in Biopolymers", Academic Press, New York.
Potts, R. B. (1952). *Proc. Camb. Phil. Soc.* **48**, 106.
Pound, G. M. (1972). *Nat. Bur. Stand. (U.S.), J. Phys. Chem. Ref. Data* **1**, 119.
Privman, V. and Schulman, L. S. (1982a). *J. Stat. Phys.* **29**, 205.
Privman, V. and Schulman, L. S. (1982b). *J. Phys. A* **15**, L231.
Quinn, G. D., Bishop, G. H. and Harrison, R. (1976). *J. Phys. A* **9**, L9.
Racz, Z. (1975). *Phys. Lett.* **53A**, 433.
Racz, Z. (1976). *Phys. Rev. B* **13**, 263.
Racz, Z. and Collins, M. F. (1975). *Phys. Rev. B* **11**, 2564.
Racz, Z. and Collins, M. F. (1976). *Phys. Rev. B* **13**, 3074.
Rahman, A. (1964). Phys. Rev. **136**, 405.
Rao, M., Kalos, M. H., Lebowitz, J. L. and Marro, J. (1976). *Phys. Rev. B* **13**, 4328.
Reatto, L. (1970). *Phys. Lett.* **33A**, 519.
Reatto, L. and Rastelli, E. (1972). *J. Phys. C* **5**, 2785.
Reghavan, V. and Cohen, M. (1975). *In* "Treatise on Solid State Chemistry", Vol. 5 (N. B. Hannay, ed.), Plenum, New York.
Reich, S. and Cohen, Y. (1981). *J. Polym. Sci.* **19**, 1255.
Rice, T. M. (1977). *In* "Solid State Physics", Vol. 32 (F. Seitz. D. Turnbull and H. Ehrenreich, eds), Academic Press, New York.
Richter, D., Baumgärtner, A., Binder, K., Ewen, B. and Hayter, J. B. (1981). *Phys. Rev. Lett.* **47**, 109.
Rikvold, P. A. and Gunton, J. D. (1982). *Phys. Rev. Lett.* **49**, 286.
Risken, H. (1965). *Z. Phys.* **186**, 85.
Rudnick, J. and Jasnow, D. (1978). *Phys. Rev. B* **17**, 1351.
Ruiz, R. (1982). *Phys. Rev. A* **26**, 2227.
Rundman, K. B. and Hilliard, J. E. (1967). *Acta Metall.* **15**, 1025.

Russell, K. C. (1980). *Advanc. Colloid Interface Sci.* **13**, 205.
Safran, S. A. (1980). *Phys. Rev. Lett.* **44**, 937.
Safran, S. A. (1981). *Phys. Rev. Lett.* **46**, 1581.
Safran, S. A. (1980). *Synth. Metals (Switzerland)* **2**, 1.
Safran, S. A., Sahni, P. S. and Grest, G. (1982). *Phys. Rev. B* **26**, 466.
Sahni, P. S. and Gunton, J. D. (1980). *Phys. Rev. Lett.* **45**, 369.
Sahni, P. S. and Gunton, J. D. (1981). *Phys. Rev. Lett.* **47**, 1754.
Sahni, P. S., Dee, G., Gunton, J. D., Phani, M. K., Lebowitz, J. L. and Kalos, M. H. (1981). *Phys. Rev. B* **24**, 410.
Sahni, P., Grest, G. and Safran, S. (1983a). *Phys. Rev. Lett.* **50**, 60.
Sahni, P., Katz, S. L. and Gunton, J. D. (1983b). Submitted for publication.
Sahni, P. S., Gunton, J. D., Katz, S. and Timpe, R. (1982). *Phys. Rev. B* **25**, 389.
San Miguel, M. and Gunton, J. D. (1981). *Phys. Rev. B* **23**, 2317.
San Miguel, M., Dee G., Gunton, J. D. and Sahni, P. S. (1981). *Phys. Rev. B* **23**, 2334.
Sancho, J. M., San Miguel, M. and Gunton, J. D. (1980). *J. Phys. A* **13**, L443.
Sarkies, K. W. and Frankel, N. E. (1975). *Phys. Rev. A* **11**, 1724.
Sato, M. and Hirakawa, K. (1977). *J. Phys. Soc. Jpn* **42**, 433.
Schneider, T. and Stoll, E. (1974). *Phys. Rev. B* **10**, 959.
Schwartz, A. J., Huang, J. S. and Goldburg, W. I. (1975). *J. Chem. Phys.* **62**, 1847; **63**, 599.
Schwartz, A. J., Krishnamurty, S. and Goldburg, W. I. (1980). *Phys. Rev. A* **21**, 1331.
Schwartz, G. (1965). *J. Mol. Biol.* **11**, 64.
Shah, J. Combescot, M. and Dayem, A. (1977a). *Phys. Rev. Lett.* **38**, 1497.
Shah, J., Dayem, A. H. and Combescot, M. (1977b). *Solid State Commun.* **24**, 71.
Siggia, E. D. (1979). *Phys. Rev. A* **20**, 595.
Siggia, E. D. and Nelson, D. R. (1977). *Phys. Rev. B* **15**, 1427.
Siggia, E. D., Halperin, B. I. and Hohenberg, P. C. (1976). *Phys. Rev. B* **13**, 2110.
Silver, R. N. (1975a). *Phys. Rev. B* **11**, 1569.
Silver, R. N. (1975b). *Phys. Rev. B* **12**, 5689.
Silver, R. N. (1977). *Phys. Rev. B* **16**, 797.
Silver, R. N. (1978). *Phys. Rev. B* **17**, 3955.
Singhal, S. P., Herman, H. and Kostorz, G. (1978). *J. Appl. Crystals* **11**, 572.
Sinha, S. (1980). "Ordering in Two Dimensions", North Holland, Amsterdam.
Sinha, D. N. and Hoffer, J. K. (1981). *Physica* **107B**, 155.
Skripov, V. P. (1974). "Metastable Liquids", Wiley, New York.
Skripov, V. P. and Skripov, A. V. (1979). *Sov. Phys. Uspkeki* **22**, 389.
Smolders, C. A., van Aarsten, J. J. and Steenbergen, A. (1971). *Kolloid-Z. Z. Polymers* **243**, 14.
Smoluchowski, R. (1951). *Phys. Rev.* **83**, 69.
Snyder, H. L., Meakin, P. and Reich, S. (1983). *Macromolecules*, to be published.
Staehli, J. L. (1976). *Phys. Status Solidi (b)* **75**, 451.
Stanley, H. E. (1971). "Introduction to Phase Transitions and Critical Phenomena", Oxford University Press, New York.
Stauffer, D. (1976). *Z. Phys. B* **25**, 391.
Stauffer, D. (1977). *J. Phys. A* **10**, L71.
Stauffer, D. (1979). *Phys. Rept.* **54**, 1.
Stauffer, D. (1981). *J. Phys. (Paris) Lett.* **42**, L99.
Stauffer, D. and Kiang, C. S. (1971). *Phys. Rev. Lett.* **27**, 1783.
Stauffer, D., Kiang, C. S. and Walker, G. H. (1971). *J. Stat. Phys.* **3**, 323.
Stoll, E., Binder, K. and Schneider, T. (1972). *Phys. Rev. B* **6**, 2777.

Stoll, E., Binder, K. and Schneider, T. (1973). *Phys. Rev. B* **8**, 3266.
Strickholm, P., Merino, E. and Ortoleva, P. (1983). Submitted to *J. Geophys. Res.*
Sundquist, B. E. and Oriani, R. A. (1962). *J. Chem. Phys.* **36**, 2604.
Sur, A., Lebowitz, J. L., Marro, J. and Kalos, M. H. (1977). *Phys. Rev. B* **15**, 3014.
Suzuki, M. (1969). *Progr. Theoret. Phys.* **42**, 1076.
Suzuki, M. (1970). *Progr. Theoret. Phys.* **43**, 882.
Suzuki, M. (1971). *Internat. J. Magn.* **1**, 123; see also *J. Stat. Phys.* **14**, 129 (1976), Appendix C.
Suzuki, M. (1976a). *Progr. Theoret. Phys.* **56**, 77.
Suzuki, M. (1976b). *Progr. Theoret. Phys.* **56**, 477.
Suzuki, M. (1976c). *Phys. Lett.* **58A**, 435.
Suzuki, M. (1977a). *Progr. Theoret. Phys.* **57**, 380.
Suzuki, M. (1977b). *J. Stat. Phys.* **16**, 477.
Suzuki, M. (1981). *Advanc. Chem. Phys.* **46**, 195.
Suzuki, M. and Ikeda, H. (1976). *Progr. Theoret. Phys.* **55**, 2041.
Swinney, H. and Gollub, J. P. (1981). *Top. Appl. Phys.* **45**.
Sykes, M. F. and Glen, M. (1976). *J. Phys. A* **9**, 87.
Sykes, M. F., Martin, J. L. and Essam, J. W. (1973). *J. Phys. A* **6**, 1306.
Sykes, M. F., Gaunt, D. S. and Glen, M. (1976). *J. Phys. A* **9**, 97.
Tanaka, T. (1978). *Phys. Rev. Lett.* **40**, 820.
Tanaka, T., Swislow, G. and Ohmine, I. (1979). *Phys. Rev. Lett.* **42**, 1557.
Tanaka, T., Fillmore, D., Sun, S. T., Nishio, I., Swislow, G. and Shah, A. (1980). *Phys. Rev. Lett.* **45**, 1636.
Thomas, G. A., Mock, J. B. and Capizzi, M. (1978). *Phys. Rev. B* **18**, 4250.
Tiapkin, Yu. D. (1977). *Annu. Rev. Mater. Sci.* **7**, 209.
Tomita, H. (1978). *Progr. Theoret. Phys.* **59**, 1116.
Tomotika, S. (1935). *Proc. Roy. Soc. Lond.* **150**, 322.
Turnbull, D. (1951). *Trans. Mettal. Soc. AIME* **191**, 661.
Turski, L. A. and Langer, J. S. (1980). *Phys. Rev. A* **22**, 2189.
van Aarsten, J. J. (1970). *Eur. Polym. J.* **6**, 919.
van Emmerick, P. T. and Smolders, C. A. (1972). *J. Poly. Sci. C*, **39**, 311.
van Emmerick, P. T., Smolders, C. A. and Geymayer, W. (1973). *Eur. Polym. J.* **9**, 309.
Verlet, L. (1967). *Phys. Rev.* **159**, 98.
Voisin, P., Etienne, B. and Voos, M. (1979). *Phys. Rev. Lett.* **42**, 526.
Volmer, M. and Weber, A. (1926). *Z. Phys. Chem. (Leipzig)* **119**, 277.
Wagner, C. (1961). *Z. Electrochem.* **65**, 581.
Wagner, H. (1978). *Top. Appl. Phys.* **28**, 5.
Wagner, H. and Horner, H. (1974). *Advanc. Phys.* **23**, 587.
Wallace, D. (1980). *In* "Proceedings of the Cargese Summer Institute on Phase Transitions", Plenum, New York.
Weins, J. and Cahn, J. (1973). *In* "Sintering and Related Phenomena" (G. C. Kuczynski, ed.), Plenum, London.
Westervelt, R. M. (1976a). *Phys. Status Solidi (b)* **74**, 727.
Westervelt, R. M. (1976b). *Phys. Status Solidi (b)* **76**, 31.
White, N. J. (1976). *J. Phys. C* **9**, L187.
Widom, B. (1975). *J. Chem. Phys.* **62**, 1332.
Williams, E. D., Cunningham S. L. and Weinberg W. H. (1978). *J. Chem. Phys.* **68**, 4688.
Wilson, K. and Kogut, J. (1974). *Phys. Rept.* **12C**, 75.
Wolfe, J. P. (1982). *Phys. Today* **35**, 46.
Wong, N. C. and Knobler, C. M. (1978). *J. Chem. Phys.* **69**, 725.

Wong, N. C. and Knobler, C. M. (1979). *Phys. Rev. Lett.* **43**, 1733; **45**, 498.
Wong, N. C. and Knobler, C. M. (1981). *Phys. Rev. A* **24**, 3205.
Yamada, T., Ohta, T. and Kawasaki, K. (1977). *J. Stat. Phys.* **16**, 281.
Zabel, H. and Peisl, H. (1979). *Phys. Rev. Lett.* **42**, 511.
Zabel, H. and Peisl, H. (1980). *Acta Metall.* **28**, 589.
Zeldovitch, Ya. B. (1943). *Acta Physicochim. (URSS)* **18**, 1.
Zia, R. K. P. (1981). *Z. Phys. B* **41**, 129.
Zwanzig, R. (1961). *Phys. Rev.* **124**, 983.

Addendum to Chapter 1

Note Added in Proof

The critical behaviour of surfaces continues to be a very active area of current research. In the following we briefly describe the most significant recent results.

A. Critical behaviour at an edge

Cardy (1983) generalized the discussion of systems with free surfaces to the case where the system is bounded by several planar surfaces which met at an edge. Then for volume $V \to \infty$ the free energy F is written as

$$F = Vf_b + Sf_s + Lf_e(\alpha) + \ldots , \tag{A.1}$$

where S is the total surface area and L the total length of the edges. The last term in eqn (A.1) involves the edge free energy $f_e(\alpha)$, which depends on the angle α between the two planes defining the edge. Cardy (1983) studies $f_e(\alpha)$ both within mean-field theory and by field-theoretic renormalization group methods analogous to those of Section VI.A. Introducing a local field H_2 acting at the edge only, a scaling behaviour

$$f_e(\alpha) = |t|^{(d-2)\nu_b} \tilde{f}_e(|t|^{-\Delta_b} H, |t|^{-\Delta_1} H_1, |T|^{-\Delta_2} H_2) \tag{A.2}$$

is established which generalizes eqn (3.16) $2 - \alpha_s = (d-1)\nu_b$ (which follows from eqn (3.23a) and the hyperscaling relation). From eqn (A.2) the exponents governing all possible magnetizations and susceptibilities may be read off; for instance, the edge magnetization behaves as $m_2 = -\partial f_e(\alpha)/\partial H_2 \propto (-t)^{\beta_2}$, with $\beta_2 = \nu_b(d-2) - \Delta_2$, and the edge susceptibility $\chi_2 = -\partial f_e(\alpha)/\partial H_2 \partial H \propto |t|^{-\gamma_2}$, with $\gamma_2 = \Delta_b + \Delta_2 - \nu_b(d-2)$, while a local susceptibility is defined as $\chi_{2,2} = -\partial^2 f_e(\alpha)/\partial H_2^2 \propto |t|^{-\gamma_{2,2}}$, with $\gamma_{2,2} = 2\Delta_2 - \nu_b(d-2)$. The correlation function of two spins at the edge decays at criticality with distance r as $r^{-(d-2+\eta_{2,2})}$, while the correlation function of a spin at the edge and a spin in the bulk decays as

Addendum to Chapter 3

Note Added in Proof

Subsequent to the completion of this article many papers have appeared (or were originally overlooked) which were not originally reviewed. A partial list of these articles as they relate to various sections of this review is given below with a few descriptive remarks.

Section I Gunton and Droz (1983) have written a general introduction to the theory of metastable and unstable states. Many of the field theoretic ideas of this review are discussed in greater detail in their monograph.

Section II An illuminating discussion of the region of validity of the classical theory of nucleation in d dimensions has been given by Binder (1983a). His treatment is based on the Ginzburg criterion.

Section III.C Mazenko and Valls (1983) have developed a real space renormalization group formalism for the Glauber kinetic Ising model. Using this formalism, they discuss the behavior and self-similarity of an Ising model quenched below T_c. Also, renormalization group analyses of the mean field model of metastable and unstable states have been given by Gunton and Yalabik (1978) and Dee *et al.* (1980).

Section IVB Klein and Unger (1983) have studied systems with long-range potentials near the classical spinodal curve. This was done using the continuum theory of Cahn and Hilliard. They found that nucleation occurs with ramified droplets. The droplets become compact in the initial stage of growth. These results are consistent with the computer simulations of Heermann and Klein (1983) discussed in Section VII.B.

Section V.A In a paper on polymer mixtures (Section XIII.H), Binder (1983b) has applied the Ginzburg criterion to determine the region of validity of the linear Cahn theory. This useful criterion can be extended to the other systems discussed in this review.

Section V.B Petschek and Metiu (1983) have studied the time dependent Ginzburg–Landau equation in two dimensions through computer simula-

tion. They analyzed spinodal decomposition in a binary mixture with a conserved order parameter. Their approach may provide a useful starting point for further studies.

Section VI.B Recent work on models with a nonconserved order parameter include the following. Monte Carlo studies have been carried out on domain growth in several two dimensional systems: The q-state Potts model (Sahni *et al.*, 1983; Srolovitz *et al.*, 1983), the clock (vector Potts) model (Kaski and Gunton, 1983), a square lattice gas with fourfold degenerate (2×1) states (Sadiq and Binder, 1983), an anisotropic planar rotor model on a triangular lattice (Mouritsen, 1983) and the antiferromagnetic model for several different quench temperatures (Kaski *et al.*, 1983). These model studies (as well as the experiments reviewed in this article) indicate that dynamical universality classes may exist analogous to those known in critical dynamics. Theoretical studies of domain growth in the antiferromagnetic model include Safran *et al.* (1983) and Grant and Gunton (1983).

Section VII Penrose and Buhagiar (1983) have discussed the kinetics of nucleation in a lattice gas model. A microscopic theory based on a version of the Becker–Doring equations is compared with the results of computer simulation studies of the model.

Section VIII The original work of Kawasaki and Ohta (1982) (Section VIII) on the dynamics of random interfaces has been extended in a series of papers. These include work on fluids (Kawasaki and Ohta 1983), a statistical dynamical theory of interacting kinks (Kawasaki and Nagai, 1983), a molecular dynamics study of interacting kinks (Nagai and Kawasaki, 1983) and an analysis of the dynamics of kinks, interfaces, vortices and the kinetics of phase transitions (Kawasaki *et al.*, 1983). Fratzl *et al.* (1983) have analyzed and compared the time evolution of the structure function and grain distribution which were obtained from computer simulations of the kinetic Ising model. They also found excellent agreement between the scaling function (scaled with the Guinier radius) obtained from Monte Carlo studies with the scaling function obtained for a variety of real systems. The scaling function is found to be independent of the temperature, alloy concentration and substance considered.

Section XI Simon *et al.* (1983) have analyzed the unmixing kinetics of various Al–Zn and Al–Ag–Zn alloys in terms of various models of nucleation and growth, as well as spinodal decomposition. Salva-Ghilarducci *et al.* (1983) have studied precipitation in ternary Al–Zn–Ag alloys by neutron SAS. Komura *et al.* (1981, 1983) have also studied phase separation by neutron SAS in Al–Zn and Al–Zn–Mg alloys. Forouki (1982) has also studied the kinetics of phase separation in an Al–Zn–Mg alloy.

Section XIII.B Maher *et al.* (1982) have studied the kinetics of a critical mixture of IW after a quench from the one-phase region into the two-phase region, followed by a reverse quench into the one-phase region. Their light scattering results are in good agreement with the theory of Ruiz mentioned in Section XIII.B. Periodic quenches have also been performed on a binary fluid by Joshua *et al.* (1983) following the original suggestion of Onuki (Section XIII.B).

Section XIII.H Binder (1983b) has developed a theory of collective diffusion, nucleation and spinodal decomposition in polymer mixtures. This work extends the earlier analyses of de Gennes and Pincus referred to in this article. Phase separation in polymer blends have been studied using light scattering techniques by Snyder *et al.* (1983) and Snyder and Meakin (1983).

Section XIII.M Weiss (1982) has presented a unified treatment for the decay of a metastable state over the entire time regime. He analyzed a Fokker–Planck model with one degree of freedom.

References

Binder, K. (1983a). IFF/KFA preprint.
Binder, K. (1983b). IFF/KFA preprint.
Dee, G., Gunton, J. D. and Kawasaki, K. (1980). *J. Stat. Phys.* **24**, 87.
Forouki, A. R. (1982). PhD thesis, University of California at Berkeley.
Fratzl, P., Lebowitz, J. L., Marro, J. and Kalos, M. H. (1983). Submitted to Acta Metall.
Grant, M. and Gunton, J. D. (1983). Temple University preprint.
Gunton, J. D. and Droz, M. (1983). *In* Lecture Notes in Physics, Vol. 183 (J. Zittartz, ed.), Springer-Verlag, Berlin.
Gunton, J. D. and Yalabik, M. C. (1978). *Phys. Rev.* **B18**, 6199.
Heerman, D. W. and Klein, W. (1983). *Phys. Rev. B* **27**, 1732.
Joshua, M., Maher, J. V. and Goldburg, W. I. (1983). University of Pittsburgh preprint.
Kaski, K. and Gunton, J. D. (1983). Temple University preprint.
Kaski, K., Yalabik, M. C., Gunton, J. D. and Sahni, P. S. (1983). Temple University preprint.
Kawasaki, K. and Nagai, T. (1983) to be published.
Kawasaki, K. and Ohta, T. (1982). *Progr. Theoret. Phys.* **68**, 129.
Kawasaki, K. and Ohta, T. (1983). *Physica* **118A**, 175.
Kawasaki, K., Ohta, T. and Nagai, T. (1983). *J. Phys. Soc. Jpn* **52**, Suppl., 131.
Klein, W. and Unger, C. (1983). *Phys. Rev. B* (in press).
Komura, S., Osamura, K., Fujii, H., Takeda, T. and Murakami, Y. (1981). *Colloid Polym. Sci.* **259**, 670.
Komura, S., Osamura, K., Fujii, H. and Takeda, T. (1983).
Maher, J. V., Easwar, N., Goldburg, W. I. and Joshua, M. (1982). *Phys. Rev. Lett.* **49**, 1850.

Mazenko, G. and Valls, O. (1983). *Phys. Rev. B* (in press).
Mouritsen, O. (1983). Aarhus University preprint.
Nagai, T. and Kawasaki, T. (1983) to be published.
Penrose, O. and Buhagiar, A. (1983). *J. Stat. Phys.* **30**, 219.
Petschek, R. and Metiu, H. (1983). *J. Chem. Phys.* (in press).
Sadiq, A. and Binder, K. (1983). IFF/KFA preprint.
Safran, S. A., Sahni, P. S. and Grest, G. S. (1983). *Phys. Rev. B* (in press).
Sahni, P. S., Grest, G. S., Anderson, M. P. and Srolovitz, D. L. (1983). *Phys. Rev. Lett.* **50**, 263.
Salva-Ghilarducci, A., Simon, J. P., Guyot, P. and Ansara, I. (1983). *Acta Metall.* (in press).
Simon, J. P., Guyot, P. and de Salva, A. (1983). *Phil. Mag.* (in press).
Snyder, H. L., Meakin, P. and Reich, S. (1983). *J. Chem. Phys.* **78**, 3334.
Snyder, H. L. and Meakin, P. (1983). Dupont preprint.
Srolovitz, D. L., Anderson, M. P., Grest, G. S. and Sahni, P. S. (1983). *Scripta Metall.* (in press).
Weiss, U. (1982). *Phys. Rev. A* **25**, 2444.

Author Index

The numbers in italic refer to the Reference pages where references are listed in full. A number in parenthesis following a page number identifies a numbered reference on that page.